(2)

SEVENTEENTH TRANSDUCER WORKSHOP

22 - 24 JUNE 1993

SAN DIEGO, CALIFORNIA

TELEMETRY GROUP

WHITE SANDS MISSILE RANGE
KWAJALEIN MISSILE RANGE
YUMA PROVING GROUND
DUGWAY PROVING GROUND
ELECTRONIC PROVING GROUND

ATLANTIC FLEET WEAPONS TRAINING FACILITY
NAVAL AIR WARFARE CENTER WEAPONS DIVISION
NAVAL AIR WARFARE CENTER AIRCRAFT DIVISION
NAVAL UNDERSEA WARFARE CENTER DIVISION NEWPORT

30TH SPACE WING
45TH SPACE WING
AIR FORCE FLIGHT TEST CENTER
AIR FORCE DEVELOPMENT TEST CENTER
AIR FORCE WEAPONS AND TACTICS CENTER
DETACHMENT 2, SPACE AND MISSILE SYSTEMS CENTER

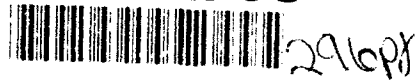

June 1993

Seventeenth Transducer Workshop

Telemetry Group
Range Commanders Council
White Sands Missile Range, NM 88002 N/A

Range Commanders Council
STEWS-SA-R
White Sands Missile Range, NM 88002-5110 N/A

New Document

SEVENTEENTH TRANSDUCER WORKSHOP

22 - 24 JUNE 1993

SAN DIEGO, CALIFORNIA

VEHICULAR INSTRUMENTATION/TRANSDUCER COMMITTEE

TELEMETRY GROUP
RANGE COMMANDERS COUNCIL

Published and Distributed by

Secretariat
Range Commanders Council
White Sands Missile Range, NM 88002-5110

DISCLAIMER

THIS DOCUMENT HAS BEEN PUBLISHED FOR INFORMATION PURPOSES ONLY. THE MATERIAL CONTAINED HEREIN DOES NOT NECESSARILY REPRESENT THE POSITION OR CONCLUSIONS OF THE RANGE COMMANDERS COUNCIL (RCC).

TABLE OF CONTENTS

TABLE OF CONTENTS (CONT'D)

TABLE OF CONTENTS (CONT'D)

TELEMETRY GROUP COMMITTEES

Chairman, E. L. LAW (NAWCWPNS (PM))
Vice Chairman, N. Lantz (DET 2, SMC)

Data Multiplex
RF Systems
Recorder/Reproducer
Vehicular Instrumentation/Transducer

MEMBERSHIP OF THE VEHICULAR INSTRUMENTATION/TRANSDUCER COMMITTEE

Raymond Faulstich (Chairman)
U.S. Army Yuma Proving Ground
STEYP-MT-I
Yuma, AZ 85365-9110

Gary Bartlett
Naval Air Warfare Center
Weapons Division
NAWCWPNS, Code C2143
China Lake, CA 93555-6001

Steve Kuehn
Sandia National Laboratories
P.O. Box 5800, Div 2645
Albuquerque, NM 87185-5800

John Ach
WL/FIBG, Bldg 24C
2145 FIFTH ST STE 2
Wright-Patterson AFB, OH
45433-7006

Lawrence Sires
Naval Air Warfare Center
Weapons Division
NAWCWPNS, Code C3213
China Lake, CA 94556-6001

Dennis Henry
Physical Science Laboratory
New Mexico State University
P.O. Box 30002
Las Cruces, NM 88003-0002

Norman E. Rector
Lawrence Livermore National
Laboratories
P.O. Box 808 M/S 154
Livermore, CA 94550

John Rupp
U.S. Army Dugway Proving
Ground
STEDP-MT-TD
Dugway, UT 84022-5000

David Crounse
Air Force Flight Test Center
6510 TESTW/TSID
Edwards AFB, CA 93523-5000

TRANSDUCER COMMITTEE OBJECTIVES

This committee apprises the Telemetry Group (TG) of significant progress in the field of transducers used in telemetry systems; maintains any necessary liaison between the TG and the National Institute of Standards and Technology and their transducers' program or other related telemetry transducer efforts; coordinates TG activities with other professional technical groups; collects and passes on information on techniques of measurement, evaluation, reliability, calibration, reporting and manufacturing; recommends uniform practices for calibration, testing and evaluation of vehicular instrumentation components; and contributes to standards in the area of vehicular instrumentation.

Transducer Workshop Summary

Workshop Number	Date	Host	General Chairman	Number Attendees	RCC TG Transducer Chairman
1	March 1960	Albuquerque, NM			
2	25-26 July 1961	Holloman AFB Alamogordo, NM	W. H. Sanders Holloman AFB, NM	46	Paul Polishuk Wright-Patterson Dayton, OH
3	21-23 June 1962	NBS Washington, DC	Arnold Wexler NBS Washington, DC	106	Paul Polishuk Wright-Patterson Dayton, OH
4	18-19 June 1964	Wright-Patterson Dayton, OH	Jack Lynch NATC Patuxent River, MD	53	Jack Lynch NATC Patuxent River, MD
5	3-4 October 1967	NBS Gaithersburg, MD	Loyt L. Lathrop Sandia Labs Albuquerque, NM	106	Loyt L. Lathrop Sandia Labs Albuquerque, NM
6	22-24 October 1969	Langley Research Crt NASA Hampton, VA	Paul Lederer NBS Albuquerque, NM	49	Loyt L. Lathrop Sandia Labs Albuquerque, NM
7	4-6 April 1972	Sandia Labs Albuquerque, NM	W. G. James AFFDL Wright-Patterson Dayton, OH	111	Pat Walter Sandia Labs First Mfg's Panel Boo-Boos
8	22-24 April 1975	Wright-Patterson Dayton, OH	Pierre F. Fuselier Lawrence Livermore Labs Livermore, CA	74	Pat Walter Sandia Labs Albuquerque, NM

Workshop Number	Date	Host	General Chairman	Number Attendees	RCC TG Transducer Chairman
9	26-28 April 1977	Eglin AFB Fort Walton Beach, FL	Kenny Cox NWC China Lake, CA	100	William Anderson NATC Albuquerque, NM
10	12-14 June 1979	North America Air Defense Command Colorado Springs, CO	Richard Hasbrouck Lawrence Livermore Labs Livermore, CA	106	William Anderson NATC Patuxent River, MD
11	2-4 June 1981	Air Force Plant Rep Office, Det 9 Seattle, WA	Leroy Bates NSWSES Port Hueneme, CA	96	William Anderson NATC Patuxent Rive, MD
12	7-9 June 1983	Patrick AFB Melbourne, FL	Kenny Cox NWC China Lake, CA	116	William Anderson NATC Patuxent River, MD
13	4-6 June 1985	Naval Postgraduate School Monterey, CA	Richard Krizan Patrick AFB, FL	112	Leroy Bates NSWSES Port Hueneme, CA
14	16-18 June 1987	Air Force Academy Colorado Springs, CO	Stephen F. Kuehn Sandia National Labs Albuquerque, NM	118	Leroy Bates NSWSES Port Hueneme, CA
15	20-22 June 1989	ESMC, Patrick AFB Cocoa Beach, FL	John T. Ach WRDC/FIBGA Wright-Patterson AFB, OH	90	Leroy Bates NSWSES Port Hueneme, CA
16	18-20 June 1991	Automotive Research Facilities San Antonio, TX	Raymond Faulstich Naval Air Test Center Patuxent River, MD	81	Leroy Bates NSWSES Port Hueneme, CA

Workshop Number	Date	Host	General Chairman	Number Attendees	RCC TG Transducer Chairman
17	22-24 June 1993		Stephen F. Kuehn Sandia National Labs Albuquerque, NM		Ray Faulstich U.S. Army Yuma Proving Ground Yuma, AZ

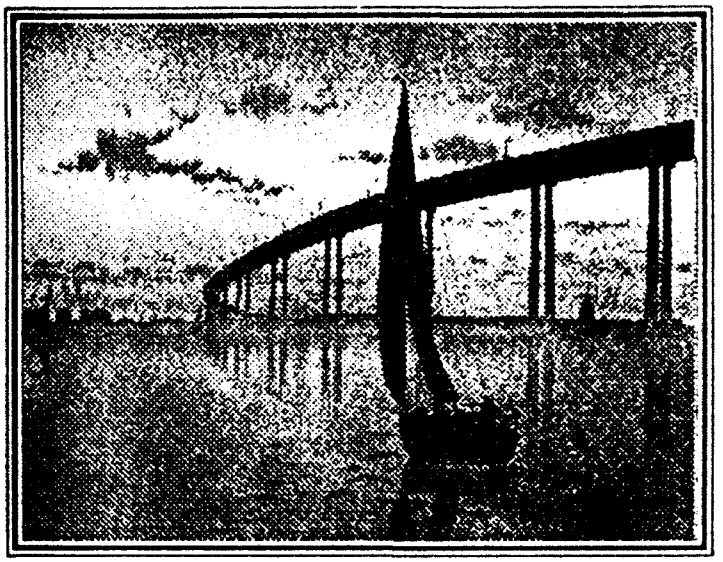

SEVENTEENTH TRANSDUCER WORKSHOP

San Diego, California
June 22-24, 1993

Sponsored by
Vehicular Instrumentation/
Transducer Committee of
Range Commanders Council
Telemetry Group

Definition of The Transducer Workshop

History

The Workshop is sponsored by the Vehicular Instrumentation/ Transducer Committee, Telemetry Group, of the Range Commanders Council. This committee develops and implements standards and procedures for transducer applications. The previous workshops, beginning in 1960, were held at two year intervals at or near various U.S. Government installations around the country.

Attendees

Attendees are working-level people who must solve real-life hardware problems and are strongly oriented to the practical approach. Their field is making measurements of physical parameters using transducers. Test and project people who attend will benefit from exposure to the true complexity of transducer evaluation, selection, and application.

Subjects

Practical problems involving transducers, signal conditioners, and read-out devices will be considered as separate components and in systems. Engineering tests, laboratory calibrations, transducer developments, and evaluations represent potential applications of the ideas presented. Measurands include force, pressure, flow, acceleration, velocity, displacement, temperature, and others.

Emphasis

The Workshop

1. Is a practical approach to the solution of measurement problems,
2. Strongly focuses on transducers and related instrumentation used in measurements engineering,
3. Has a high ratio of discussion to presentation of papers, and
4. Allows attendees to share knowledge and experience through open discussion and problem solving.

Goals

The workshop brings together those people who use transducers to identify problems and to suggest some solutions, identifies areas of common interest, and provides a communication channel within the community of transducer users. The primary goals are to:

1. Improve the coordination of information regarding transducer standards, test techniques, evaluations, and application practices among the national test ranges, range users, range contractors, other transducer users, and transducer manufacturers;
2. Encourage the establishment of special sessions so that attendees with measurement problems in specific areas can form subgroups and remain to discuss these problems after the workshop concludes; and
3. Solicit suggestions and comments on past, present, and future Vehicular Instrumentation/Transducer Committee efforts.

General Chairman

Stephen F. Kuehn
Sandia National Laboratories
P.O. Box 5800
Department 2645
Albuquerque, NM 87185-5800
(505) 844-8383

Program

MONDAY, JUNE 21, 1993

2000 Social Hour, at the Bahia Resort Hotel, courtesy of the Vehicular Instrumentation/Transducer Committee. All attendees welcome!

TUESDAY, JUNE 22, 1993

0730 REGISTRATION

0800 **Steve Kuehn**, General Chairman
Seventeenth Transducer Workshop
Introductions: **Ray Faulstich**, Chairman
Vehicular Instrumentation/Transducer Committee, RCC/TG

0830 **Session 1: Transient Measurements**
Chairman: **Charles Bullock**, Army Research Laboratory
Cochairman: **John Rupp**, Dugway Proving Ground

- "Pyro-Shock, Impact and Other Transients: Some Thoughts on 'TQM' Total Quality Measurements," **Peter K. Stein**, Stein Engineering Services
- "A Miniature Blast-Gauge Charge Amplifier System," **James L. Rieger** and **Robert Weinhardt**, Naval Air Warfare Center Weapons Division
- "Small Diameter Bar Gauges for Fast Response Airblast Measurement," **Carl Peterson** and **Phil Coleman**, S-Cubed

1000 BREAK

1015
- "Novel Applications of Miniature Hopkinson Bar Sensor," **W. Randolph Davis** and **W. Scott Walton**, Aberdeen Proving Ground
- "Isolation of a Piezoresistive Accelerometer Used in High Acceleration Tests," **Vesta I. Bateman**, **Fred A. Brown**, and **Neil T. Davie**, Sandia National Laboratories.

- "Dynamic Pressure Calibration Instruments and Sensor Transient Response," **James F. Lally**, PCB Piezotronics, Inc.
- "Compact Fast Response Transducer for Direct Heat Flux Measurement," **James G. Faller**, Aberdeen Proving Ground

1215 LUNCH

1330 **Session 2: Data Acquisition**

Chairman: **William Shay**, Lawrence Livermore Labs

Cochairman: **Daniel Skelley**, Naval Air Warfare Center Aircraft Division

- "A Comparison of Video Compression Techniques for Instrumentation," **James L. Rieger** and **Sherri L. Gattis**, Naval Air Warfare Center Weapons Division
- "Distribution of Solar Flare Data Using Available Communication Channel," **James L. Rieger** and **David Rosenthal**, Naval Air Warfare Center Weapons Division
- "Information Capture in Real Time at High Speed," **Harry A. Shamir**, Colorcode, UnLimited
- "Micro-Pressure Sensors" (Mini-paper), **Ben Granath** and **Dave Jaros**, PCB Piezotronics, Inc.

1515 BREAK

1530
- "A Program to Validate Inspection Technology for Aging Aircraft," **Patrick L. Walter**, Sandia National Laboratories
- "A Pressure Sensor Module for Space Shuttle Main Engine Fuel Application," **Seun K. Kahng, Qamar A. Shams**, and **Vincent B. Cruz**, NASA Langley
- "High Frequency Data Gathering through Digital Data Acquisition," **Paul V. Villhard**, McDonnell Douglas Aerospace
- "'DIDO': A Versatile Signal Conditioner for Hostile and Noisy Environments," **Charlie Gilbert, Mark Groethe**, and **Phil Coleman**, S-Cubed

WEDNESDAY, JUNE 23, 1993

0800 **Session 3: Calibration Techniques**

Chairman: **Richard Krizan**, Patrick AFB

Cochairman: **Roger Noyes**, EG&G Energy Measurements, Inc., Las Vegas

- "Static Versus Dynamic Calibration of Miniature Pressure Transducers," **David Banaszak** and **Gary Dale**, Wright Laboratory
- "Measurement of Frequency Dependent Sensitivity and Phase Characteristics of Eddy Current Displacement Transducers," **B. T. Murphy, G. Rombado**, and **J. K. Scharrer**, Rockwell International
- "The Effects of Cable Connections on High Frequency Accelerometer Calibration," **B. F. Payne**, National Institute of Standards and Technology
- "Smart Sensors," **Steven C. Chen**, PCB Piezotronics, Inc.

1000 BREAK

1015 "Smart Sensors" Panel Discussion

Moderator: **Richard Talmadge**, Wright Laboratory

Panel Members: **Robert D. Sill**, Endevco Corporation
Steven C. Chen, PCB Piezotronics, Inc.
John Gierer, McDonnell Douglas Aerospace
John Judd, Vibra-Metrics, Inc.

1215 LUNCH

1330 Tour of Endevco Corporation facilities, San Juan Capistrano, California

1830 Banquet at Hotel

THURSDAY, JUNE 24, 1993

0800 **Session 4: Applications**

Chairman: **William Anderson**, Naval Air Warfare Center Aircraft Division

Cochairman: **James L. Rieger**, Naval Air Warfare Center Weapons Division

- "Development of the BOA Missile Angle-of-Attack Sensor," **Steven J. Meyer** and **Edmund H. Smith**, Naval Air Warfare Center Weapons Division
- "Acceleration and Force Transducer Errors," **Wayne Tustin**, Equipment Reliability Group
- "Performance Evaluation of Dynamic Pressure Sensors and Accelerometers Using a Particle Impact Noise Detector," **Martha Pierce Willis**, Rockwell International
- "A Miniature, Digital Accelerometer for Real-Time Measurements," **John Cole** and **Doug Braun**, Silicon Designs, Inc.

1000 BREAK

1015
- "An Ultrasonic Angular Measurement System," **Justin D. Redd**, Air Force Flight Test Center
- "Commercial Pressure Transducers for Military and Aerospace Applications," **Daniel R. Weber** and **William Maitland**, Data Instruments, Inc.
- "Dynamic Force and Strain Gauge Applications Using PVDF Polmer Sensors," **Donald E. Johnson**, Ktech Corporation
- "Danish Accreditation in the Field of Acoustics," **Torben Licht**, Bruel & Kjaer

1215 CLOSING REMARKS: General Chairman

1230 WORKSHOP CONCLUDES

General Information

The Seventeenth Transducer Workshop will be held June 22-24, 1993, at the Bahia Resort Hotel in San Diego, California.

Registration

The registration consists of a completed registration form, a written "Murphyism," and a fee of $100.00 (payable in advance or at the door) to:

Ray Faulstich, Treasurer
Transducer Workshop
P. O. Box 235
Yuma, AZ 85366-0235

A "Murphyism" can describe any measurement attempt that went awry with the objective of learning from our errors and keeping our feet on the ground. It should be something generic rather than common human oversight: something from which we can learn. The tone should be anonymous so no person, organization, or company is embarrassed. While a "Murphyism" is not a requirement, submissions are strongly encouraged and the best will be included in the program.

Advance registration is desirable. Please use the enclosed registration form, include a check or money order for $100.00 payable to the Transducer Workshop, and mail to the Workshop Treasurer by May 21, 1993. **(Note: Purchase orders are not acceptable.)**

The registration fee covers the cost of coffee, tea, soft drinks, doughnuts, evening banquet, and a tour. A copy of the workshop proceedings is supplied to all attendees. Late registration will be provided at the workshop registration desk in the hotel.

Hotel Accommodations

Bahia Resort Hotel
998 West Mission Bay Drive
San Diego, California 92109
(619) 488-0551

A fixed block of rooms has been reserved at special rates for the Transducer Workshop. The following rates include tax and are valid for the weekends preceding and following the workshop: Single $77, Double $87, Triple $97, and Quadruple $107. Please mention the RCC/TG Transducer Workshop when making reservations. Early hotel reservations are strongly encouraged. Hotel reservations must be received by May 21, 1993 for these rates to apply.

Guests

No formal program will be planned for spouses or guests. However, they will be most welcome at the Social Hour on Monday and the banquet on Wednesday ($20.00 additional per guest for the dinner).

Tour - Wednesday Afternoon

A tour of Endevco is planned for Wednesday, June 23, 1993. Please indicate on the registration form if you will be accompanied by guests so that adequate transportation will be provided.

Format and Background

Workshops are just what the name implies: everyone should come prepared to contribute something from their knowledge and experience. In a workshop, the attendees become the program in the sense that the extent and enthusiasm of their participation determine the success of the workshop.

Participants will have the opportunity to hear what their colleagues have been doing and how it went; to explore areas of common interest and common problems; and to offer ideas and suggestions about what's needed in transducers, techniques, and applications.

Additional Information

May be obtained from the General Chairman, or:

Committee Chairman and Treasurer
Raymond Faulstich
U.S. Army Yuma Proving Ground
STEYP-RS-EL
Yuma, AZ 85365-9110
(602) 328-6382
DSN 899-6382

Facilities Chairman
Lawrence Sires
Naval Air Warfare Center Weapons Division
Code C3213
China Lake, CA 93555-6001
(619) 939-7404
DSN 437-7404

Papers Chairman
John Ach
Wright Laboratory
WL/FIBG
Wright-Patterson AFB, OH 45433-7006
(513) 255-5200, Ext. 300
DSN 785-5200, Ext. 300

SESSION 1

TRANSIENT MEASUREMENTS

PYRO-SHOCK, IMPACT, EXPLOSIONS AND OTHER HIGH-SPEED TRANSIENTS:

SOME THOUGHTS ON "TQM" — TOTAL QUALITY *MEASUREMENTS*

by Peter K. Stein, President
Stein Engineering Services, Inc.
5602 E. Monte Rosa
Phoenix, AZ 85018-4646

Telephone & Telefax: (602)—945—4603

Seventeenth Transducer Workshop
Range Commanders Council
San Diego, California, June 22-24, 1993

ABSTRACT

The measurement of a high speed transient requires, in general, the reproduction of its wave shape.

Preventing the achievement of this mission are distortions due to Input–Output Amplitude characteristics, to Magnitude vs. Frequency and Phase vs. Frequency characteristics plus the response of the measurement system to extraneous environmental influences. Problems of rise–time, undershoot and peak–depression are also present.

The author will refer to these Distortion Mechanisms as Amplitude Distortion, Magnitude Distortion and Phase Distortion, for short.

Diagnostic data about the measurement system and about its performance in the operating environment are necessary in order to validate the acquired data. The requirements are given in the paper.

Data analysis and interpretation are not God–given rights guaranteed by the Constitution. They are rights which the Measurement Engineer has to earn through the Data Validation process. Before measurements may be analyzed or interpreted they must be raised to the level of *Total Quality Measurements* – the forgotten *TQM*.

This paper presents techniques, based on the Unified Approach to the Engineering of Measurement Systems (Ref 1), which achieve these aims.

The data validation processes are all internal, within the measurement system and the acquired data. No comparison with theoretical or predicted value is ever suggested.

Measurement Systems must, however, be **designed** to accommodate these validation procedures. The procedures must be built into the test program. They cannot, in general, be added after-the-fact.

One of several requirements discussed in this paper is the ability to provide zero excitation – bridge supply – interrogating input – power – whatever nomenclature is used, to impedance-based transducers such as resistance-strain-gage-based trans-ducers and strain gages. Preferably such a choice should be computer programmable.

Such a check is mandatory for all explosively initiated tests. All chemical explosions are accompanied by magnetic and electric fields. In automotive air bag inflation tests, for example very large electrostatic discharge voltages have been observed.

The list of manufacturers known to the author and who provide signal conditioning with such an option, is very short indeed and a sad commentary on modern signal conditioning design (see Appendix).

Procedures similar to the ones described in this paper for strain-gage-based and piezoelectric transducers are given in Ref 1 for thermocouples. The bulk of the methods given in this paper are, however, applicable to all transducers for all transient measurements in all disciplines.

THE WAVE SHAPE REPRODUCTION OF A TRANSIENT

The measurement of a high speed transient requires, in general, the reproduction of its wave shape.

As shown in Ref. 1, the reproduction of the wave shape of any signal requires:

- Operation in the distortion-free linear range of the *Input–Output Characteristics*.

Any Non-Linearities in the Input-Output Characteristics result in the creation of frequencies at the Output which were not present at the Input, known as Frequency–Creation (see also Ref. 2). These created frequencies may be higher than or lower than the input frequencies; sums and differences of them; integer or non-integer multiples or sub-multiples of the input frequencies and of their sums and differences, etc. No amount of filtering may be able to hide the effects of those *created frequencies*. The result is Wave Shape Distortion due to Amplitude-Based mechanisms.

- Operation in the flat range of the *Magnitude vs. Frequency–Response Characteristics*.

Operation outside this range results in Wave Shape Distortion due to Magnitude vs. Frequency-Based mechanisms.

- Operation in the linear portion of the *Phase Shift vs. Frequency–Response Characteristics* or in the Constant Time-Delay portion of the *Time-Delay vs. Frequency–Response Characteristics*.

Since the derivative of the phase shift curve with respect to frequency is the *Time Delay* of the signal through the measurement system, *Constant Time Delay* is a consequence of *Linear Phase Shift*. Operation outside these ranges results in Wave Shape Distortion due to Phase vs. Frequency-Based mechanisms.

Data Validity Diagnostic Procedures

The measurement of high speed transients also requires additional diagnostics to assure data validity. Since these have been discussed extensively in Ref. 1 only an abstract of the essence of the problems and approaches to their solution will be given here.

Any publication which does not present evidence of these diagnostic validity checks contains data which cannot really be interpreted as representing the process for which the experimental observations are reported in that paper. Without the validation procedures presented here, the acquired data do not represent **Total Quality Measurements**.

Note that **nowhere** is there even a hint or suggestion to compare the experimental data with theoretical predictions. These are usually less valid than the data! Once the data are validated they become the criterion to which any theory is compared.

A PRIORI KNOWLEDGE REQUIRED

Before a Transient Measurement can be planned, executed or interpreted, the following knowledge must exist about the Measurement System being used, and the Process being investigated.

About the Measurement System

The Linearity (Input–Output) Characteristics and the Frequency–Response Characteristics for Magnitude and Phase must be known for the Measurement System.

For the Frequency–Response Characteristics for Magnitude, the Roll-Off–Characteristics at both ends of the curve must be known to at least one or two decades below the lower 3 dB point and above the upper 3 dB point. If those Roll–Off–Characteristics can not be obtained, then the Transient Response of the system to a Step must be known, both to an expanded and a compressed time scale.

It will be seen that these latter data are contained in the **Shunt Calibration** record and are of extreme importance in the data interpretation.

No transient record can be interpreted without the above information being available.

About the Process

The Amplitude vs. Frequency-Content of the original signal as emitted by the Process must be known so that the frequency response and linearity specifications can be established for the measurement system. This knowledge also permits selection of sampling rates and/or carrier frequencies for minimum data loss during its acquisition. (See also Refs 1, 3)

The Horse Before the Cart ?

The Measurement Engineer finds him/her-self in the usual *Closed-Loop* quandary of needing to know the answer before the question can be phrased — i.e., the frequency spectrum of the signal and the amplitudes, before the measurement system can be selected to observe them.

In the case of steady–state signals, the solution is easier than for transient measurements, because preliminary observations can be made which are not possible in transient situations. The design process takes only time. Ref. 1 provides a step-by-step process for the planning of both types of test which will be summarized here only for the transient case.

For transient measurements, the diagnostic process requires channel capacity. In parallel with whatever measurement system has been selected, there must be a **totally analog measurement channel** to provide the data on amplitudes and frequencies before anti–aliasing filters for purposes of either sampling criteria or channel separation criteria (Ref. 3) have distorted the original data.

Such **analog channels** must contain only analog components such as cathode ray oscilloscopes or direct–record *analog magnetic tape recorders along with analog* (AC or DC) amplifiers and signal conditioning. No FM systems are permitted and no transient capture systems are permitted, since those have already been pre–filtered resulting in perhaps unwitting data distortion.

It is true that the old analog systems did not have much amplitude–reproduction accuracy — but they had sufficient frequency–reproduction capabilities to provide the information needed here.

How to Break the Closed Loop

The methodologies presented above may seem difficult to apply, but if the mission is to acquire defensible, provably valid, **Total Quality Measurements**, there is only one other choice: the data validation methods which will be discussed, which permit the following conclusion to be reached, if it applies:

These data, as obtained, have not been influenced (distorted) by the measurement system used, or through its environment, by more than x percent.

If the validation methods presented in this paper are applicable, then the pre-test or parallel–**analog**-channel diagnostic procedures identified above, may be omitted

In most practical applications the validation methods discussed below are the only viable ones.

DOCUMENTING THE SYSTEM RESPONSE TO A STEP

It is customary to through–calibrate measurement systems with step inputs or with repeated step inputs such as a square wave. These steps are usually produced by one of two means and can be used to document the *Rise Time* and *Undershoot* Characteristics of the Measurement System forward of the injection point. Time scale expansion (for *Rise Time*) or contraction (for *Undershoot*) may have to be used.

To factor in the characteristics of the component(s) behind the injection point, the techniques presented in this paper can be used.

The Production of Step Inputs

Resistance Injection – Shunt Calibration:

A *Calibration Resistor* is switched in parallel with one of the strain gages (or other resistively–based transducers) to produce a step–change in resistance which propagates through the measurement system. If the switch is turned on and off periodically such as by a contact modulator (chopper), a pulse train (or square wave) of resistance injection is obtained. The repetition rate for such a modulator must be properly selected or reproduction of the peak-peak value, which carries the calibration signal, will not occur. See Ref. 1.

If the Calibration Resistor, R_c is switched directly across the strain gage, R, then the unit resistance change which has been produced is:

$$\Delta R/R = -R/(R + R_c)$$

Otherwise other effects such as lead wire resistances must be taken into account. Note that there is a relationship established during the calibration of the transducer itself

$$\Delta R/R = K.\ \Delta Q$$

where Q is the measurand acting on the transducer. It is thus possible to compute a $\Delta Q_{simulated}$ by the R_c shunt operation by equating the above relationships.

$$\Delta Q_{simulated} = -(1/K)[R/(R + R_c)]$$

A direct relation ship between ΔQ and R_c can also be obtained during the transducer calibration process, not relying on any equations or assumptions – a preferred procedure.

So long as the switching time rise–time is less than 1/5th the output step rise–time, the time–expanded (short–term) portion of the response to that step represents the *System Rise-Time*, t_{r-s}, from the transducer terminals forward.

The system *Undershoot Characteristics* are determined from the time-compressed (long–term) portion of the response to that step.

Voltage / Current Injection:

Measurement systems which incorporate thermocouples, piezoelectric transducers or other transducers with self-generating responses, but even some strain-gage-based systems, may be through-calibrated by injecting a step or square wave of voltage or current. The rise-time of the response to that step will represent the rise time of the measurement system forward from that transducer, provided the rise-time of the input step is less than 1/5th that of the output step (see Section on Upper Frequency Limit).

The system *Undershoot Characteristics* are determined from the time-compressed (long-term) portion of the response to that step.

THE FREQUENCY RESPONSE CURVE FOR MAGNITUDE

Wave shape distortion of a transient is possible due to insufficient bandwidth and / or due to resonances. In both cases, the signals may still be in the linear, distortion-free range of the Input-Output Characteristics, but the wave shape will have been compromised.

Non-Resonant Frequency Response Curve

Upper Frequency Limit: Rise Time

Since every system exhibits an upper frequency limit, every measurement system will exhibit rise-time problems.

Fig. 1 illustrates a typical flat frequency response curve with several time constants or upper frequency break-points limiting high-frequency behavior. The absolute values of the asymptotic slopes identify the order of the differential equation needed to model the system in that frequency range. The ultimate roll-off slope is indicated here by "-p" and should be known.

Each unit of slope is the equivalent of 20 dB/decade, since there are, by definition, 20 dB in every decade. By consequence there are 6.02 dB in every octave (doubling or halving of frequency), which is usually rounded off to 6 dB/octave. The numerical slopes have more physical meaning to the measurement engineer. The **-3 dB point, half power point, -30% response point, upper frequency limit,** f_2, is arbitrarily defined as the frequency at which 3 dB (about 29.7%) of the signal has been lost due to magnitude-based distortion. Only in a first order system is that frequency meaningful in terms of system characteristics. It represents the meeting point of the two asymptotes which govern such a first-order system.

Fig. 2 illustrates the transient response to a step which a 1st-order, 2nd-order, p-th order system would have, depending on the final value of the roll-off slope.

The **10% to 90% rise-time** is defined as the time it takes for the signal to rise from 10% of its value to 90% of its final value. It is a concept totally different from time-constant or the 36.9% or 63.1% response times. Those numbers are associated only with first-order systems where they represent measures of the one and only existing time constant. The systems shown have multiple time constants or break frequencies and only the **rise time** concept may be applied.

There is a convenient relationship which is the result of a limit theorem in pulse amplifier design which relates the two concepts in the frequency and the time domains for systems with an infinite ultimate roll-off slope at infinite frequency.

$$[f_{2,-3\,dB}](\text{in Hz}) \times [t_{r(10\text{-}90\%)}](\text{in secs}) \Rightarrow 0.35 \pm 10\%.$$

The relationship applies only to **monotonic, non-resonant** systems, and the 10% tolerance accounts for finite roll-off slopes. (Refs. 4, 5, 6). It does **not** apply to spatially averaging transducers such as side-mounted strain gages or pressure transducers, which exhibit resonant humps. For systems with 10% – 25% overshoot, Ref. 7 suggests a limit value of 0.45.

The same references present another limit theorem from pulse amplifier design considerations:

Rise times for an infinite number of series-connected components add as the square root of the sum of the squares of the individual components.

$$t_{r\text{-}s} = \sqrt{[\Sigma\,(t_{r\text{-}i})^2]}$$

where $t_{r\text{-}i}$ = the individual component rise times

This also requires a roll-off slope in the magnitude vs. frequency domain which approaches infinity as frequency approaches infinity.

For finite ultimate roll-off slopes, the approximation, although not good enough for data *correction*, can be used for data *validation* through the application of a *deviation minimizing design philosophy*.

Let $t_{r\text{-}o}$ = rise time observed from the data
$t_{r\text{-}s}$ = measurement system rise time
$t_{r\text{-}p}$ = phenomenon rise time

$$t_{r\text{-}o} \approx \sqrt{[(t_{r\text{-}s})^2 + (t_{r\text{-}p})^2]} \quad \text{(see Fig. 3)}$$

or $$t_{r\text{-}p} \approx (t_{r\text{-}o}) \cdot \sqrt{[1 - m^2]} = t_{r\text{-}o}\,(1\text{-}n)$$

The symbol ≈ means: is approximately
where m = $[(t_{r\text{-}s})/(t_{r\text{-}o})]$ = known
and n = error made due to neglect of m^2

The following table can be constructed:

Value of m	Maximum Error due to Neglect of n
1/3	6 %
1/4	3 %
1/5	2%
1/10	1/2%

So long as the observed rise time is at least 5 times the system rise time, the rise-time distortion due to the measurement system is less than 2%, a not unreasonable target for transient data.

This criterion can be used to establish, before a test even starts, the limiting value of acceptable / believable rise times on a test.

$$t_{r\text{-}o\text{-}acceptable} > 5.\ t_{r\text{-}s} \quad \textbf{for better than 2\% rise time validity.}$$

Thus, even though nothing may be known about the process being observed, the influence of the measurement system on the observation can be estimated. Even if the approximation were 20% in error, the rise time validity would be only 3% instead of 2% – deviation minimizing design principles.

Applications Note:

In Hopkinson / Davies Bar applications for accelerometer calibration at high "g" levels, the **strain-rate, i.e., the rise-time of the strain-time record** is the calibration signal! The above validation procedures must be applied. In Hopkinson / Davies Bar applications for determining the rise time of strain gages, the above validation procedures must also be applied.

FIG. 1: FREQUENCY RESPONSE CURVE FOR MAGNITUDE SHOWING ASYMPTOTIC LIMITS AT THE HIGH FREQUENCY END

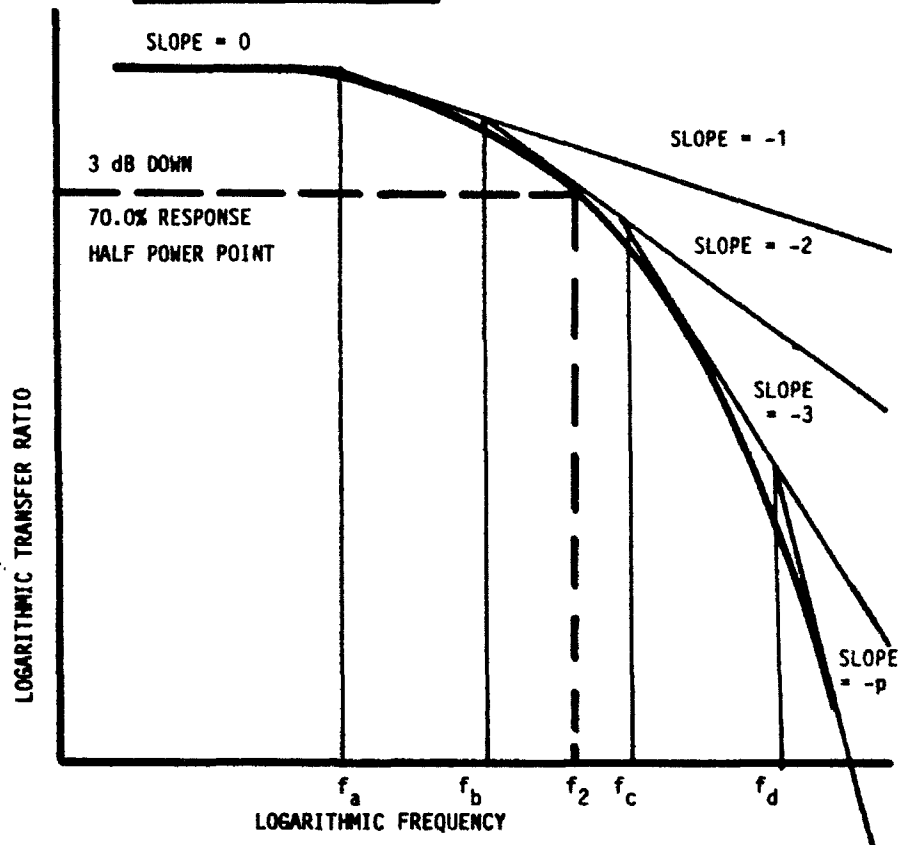

FIG. 2: RESPONSES TO A STEP ASSOCIATED WITH ULTIMATE ROLL-OFF SLOPES AND DEFINING THE 10 - 90% RISE TIME

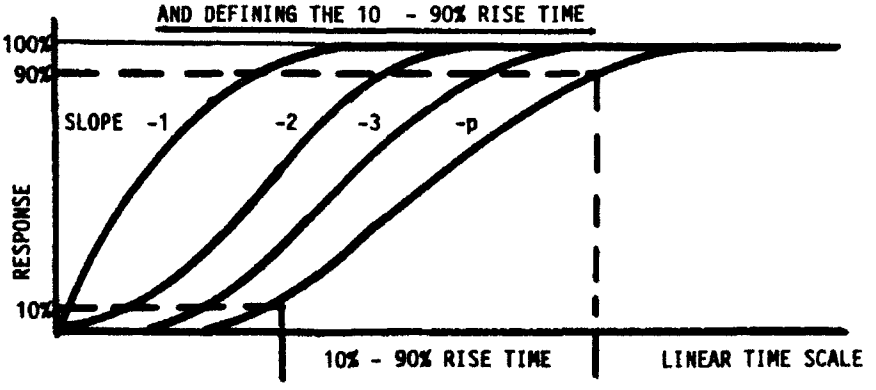

FIG. 3: THE PROBLEM OF RISE-TIME VALIDATION: DID THE MEASUREMENT SYSTEM INFLUENCE THE DATA FROM THE PHENOMENON?

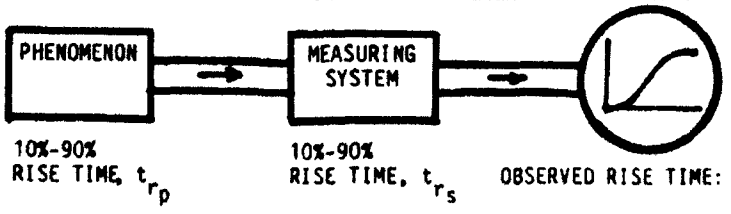

Lower Frequency Limit: Undershoot

Direct (DC) Coupled Systems:

Unless the measurement system is Direct (DC) Coupled, there may undershoot in its output when a step or a pulse is applied at its input.

Governed by Integer–Slope Roll–Offs:

Fig. 4 illustrates a typical flat frequency response curve with several time constants or lower frequency break–points limiting low-frequency behavior. The absolute values of the asymptotic slopes identify the order of the differential equation needed to model the system in that frequency range. The ultimate roll–off slope is indicated here by "q" and should be known.

The same comments translating slopes into decibels apply as did to the Upper Frequency Limit. Slopes of $\pm q = \pm 20.q$ dB/decade or approximately $\pm 6.q$ dB/octave. Again, the numerical slopes are more informative to the measurement engineer than the dB values. The **-3 dB point, half power point, -30% response point, lower frequency limit, f_1**, is arbitrarily defined as the frequency at which 3 dB (about 29.7%) of the signal has been lost due to magnitude–distortion. Only in a first order system is that frequency meaningful in terms of system characteristics. It represents the meeting point of the two asymptotes which govern such a first-order system.

Undershoot to a Step Input:

Fig. 5 illustrates the transient response which a 1st–order, 2nd–order, 3rd–order, q–th order system would have, depending on the final value of the roll–off slope. See also Refs. 4, 5, 6. A time-compressed record of the **shunt calibration** or **voltage injection step** will thus reveal the system order: the number of zero-crossings, plus 1.

The **Undershoot** is defined as the maximum negative excursion of the response per unit of maximum positive response, usually expressed in percent.

Physical Response Explanation:

Any system with a frequency response for magnitude which is a straight line of slope q and a frequency response curve for phase which is $q.\pi/2$ is a q–th order differentiator. If the frequency response of the system goes from slope 0 in the flat, high-frequency portion, through 1, 2, 3, etc., to q at the low-frequency end, then the system can act only as an **imperfect** q–th order differentiator. This argument provides a physical explanation of the apparent oscillations in an over–damped, non-resonant system, as illustrated in Fig. 6. These are not resonances, they are valiant attempts of the system to act as a an approximate–q–th order differentiator.

Second-Order System Criteria

For a 2nd–order system, let the low–frequency break points be $f_a < f_b$ with $b = f_a/f_b < 1$; then Fig. 7 relates the ratio, b, to the undershoot, U in the curve with the arrow to left. It should be noted that for 1% undershoot, the break points must be a factor of 100 apart! for 5% undershoot they must be separated by a factor of about 13. The curve with the arrow to the right permits determination of the zero-crossing time T_o.

Practical Application: A piezoelectric transducer connected to an AC-coupled amplifier would represent a typical 2nd–order system of the type being discussed.

Equivalent 2nd–Order System: Given the two break points f_a and f_b, it is possible to calculate the pure 2nd–order system with the same behavior characteristics as the one obtained by series-connecting two first-order systems (Ref. 8).

f_n = undamped natural frequency = $\sqrt{(f_a.f_b)}$
h = damping ratio = $(f_a+f_b) / 2\sqrt{(f_a.f_b)}$

The two time constants would, of course, be:

$$\tau_a = 1 / [2.\pi.f_a] \qquad \tau_b = 1 / [2.\pi.f_b]$$

Those values could be substituted into the general equations for steady state and transient responses of the totally–equivalent 2nd–order system found in Ref. 8.

Undershoot to a Square Pulse Input:

Whereas only 2nd–and–higher order systems showed undershoot to a step, even first-order system exhibit undershoot to a pulse. The phenomenon is illustrated in Fig. 8 for a square pulse of duration "a". The response of a low–frequency limited, high–pass first-order system to a step is: $e^{-t/\tau}$. At time t = a, the value of the function is: $e^{-a/\tau}$, at which point the -1 step occurs. Therefore the undershoot

$$U = 1 - e^{-a/\tau} \approx -a/\tau$$

For values of $U < 0.1$ the approximation is excellent. For higher-order systems different criteria must be used.

Practical Application: If the maximum permissible undershoot, U_{max} is (1/2) small scale division on the read–out or half the least significant bit, a reasonable design objective has been set. Since one can not interpret such signals, their existence should cause no problems. For a 1st-order system such as an AC-coupled CRO observing a strain gage output expected to a square pulse, then:

$$\text{Let } U_{max} = -a_{max}/\tau$$

Then the maximum observed pulse width for which the undershoot will be less than maximum is:

$$a_{max} < U.\tau.k$$

where $k > 1$ is a pulse shape factor for pulses perhaps more gentle than a square pulse. See also Refs. 9, 10, 11. For a square pulse, k=1.

As the data are acquired during the test, the pulse widths observed in the least favorable way: from zero crossing to zero crossing, will serve as guide as to whether or not the undershoot shown in the record is data or measurement–system–created artifact. An example is shown in Fig. 9:

$U_{max} = -0.01$ 2 mm divisions on an oscilloscope on which full scale is 10 cm, i.e. 1%

$\tau = 0.1$ sec for an AC-coupled CRO as the only low–frequency–limiting component in the measurement system.

a_{max} = 1 millisecond.

On Photo 9, Fig. 9 the pulse at the output is 0.25 msec wide and the undershoot of some 56% (shown as "B") must therefore be data. In this case it is a negative reflected stress wave during an impact test. For higher-order systems the superposition principle shown in Fig. 8 can be used.

FIG. 4: FREQUENCY RESPONSE CURVE FOR MAGNITUDE SHOWING ASYMPTIC LIMITS AT THE LOW-FREQUENCY END.

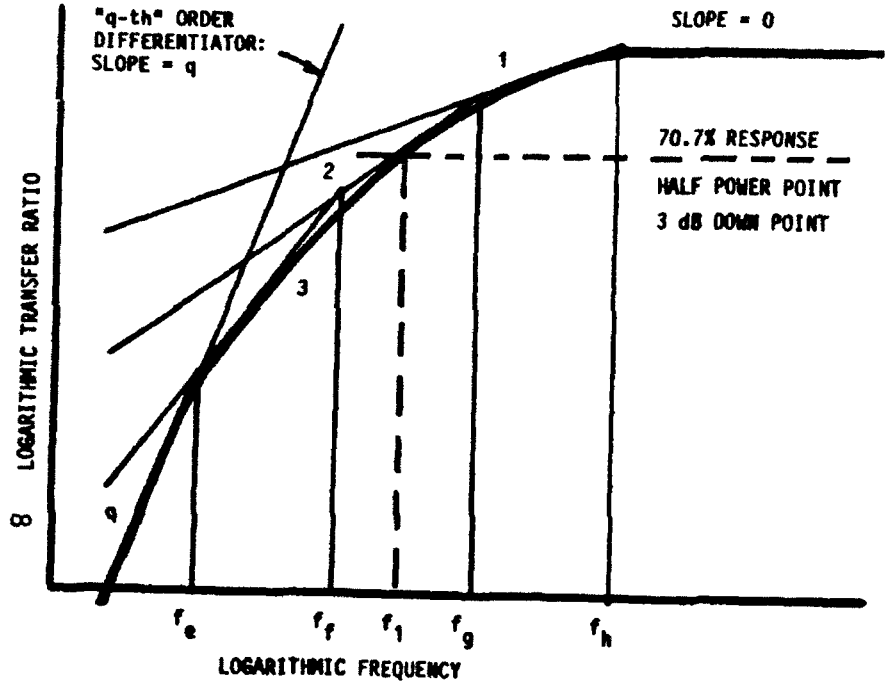

FIG. 5: RESPONSES TO A STEP ASSOCIATED WITH ULTIMATE ROLL-OFF SLOPES AND DEFINING "UNDERSHOOT"

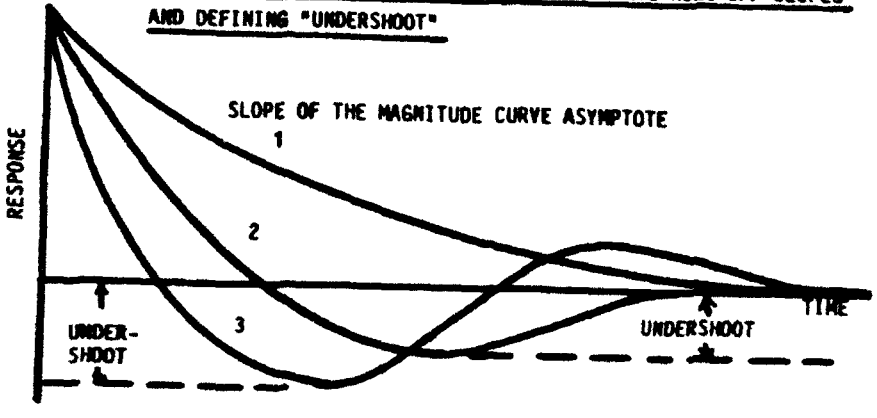

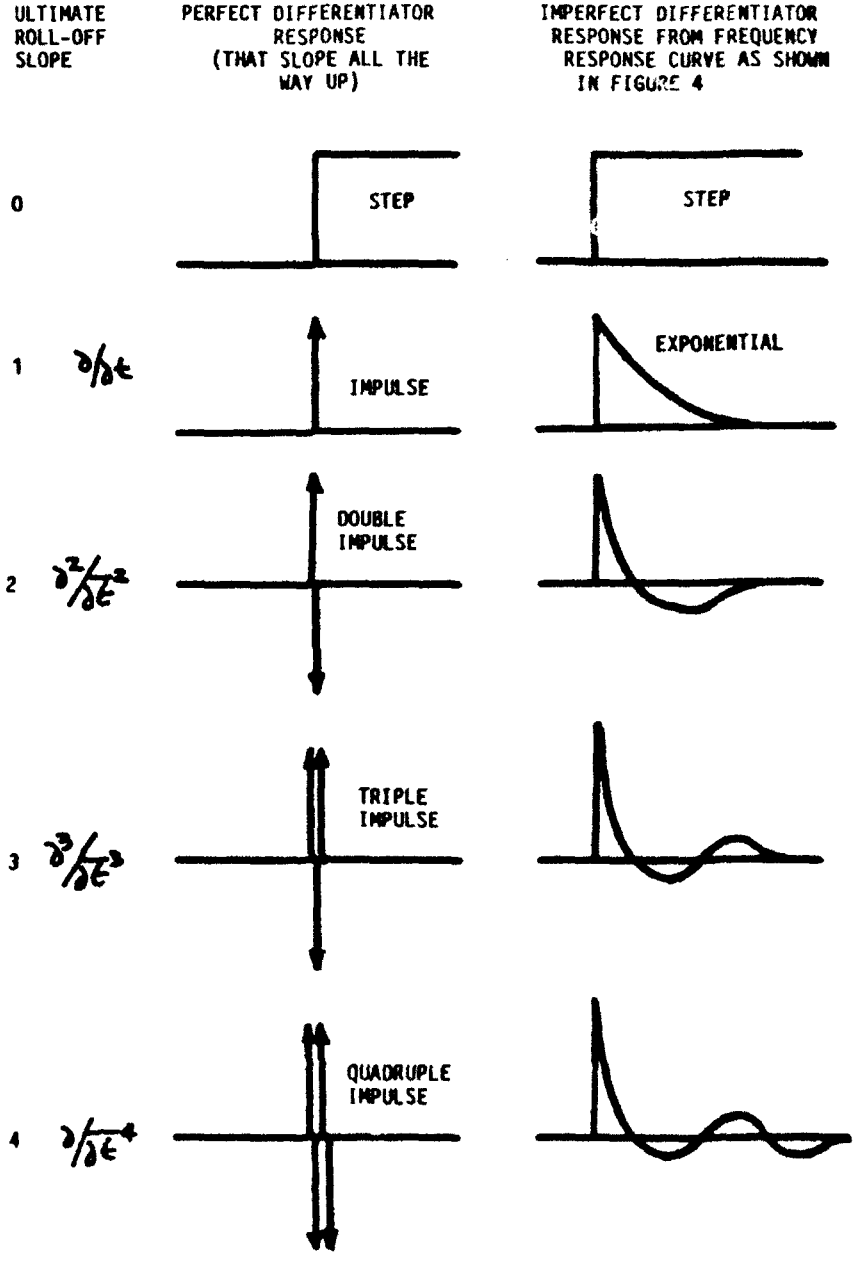

FIG. 6: PHYSICAL EXPLANATION FOR UNDERSHOOT AND ZERO CROSSINGS

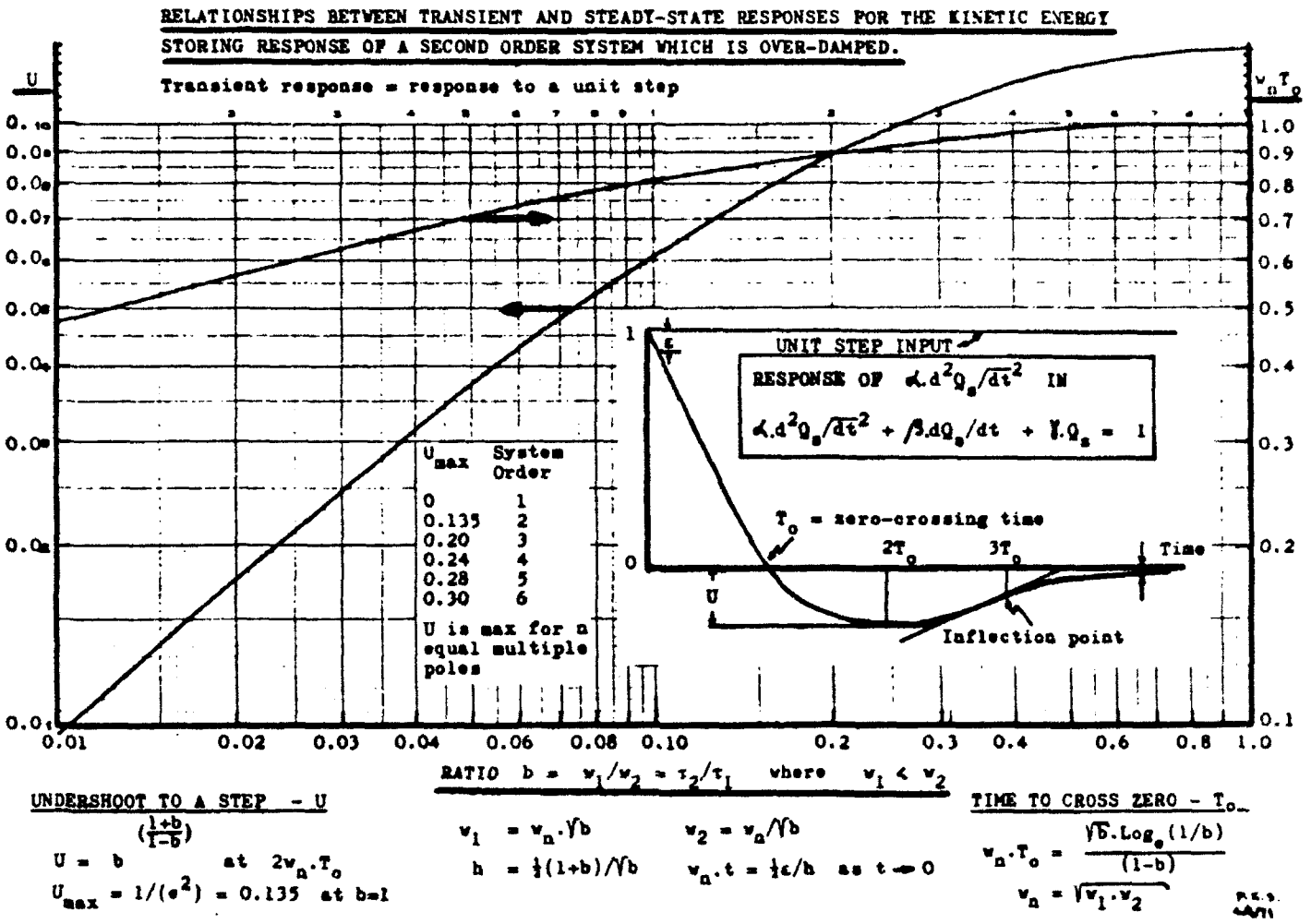

FIG. 7: UNDERSHOOT AND ZERO-CROSSING IN SECOND-ORDER SYSTEMS FOR STEP RESPONSE

Note that the above chart is based on radian frequency: w in rad/sec = $2\pi f$ in Hz

From Ref. 28

NOTE: In the above design chart, $w_1 = 2\pi f_a$ and $w_2 = 2\pi f_b$
τ_1 and τ_2 are the time constants associated with w_1 and w_2.
The equation for Undershoot is for $b < 1$, i.e. not critically damped systems. The result for b = 1, critical damping, is also given.

FIG. 8: RESPONSE OF A FIRST-ORDER SYSTEM TO A PULSE USING THE PRINCIPLE OF SUPERPOSITION

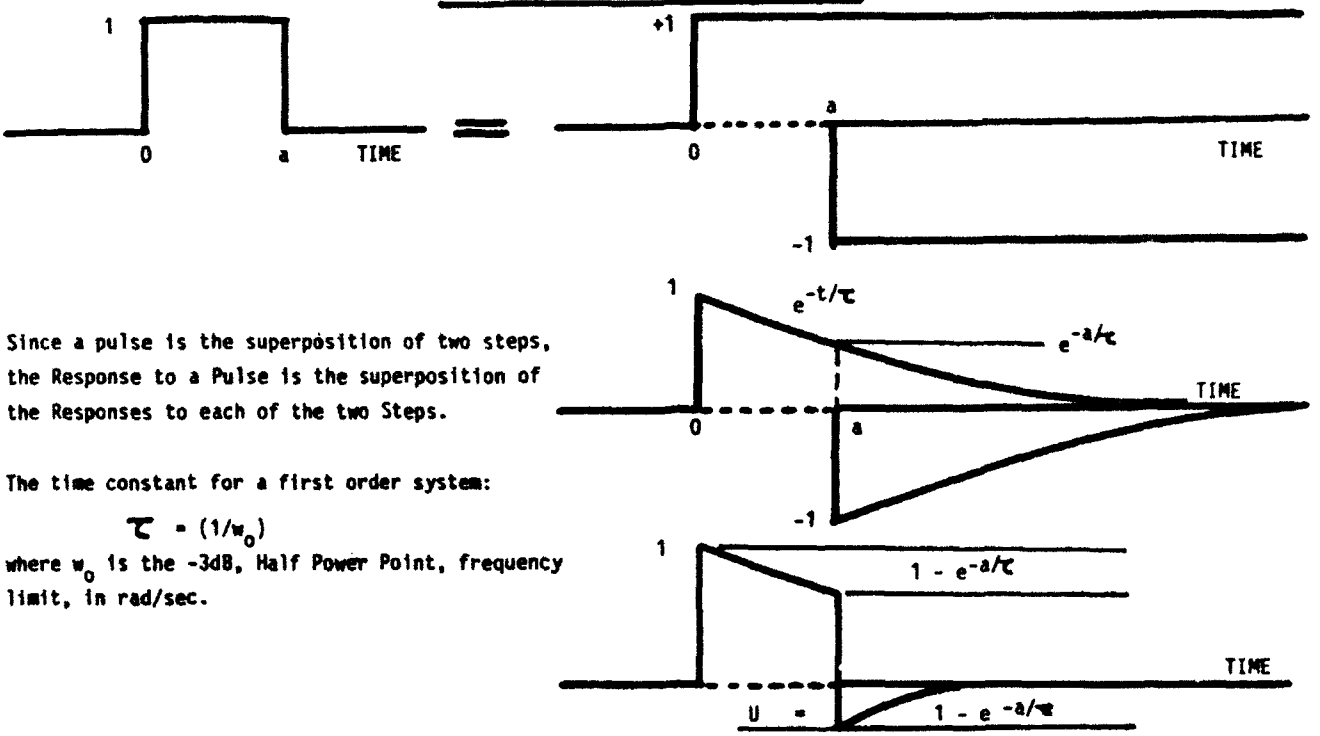

Since a pulse is the superposition of two steps, the Response to a Pulse is the superposition of the Responses to each of the two Steps.

The time constant for a first order system:

$$\tau = (1/w_0)$$

where w_0 is the -3dB, Half Power Point, frequency limit, in rad/sec.

FIG. 10: FREQUENCY RESPONSE OF A TYPICAL COMMERCIAL ACCELEROMETER (From Ref. 17)

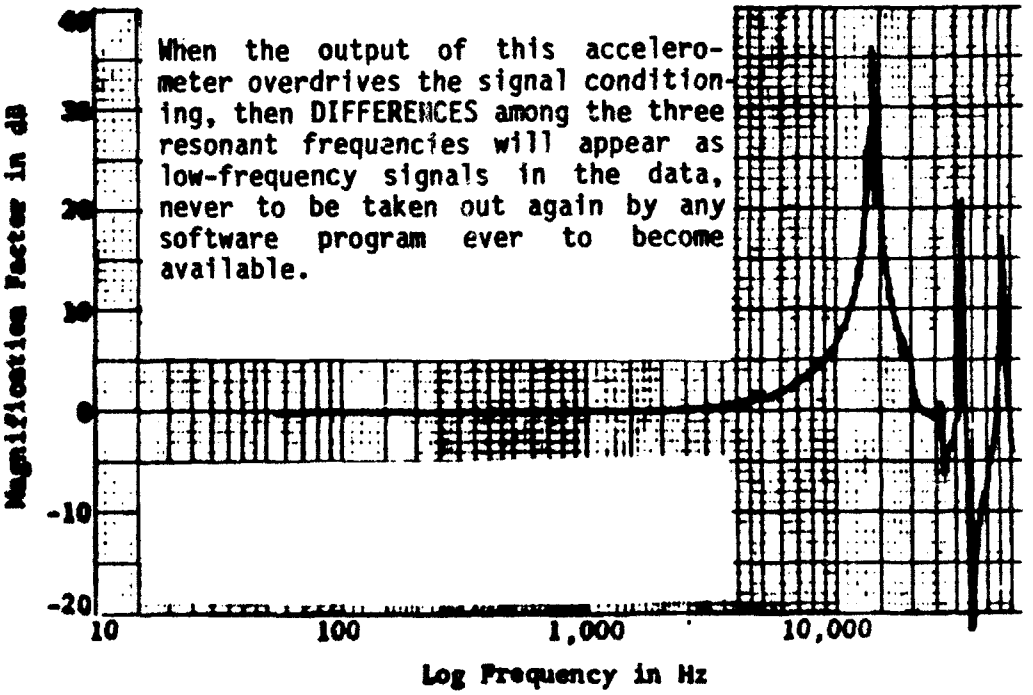

FIG. 9: CASE STUDY FROM AN IMPACT TEST USING BONDED RESISTANCE STRAIN GAGES

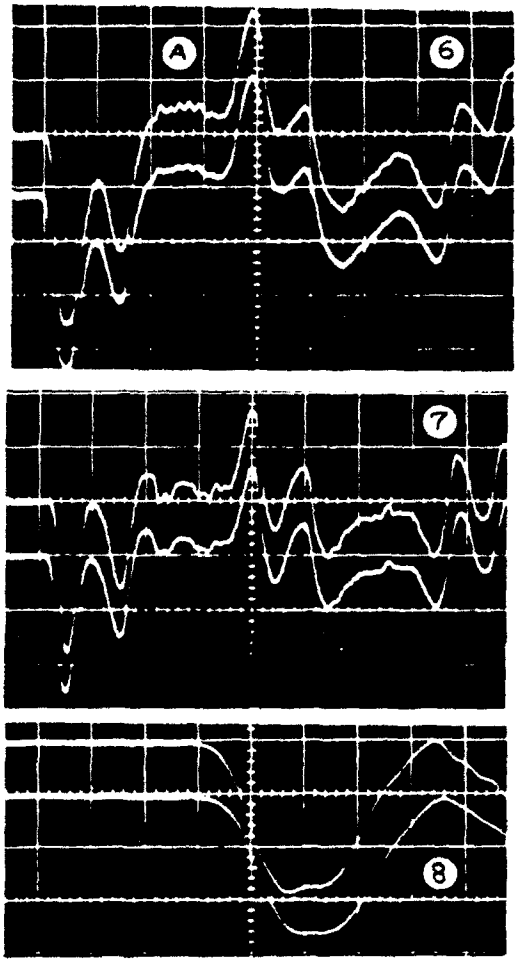

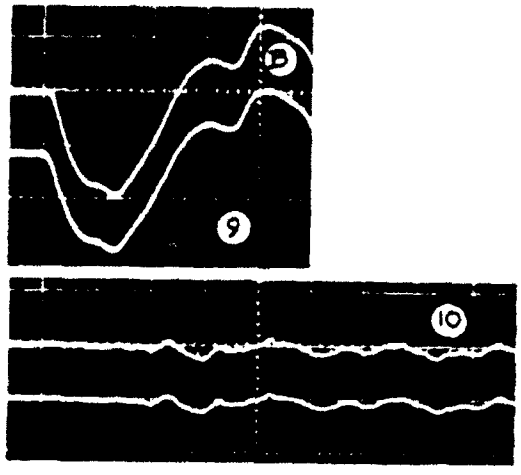

IMPACT TEST RESULTS

PHOTO	HAMMER	TIME SCALE
6	8-oz	0.1 msec/cm
7	2-oz	0.1 msec/cm
8	2-oz	20 usec/cm
9	--	0.1 msec/cm
10	8-oz	0.1 msec/cm(*)

Y_1 = 2mv/cm

Y_2 = 200 mv/cm

Other settings and components same as before.

(*) No current through gages

IMPACT-INDUCED VOLTAGES: PHOTO 10

Reduced by design but still visible.

MEASURING SYSTEM

Constant current circuit, four terminal strain-gage arrangement with inductively cancelling gage connection.

Two-conductor shielded cables from current source to gages and from gages to CRO. Specimen, current source chassis, cable-shields all connected to CRO ground. For each photo except #5: TOP TRACE: from gages directly to CRO bottom trace: from gages through 123 pre-amp to CRO MEASUREMENT SYSTEMS ENGINEERING LABORATORY ARIZONA STATE UNIVERSITY May 1970 Nettles & Stein

THE "UNDERSHOOT" NEGATIVE-STRAIN SIGNAL: PHOTO 9 - "B":

The top trace can be validated by the methods presented in this paper. The numerical example at the bottom of page 5 applies. Pulse width is 0.25 msec, hence the negative strain IS a from a reflected stress wave. The bottom trace can not be validated since amplifier characteristics are not provided by the manufacturer.

THE RISE-TIME OF THE STRAIN PULSE IN PHOTO 8:

The top trace can be validated to be the strain-wave rise-time not distorted by more than 2%. The bottom trace can be shown to be invalid and dominated by the amplifier rise-time. (From Refs. 8 and 29)

Resonant Systems

Many measurement systems with which transient measurements are performed contain at least one transducer with a highly undamped resonance. Such devices may be piezoelectric or piezoresistive (strain gage) accelerometers, pressure transducers, load cells, etc. Their damping ratios are often between 0.001 and 0.01, with dynamic magnifiers, "Qs" or resonant peaks of 50:1 to 500:1. Figure 10 illustrates a typical response.

Practical Application: Note that the response is not shown as pure 2nd–order because real hardware has numerous resonances due to internal transducer parts, mounting techniques, etc. The dominant resonance looks closely enough like a pure 2nd–order system most of the time, that it is shown as such in many illustrations. It is a misleading model.

Test Conditions Under Impact Excitation:

Impact, by definition, is suddenly applied energy. Energy consists of pairs of quantities such as Force and Displacement, Pressure and Volume, Voltage and Charge.

Energy, E, can not be transmitted in zero time, t, since that would require infinite power, P. Dimensionally:

$$|E| = |P|.|t|$$

Thus the propagation of energy occurs as pairs of energy components and as a function of time into the structure being impacted. This condition can be described by a pair of non-linear, simultaneous, partial differential wave equations in space and time.

Like all waves, these will be reflected from discontinuities and refracted through them. Such discontinuities may be joints such as rivets, bolts, spot welds, adhesive layers, etc., or changes in geometry or section. Reflected waves return to the point of impact, often to be reflected from and refracted through it. The cycle continues until the energy generated by the impact is dissipated. The excitation to which a transducer mounted on the impacted structure is exposed, therefore, is not only the initial impulse created by the impact, but a multiplicity of reflected impulses which arrive at the transducer in **no predictable sequence and with no predictable timing**. The time scale is too short and the reflections are governed by such local conditions that mathematical modeling has not yet succeeded in predicting these events.

Problems Created by the Test Conditions and Some Solutions:

There are two kinds of problems created by these Test Conditions as described:

Overload of the Transducer and its Destruction: The initial pulse and/or the superposition of the many reflections can overload and destroy the transducer mechanically. Only a (mechanical) filter between the Transducer and the Structure can prevent such a failure unless a high–range transducer is used, in which case the output level may be too small compared to the noise level. Typical manufacturers of mechanical filters are Refs. 12 , 13 and 14. There is considerable research on this topic being carried out by Dr. Vesta Bateman at Sandia National Labs, Albuquerque with periodic reports at Shock & Vibration Symposia and Range Commanders Council Transducer Workshops. The problem is especially severe for applications where the transducer must survive a very high-g pulse and subsequently record low accelerations.

Overload the Signal Conditioning Creating Low–Frequency Signals due to Intermodulation Distortion: When a sequence of pulses arrives at the resonant transducer, they may do so in such a phase relationship to each other that they subtract each other's effects and diminish the resonant vibrations set up by the first. They may also reinforce each other and build up the resonance stimulated by preceding pulses. Fig. 11 illustrates the problem from Refs. 15, 16, 17 summarized in Ref. 2.

When a system with multiple, closely-spaced resonances, such as a real transducer, is excited at high amplitudes, the resulting responses may drive the signal conditioning into the non-linear range of its Input-Output Characteristics.

Difference frequencies *among these resonances will form. These difference frequencies may appear in the low–frequency range occupied by the real signals to be measured and any filtering of the high frequencies which is performed, will not affect these "aliased" frequencies.*

Let the excitation be from only two impact-stimulated resonant frequencies:

$$(IN) \quad = \quad \mathrm{Sin}\omega_1 t + \mathrm{Sin}\omega_2 t$$

and let the non-linear Transfer Characteristics be:

$$(OUT) = k + a(IN) + b(IN)^2 + \cdots \qquad \text{then}$$

$$(OUT) = k + a.\mathrm{Sin}\omega_1 t + a.\mathrm{Sin}\omega_2 t + (b/2)(1-\mathrm{Cos}2\omega_1 t) + (b/2)(1-\mathrm{Cos}2\omega_2 t) + \mathbf{b.Cos(\omega_1 - \omega_2)t} - b.\mathrm{Cos}(\omega_1+\omega_2)t \ \ldots .$$

Note that higher frequencies, $2\omega_1$, $2\omega_2$, and $(\omega_1 + \omega_2)$ have been created, but also a lower frequency $(\omega_1 - \omega_2)$ which might well lie in the same frequency range in which signals exist, never again to be separated from them. The process is also *called Transient Intermodulation Distortion, see Refs. 18, 24.*

The phenomenon is not predictable or designable. It was to answer the question: *"Has this contaminating phenomenon occurred during a test as determined from post–test diagnostic procedures,"* that Pat Walter was sent to the Laboratory for Measurement Systems Engineering at Arizona State University by his employer, Sandia National Laboratories, Albuquerque under a fully funded doctoral study *grant. Refs. 15, 16, 17 provide the positive answers to that question.*

By performing an **energy spectral density analysis** on the acquired data, it is possible to determine whether such low–frequency creation has occurred during the test and whether the right to filter out the high–frequency signals, can be established. **Filtering data is not a God–given right guaranteed by the Constitution. It is a privilege which *must be earned.***

A beautiful bench-top demonstration for training / education purposes is shown in Refs. 19 and also 2.

Another way to solve the problem is to build an electrical filter into the transducer, after the piezoelectric / piezoresistive elements but before the first "active" electronic amplifier, to prevent amplifier overload, which is where the damage is done. Based on Dr. Walter's dissertation, such transducers are now available commercially from several sources. Refs. 20, 21, 22, 23, 38 for example. Fig. 12 illustrates a typical comparison between traducers with and without internal filters.

In piezoelectric transducers the first filter pole actually uses the capacitance of the piezoelectric element itself. Other poles are incorporated before the first amplifier which could easily be driven non-linear.

FIG. 11: RESPONSE OF A LINEAR SECOND ORDER SYSTEM TO MULTIPLE EXPONENTIAL PULSES.

(System damping ratio = 0.01 of critical. Natural Period = 0.02)

Pulses arrive at t=0, 0.21, 0.30 Pulses arrive at t=0, 0.20, 0.30

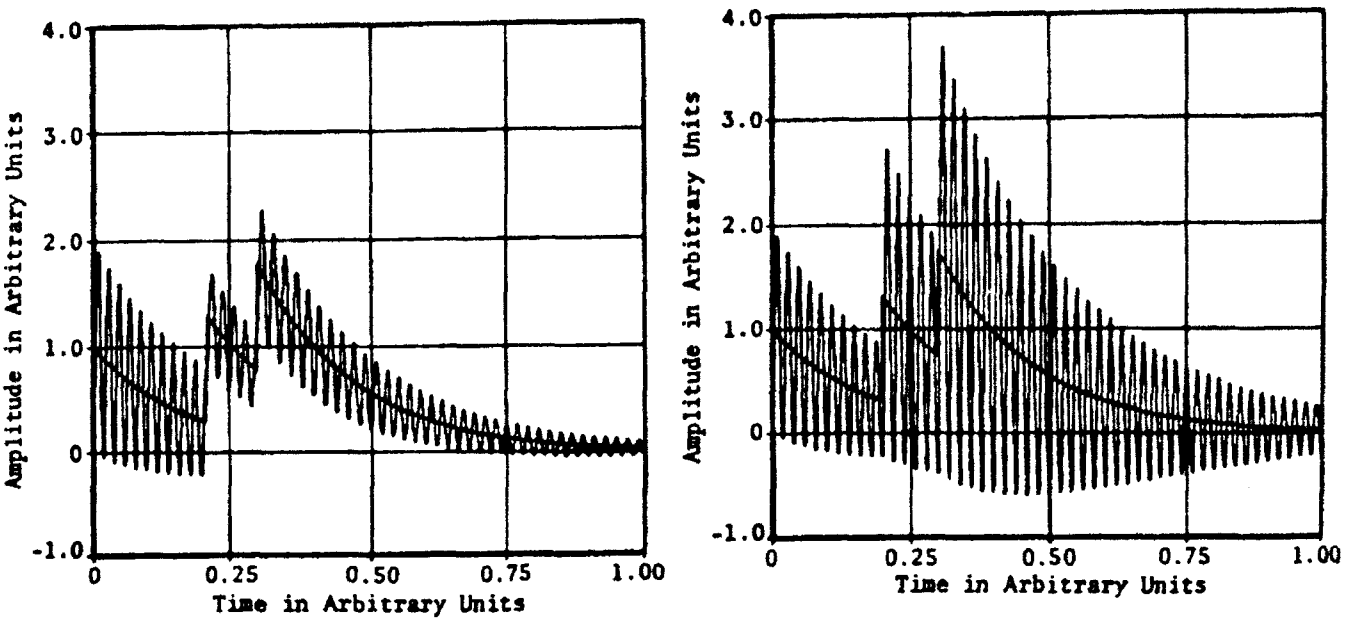

Note that if the distortion-free linear input range is 2.5 Units, that the right-hand response, driven non-linear, might create low frequencies not present in the signal.

FIG. 12: PCB ACCELEROMETER FREQUENCY RESPONSES WITH AND WITHOUT INTERNAL FILTER

(From Ref. 23)

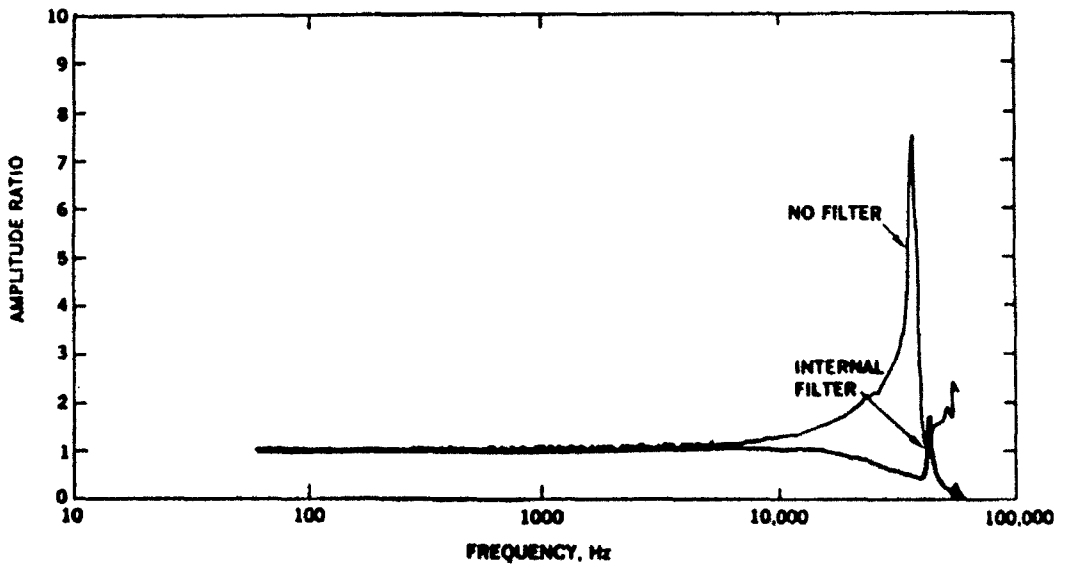

ACCELEROMETERS WITH AND WITHOUT AN INTERNAL FILTER USING A LINEAR AMPLITUDE RATIO VERTICAL SCALE (PCB 308M23 AND PCB 305A)

THE FREQUENCY RESPONSE CURVE FOR PHASE

Phase-Based Distortion due to Nonlinearity:

In measurement systems for steady-state dynamic measurands, the effect of phase shift on wave shape is well known. Fig. 13 illustrates *different wave shapes* for which the *frequency content* is the same. Only the phase angle between the two frequency components is varied. Since the human ear is insensitive to that kind of phase shift, all the wave shapes illustrated, will sound the same, provided the 180° phase shift condition is adjusted to be within the audio system's linear (distortion-free) range.

Ref. 25 presents a persuasive case study in which several frequency response curves for phase shift are used to process the same transient signal. Wave shape reproduction is obtained only for the *linear phase shift* characteristics, as illustrated in Fig. 14.

Some wave shapes which are completely different, differ **only** in their phase shift curves. Fig. 15 shows a Terminal Peak Sawtooth Pulse and an Initial Peak Sawtooth Pulse. Fig. 16 illustrates that the **Magnitude** of the Fourier Transform is the same for both wave shapes but that the **Phase Shift only** is responsible for their different appearance. (From Ref. 25.)

For frequency-content reproduction only, the linear phase shift law enunciated below, need not be obeyed.

Linear Phase Shift Requirement

The requirement for linear phase shift characteristics for wave shape reproduction is presented in Ref. 1 and reproduced below. Wave shape reproduction can only result if all frequencies in the wave shape are delayed the same amount in time as they pass through the measurement system. If **t_o = constant then phase shift must be linearly proportional to frequency.** Actually the time delay is the slope of the phase shift curve. Thus **Time Delay vs. Frequency Curves** are really more helpful than Phase Shift vs. Frequency Curves. Some manufacturers provide those. See Fig 17 showing characteristics of filters from *Frequency Devices* from Refs. 26 & 36. *Precision Filters* shows filter characteristics in a similar manner. Refs. 26 & 37.

Linear phase shift or constant time delay is also required for coincidence measurements and sample-and-hold operations.

PHASE SHIFT - TIME DELAY - RETARDATION: RELATIONSHIPS

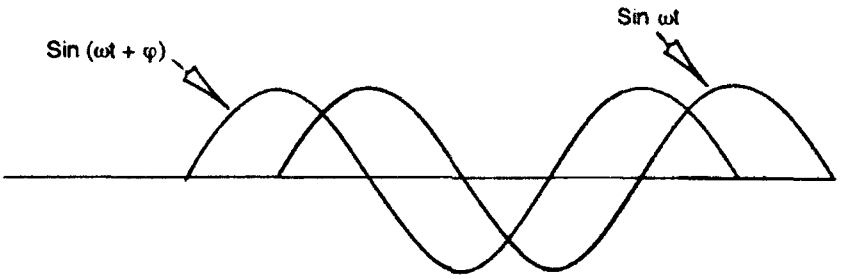

Time Delay	$-t_o$	← Period = T →	Time Dimension
Phase Shift	φ	← Cycle = 2π →	Radians - Angle
Retardation	$-\delta$	← Wave Length = λ →	Distance Dimension

Relationships by Direct Proportion from the Figure

$\varphi/-t_o = 2\pi/T = \omega$ **$\varphi = -t_o\omega$** **For t_o = constant, linear phase shift law results**

$-\delta/-t_o = \lambda/T = c$ $\delta = t_o.c$ ω = frequency in radians/second

$\varphi/-\delta = 2\pi/\lambda = \omega/c$ $\varphi = -\omega.\delta/c$ c = wave propagation speed

Applications Note:

The **shunt calibration** or **step-voltage injection** record, time-expanded, gives the system **rise time** characteristics for the entire measurement system except the input transducer and its lead wires. Those can be factored in using the relationships given in this paper to obtain the value for $t_{r\text{-}s}$.

One problem which may arise, is that many input transducers are not monotonic in frequency response, in fact, they may be highly resonant. The relationships established in this paper will not apply to those cases. If the pre-filtered transducers are used, then the problem becomes more tractable.

When time-compressed, the step-response record will show the system's **undershoot** characteristics forward of the injection point. So long as the input transducer is DC-coupled, that will also be the total system's response.

When an AC-coupled input transducer is used the problem is more difficult. Beyond second order systems for which a design chart is shown in Fig. 7, the author is not aware of general solutions. It is also not in the measurement engineer's favor to work with measurement systems with low-frequency roll-offs exceeding 2, for transient measurements.

If that does become necessary, then new criteria need to be developed, and the author will gratefully include those in up-dated versions of this paper.

A piezoelectric transducer with an AC-coupled amplifier feeding into an AC-coupled oscilloscope is already a third-order system for which a general solution is not yet available to the author's knowledge.

EFFECT OF PHASE SHIFT ON WAVE SHAPE

$$\sin \omega t + \tfrac{1}{3} \sin(3\omega t + \phi)$$

ABSCISSA ARE FRACTIONS OF A PERIOD

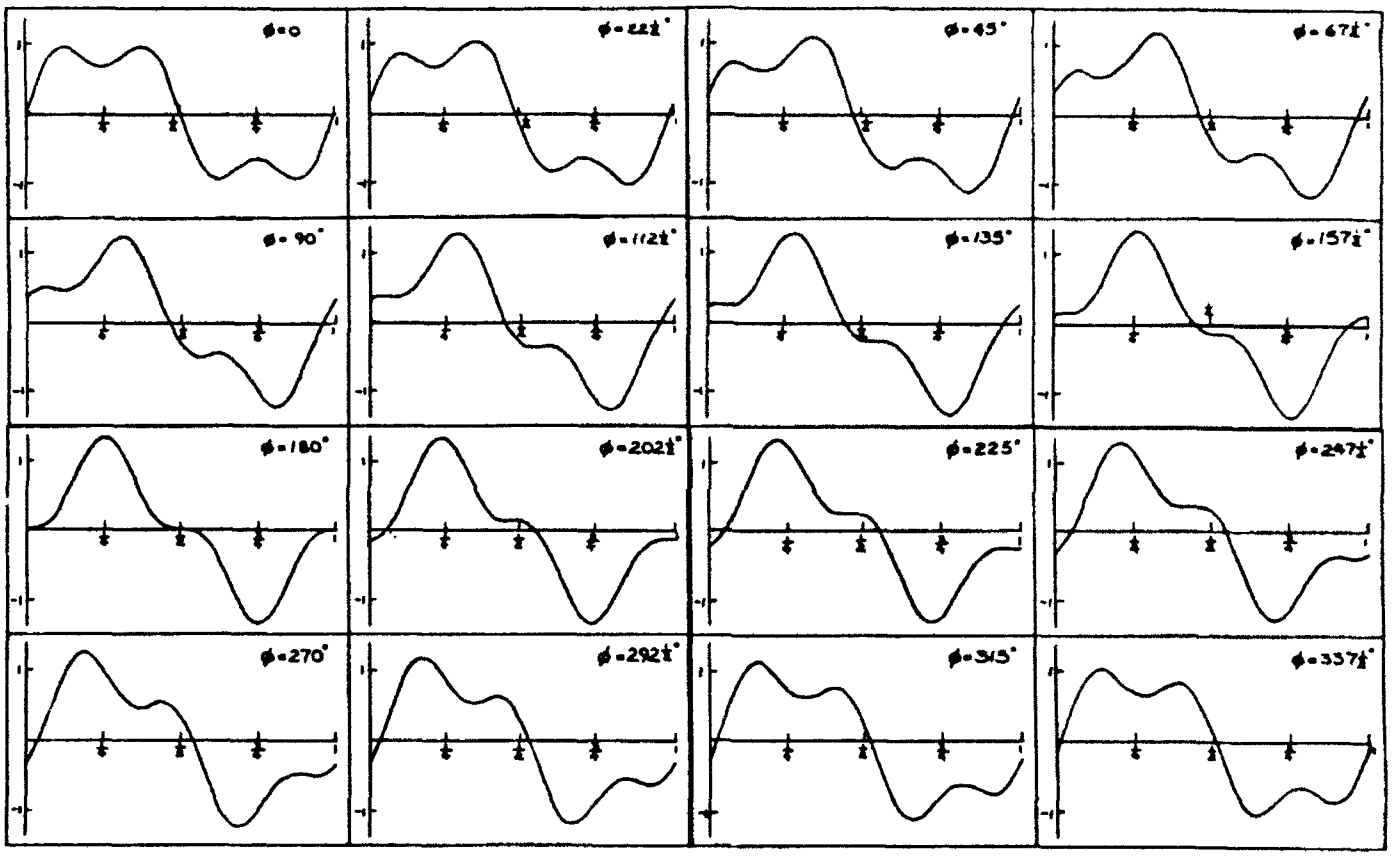

FIG. 13: EFFECT OF PHASE SHIFT ON WAVE SHAPE

(From Ref. 30)

FIG. 14: EFFECT OF FREQUENCY RESPONSE CURVE FOR PHASE ON WAVE SHAPE REPRODUCTION OF A TRANSIENT

Frequency-Response Curves for Phase used in this study (Ref. 25)

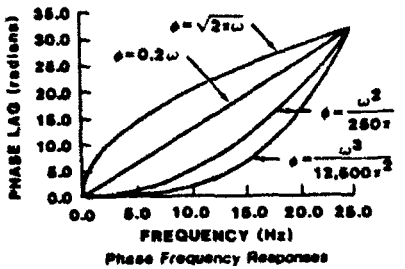

Phase Frequency Responses

Wave Shapes

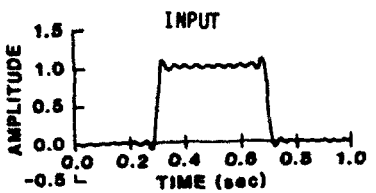

Fig.14a: Amplitude

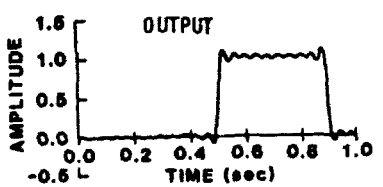

Fig.14b: Linear Phase Shift

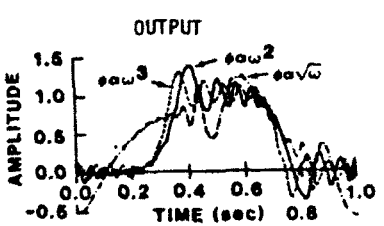

Fig.14c: Nonlinear Phase Shifts

FIGS 15 & 16: TWO WAVE SHAPES OF IDENTICAL MAGNITUDE SPECTRUM BUT DIFFERENT PHASE SPECTRA (From Ref. 25)

FIG. 15: THE WAVE SHAPES

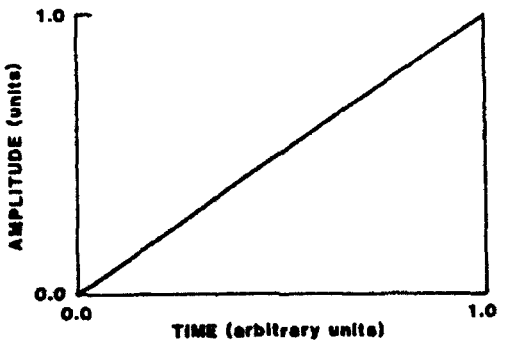

Fig.15a: Terminal Peak Sawtooth Pulse

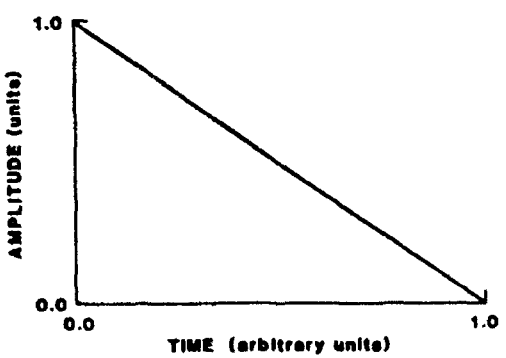

Fig.15b: Initial Peak Sawtooth Pulse

Fig.15: Sawtooth Pulses

FIG. 16: THE MAGNITUDE AND PHASE SPECTRA

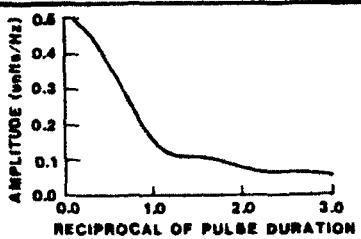

Fig.16a: Magnitude of Fourier Transform of Both Terminal and Initial Peak Sawtooth Pulses

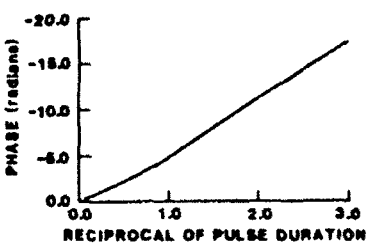

Fig.16b: Phase of Fourier Transform of Terminal Peak Sawtooth Pulse

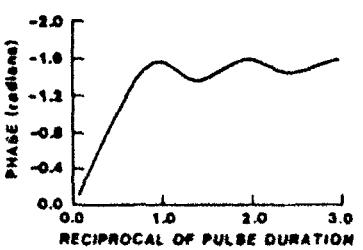

Fig.16c: Phase of Fourier Transform of Initial Peak Sawtooth Pulse

Fig.16: Fourier Spectra of Sawtooth Pulses of Figure 6

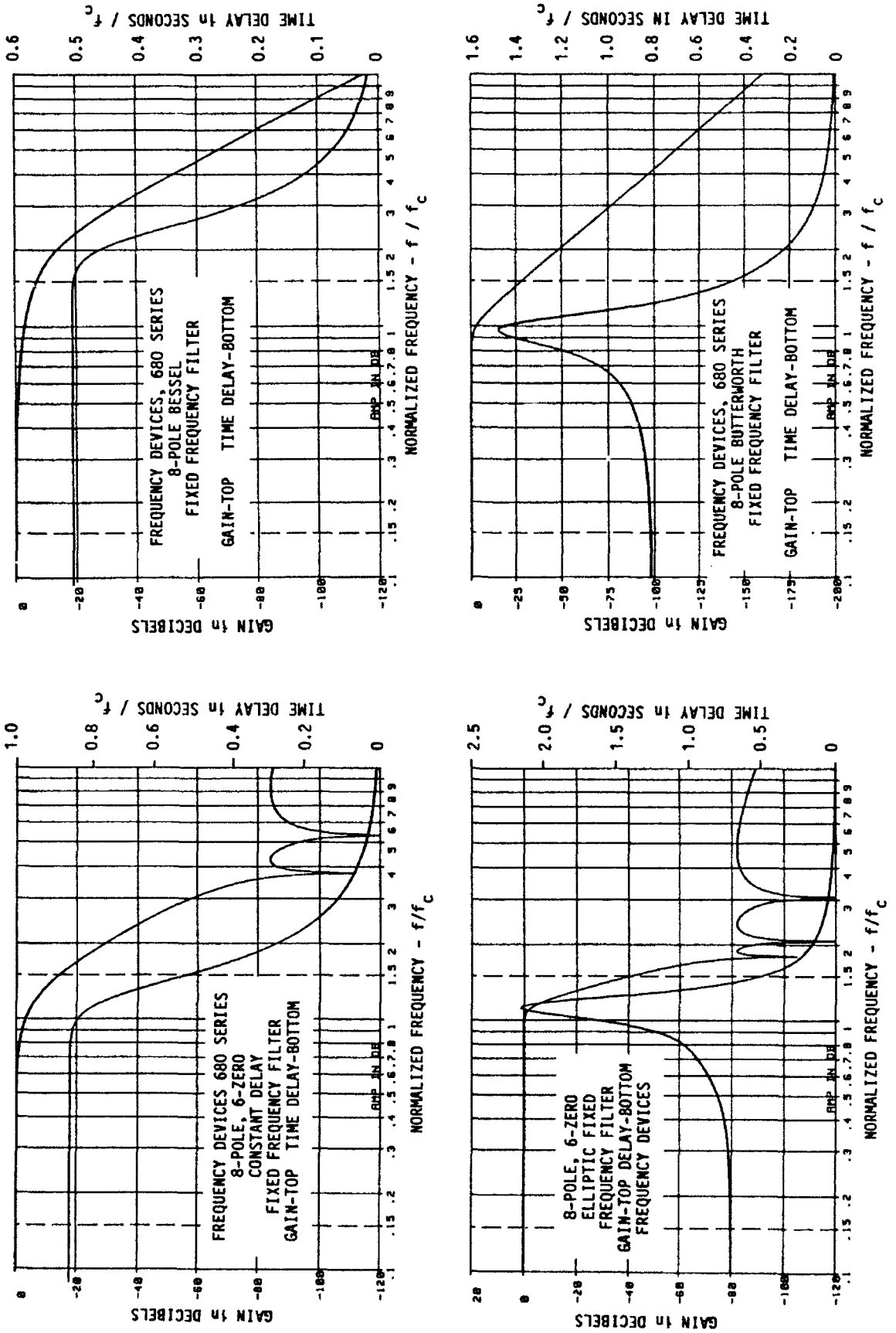

FIGURE 17: TYPICAL FILTER CHARACTERISTICS FOR FREQUENCY RESPONSE FOR MAGNITUDE AND FOR DELAY TIME

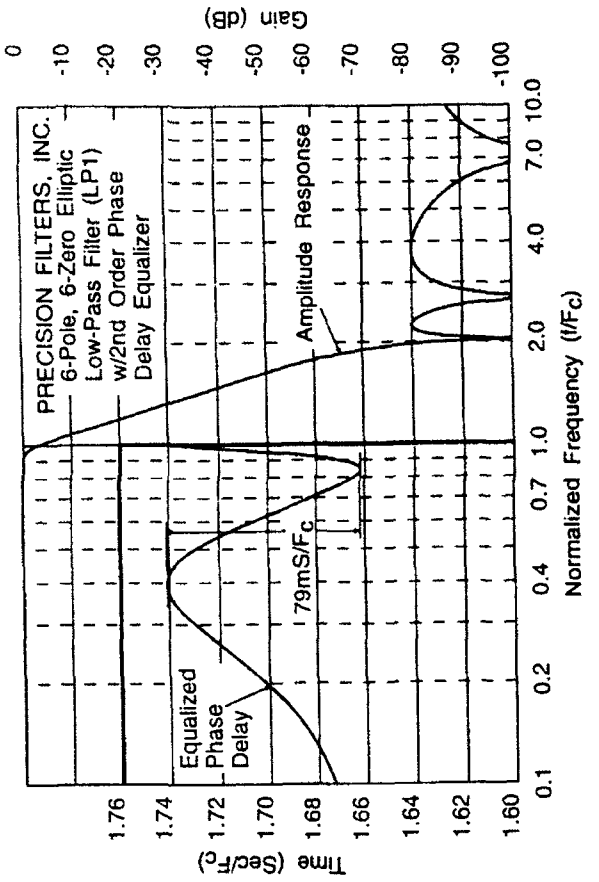

Group Delay, Time Delay and Phase Delay

Douglas Firth, Senior Applications and Project Engineer at *Precision Filters* (Ref. 37) distinguishes between:

- *Group Delay* (called *Time Delay* in this article) which he defines as the slope of the Phase Shift vs. Frequency Curve, and
- *Phase Delay* which is determined for individual frequencies and is used for correction procedures. It is defined as the phase shift expressed as a fraction of a cycle, divided by the frequency. Thus if there is a 90-degree phase shift at 1 kHz, the Phase Delay at that frequency is 90/360 divided by 1000 or 250 microseconds.

The performance curves for three *Precision Filters* models are shown in Fig. 17-A illustrating both the *Phase Delay* and *Group Delay* characteristics along with the *Amplitude Response* curves.

It should again be noted that *Wave Shape Reproduction* requires a flat "Delay" curve and that phase-induced wave shape distortion will occur in the non-flat region.

When Non-Linear Phase Shift Is Permissible

When the object of the test is reproduction of **only** frequencies or frequency-patterns, such as for modal analysis, then non-linear-phase-shift filters with very steep magnitude vs. frequency roll-offs are acceptable. Wave shape reproduction will then neither occur nor be a criterion.

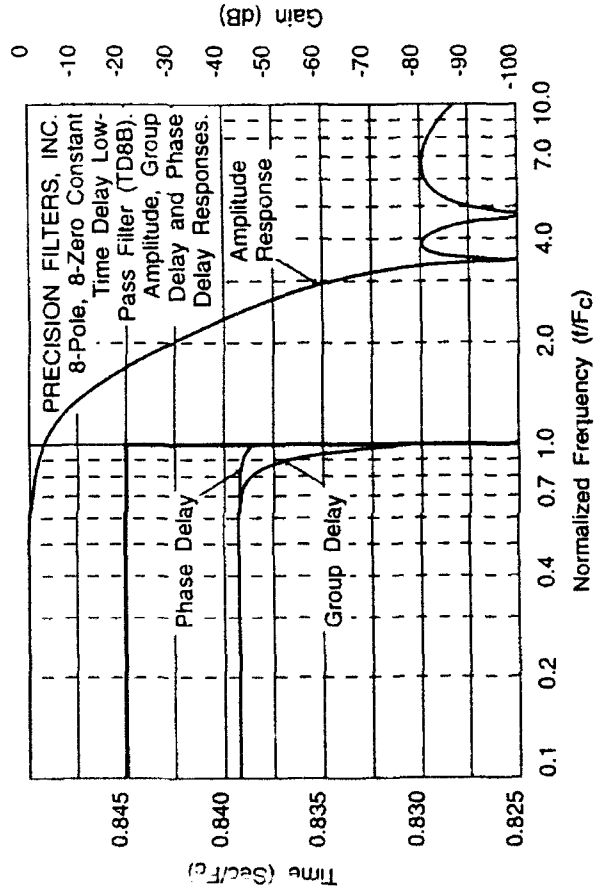

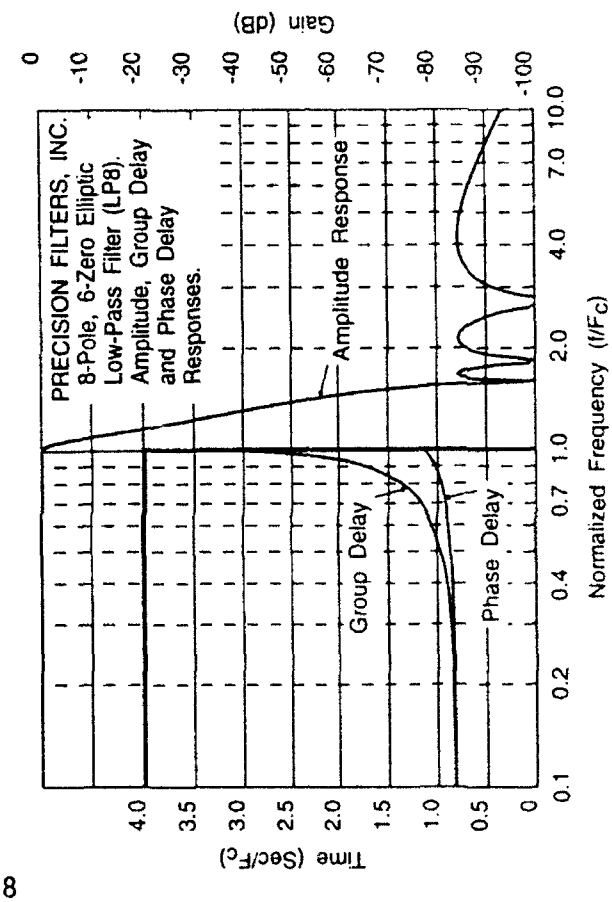

NOISE DOCUMENTATION
DUPLICATE GAGES

Shock-Separation Test 25 Feb 1990

Supply voltage = 5 V_{DC}

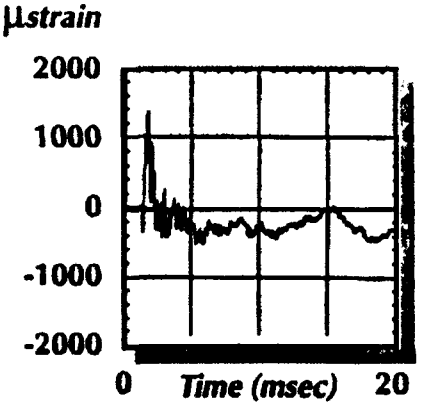

Supply voltage = 0

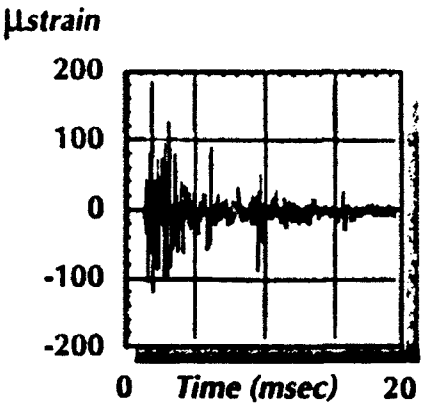

FIG. 18: TWO CASE STUDIES OF IMPACT-INDUCED VOLTAGES IN STRAIN GAGES
DETAILED DESCRIPTIONS OF THESE TESTS AND OTHERS ARE IN REF. 27

NOISE DOCUMENTATION
DUPLICATE GAGES

Scale Model in Blast Tube 22 Jan 1987

Supply voltage = 0

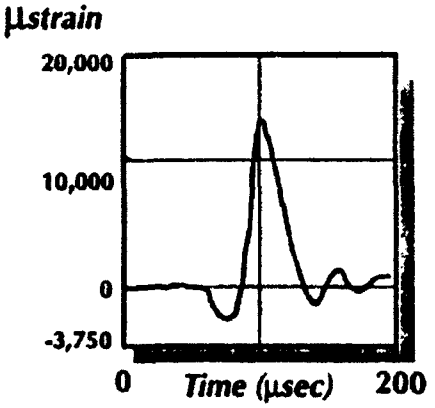

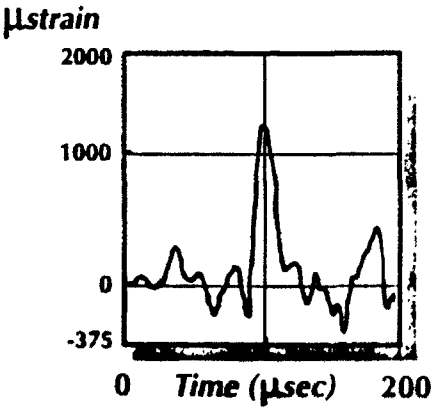

CHECK CHANNELS

Because all components (transducers) in a measurement system respond in all ways in which they can to all factors in the environment, certain diagnostic checking procedures must be built into all measurement systems. For the measurement of high speed transients, some of these diagnostic checks are absolutely crucial to data integrity.

Ref. 1 presents a detailed discussion of these diagnostic checks. They fall into three categories:

- **CHANNELS UNINTERROGATED (UNPOWERED)**

  Switched Check Channels take time.
  Parallel Check Channels take channel capacity.
  Their output represents 2 important noise levels (Ref. 1):
  All *self-generating (voltage) responses.*

  Transducers with a Desired Non-Self-Generating (Impedance-Based) Response.

  All transducers such as piezoresistive or strain-gage-based transducers, especially under high-speed transient conditions, will emit a transient voltage caused by the transient strain and by other mechanisms. These voltages are therefore correlated to the signal (strain, force, pressure, etc.), occupy the same frequency range as the signal and the same time scale. They **cannot be detected or eliminated** with frequency-selective filtering, time-domain, or statistical techniques, the traditional "tools of the trade".

  In addition, voltages may be generated in transducers by other mechanisms: thermoelectric, triboelectric, photovoltaic, magnetically induced, electrically induced, etc.

  The only two methods to identify their presence are:

- **To remove the Interrogating Input** (Bridge Power or Current for a resistive transducer) during the test. In high-speed transient tests either two tests must be conducted: one with and one without bridge power, or a second channel (check channel) must be mounted near the measuring channel and not powered. The rest of the signal conditioning for both channels must be identical.

  The number of manufacturers of signal conditioning with an *"Excitation Off"* control is just over a dozen. See the Appendix for a list of those with which the author is familiar. The first instrument with this feature, to the author's knowledge, was the Ellis BAM-1, Bridge Amplifier & Meter, of about 1953 which enjoyed a production run of almost 40 years, lastly as the Vishay – Ellis BAM-1 of the Measurements Group, Inc., see Appendix. The author still treasures his unit.

- **To reverse polarity** at the bridge (transducer) input and output simultaneously. If the output changes, then half of that change is due to voltages generated by the application of the measurand. This diagnostic procedure requires two tests to be run: one with each Interrogating Input (excitation) polarity.

  Since the effect of these Self-Generated voltages is usually of the order of 10% of total output but can be as high as 80%, such checks are mandatory for all high-speed transient tests. See Ref. 27 for case studies.

  Two recent examples are shown in Fig. 18, from McDonnell–Douglas Corp., and Lawrence Livermore National Lab. See also Photo 10 in Figure 9 which shows the strain-induced self-generating voltages in the illustrated impact experiment, to the same scale as the signals.

- **CHANNELS NOT EXPOSED TO THE MEASURAND**

  Their output represents 2 different important noise levels (Ref. 1): The total measurement system responses to the Undesired Environmental Stimuli.

  A channel not exposed to the stimulus is therefore helpful. Its signal conditioning must be identical to the one for the measuring channel. This check channel shows different environment–response effects than an un–powered channel.

  A *pressure transducer mounted in a blind hole which is* vented to atmosphere, for example, permits evaluation of the effect of ambient accelerations, temperatures, etc., on the measurement. It can also be calibrated by application of pressure through the vent, during a test (Refs. 1, 35).

  The *dummy strain gage* consisting of a strain gage of the same Lot Number mounted on an unstrained piece of the same material as the measuring gage, installed at the same time by the same person under identical conditions, and maintained in the same environment as the measuring gage, is the typical example of this compensation or diagnostic method, used since the commercialization of the strain gage in 1938.

  If the Interrogating Input or Bridge Supply is also disconnected, the desired responses as stimulated by the undesired environments are isolated and documented by this method. This is an important noise-documentation procedure.

- **CHANNELS NOT RESPONSIVE TO THE MEASURAND**

  Depending on design, output is diagnostic of specific environment-response interactions.

  Transducers with a Desired Non-Self-Generating (Impedance-Based) Response.

  Piezoresistive single crystals such as p-type Silicon, have a maximum Resistance-Strain Sensitivity (Gage Factor) when cut along the (1,1,1) crystallographic axis and a minimum (almost negligible) Gage Factor when cut along the 1,0,0) axis. Check channel transducers made of (1,0,0) cut crystals are commercially available (Refs. 32). Some models simply contain unstrained gages (Ref. 31). They have the same resistance vs. nuclear radiation characteristics and often the same resistance vs. temperature characteristics as the "normal" channels and serve as checks for those effects.

  Endevco's Model 7270A-Z is an acceleration-insensitive "accelerometer" built on yet a different principle, checking for still different environment-response effects.

  Transducers with Desired Self-Generating (Voltage-Based) Response:

  Piezoelectrically-Based Transducers

  Piezoelectric transducers are commercially available in three major families for measurands such as acceleration, shock, "vibration", force, pressure, etc.

- **Naturally Piezoelectric Single Crystals** such as quartz, which, when cut along a specific crystallographic axis, exhibit a high (often maximum) piezoelectric response: electrical charge produced by mechanical deformation.

  It is possible to cut such crystals along axes of minimum piezoelectric response but the author is not aware of a commercially exploited application for check channels. Such Z-cut Quartz would not show any thermal effects, however.

  Some manufacturers who use quartz do, however, make special items on request (See Ref. 20 for one example)

- **Polarized Ferroelectric Ceramics**, man-made in powdered form and fired into the desired geometry in a mold. A high electric field is then applied to the material which is

maintained at a temperature above *critical temperature*.

The electric field aligns the randomly oriented domains in the ceramic which becomes polarized or poled.

When the temperature is lowered back to room temperature, the material remains polarized (or poled) when the electric field is removed. The *critical temperature* can be defined as that temperature above which the phenomenon described above, occurs.

A thusly polarized ferroelectric ceramic becomes piezoelectric. A piece of the same material and identical geometry which has not been polarized, will not act in a piezoelectric manner. But it will have responses identical to its polarized twin, to many, but not all, environmental factors. The polarization field is, to some extent, the analog of the bridge supply voltage for resistive transducers, except that it can not yet be turned off and on for a single transducer during a test.

Check channel accelerometers made from unpolarized materials but otherwise identical to the polarized models were first proposed and used by Pierre Fusilier, then Head of the Transducer Group at Lawrence Radiation Laboratory in the early 1960s. A recent (1992) use of that type of check channel is given in Ref. 33. Various National Laboratories such as Lawrence Livermore, Sandia and Los Alamos as well as Boeing have used such check channels over the last 3 decades. So far as the author is aware, they are made by only one manufacturer on demand (Ref 34) but see Bill Shay's comments in Ref. 33.

- **Polarized Flexible Polymers.** The commercial exploitation of these materials is not yet sufficient to have resulted in the use of any unpolarized check channels to the author's knowledge.

Thermoelectrially Based Transducers

A thermocouple design which can be made non-responsive to temperature is described in Ref. 1. The principle has been extensively and successfully used by Dr. Ray P. Reed of Sandia National Laboratories as a diagnostic technique in thermocouple circuits (Ref. 45 as just one example).

DETECTION OF TRANSDUCER DAMAGE THROUGH OVERLOAD

Transient excitation of transducers such as load cells, pressure transducers, accelerometers and strain gages through application of pyro-shock, explosions or impact can easily result in transducer damage through overload. As for any mechanical structure, direct and incontrovertible evidences of such overload are:

- Zero Shifts
- Modal Parameter Changes
- Transverse / Cross Sensitivity Changes
- Common Mode Rejection Ration Changes

Such changes occur either due to yielding / permanent distortion of parts of the structure or due to shifts in joints such as screws, bolts, spot welds, rivets, adhesive layers, etc.

Among evidences of overload-induced-damage are changes in:

- Calibration Factor, Transfer Ratio, Sensitivity
- Linearity
- Stability (drifts of readings with time)
- Self-Temperature Compensation (Often the most serious effect of almost unbelievable magnitude)
- Creep and Hysteresis

Among the very few detailed studies of such effects for strain-gage-based transducers is Ref. 39 supplemented by Ref. 40. After a 500% overload of a load cell, the zero shift was 100% of Full Scale and the temperature effect on zero had gone from a few ppm/°F to 280 ppm/°F! The effect was linear for that load cell. The load cell was still mechanically and electrically continuous. Such overload-induced zero-shifts can actually be exploited to estimate overloads experienced by transducers (Ref. 41). The effects identified above are the reasons why transducers, in general, are made with as few internal joints as possible. Flexures are sometimes machined with almost incredible ingenuity to avoid any and all joints. Many piezoelectric accelerometers, however, have layered (sandwich) constructions including screw joints. Units specifically designed for the kind of tests described in this paper avoid these constructions (Ref. 44).

Zero Shifts: The zero-shift criterion is applicable only to DC-responding transducers although piezoelectric transducers also exhibit this result on a short-term basis (Ref. 44).

For resistance-based transducers such as strain-gage-based ones, there are now two requirements for detection of such overloads.

- The initial zero (output for zero input) for every transducer must be determined on its receipt and marked on the specification sheet which accompanies the transducer. The manufacturer usually provides only the maximum amount of unbalance and not the specific value for a specific serial number of transducer.
- The signal conditioning must permit the measurement of this initial unbalance. *If the signal conditioning is equipped with an auto-zero feature, there must be a defeat mechanism for that feature.* Ref. 42 cites the case where the absence of such a defeat feature hid a 75% of full scale overload-induced zero-shifts for a long time until a check was made using a different signal conditioning. Ref. 43 cites the McDonnell-Douglas, Huntington Beach, CA criteria for discarding a transducer with more than 1% of full scale zero-shift. These are just two references out of many.

If the Balance Control has no scale so that a return to an initial condition is not possible, such marks must be added.

This Appendix does not identify which of the signal conditioning units listed, provide this auto-balance defeat feature. Prospective users are encouraged to determine this condition before use.

Modal Parameter Changes: The Resonant Frequency and/or Damping Ratio / Bandwidth, and/or Dynamic Magnifier – "Q" - T_{max} must be determined on the as-received transducers and marked on the specification sheet which accompanies it. Manufacturers do not, in general, provide these data for specific serial numbers. Only ranges for model numbers are given.

For piezoelectric transducers, but also for full-scale structures such as off-shore oil wells and bridges, these properties are very sensitive damage criteria.

Transverse Sensitivity Changes: Because of the possible movement of the internal parts due to shock excitation, the symmetry with which the transducer was originally constructed may have been destroyed, seriously affecting its transverse or cross sensitivity.

Ref. 46 cites a test where 160 accelerometers were used on a spacecraft modal survey. The 120 accelerometers owned by the company performing the test had been checked for transverse sensitivity coefficient and any units over 5% had been rejected. The 40 rented units furnished by the spacecraft contractor had not been so checked. 33 of the 40

units showed a transverse sensitivity coefficient of between 5% and 30% and had to be replaced. Unfortunately this was only checked after the test had yielded questionable results.

The test conductor has since developed an automatic data validation program as part of the data acquisition system, which identifies spurious accelerometer data created by transverse sensitivity responses (Ref. 26).

Common Mode Rejection Ratio: The ability of a differentially coupled transducer to reject common mode, such as the line pressure in a differential pressure transducer, is also a sensitive damage criterion. Almost no differential pressure transducer manufacturer in the world quotes the common mode rejection ratio and its linearity limits and frequency response limits. Testing differential pressure transducers for common mode rejection ratio is expensive and time consuming. Thus this method of determining transducer damage is not very useful.

A good but rough criterion of overload damage, easily verified, is the lowest line pressure (or common-mode-Q) which first produces a noticeable zero shift at the differentially coupled output. This must also be determined on the transducer in its as-received condition since it is never specified for particular serial numbers and differs greatly among them.

However, a transducer for which damage has been established by one of the three other techniques should never be used for differential measurements. There are enough problems in that field (Refs. 1 and 47) that the ones created by overloaded transducers do not need to be added.

TOTAL QUALITY MEASUREMENTS – TQMs

TQMs ARE VALIDATED FORAT LEAST:
(see also Ref. 48)

Rise Time & Undershoot
Frequency loss due to due Anti-Aliasing
Frequency loss due to Pre-Filtering
Peak Reproduction (*)
Frequency Content Reproduction
Wave Shape Reproduction
First Cycle Stability (*)
Undesired Voltage / Impedance Responses due to the Measurand
Undesired Voltage / Impedance Responses due to Undesired Environments
Desired Responses due to Undesired Environments
Boundary Condition *Golden Calf* Effects (*)
Common Mode & Cross Sensitivity Effects
Overload Damage Effects
Sweep Speed / Frequency Velocity Effects
(for Steady State Tests, not discussed here, but see Ref 48)
Impulse-Excited-Ringing-Created Overload
(for Transient Tests, the topic of this paper)

(*) Not specifically discussed in this paper but see Ref. 1.

CONCLUSIONS:

Tests involving pyro–shock conditions, impact, explosions and other high speed transients must be planned, executed and validated according to strict rules of the discipline: *The Engineering of Measurement Systems.*

Data that have been acquired without incorporating these validation procedures are suspect and cannot be assumed to represent the process which was observed. They do not represent **Total Quality Measurements**.

It is often impossible to correct contaminated data by any software process yet established. Unless these validation procedures are built into the measurement system design, the data acquired with such a system cannot be checked and any conclusions drawn from the test are at the risk of the experimenter.

No papers dealing with these topics should be accepted for presentation or publication unless the author clearly identifies the diagnostic validation procedures and system characteristics which were used. All Uncertainty Analyses and Error Analysis must be **preceded** by these checks.

The material presented in this paper and in Ref 1 was taught in the Junior course in Measurement Systems Engineering, Fall 1959 – Spring 1977, Arizona State University as part of a program leading to BS, MS and PhD degrees in Measurement Systems Engineering.

The fact that a recent International Congress programmed 13 papers on these topics, which showed no evidence of data validation procedures for tests such as mentioned here, is an almost inconceivable condition near the end of the 20th Century.

The question posed at the beginning of this paper must always be answered:

Could these data have been produced by that measurement system, without distortion, without "noise" levels and without affecting the process being observed, all within whatever limits of validity have been specified!

APPENDIX

From the foregoing discussion, the following requirements can be placed on signal conditioning for resistance-based transducers:

THREE (Among Many)
SIGNAL CONDITIONING REQUIREMENTS
FOR RESISTANCE–BASED TRANSDUCERS

- *Interrogating Input Disconnect*: Bridge Power Defeat.
  (For very low-frequency tests, polarity reversal may replace the disconnect feature)
  To check for Self-Generating Voltage Responses
- Step–Resistance Change: Shunt Calibration
  To check Rise Time & Undershoot Characteristics
- Balancing Circuit Disconnect: Auto-Zero Defeat
  (Balancing circuit reference position may be acceptable)
  To check for Transducer Damage

Manufacturers of Signal Conditioning with Excitation OFF Provision and Step Calibration

The number of manufacturers of signal conditioning for impedance–based transducers in which the *Bridge Supply, Excitation, Interrogating Input* can be switched to *Zero* or *Off* is very limited. To the author's knowledge, which is not exhaustive, the following manufacturers provide that possibility on some of their models, either in a manual or computer programmable manner. Contact names are given where the author has them. Anyone with additional information on other manufacturers is asked to be so kind as to share that with the author: Phone & FAX: 602-945-4603.

Amacron
Jack J'maev, President
901 South Idaho, # 4
La Jabra, CA 90631
Phone: 310-690-8505

Model 02J14 Bridge Completion and Calibration Eurocard Module; excitation-defeat relay.

Apix
Chris and Pete Tsipouras
23198 Hermitage Circle
Boca Raton, FL 33433
Phone: 407-391-8956 FAX: 407-391-8963

Model 1EX-1A Isolated Milliamp Output Excitation Module

Aydin Vector Division
Farhad Daghigh
Digital Products Sales
P. O. Box 328
Newtown, PA 18940-0328
Phone: 215-968-4271 FAX: 215-968-3214

Model SSC-2008 Super Signal Conditioner; programmable bridge supply OFF
Model PCU-800 Series Signal Conditioner & PCM Encoder; programmable bridge supply OFF

Campbell Scientific, Inc.
Paul D. Campbell, President
815 West 1800 North
Logan, UT 84321-1784
Phone: 801-753-2342 FAX: 801-752-3268

Model 21X Data Logger (not for dynamic applications) Bridge power reversed at each reading. No shunt calibration.

Dynamics Division of Waugh Controls Corp.
Tony Mastroianni, Product Manager
9001 Fullbright Avenue
Chatsworth, CA 91311-6172
Phone: 818-998-8281 FAX: 818-407-1320

Model 8000; programmable bridge supply OFF

Ectron Corp.
Walter Hanford, Vice-President, Marketing
8159 Engineering Rd.
San Diego, CA 92111
Phone: 619-278-0600 FAX: 619-278-0372

Model 765 Programmable Transducer Conditioning Amplifier; programmable bridge supply OFF.
Transducer Conditioning Amplifier Models 563H, 753A, 755; remote or front panel switch for bridge supply OFF

Endevco Corp
Bob Clark
30700 Rancho Viejo Road
San Juan Capistrano, CA 92675
Phone: 714-493-8181 FAX: 714-661-7231

Model 4430, programmable bridge supply OFF

Encore Electronics, Inc.
Marcel Zucchino, President
RD 2, Route 50
Saratoga Springs, NY 12866
Phone: 518-584-5354

Model 610, manual bridge supply OFF

Instrum
Charles Armenia, President
176 West Pomona Avenue
Monrovia, CA 91016
Phone: 818-303-4210 FAX: 818-357-8863

Models 2705, 2706, manual bridge supply OFF optional

Measurements Group, Inc.
Steve Katz, Vice-President of Sales
P. O. Box 27777
Raleigh, NC 27611
Phone: 919-365-3800 FAX: 919-365-3945
Model VE BAM-1, manual bridge supply OFF
Model 2400, programmable bridge supply OFF
Models 3500, 3800; manual switch
Models 2100, 2200, 2300; manual switch

Neff Instrument Corp.
Louis Lang, Marketing Manager
700 South Myrtle
Monrovia, CA 91016
Phone: 800-423-7151 FAX: 818-303-2286

Series 300 Transducer Signal Conditioner Module; optional bridge supply OFF
Model 490 Data Acquisition & Recording System; programmable bridge supply OFF

Optim Electronics, Corp.
Roger Moore, President
Middlebrook Technology Park
1201 Middlebrook Road
Germantown, MD 20874
Phone: 301-428-7200 FAX: 301-353-0129

Model AD 682SH-1 Differential Input Module for all Megadac models

Pacific Instruments, Inc.
John Hueckel, President
215 Mason Circle
Concord, CA 94520
Phone: 510-827-9010 FAX: 510-827-9023

Model 8250 Transducer Conditioning Amplifier
Model 8650/8655 Transducer Conditioning Amplifier
Model 9250/9255 Programmable Transducer Amplifier
Model 9300 Transducer Amplifier, Programmable
Model 9350/9355; programmable
All have Excitation Interrupt, programmable on models so identified.

Precision Filters, Inc
Don Chandler, President
240 Cherry Street
Ithaca, NY 14850
Phone: 607-277-3550 FAX: 607-277-4466

Model 27000 System, Transducer Amp/Filter Module

Wems, Inc. Formerly Teledyne Signal Conditioning
Mr. David Anoushirvany
Chief Engineer, Signal Conditioning
4650 West Rosecrans
Hawthorne, CA 90250
Phone: 310-644-0251 FAX: 310-644-5334

Model 849333 PCU, Pre-Conditioning Unit; manual bridge supply OFF.
Model 858900 Programmable PCU

REFERENCES:

1. Stein, Peter K. **The Unified Approach to the Engineering of Measurement Systems, Part I – Basic Principles**. Monograph, April 1992, 134 pp, soft cover. Stein Engineering Services, Inc., 5602 E. Monte Rosa, Phoenix, AZ 85018. Phone & FAX 602-945-4603. $15 cash with order, $20 with invoice. ISBN # 1-881472-00-0.

2. Stein, Peter K. *Dynamic Measurements on and With Non-Linear Systems: Problems and Approaches*. Presented at: IMEKO IX, 9th International Measurement Conference, May 24-18, 1982, Berlin, Germany. **Proc. First International Modal Analysis Conference – IMAC 1, November 8-10, 1982**, pp. 358-389, Soc. for Experimental Mechanics, Bethel, CT. **Proc. 12th Transducer Workshop, June 7-9, 1983**, pp. 2-35. Range Commanders Council Secretariat, White Sands Missile Range, NM, 88001. Also **Lf/MSE Publ. 76,** from Stein Engineering Services, Inc., 5602 E. Monte Rosa, Phoenix, AZ 85018 with revisions through 1985.

3. Stein Peter K. *Better the Imperfect Truth than Perfectly Accurate Garbage*, **Experimental Techniques**, November 1985, Editorial, p. 3. Also Sheet 24 in Lf/MSE Reprint 67, 1989 edition. Stein Engineering Services, Inc., 5602 E. Monte Rosa, Phoenix, AZ 85018.

4. Ghaussi, M. S. **Principles and Design of Linear Active Circuits**, McGraw–Hill Book Co., 1965. pp. 487-490

5. Valley, George E., Jr. & Henry Wallman. **Vacuum Tube Amplifiers**, McGraw–Hill Book Co., 1948. p. 66.

6. Elmore, William C. & Matthew Sands, **Electronics: Experimental Techniques**, McGraw–Hill Book Co., 1949. pp. 128-141.

7. Sauceda, Robert & Earl E. Schiring, **Introduction to Continuous and Digital Control Systems**, MacMillan, 1968, p. 452.

8. Stein, Peter K. **Measurement Engineering, Vol. I – Basic Principles**, Chapter 5, 4th edition, 1967 through to 6th edition 1970. Stein Engineering Services, In., 5602 E. Monte Rosa, Phoenix, AZ 85018.

9. Anon. **Instruction Manual for Endevco Piezoelectric Accelerometers**, Publ 101, 1979, Endevco. 30700 Rancho Viejo Rd., San Juan Capistrano, CA 92675

10. Gurtin, M. E. The Effect of Accelerometer Low–Frequency Response on Transient Measurements, **Experimental Techniques**, June 1961, pp. 206 ff.

11. Rhodes, J. E. Transducer System Frequency Requirements for Transient Measurements, Endevco, Tech Data Sheet, 9/22/60. See Ref. 9 for source.

12. Anon. **Specification Sheet**, Endevco Model 7255 Accelerometer. Source, see Ref. 9.

13. Anon. **Specification Sheet**, UA 0553 and UA 0559 Mechanical Filter for Accelerometers. Brüel & Kjær Instruments, Inc., 185 Forest St., Marlboroug, MA 01752.

14. Anon. **Specification Sheet**, Accelerometer Mounting Wax, Model 080A24. PCB Piezotronics, Inc., 3425 Walden Avenue, Depew, NY 14043

15. Walter, Patrick L., & H. D. Nelson, *Limitations and Corrections in Measuring Structural Dynamics*, **Experimental Mechanics**, Sept. 1979, pp. 309-16.

16. Walter, Patrick L. *Deconvolution as a Technique to Improve Measurement–System Data Integrity*. **Experimental Mechanics**, August 1981, pp. 309-314.

17. Walter, Patrick L. *Limitations and Corrections in Measuring Dynamic Characteristics of Structural Sys-ems*, **PhD Dissertation**, Arizona State Univ, Tempe, AZ 85287, 1978, **Sandia Document 78-1015**, Oct. 1978, Sandia National Labs, Albuquerque, NM. Also in: Patrick L. Walter, *Bridge Transducers*, Ch. 8 in **Instrumentation and Control, Fundamentals and Applications**, Chester L. Nachtigal, Ed. Wiley & Sons, 1990, pp. 265-308.

18. Thomsen, Carsten & Henning Møller. *Swept Measurements of Harmonics, Difference–Frequency and Intermodulation Distortion*, **Brüel & Kjær Application Notes**, no date. Source, see Ref. 13.

19. Wright, Charles P. *Dynamic Data Invalidity due to Measurement System Non-Linearity*, **Proc. Western Regional Strain Gage Committee, Feb. 12-13, 1985 Meeting, Phoenix, AZ**. From WRSGC, 44 N. Benson Ave., Upland, CA 91786. Also in Ref. 2, 1985 revision.

20. PCB Piezotronics, Inc., 3425 Walden Ave, Depew, NY 14043. Jim Lally CEO. PCB manufactured special transducers for the author such as a spark plug mounted pressure transducer with its input welded shut, to serve as check channel for vibrations. "Customized arrangements become future products!" says Richard Lally. Example: *Model 305M23 Accelerometer* in Fig. 12. "There have been 400+ variations of our Model 308 Accelerometer", he emphasizes.

21. Endevco Corp., 30,700 Rancho Viejo Rd., San Juan Capistrano, CA 92675. Ex. *Models 2255A, 2255B Isotron Accelerometers*. Bob Clark.

22. Vibra•Metrics, Inc., 1014 Sherman Ave, Hamden, CT 06514. Ex. *Model AN115 Accelerometer*, John Judd, Pres

23. Schelby, Frederick. *A Systems Approach to Measuring Short–Duration Acceleration Transients*. **Proc. 12th Transducer Workshop, June 7-9, 1983**. Range Commanders Council Secretariat, White Sands Missile Range, NM 88001.

24. Jung, Walter, M. L. Stephens & C.C. Todd. *An Overview of SID and TIM, Parts I & II*. **Audio Jnl.** June 1979, pp. 59-72; July 1979, pp. 38-47.

25. Walter, Patrick L. *Effect of Measurement System Phase Response on Shock Spectrum Computation*. **Shock & Vibration Bulletin, Bull. 53, Part 1**, May 1983, pp. 133-141.

26. Wright, Charles P. *Knowledge-Based Systems for Test Data Acquisition and Reduction*. **Lf/MSE Reprint 82**, Lecture notes for the Short Course: The Engineering of Measurement Systems. Stein Engineering Services, Inc., 5602 E. Monte Rosa, Phoenix, AZ 85018. (*Frequency Devices*, 25 Locust St., Haverhill, MA 01832) (*Precision Filters*, 240 Cherry St., Ithaca, NY 14850).See also Ref. 48.

27. Stein, Peter K. *Our Engineering Education: The Not–So–Scientific Method*. Presented at The Role of Laboratories in Engineering Education Session, American Society of Mechanical Engineers Winter Annual Meeting, Dec. 3, 1979, New York City. Revised version: **Lf/MSE Newsletter No. 38, Summer 1992,** pp. (ii)-24, Stein Engineering Services, Inc., 5602 E. Monte Rosa, Phoenix, AZ. Also **Lf/MSE Publ. 74**, July 1992, from the same source.

28. Stein, Peter K. *Some Notes on Second Order Systems: Responses of Systems to Steps and Pulses*. **Lf/MSE Publ. 35/36/40**, 1st ed. , 1971; current ed., 1985. Stein Engineering Services, Inc., 5602 E. Monte Rosa, Phoenix, AZ 85018

29. Stein, Peter K. *The Unified Approach to the Engineering of Measurement Systems: Yesterday's Recipe for Tomorrow's Source of Measurement Engineers: Part II – Transient Measurements: A Junior Level Final Examination – Mechanical Impact: Traveling Wave Phenomena – A Problem*

in Data Validation. **Publ. 85**, Mar. 93 same source as Ref. 30.

30. Stein, Peter K. *The Myth of Wave Shape Reproduction*, in **Lf/MSE Publ. 65**, 1st ed. 1968; current ed. 1975. Stein Engineering Services, Inc., 5602 E. Monte Rosa, Phoenix, AZ 85018.

31. *Model 2266 Series Radiation Resistant Piezoresistive Accelerometers. Model 7231C–Z Accelerometers* contain unstrained gages. Endevco, see Ref. 34 for address.

32. Kulite Semiconductor Products, Inc., Ron Moores, Marketing V-P, 1 Willow Tree Rd., Levonia, NJ 07605. (201)-461-0900. Any of their strain gages with "O" replacing the "P" gage designation, per April 11, 1976 memo from John Kicks, then Manager, Sales & Product Engineering.

33. Shay, William, Lawrence Livermore National Laboratory, *Case Studies in Noise Documentation: Case Study #2: A "Dummy" Transducer as Check Channel in a Noisy Environment*, **Lf/MSE Newsletter No. 39,** January 1993, Stein Engineering Services, Inc., 5602 E. Monte Rosa, Phoenix, AZ 85018.

34. Endevco, 30,700 Rancho Viejo Rd., San Juan Capistrano, CA 92676-1789. Bob Clark: "There will be a new listing in our printed price list which will reflect the availability of such devices", Oct. 12, 1992 memo.

35. Stein, Peter K. *The Measurement of High Frequency Fluctuations between Impeller Blades in an Operating Gas Turbine Compressor,* **ASME Paper 60-WA-337**, 1960. Also Chapter 15 in Ref. 8 since its 1st, 1960 Edition. (Reporting work done by the author at AiResearch Manufacturing Company of Arizona, now Allied Signal, Garrett Turbine Engine Division, in 1956.)

36. Frequency Devices, Inc., Dr. Robert E. Steer, Jr., President. 25 Locust Street, Haverhill, MA 01832. In addition to the filters shown, FDI provides the 848 series of programmable modules and the model 9002, 9016 and 9064 instruments that have the same transfer functions available.

37. Precision Filters, Don Chandler, President, 240 Cherry Street, Ithaca, NY 14850.

38. *Models 720 Series & 793L Accelerometers.* Wilcoxon Research, 21 First Field Rd., Rockville, MD 20878. 301-330-8811. Eric Saller, Senior Applications Engineer.

39. Tovey, F. Michael. *Effects of Overload on Load Cell Performance.* **Experimental Techniques**, Vol. 5, No. 3, Sept. 1981, pp. 8-9. The missing figure is published in Ref. 40. Tovey's paper also appears in **Proc. Western Regional Strain Gage Committee, Feb. 1978 Meeting** from WRSGC, 44 N. Benson Ave., Upland, CA 91786.

40. Stein, Peter K. **Lf/MSE Publ. 67, Sheet 23**, Stein Engineering Services, Inc., 5602 E. Monte Rosa, Phoenix, AZ 85018-4646.

41. Stein, Peter K. *Some Little Known Literature and Effects in Strain–Gage–Based Force Transducers,* **Proc. International Conference on Measurement of Force & Mass, Sept. 11-14, 1984, Kobe, Japan**, pp. 303-308, Society of Instrument & Control Engineers (SICE), Japan, 1984.

42. Potvin, Robert. Comment about Northrop Aircraft experience in **Proc. Western Regional Strain Gage Committee Meeting, August 11-12, 1992**. WRSGC, 44 N. Benson Ave., Upland, CA 91786.

43. Shull, Larry, Comment about McDonnell-Douglas procedures in Ref. 42 above.

44. Chu, Anthony & Arthur Gilbert. *Zero Shift of Piezoelectric Accelerometers in Pyroshock Measurement.* **Proc. 56th Shock & Vibration Symposium, Oct. 22-24, 1985**, Shock & Vibration Information Analysis Center (SAVIAC), c/o Booz-Allen & Hamilton Inc., 2711 Jefferson Davis Highway, Suite 600, Arlington, VA 22202-4158. Also from Endevco at the address cited in Ref. 34.

45. Reed, Dr. Ray P. *Validation Diagnostics for Defective Thermocouple Circuits*, **Proc. 6th International Conf on Temperature, Its Measurement & Control in Science & Industry**, 1982, Vol. 5, No. 2, pp. 931-938. American Inst of Physics, NY.

46. Wright, Charles P. **Personal Communication,** April 1981, 2550 Date Circle, Torrance, CA 90505.

47. Stein, Peter K. *The Measurement of Differential Quantities: Problems and Approaches*, preprint of a paper presented at the Annual Meeting, Soc. for Engineering Education, June 1972, **Lf/MSE Publication 43**, 40 p. Stein Engineering Services, Inc., 5602 E. Monte Rosa, Phoenix, AZ 85018, Phone & FAX: 602-945-4603

48. Vellutini, G.A., C. P. Wright. *Knowledge-Based Systems for Test Data Acquisition/Reduction,* **Proc. 11th Aerospace Testing Seminar**, Institute of Environmental Sciences, October 1988.

A Miniature Blast-Gauge Charge Amplifier System

James L. Rieger, PE/PTBW* Robert Weinhardt†

May 3, 1993

Abstract

Transducers whose outputs are characterized as a charge require signal conditioning to convert the charge produced to a voltage or current for use in instrumentation systems. Blast gauges, in particular, require processing which preserves the transient nature of the data and very fast risetimes, which would otherwise be degraded by long cable runs and parasitic capacitances. A *charge amplifier* which amplifies and converts a charge to a low-impedance voltage suitable for driving coaxial lines is described, along with theory of operation. Charge amplifiers of the type described are relatively unaffected by temperature and power supply variations, and occupy less than two square inches of printed circuit board space per channel.

Key words: charge amplifier, blast gauge, transducer

1 The Nature of 'Charge'

Charge is one of the four imponderable units necessary to describe all physical phenomena, as are length, time, and force or mass. The unit of charge is the *coulomb*; the charge on an electron is 1.602×10^{-19} coulombs.

2 Capacitors As Charge Transducers

A capacitor is a storage device, which holds and concentrates charge as electrons collect on one capacitor surface attracted by the opposite charge on the other surface separated by an insulator. Because a capacitor has in its construction an insulator between its input conductors, electrons never cross from one side to the other.

*Mr. Rieger is a Fellow of the Naval Air Warfare Center, Weapons Division, China Lake, CA
†Mr. Weinhardt is with the Naval Air Warfare Center, Weapons Division, China Lake, CA

When a voltage (which represents a 'potential') is placed across a capacitor, the capacitor charges to that external voltage through some inevitable source resistance, as shown in Figure 1.

The equation for the capacitance of a parallel-plate capacitor is

$$C = \frac{A}{\epsilon_r \epsilon_0 d} \qquad d \ll A \tag{1}$$

Where A is the area of either plate (both plates the same size); d the distance between the plates; ϵ_0 the permittivity of free space, or $\frac{1}{36\pi} \times 10^{-9} \approx 8.85 \times 10^{-12}$ farads/meter; and ϵ_r the relative permittivity of the insulation material used, which has a practical range of $1 \rightarrow 15$ or so.

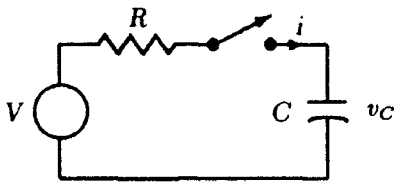

Figure 1: Classic Capacitor Charging Circuit

Voltage developed across a capacitor with no initial charge and with the switch shown closed at $t = 0$ is

$$v_c(t) = V \times (1 - e^{\frac{-t}{RC}}) \tag{2}$$

where V, R, C are fixed voltage, resistance, and capacitance, respectively, and v_c and i_c are functions of time t. Eventually (after a 'long time'), the entire battery voltage is present across capacitor C. At any point, by definition, the charge in the capacitor is given by

$$q = Cv_c \tag{3}$$

and the charge and voltage across the capacitor are always proportional. While the external resistance affects the rate at which the capacitor charges, power loss across any finite resistor for a complete charge of the capacitor is the same.

When the circuit of Figure 1 is modified to add more capacitors in series as shown in Figure 2, the resulting capacitance is decreased, but the same charge is present on each capacitor no matter what each individual capacitor's value is.

Since the voltage across the capacitor string eventually equals the voltage V (that is, $V \propto v_{c_1} + v_{c_2} + v_{c_3}$ and $\lim_{t\to\infty}(v_{c_1} + v_{c_2} + v_{c_3}) = V$), the voltage across each capacitor will be whatever satisfies Eq'n 3. Also, if the series capacitance is lower than that in the circuit of Figure 1 and R remains the same, each capacitor will charge more quickly to its final value than the single capacitor in the circuit in Figure 1, a result that is probably counterintuitive, though a consequence of Eq'n. 2.

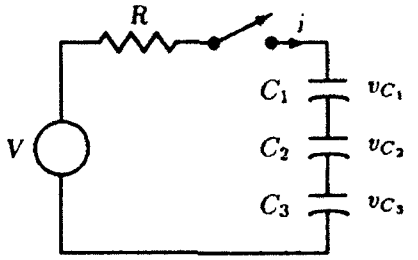

Figure 2: Multiple Capacitor Charging Circuit

The current through the capacitor and the rest of the circuit in Figure 1 is identical, since there is but one current loop, but current is most easily calculated for the resistor since Ohm's Law holds. Then circuit current corresponding to the expression in Eq'n. 2 is

$$i = \frac{v}{r} = \frac{e^{\frac{-t}{RC}}}{R} \tag{4}$$

which is an exponential, decreasing to zero as $t \rightarrow \infty$. The rate at which $i(t)$ decreases is again due to the resistance R. Current and charge in the capacitor are related by the expression

$$q = it \tag{5}$$

so the charge in a capacitor could be measured by integrating $i(t)$ over time t, although the charge rate would be determined by any resistance used in the integrator.

A capacitor can be thought of as a *transducer* in the sense that it changes charge to voltage.

3 Charge Sources

A perfect voltage source can be thought of as a voltage source independent of load, capable of supplying infinite current. A perfect current source is capable of supplying a specified output current into any load no matter how high the voltage need be. Internal resistance of a perfect voltage source is zero; internal conductance (reciprocal of resistance) of a perfect current source is zero as well. Approximations of perfect voltage and current sources, especially over a more limited range of loadings are indeed possible. A perfect *charge* source produces a charge independent of load capacitance at least over some range, and is approximated by a voltage and a large (infinite?) series capacitance. Hence as in Figure 3, the charge produced is independent of the capacitance of the load, which consists of cable and parasitic capacitances and of the observation capacitor across which a voltage is measured.

As R. P. Reed notes in his paper [**Sandia**, p. 42] a piezoelectric transducer *should* be considered as a charge source, not as a voltage or current source. The proper load for a charge source is a capacitor, not a resistor, since the capacitor stores the charge and a resistor dissipates the charge as heat.

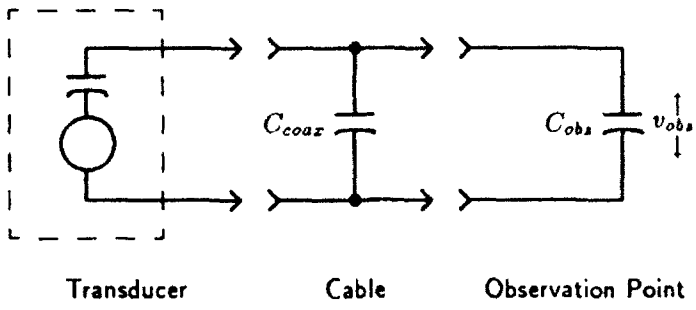

Figure 3: Measurement Equivalent Circuit

By knowing the observation capacitance and any parasitics that can't be ignored, a voltage observed across the observation capacitance can then be measured and the output charge deduced by application of Eq'n. 3. Unfortunately, the act of measuring the voltage across the capacitance inevitably discharges the capacitor. Measurement of the current through the capacitor would involve integration of the current to obtain the charge, which would involve added series resistance, thus inevitably slowing the charging process.

4 An Active Charge Amplifier

Use of the feedback characteristics of a modern operational amplifier can make a near-perfect charge measurement circuit, as shown in Figure 4.

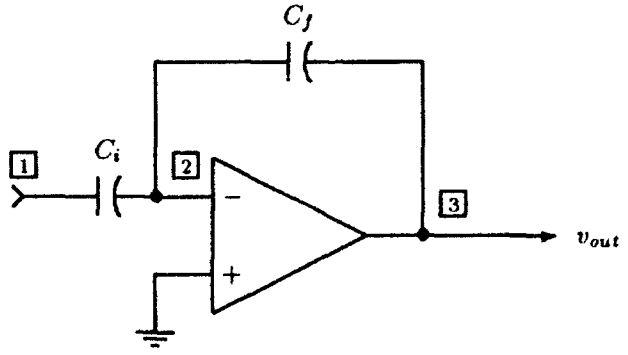

Figure 4: Ideal Charge Amplifier

When a charge enters at point [1], a current flows through capacitor C_i toward point [2]. The output of the amplifier, which was initially zero, is driven negative by the difference in voltage between its positive input, at zero volts, and the negative input into which a positive voltage occurs as a result of the current flow. Impedance of the amplifier inputs is

infinite (or nearly so) and gain of the amplifier is also infinite (or nearly so), so the voltage level at point [3] falls to a point at which C_f charges such that the voltage at point [2] is forced back toward zero. The feedback action continues to maintain point [2] at very near zero volts regardless of any change in charge at point [1]. Since no current flows into the operational amplifier at point [2], the currents through the two capacitors must be the same. The voltages at point [2], which is maintained at zero due to the feedback, thus the voltage across capacitor C_f, which is also v_{out}, is whatever voltage is necessary to produce the current necessary to charge C_f in accordance with Eq'n. 5. Since the currents are equal, the voltages across the two capacitors (which still must satisfy Eq'n. 3) are inversely proportional to the capacitances of C_f and C_i. Gain of the entire system, for a charge q_{in} present at point [1] (and thus across capacitor C_i to ground) is thus given by

$$v_{out} = -\frac{C_i}{C_f} \times q_{in} \tag{6}$$

Assuming that the charge source produces a constant charge into capacitive loads between limits which include C_i (in parallel with parasitic capacitances, if appropriate), the system produces a low-impedance voltage proportional to input charge as desired. Once C_i is selected, C_f is then selected for desired charge gain for the circuit. If C_i is selected to be as small as possible for a given charge source, charge time is minimized and the effect of nonzero source resistance (an 'ideal' charge source has a zero source resistance, but real ones have at least some resistance).

If the circuit is considered to be a voltage amplifier, driven by a perfect voltage source rather than a charge source, the gain of the circuit is equal to the ratio of C_f to C_i due to the ratio of the impedances of the two capacitors, except that at DC the impedances of both capacitors are infinite, so the circuit gain is undefined.

If the circuit is considered in terms of operational amplifier circuitry from analog computation, the circuit is both an integrator and a differentiator of an input voltage, and performs the operation

$$v_{out} = \int_0^t d\tau = t + c_0 \tag{7}$$

where τ is a dummy variable and $c(0)$ is a constant term which is set to zero by the feedback resistor.

5 Real Vs. 'Ideal'

The amplifier circuit in Figure 4 will not work for long with 'real' devices, although it will work well enough for most purposes except for one. Since there is no DC path in the loop for the negative input (the 'summing point') the amplifier's DC output will drift to one of the supply rails and stay that way. Hence the response of this amplifer cannot extend down to DC. A circuit which provides DC stability is shown in Figure 5, which differs only by addition of feedback resistor R_f.

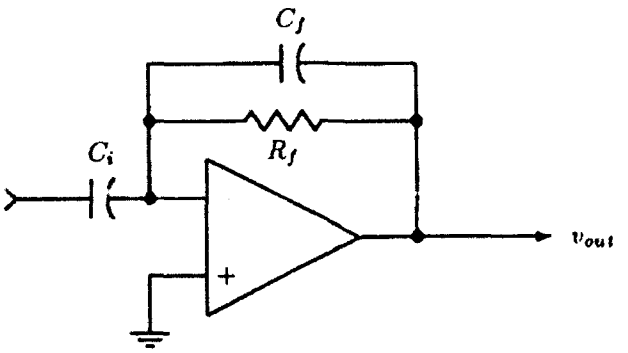

Figure 5: Practical Charge Amplifier Circuit

DC gain of the circuit (interpreted to mean output voltage for a constant charge) is zero, and response falls below gain predicted by Eq'n. 6 when $R_f = \frac{1}{2\pi fC}$. For the circuit we built, using $R_f = 1.5\,\mathrm{M}\Omega$ and $C_f = .01\,\mu f$, the low-frequency 3 dB corner is at 10.6 Hz, which presents no problem with a blast gauge; by a different selection of amplifier, the response could be extended below 0.1 Hz if needed for seismic measurement, etc.

6 Response Time and Slew Rate

Real amplifiers have other limitations as well, and operational amplifiers used for general communications work will not perform well in use as a charge amplifier. Typical internally-compensated amplifiers have frequency responses to around 1 MHz at unity gain; the amplifier used for this application (the Élantec EL 2073) has a unity gain of 400 MHz, and a gain-bandwidth product at any gain of 200 MHz. As a consequence, gain to a 1 MHz signal is several hundred, assuring that the feedback circuit necessary for accuracy is stiff enough to act quickly when the input changes abruptly. A two-volt step on the output when loaded by a 50Ω output cable and series resistor responds at a rate of at least 175 $V/\mu s$, thus rising fast enough for 40 ns pulses to be resolved at full amplitude.

7 Line Drivers

The output of the charge amplifier drives a coaxial cable of whatever length is necessary for the desired system. The coaxial cable acts as a 50Ω load at any frequency of interest (at least several hundred MHz) if terminated in a single 50Ω resistance at the far end, or is infinite in length. For exceptionally long cable runs, tilt equalization may be necessary for frequency flatness, but this is a function of the cable and not the amplifier. A properly terminated cable does *not* appear as a capacitor, only as a resistor. When properly terminated, as any circuit, the output voltage will be exactly one-half the output voltage at the amplifier.

8 Power Supply Considerations

An operational amplifier circuit does not depend on the power supplies which operate it as references, and the absolute voltage on either power supply and the ratio between the voltages should not matter so long as the output is not saturated and pinned to one of the supply rails. In actuality, some power supply feedthrough does affect any amplifier. For the Élantec EL 2073, power supply rejection is typically 80 dB at DC and 40 dB at 30 MHz, so a power supply variation of ±10% at 30 MHz would cause a ±5 mV change in the output voltage, which is about 1% of full scale. Since a power supply variation as extreme as that described here is unlikely (and unacceptable), power supply noise should be essentially unreadable.

9 Calibration

While a charge amplifier converts charge to voltage, the actual physical phenomenon to be measured is not a charge but a pressure, which is measured by stimulation of a transducer to produce charge. Transducers made from polyvinylidene fluoride [PVDF] produce outputs in accordance with the formula

$$q = 0.25 \times p^{.637} \quad \mu C/cm^2 \tag{8}$$

where the multiplier and exponent were determined experimentally and p is in gigapascals [GPa]. A one square centimeter gauge thus produces an output of about 0.7 μC when an excitation pressure of 50 *kbar* or 5 GPa.[1] Unlike crystals which have been used historically, PVDF gauges are flat and can be sandwiched between layers of material and sized to fit space available. Producing a test signal for a transducer and charge amplifier involves either hitting the gauge connected to the amplifier with a calibrated hammer or (in the absence of a gauge) supplying a charge from a large capacitor or a switched low-impedance voltage source. A typical gauge used to demonstrate a breadboard circuit had a 10 mm^2 active area, and thus produced an output of 0.07 μC, which produces an output of

$$v = \frac{q}{C} = \frac{7 \times 10^{-8}}{0.22 \times 10^{-6}} = 318\,mV$$

into the 0.22 μF load presented by C_i of the amplifier in Figure 6. Using a 0.1 μF feedback capacitor, the output voltage pulse is

$$0.318 \times -\frac{.22}{.01} = -7\ V$$

If a 50Ω output resistor and cable load are used, the effective gain would be reduced by half, to 11 $V/\mu C$.

[1] A *bar* is a single standard atmospheric pressure, around 14.3 pounds per square inch absolute [PSIA]. A *pascal* [*Pa*] is the preferred metric unit, with atmospheric pressure equal to 10^5 Pa.

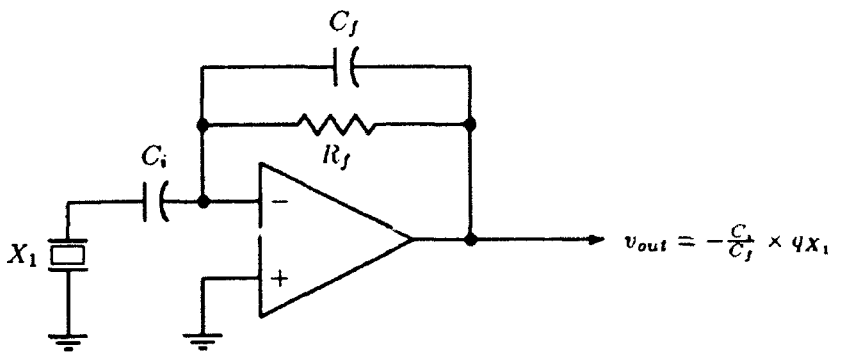

Figure 6: Transducer and Charge Amplifier Test Circuit

Gain of the amplifier for the AC term of the circuit is $-\frac{C_i}{C_f} = -\frac{0.1 \times 10^{-6}}{0.22 \times 10^{-6}} = -22\ V/\mu C$. The negative sign is a consequence of the inversion in the amplifier, and to get a positive output (usually what is desired), the leads of the gauge would be connected so that the charge output from the gauge is negative.

10 What a Charge Amplifier Is Not

A charge amplifier measures an input charge (or more precisely, as shown, the *change* in input charge). A transducer whose reaction to measured stimulus is not an appropriate input signal for a charge amplifier circuit. Consider the case of a classic 'condenser microphone', where one of the plates of a charged capacitor is used as a diaphragm, varying the capacitance of the transducer capacitor in response to the change in position of the diaphragm. If the charging resistance and voltage are high, the charge does not change appreciably since the average capacitance of the transducer does not change, but in accordance with Eq'n. 3, if q stays constant and c varies, the instantaneous voltage across the capacitor varies as well. A signal-conditioning circuit for such a system is shown in Figure 7.

Due to the high resistances and voltages necessary,[2] the capacitor-based transducer circuit does *not* use the same signal conditioning as a charge source, which appears as a very low resistance.

11 Customer Unit

A printed circuit board of approximately $6\frac{1}{2}'' \times 3''$ and containing four such amplifiers and a regulator system to provide $\pm 6\ V_{dc}$ for system operation from higher-voltage remote supplies

[2]Transducers called *electrets* replace the high-impedance high voltage with a 'permanent' charge, but still produce very high-impedance outputs.

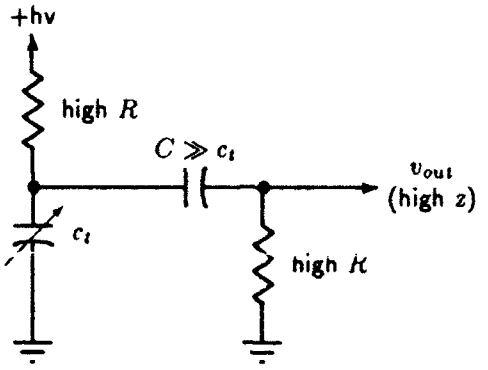

Figure 7: Variable-Capacitance Transducer Circuit

was built for a customer for use in a sled test of warhead devices at China Lake. While the board could have been made smaller, it was not necessary to do so for that particular use. The board was double-sided and used the top as a ground plane; heat sinking was not required, and the amplifiers were capable of driving the 75 Ω coaxial lines used in the system directly. The card has been in use for multiple tests since February of this year (1993).

12 Conclusion

A charge amplifier circuit as described in this paper can be used to measure blast pressures in the ranges produced by PVDF and similar gauges. The charge amplifier described produces higher frequency response and more accurate rendition of the charge profile of the input transducer in a smaller package and a lower cost than circuits previously used.

13 References

For further illumination on some of the material discussed in this paper, the following references are recommended.

1. Élantec data book: **High Performance Analog Integrated Circuits**, Milpitas, CA, 1992

2. Sandia National Laboratories: **PVDF Shock Sensor Workshop Proceedings**, 11 13 December 1990

3. Tobey, Gene; Graeme, Jerald; and Huelsman, Lawrence (editors): **Operational Amplifiers—Design and Applications**, pp. 233-235, McGraw-Hill, New York, 1971

NOVEL APPLICATIONS OF MINIATURE HOPKINSON BAR SENSORS

W. Randolph Davis
W. Scott Walton
Combat Systems Test Activity
Aberdeen Proving Ground, MD 21005

ABSTRACT

Miniature Hopkinson bars have been found to be useful in several applications. Measurement of shock induced in a plate by a projectile impact or by explosion is difficult to measure in the immediate vicinity of the event. A simple transducer has been developed which is both inexpensive and rugged. The transducer allows measurement of shock wave levels on the surface immediately opposite the impact/explosion. The same concept has been used to measure the impact force of a firing pin in small arms. A transducer is chambered in the weapon in a normal manner and the gun is fired to impact the firing pin on the transducer. The firing pin force and impulse are then measured at a variety of temperatures and can be compared to the impulse required to ignite a primer.

BACKGROUND

The Hopkinson bar [reference 1] was originally used to measure the momentum from explosive detonations and projectile impacts. An instrumented Hopkinson bar has been used for the past ten years to measure airblast pressure during the simulation of nuclear weapon tests [reference 2].

All of these events (explosive detonations, projectile impacts, and atomic weapon detonations) are violent, and usually destroy any transducer in the immediate vicinity of the event. Such events are also very short in duration. This paper will describe the use of an instrumented Hopkinson bar to measure two events that are short in duration, and are typically destructive to standard commercial transducers.

FIRING PIN FORCE TRANSDUCER

The historic method of measuring firing pin impulse involved the insertion of a copper plug into the firing chamber. The depth of the indent caused by the firing pin impact was then measured. The firing pin must impart a large enough impulse to indent the primer (and detonate a small explosive), but it must not pierce the primer and allow the release of high pressure gases.

The efforts to use electronic instrumentation to measure firing pin impulse began when a weapon failed to fire reliably at -60 degrees F. One disadvantage of the copper insert is that the temperature of the weapon will change the measurement value. The hardness (and strength) of the copper varies with temperature. The depth of penetration value also has

disadvantages because it cannot be easily converted into engineering values except by calibration using a falling weight in a drop tower, such as the primer tester shown in figure 1. The calibration procedure must be repeated for each lot of copper inserts, and small variations in the condition of the copper inserts, such as surface finish and the presence of a hard surface layer, dramatically affect the results.

Typical commercial load cells were not suitable for this application for a number of reasons:

1. The load is of very short duration (200 microseconds), which requires higher frequency response than most commercial transducers can provide.

2. Physical space is too small to accommodate typical commercial transducers (the sensor must fit inside the cartridge case of 5.56, 7.62 or 9mm ammunition).

3. A soft impact material is needed (to prevent firing pin damage) and the impact causes local deformation of the sensing element.

Figure 1. Photograph of primer testing machine.

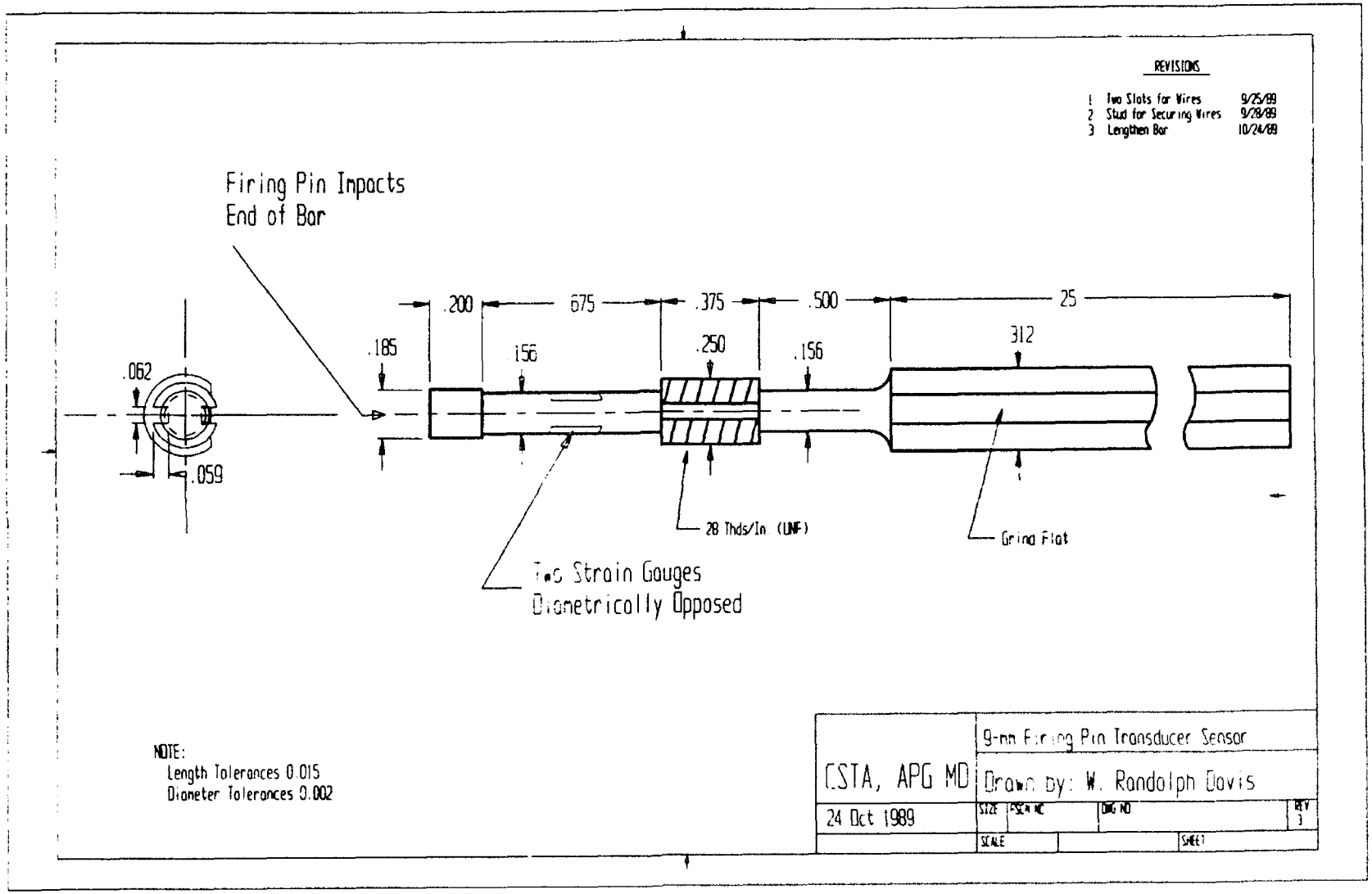

Figure 2. Sketch of Firing Pin Force Transducer (FPFT).

The Firing Pin Force Transducer (FPFT) was developed to overcome these problems. Figure 2 shows the mechanical layout. A photograph of the sensor is shown in Figure 3. A pair of one-eighth inch, 350 ohm foil strain gages were attached to the rod and electrically connected in series as one leg of a Whetstone bridge to eliminate any measurement of bending. Commercial signal conditioning and short cables were used to obtain a frequency response of 100 KHz. Both steel and brass have been used as materials for the FPFT.

The transducer rod is inserted into the muzzle of a weapon until the sensor end protrudes through the breech. The facsimile cartridge is then screwed onto the rod so that the end of the rod assumes the position of a primer. The weapon is then locked and fired to allow the firing pin to impact the transducer. A waveform (as shown in Figure 4) is recorded and corrected as follows:

$$\text{Strain} = 4*V_s/(V_b*G*F)$$

Where:

V_s = Signal Voltage
V_b = Bridge Supply Voltage
G = Preamplifier Gain
F = Gauge Factor(of Strain Guage

$$\text{Stress} = E*\text{Strain}$$

E = Young's Modulus for the Rod Material

$$\text{Force} = \text{Stress}*\text{Area}$$

Figure 3. Photograph of Firing Pin Force Transducer (FPFT) mounted in cut-away model of 9mm pistol.

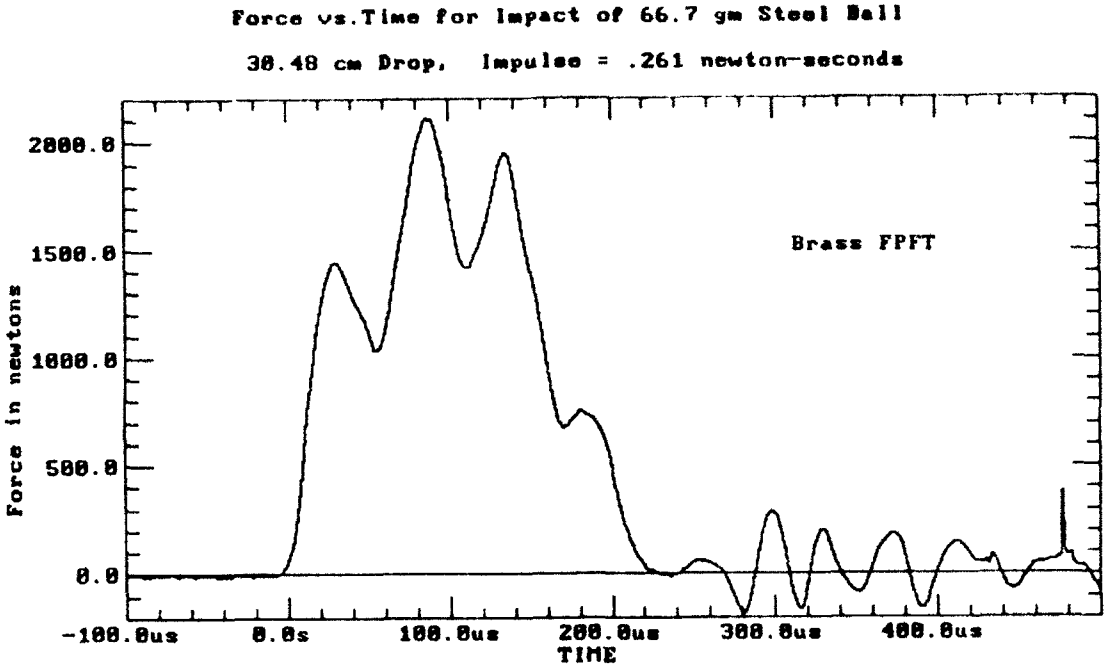

Figure 4. Force vs. time measured by Firing Pin Force Transducer (FPFT) in primer testing machine. Note 25 KHz oscillations due to long firing pin.

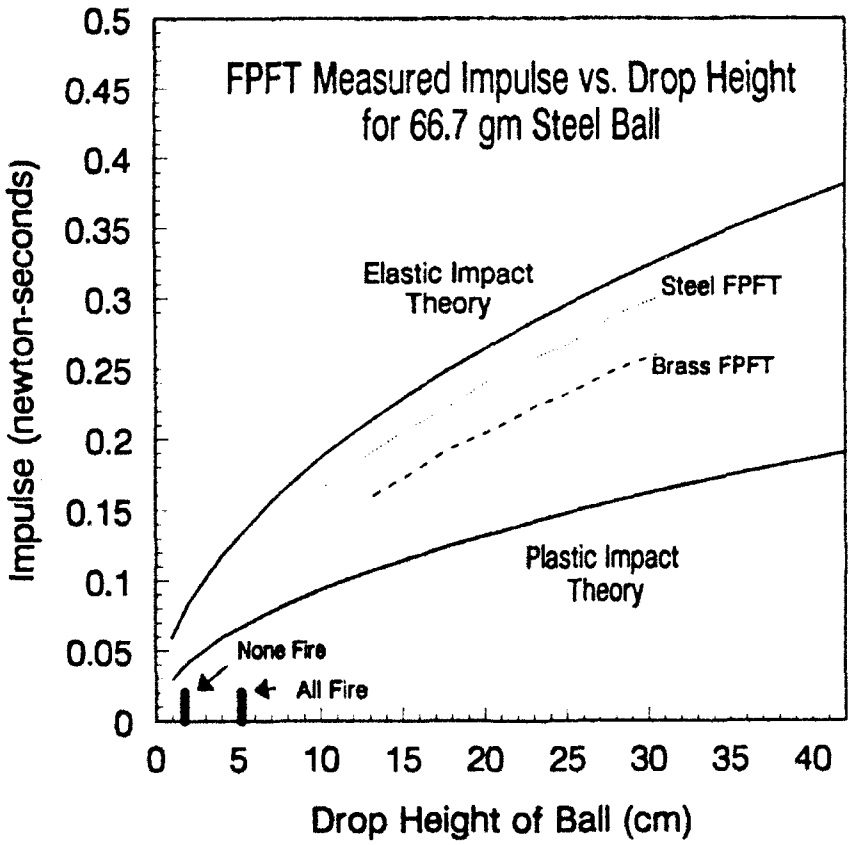

Figure 5. Correlation between impulse measured by FPFT and drop height. Test limits for 9mm primer functioning are also shown.

The impulse produced by the firing pin impact is then calculated by integrating the force vs. time curve (i.e impulse = area under the curve). The FPFT can be used in the primer tester (shown in figure 1) as well as in a weapon. Impulse measurements correlate to the ball drop height (as shown in figure 5), and to the impulse needed to initiate a primer. Impulse measurements in weapons are used to evaluate firing pin performance at various temperatures to ensure that soldiers will have a weapon that operates whenever it is needed.

INERTIAL HOPKINSON BAR (IHOP) SENSOR

The second application involves the study of impact dynamics during high amplitude shock caused by projectile impact on armor plate. Measurements are needed to evaluate armor plate welding techniques and evaluate the shock loads that equipment inside armored vehicles must withstand during the impact of enemy projectiles.

Most shock sensors are unable to survive in the immediate vicinity of an impact. Guages glued to the back surface of a plate behind the event tend to debond because of the sudden acceleration and large dynamic strain. Commercial transducers often break completely or produce erroneous results because of contamination by high frequency shock (in excess of 1 million g's at 1 MHz). Reference 3 describes the difficulties of such measurements.

The Inertial Hopkinson Bar (IHOP) sensor is shown in figure 6. As the plate is struck by a projectile, the resulting shock causes the back surface to move at velocity V. This sudden velocity change causes a stress S in the bar, which can be calculated as:

$$S = D*C*V$$

where S = Stress
D = Density
C = Velocity of longitudinal wave propagation
V = Velocity caused by impact (ie sudden velocity change)

The strain gages sense this stress wave, just as in the previous firing pin force application, but is this cause, the strain is proportional to velocity:

$$V = \frac{Strain*E}{D*C}$$

where Strain = Measured strain
E = Young's modulus of elasticity
D = Density
C = Velocity of longitudinal waves

A photo of the IHOP sensor is shown in figure 7. The response of the IHOP sensor to a BB impact is shown in figure 8, and compared to the response of other instruments (a laser vibrometer and the CSTA velocity gage).

The most important feature of the IHOP sensor is its robustness. Because it is welded on the armor plate, it can survive even when the plate is

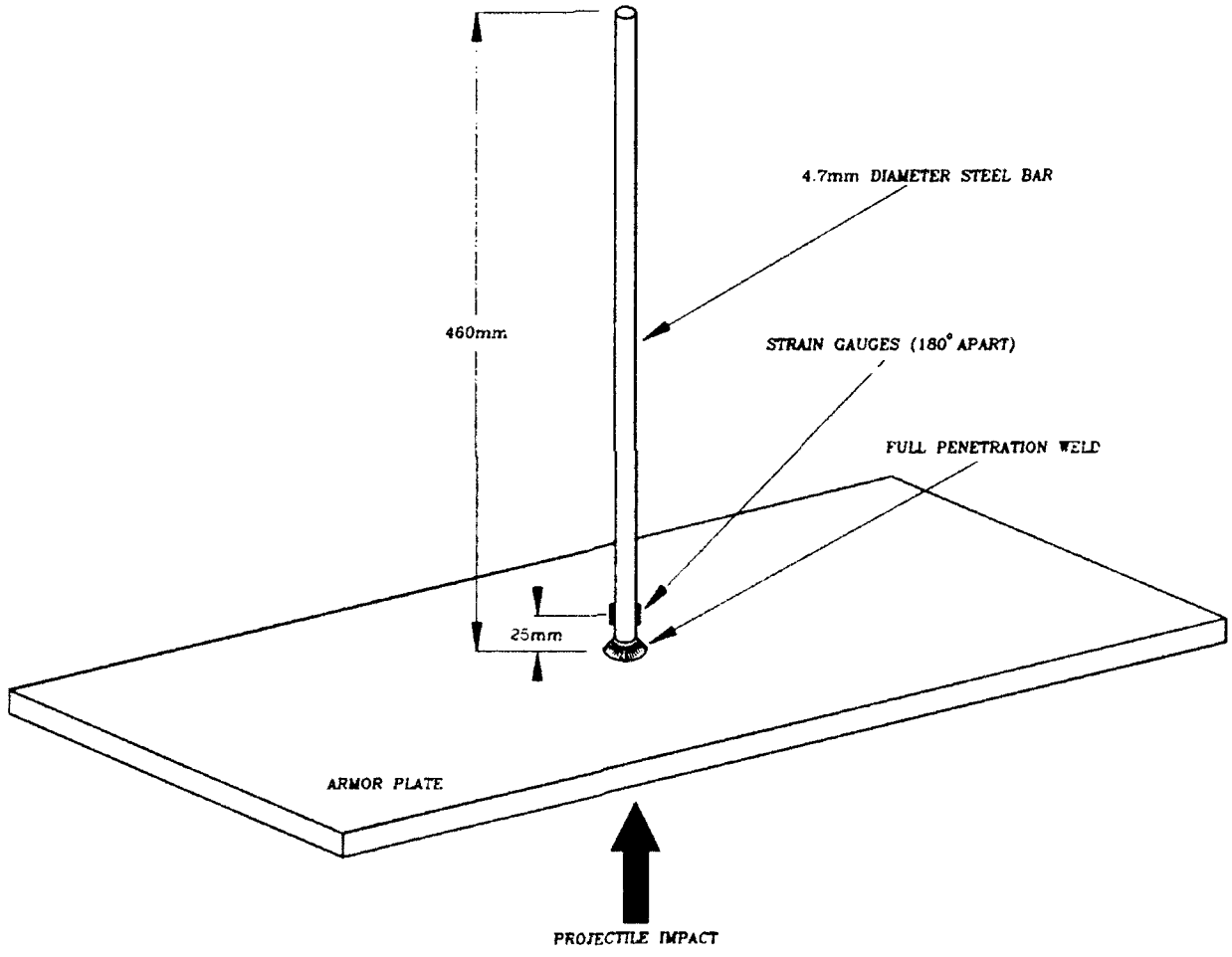

Figure 6. INERTIAL HOPKINSON BAR SENSOR

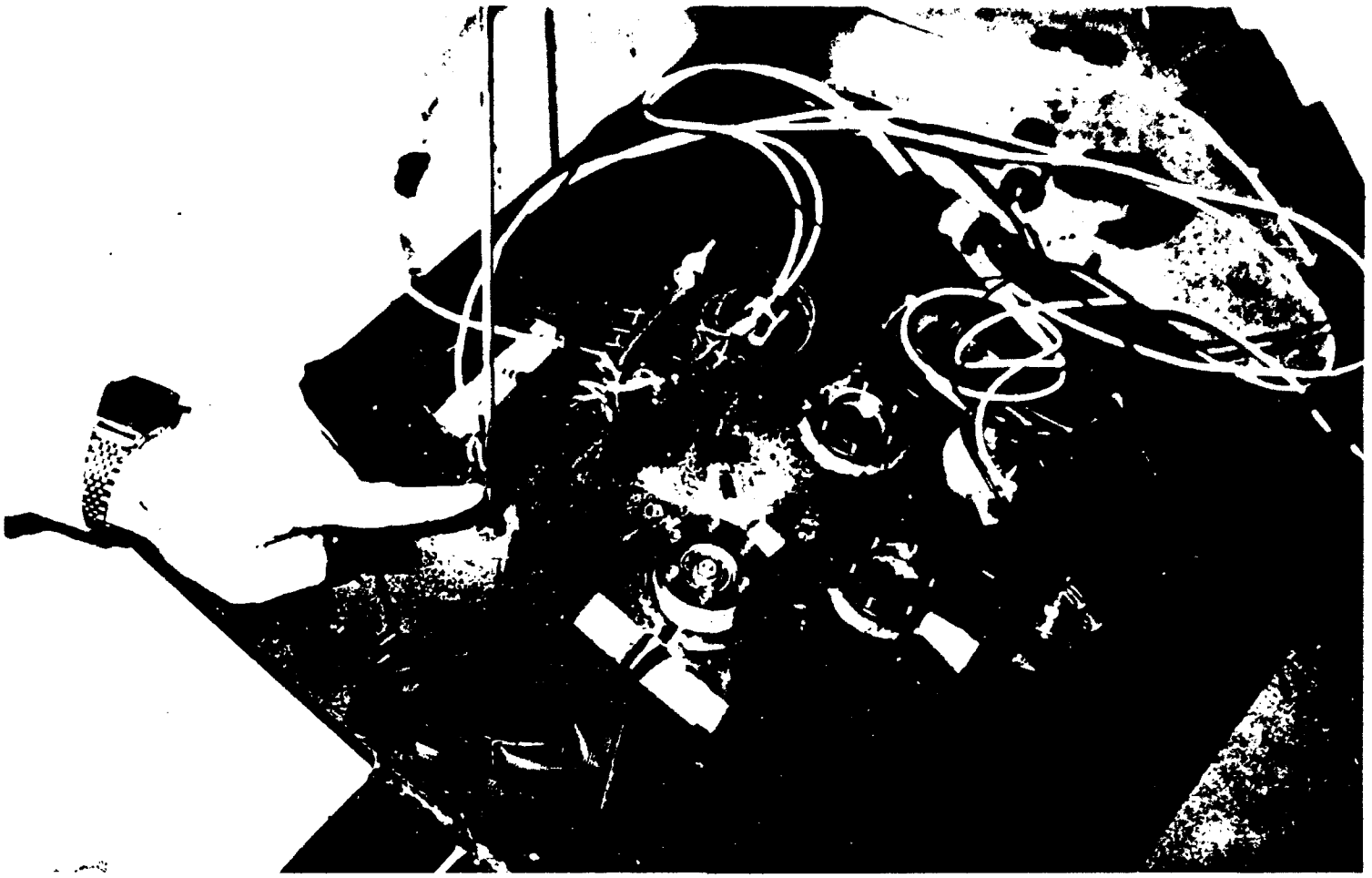

Figure 7. Photograph of IHOP sensor mounted on armor plate.

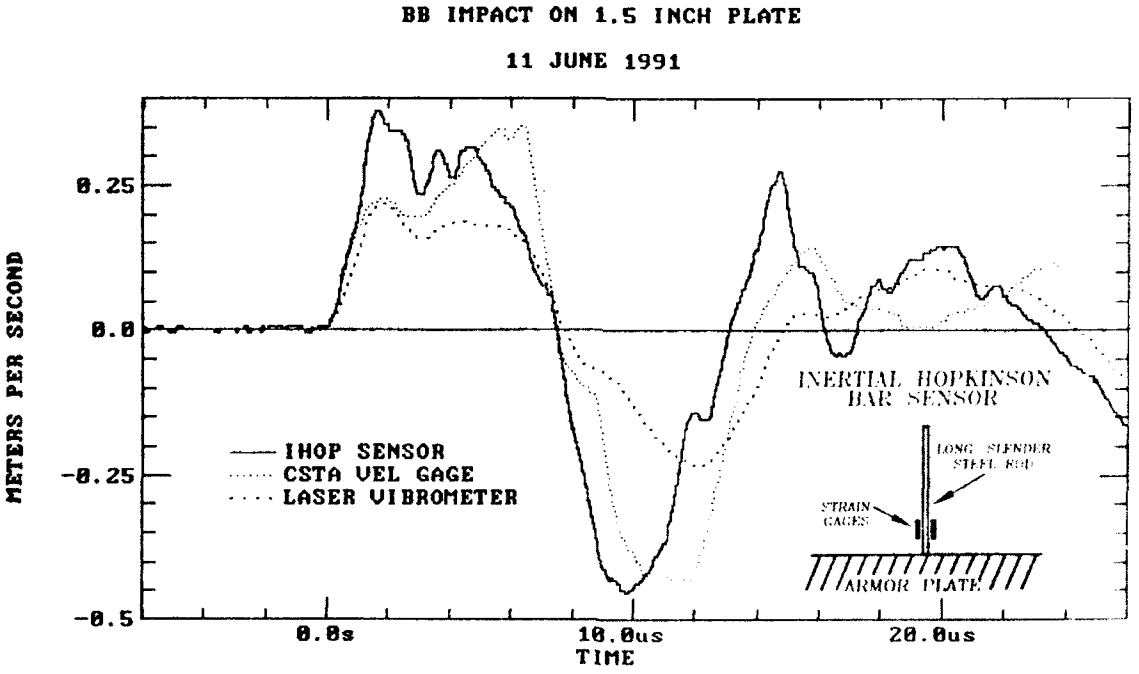

Figure 8. Comparison of IHOP sensor response to various other measurements during the impact of a .177 caliber BB on a 1.5" steel plate.

deformed by severe shock. The strain guage is a very small mass. The most vulnerable portion of the IHOP sensor is the small solder joints on the strain gage, which usually survive where others sensors fail.

FREQUENCY RESPONSE

A significant effort was required to get 1 MHz frequency response for the IHOP sensor. Strain gages with 120 ohm resistance and very short cables were used. Because no commercial signal conditioning unit provides 1 MHz response, a battery was used for excitation, and a high impedance, 15 MHz amplifier with fiber optic isolation was used to measure the strain gage response. By contrast, it was noted that long (150 meter) cables typically have a capacitance of .02 microfarads or larger. When combined with high resistance (350 ohms or greater) strain gages, frequency response is typically limited to 10 KHz.

Dispersion of different frequency stress waves causes a "mechanical" frequency response problem. Note that as shown in figure 9, large diameter bars cause 'ringing" at increasingly lower frequencies. Hence small diameter rods are needed to obtain short rise times and high frequency response, as shown in Table 1. "End effects" make the "mechanical ringing" most severe near the end of the rod that is excited. On the IHOP sensor used in our experiments, the strain gage was placed 2.5 cm (5.3 diameters) away from the plate surface. Fast rise time, short duration events caused "ringing" at roughly 1 MHz.

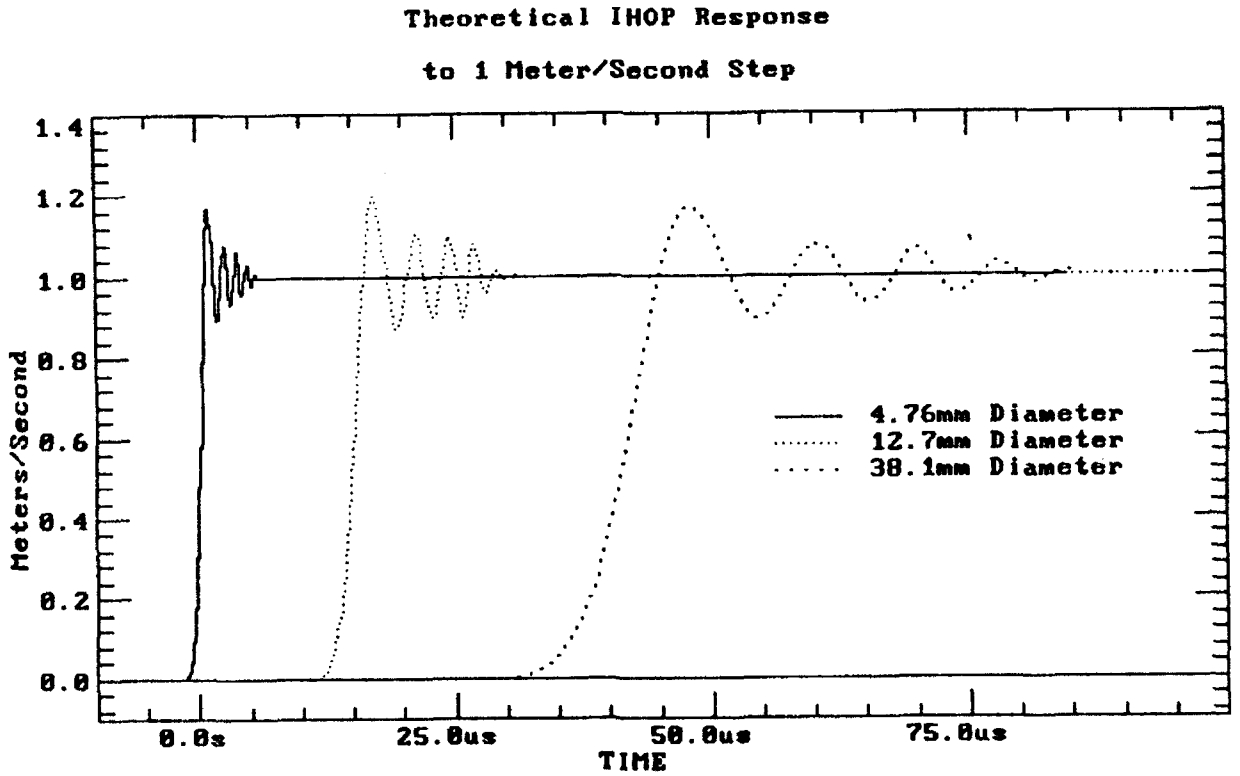

Figure 9. Theoretical prediction of the response of various diameter steel bars to a step function. Monitoring location is 5.3 diameters from impact end. Signals have been offset in time for clarity.

Table 1. Theoretical Initial Rise Time and Subsequent Fluctuations for Hopkinson Bar Response to a Step (from Figure 9).

Bar Diameter (mm)	Initial Rise Time (microseconds)	Bandwidth =.35/Risetime (Hz)	Subsequent Fluctuations (Hz)
4.76	1.025	340,000	1,000,000
12.7	2.718	130,000	350,000
38.1	8.145	43,000	140,000

An analytical technique for correcting the mechanical "ringing" caused by dispersion is described in reference 4. In the experiments using the IHOP sensor, the correction technique was of limited value. It is assumed that the reason the correction technique did not help was because most of the "ringing" observed was due to "end effects" rather than dispersion.

CONCLUSIONS

The Hopkinson bar concept has been used to measure pressure, force, and velocity. The Hopkinson bar sensors described have been developed for the same reasons that the original bar was developed: i.e. we needed to make measurements during violent events that destroy other transducers. Our conclusions are:

A. The Hopkinson bar transducers survive where others fail.

B. The Hopkinson bar transducers have limited frequency response:

1. Low frequency response is controlled by the length of the bar. For the FPFT a 25" bar was needed to measure 220 microsecond events.

2. High frequency response is controlled by:

a.) Electronics. Typical frequency response is 10 KHz. Special effort must be used to obtain 1 MHz response from a Wheatstone bridge.

b.) Mechanical dispersion. A small diameter rod is needed for high frequency response.

C. For future experiments with Hopkinson bar sensors requiring high frequency response, the following changes should be tried:

1. Try to use an even smaller diameter bar. Limits to bar diameter are controlled by the ability to get a good weld to the armor plate and the ability to bond the strain gages to the bar.

2. Place the strain gage further away from the end of the bar that is excited (at least 10 diameters away to avoid "end effects").

3. To improve the low frequency response, a longer bar is desired. An experiment with a "coiled" bar should be tried to determine if a long bar can be packaged in a compact location without compromising measurement accuracy.

REFERENCES

1. Hopkinson, B., "A Method of Measuring the Pressure Produced in the Detonation of High Explosives or by the Impact of Bullets," Philosophical Transactions, Series A, Royal Society of London, Vol. 213, 1919, pp 437-457.

2. Baylot, James T., and Hall, Robert L, "Analysis of Hopkinson Bar Gage for Measurement of Very High Airblast Pressure", Proceedings of the 62nd Shock and Vibration Symposium, Volume II, pp 412-421, Oct 1991.

3. Walton, W. Scott, "Pyroshock Evaluation of Ballistic Shock Measurement Techniques". Proceedings for the 62nd Shock and Vibration Symposium, Volume II, pp 422-431, Oct 1991.

4. Gorham, D. A., "A Numerical Method for the Correction of Dispersion in Pressure Bar Signals," J. Phys. B: Sci. Instrum., Vol 16, 1983, pp 477-479.

ISOLATION OF A PIEZORESISTIVE ACCELEROMETER USED IN HIGH ACCELERATION TESTS*

Vesta I. Bateman
Fred A. Brown
Neil T. Davie
Sandia National Laboratories
Albuquerque, New Mexico 87185

ABSTRACT

Both uniaxial and triaxial shock isolation techniques for a piezoresistive accelerometer have been developed for pyroshock and impact tests. The uniaxial shock isolation technique has demonstrated acceptable characteristics for a temperature range of -50°F to +186°F and a frequency bandwidth of DC to 10 kHz. The triaxial shock isolation technique has demonstrated acceptable results for a temperature range of -50°F to 70°F and a frequency bandwidth of DC to 10 kHz. These temperature ranges, that are beyond the accelerometer manufacturer's operational limits of -30°F and +150°F, required the calibration of accelerometers at high shock levels and at the temperature extremes of -50°F and +160°F. The purposes of these calibrations were to insure that the accelerometers operated at the field test temperatures and to provide an accelerometer sensitivity at each test temperature. Since there is no NIST-traceable (National Institute of Standards and Technology traceable) calibration capability at shock levels of 5,000 g - 15,000 g for the temperature extremes of -50°F and +160°F, a method for calibrating and certifying the Hopkinson bar with a transfer standard was developed. Time domain and frequency domain results are given that characterize the Hopkinson bar. The NIST-traceable accuracy for the standard accelerometer in shock is ±5%. The Hopkinson bar has been certified by the Sandia Secondary Standards Division with an uncertainty of 6%.

INTRODUCTION

Sandia National Laboratories (SNL) conduct impact testing for a variety of structures as discussed in other papers [1,2]. During an impact test, metal to metal contact may occur within the structure and produce high frequency, high amplitude shocks. The high frequency portion of this transient vibration has been observed to excite an accelerometer into resonance even though this resonance exceeds 350 kHz. An accelerometer may fail in this situation. Even if the accelerometer does not fail, the amplitude of the resonating accelerometer response can be so large that the data are clipped and rendered useless. If the data are not clipped, a digital filter must be applied to eliminate undesirable accelerometer resonant response. In

*This work was performed at Sandia National Laboratories and was supported by the U.S. Department of Energy under Contract DE-AC04-76-DP00789.

anticipation of accelerometers' resonating during a test, the data channels may be set to accomodate the large amplitude of the accelerometer resonance. The result is usually an unacceptably small signal to noise ratio. If possible, it is more desirable to prevent excitation of the accelerometer resonance. This may be accomplished by mechanically isolating the accelerometer from the high frequency excitation without degrading the transducer response in the bandwidth of interest.

In the past, several techniques have been used at Sandia National Laboratories to mechanically isolate accelerometers and instrumentation packages containing accelerometers from high frequency, high amplitude shock environments. These techniques include various configurations of adiprene, polysulfide rubber, water soluble wax, and urethane rubber [3,4,5]. The techniques have been successful in mechanically isolating the accelerometers but have a limited, useable frequency range of 2 kHz or less. The useable frequency range is specified as those frequencies for which the sensitivity deviation is $\pm 5\%$ or less. In one application, a mechanical isolator was combined with an electrical analog filter, tuned for the isolator resonance, to achieve a useable frequency range of 10 kHz. A commercially available, mechanical isolator has also been evaluated. However, this isolator exhibited nonlinear behavior over its acceleration capability of 1500 g. A commercial piezoelectric accelerometer with integral electronics and mechanical isolation is available but is generally not used in our field testing because of signal conditioning requirements, cable-whip and zero-shift problems, and a limited useable frequency range of about 1 kHz.

A bandwidth of 10 kHz is needed for many applications because more sophisticated analyses are being performed with the field data. The isolation techniques were designed and evaluated for the desired bandwidth of 10 kHz. These techniques are used with a piezoresistive accelerometer which is frequently used for field tests of various high reliability structures which must withstand severe shock environments. The piezoresistive accelerometer has several desirable characteristics: DC response, low power requirements, minimal zero shift, and high resonant frequency. One undesirable characteristic is that the piezoresisitive accelerometer is undamped. A high frequency input causes it to resonate, and the resulting large amplitude may exceed the measuring capability of the instrumentation system. The resonant behavior is prevented with a mechanical isolator that has a damped resonance between the upper limit of the useable frequency range and the accelerometer's resonance. For example, the uniaxial isolator assembly has a damped resonance at about 50 kHz. This resonance allows attenuation of frequency input to the accelerometer above 50 kHz, and is useable for the piezoresistive accelerometer models with ranges equal to or greater than 6,000 g.

There are several goals in the design of a shock isolation technique. Primarily, the technique must have repeatable response characteristics. Secondly, the technique must allow calibration of the shock isolated accelerometer assembly prior to and after a field test. Lastly, the

technique must show linear amplitude and frequency characteristics. These goals have been achieved with the mechanical isolators developed at Sandia National Laboratories for a piezoresistive accelerometer [6,7]. The uniaxial shock isolation technique has demonstrated acceptable characteristics for a temperature range of -50°F to +186°F and a frequency bandwidth of DC to 10 kHz. The triaxial shock isolation technique has demonstrated acceptable results for a temperature range of -50°F to 70°F and a frequency bandwidth of DC to 10 kHz. Additionally, these characteristics have been verified by the calibration of the Hopkinson bar used for testing of the isolation techniques [8]. This paper will discuss the testing that has been conducted to demonstrate the performance of the isolation techniques and the calibration of the Hopkinson bar that has been performed to verify the results.

UNIAXIAL AND TRIAXIAL ISOLATION DESIGNS AND CALIBRATION

The uniaxial and triaxial isolation techniques are shown in Figure 1. The uniaxial technique consists of an aluminum disk that has a slot for the accelerometer. The disk is divided into two halves that are held together by two screws. A layer of polysulfide rubber compound (PRC-1422) is positioned on each side of the accelerometer in the slot. Brass locator pins (not shown) hold the PRC-1422 and accelerometer layers in place in the slot. An integral stud on the bottom of the disk is used to attach the uniaxial isolator assembly to the test structure (25 in-lbs mounting torque). Shrink tubing is used on the brass pins in the disk technique to prevent metal to metal contact during lateral shocks.

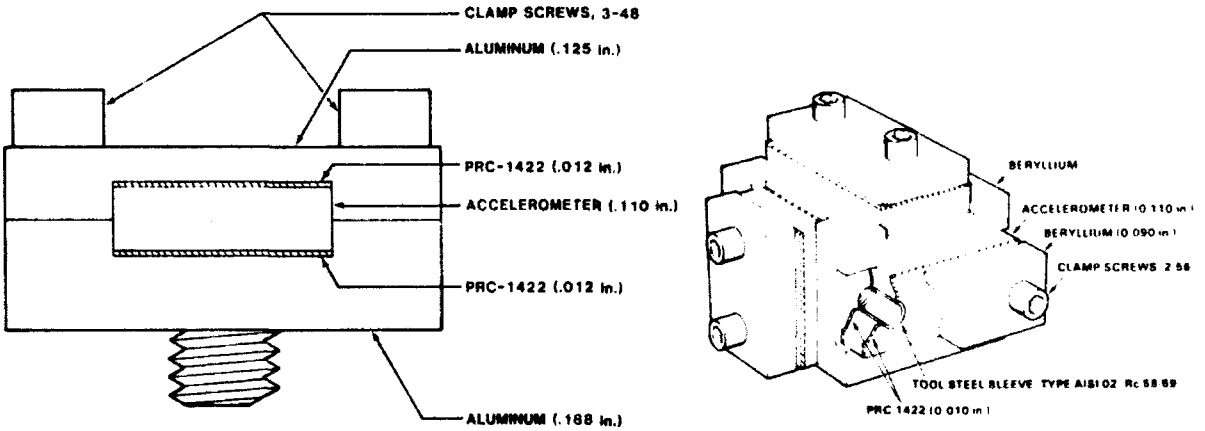

a) Uniaxial Isolation Technique **b) Triaxial Isolation Technique**

Figure 1: Uniaxial and Triaxial Isolation Techniques for a Piezoresistive Accelerometer.

The triaxial isolation technique, also shown in Figure 1, consists of a 0.6 in. cube of either 7075 aluminum or beryllium that has been machined with a slot on each of three orthogonal faces. The piezoresistive accelerometers are mounted in the slots with a layer of PRC-1422 on either side in the same manner as the uniaxial isolation technique. Hardened steel sleeves are

covered with shrink tubing to prevent metal-to-metal contact and are pressed into the mounting holes in the accelerometer. The sleeves are 0.125 in. long and provide correct spacing between the top plate and the bottom of the slot so that a consistent compression is maintained on the elastic material, PRC-1422. The plate, accelerometer, and layers of PRC-1422 are held in place with 2-56 screws that are torqued to 60 in-oz. A torque of 40 in-lbs is used for the triaxial isolation assembly mounting stud.

All accelerometers in this study were calibrated in the Sandia Calibration Laboratory using three methods: 1) shaker calibration; 2) centrifuge calibration; and 3) dropball calibration. The three methods are traceable to the National Institute of Standards and Technology, NIST, formerly NBS as described elsewhere [6]. Two commercially available mechanical isolators were evaluated using 6000 g piezoresistive accelerometers. Although the dropball and centrifuge calibrations were acceptable, both commercial isolators showed a deviation of 36% at 5 kHz in the shaker calibration at 5 g input as shown in Figure 2a. A uniaxial isolator assembly calibration at 30 g input is also shown for comparison. The damped resonance at 5 kHz is in agreement with the manufacturer's specifcations for the commercial isolator. The shaker data indicates that the useable frequency range, defined as less than 5% deviation from the 100 Hz reference, is about 1 kHz. Additionally, the commercial assemblies were evaluated on the Hopkinson bar, described in a later section, at two levels of 500 g and 1500 g with a pulse duration of 100 μs. These tests showed amplitude nonlinearities in the commercial isolator.

Figure 2b shows a shaker calibration at 30 g input for a uniaxial isolator assembly. This isolator had a sensitivity variation of less than $\pm$0.5% for the $\pm$5000 g centrifuge calibration (not shown). Figure 2c depicts a dropball calibration of the uniaxial isolator. Since the isolators were satisfactorily calibrated by all three methods, a more detailed evaluation of the shock isolation techniques was undertaken to investigate the linearity of amplitude and frequency characteristics on the Hopkinson bar in the Sandia Shock Laboratory.

HOPKINSON BAR CONFIGURATIONS FOR CHARACTERIZATION OF SHOCK ISOLATION TECHNIQUES

Accelerometer calibrations at temperatures other than ambient can only be conducted with the shaker due to limitations of existing equipment at the SNL Secondary Standards Lab. For shock accelerometers, it is desirable to calibrate with the dropball or with another shock producing technique such as the Hopkinson bar. The Hopkinson bar easily lends itself to temperature conditioning because the end of the bar, where the accelerometer is mounted, is simply inserted into a temperature chamber. For this reason, shock calibrations for the shock isolation techniques at the temperature extremes of -50°F and +186°F were conducted with a Hopkinson bar located in the SNL Shock Laboratory. The configuration for a normal input is shown in Figure 3. Normal input in this configuration is an input that is normal to the mounting surface and is also parallel to the integral mounting stud. Both the

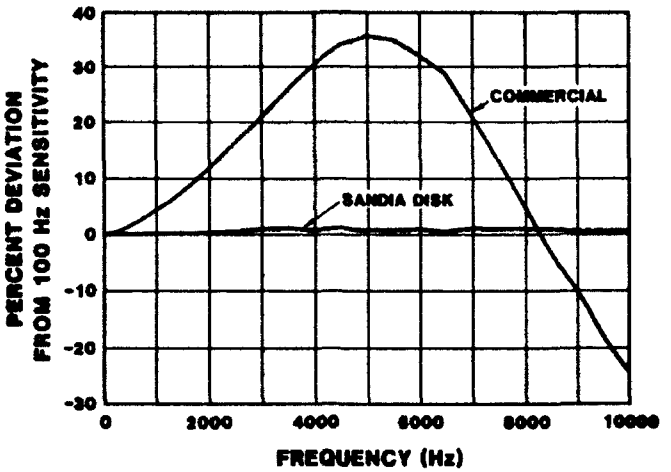

a) Shaker Calibration Comparison for Uniaxial and Commercial Isolators

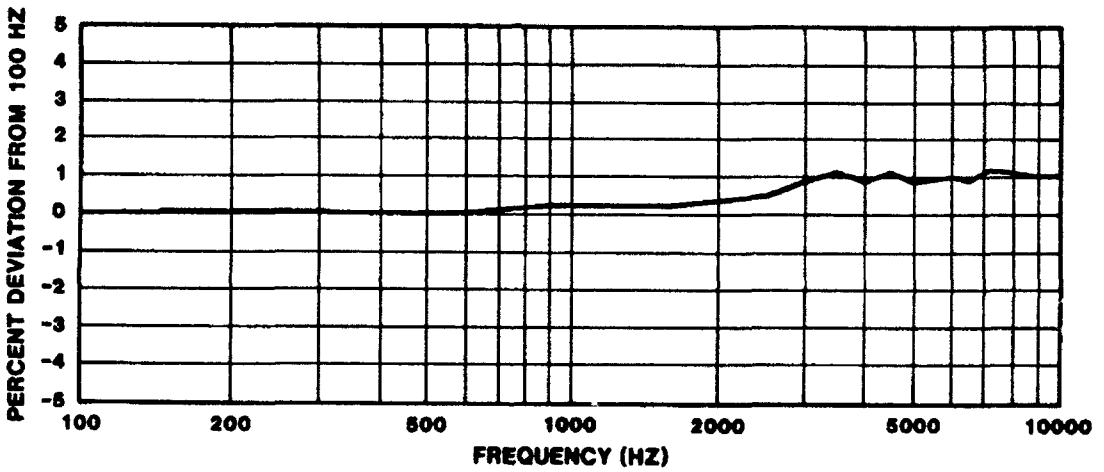

b) Shaker Calibration of Uniaxial Isolator

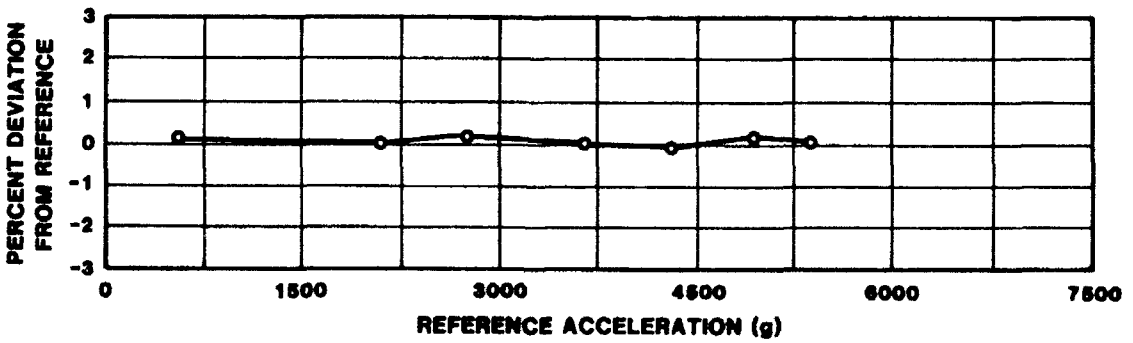

c) Dropball Calibration of Uniaxial Isolator

Figure 2: Calibrations for Commercial and Uniaxial Isolators

uniaxial technique and one axis of the triaxial isolation technique are tested with the normal input. The other two axes of the triax are characterized with a transverse input created by the Hopkinson bar configuration in Figure 4. A transverse input is perpendicular to the mounting stud or parallel to the mounting surface. An in-axis response is the response of an accelerometer whose sensitive axis is in the direction of the shock. An out-of-axis response is the response of an accelerometer whose sensitive axis is not in the direction of the shock. The uniaxial isolation technique and one axis of the triaxial isolation technique have in-axis response for a normal input. Each of the two other orthogonal axes of the triaxial isolation technique can have in-axis response for a transverse input.

These two Hopkinson bar configurations are used to characterize the response of the isolation techniques in both the time domain as a sensitivity calculation and in the frequency domain as frequency response functions. The sensitivity calculation is described below. The frequency response functions are calculated in the same manner as reported previously [6] except that an accelerometer mounted on the end of the bar is used as the reference acceleration for transverse inputs.

The theory of stress wave propagation in a Hopkinson bar is well documented in the literature [9,10]. The results of this theory are summarized as follows:

A Hopkinson bar is defined as a perfectly elastic, homogeneous bar of constant cross-section.

A stress wave will propagate in a Hopkinson bar as a one-dimensional elastic wave without attenuation or distortion if the wavelength, λ, is large relative to the diameter, D, or $10D \leq \lambda$.

For a one-dimensional stress wave propagating in a Hopkinson bar, the motion of a free end of the bar as a result of this wave is:

$$v = 2c\varepsilon \tag{1}$$

or,

$$a = 2c\left[\frac{d\varepsilon}{dt}\right] \tag{2}$$

where v and a are the velocity and acceleration, respectively, of the end of the bar, $c=\sqrt{E/\rho}$ is the wave propagation speed in the bar, E is the modulus of elasticity, ρ is the density for the Hopkinson bar material, and ε is the strain measured in the bar at a location that is not affected by reflections during the measurement interval.

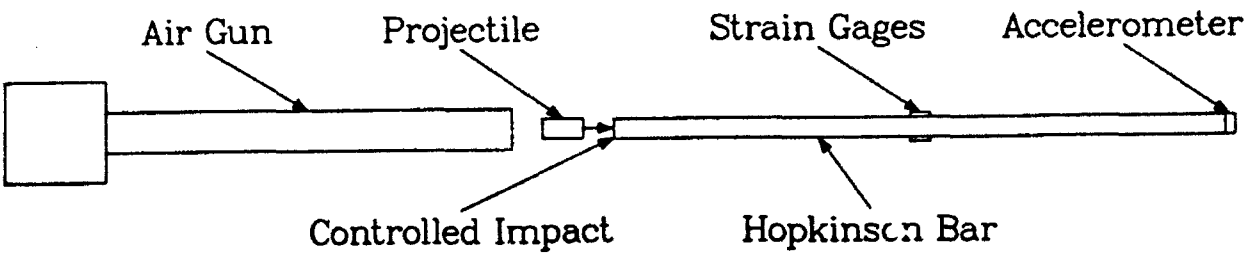

Figure 3: Hopkinson Bar Configuration for Normal Input.

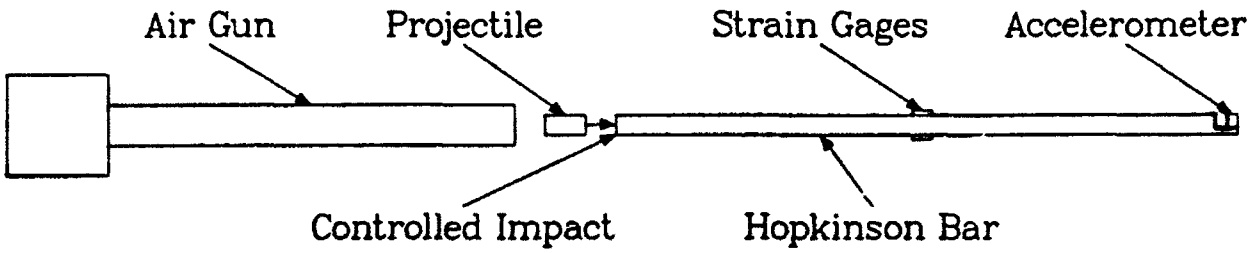

Figure 4: Hopkinson Bar Configuration for Transverse Input.

The motion of an accelerometer mounted on the end of the bar will be governed by equations (1) and (2) if the mechanical impedance of the accelerometer is much less than that of the bar or if the thickness of the accelerometer is much less than the wavelength. The requirement on the strain gage is that the gage length (g.l.) be less than the wavelength or $\lambda \geq 10$ g.l.

The Shock Laboratory Hopkinson bar, used for accelerometer testing, is shown schematically in Figures 3-4 and is made of 6 Al, 4 V titanium alloy (6% aluminum and 4% vanadium) with a 72 inch length and a 0.76 inch diameter. The bar is supported in a way that allows it to move freely in the axial direction. A low pressure air gun is used to fire a 2 inch long hardened tool steel projectile at the end of the bar. This impact creates a stress pulse which propagates toward the opposite end of the Hopkinson bar. The amplitude of the pulse is controlled by regulating the air gun pressure, which determines the impact speed. The shape (approximately a half sine) and duration of the pulse are controlled by placing various thicknesses of paper (3x5 index cards) on the impact surface. The two strain gages are located 49.75 inches from the end on which the accelerometer is mounted and are mounted at diametrically opposite positions on the bar. The 49.75 inch

strain gage location is in the mid-portion of the bar and allows a longer incident pulse, if desired. These gages are connected in opposite arms of a Wheatstone bridge to measure the net axial strain.

Once recorded, the strain and acceleration records can be compared by using either velocity or acceleration as shown in (1) and (2). When these comparisons are made, the time delay of the acceleration record, which is equal to the time for the wave to propagate from the strain gage to the end of the bar, must be taken into account. Hopkinson bar accelerometer calibration methods documented in the literature [11-13] generally use velocity, in which case the accelerometer record is integrated and compared directly to the strain record converted to velocity by the factor 2c. This provides smooth curves for comparison of time histories, however much of the higher frequency information is lost due to the integration process. Since it was desired to preserve the frequency response of the data, acceleration is used for the comparison of the data. Consequently, the time derivative of the strain records was required, and the resulting signal may be contaminated by high frequency noise created in the process of calculating the derivative. This problem was essentially eliminated by: 1) adequate sample rate of 500 kHz or higher; 2) low pass digital filtering with a cutoff frequency well above the frequency range of interest (10 kHz); and most importantly, 3) an accurate differentiation algorithm which was derived using the Fourier series reconstruction techniques in [14]. This algorithm results in an exact derivative of the digitized signal providing the Sampling Theorem has not been violated, that is, the data is not aliased [15].

The selected technique for calculating the sensitivity change at temperatures other than ambient, using the acceleration derived from the Hopkinson bar strain measurements, can be used only to estimate the change in sensitivity due to temperature because of the uncertainties associated with the measurements. Most of the errors are deterministic and will be cancelled when the percentage sensitivity change due to the -50°F temperature is calculated in the following equation [8]:

$$C = \left[\frac{A_{Ac-50}}{A_{Ac-A}} \cdot \frac{A_{Hop-A}}{A_{Hop-50}} - 1 \right] \times 100 \qquad (3)$$

where:

C = Percentage sensitivity change at -50°F as compared to ambient,

A_{Ac-50} = Shock amplitude measured by accelerometer at -50°F,

A_{Ac-A} = Shock amplitude measured by accelerometer at ambient,

A_{Hop-A} = Shock amplitude derived from strain gages for ambient test, and

A_{Hop-50} = Shock amplitude derived from strain gages for -50°F test.

A similar equation is used for the sensitivity change at +186°F.

UNIAXIAL ISOLATION TECHNIQUE PERFORMANCE

Twelve piezoresistive accelerometers mounted in the uniaxial isolation technique were used to assess the performance of the technique at -50°F and +186°F. Each accelerometer was subjected to five 5000 g pulses with a duration of 100 μs at each of five temperatures: ambient (70°F), -50°F, ambient, +186°F, and ambient. The accelerometers were tested at ambient after each test at a temperature extreme because the temperatures of -50°F and +186°F are beyond the manufacturer's operational range, -30°F to +150°F. The last ambient test ensured that the accelerometer was still operational after exposure to the extreme temperature environment.

The uniaxial isolation technique was characterized in the time domain with equation (2). The data from the strain gages and the accelerometers were digitally filtered at 17 kHz prior to the sensitivity calculation. The average sensitivity change at -50°F was 6.0% or -0.05%/°F. The average sensitivity change at +186°F was -4.3% or -0.04%/°F. These results are lower than the -0.06%/°F quoted in the manufacturer's specifications.

An acceleration-to-acceleration frequency response function was calculated for the uniaxial isolation technique at the two temperature extremes and compared to the frequency response function at ambient temperature. The calculations were made in the same manner as those published previously [6], and the frequency resolution for these calculations is 244 Hz. The magnitudes of the frequency response functions are shown in Figure 5 which shows that the magnitudes at 10 kHz deviate less than 10 percent from the magnitude at low frequency for all three temperature conditions. The frequency response function phase (not shown) varies in an approximately linear manner up to 10 kHz for all three temperature conditions. The deviation in the frequency response function magnitude above 20 kHz can be explained by the coherence functions (not shown) which show the coherence between the input and the output accelerations is less than one above 20 kHz. The computational anomaly, indicated by the lack of coherence, creates an apparent resonance above 20 kHz that is not a mechanical resonance in the uniaxial isolation technique.

TRIAXIAL ISOLATION TECHNIQUE PERFORMANCE

The triaxial isolation assembly, using a beryllium block, has been characterized at both ambient and at -50°F. Two beryllium triaxes were characterized at two levels: 2500 g and 5000 g, but only the results for the 5000 g input are shown here. The 2500 g results are similar. Each accelerometer in each triax was subjected to five 2500 g, 70 μs pulses and to five 5000 g, 70 μs pulses at the two temperatures: ambient (70°F) and -50°F.

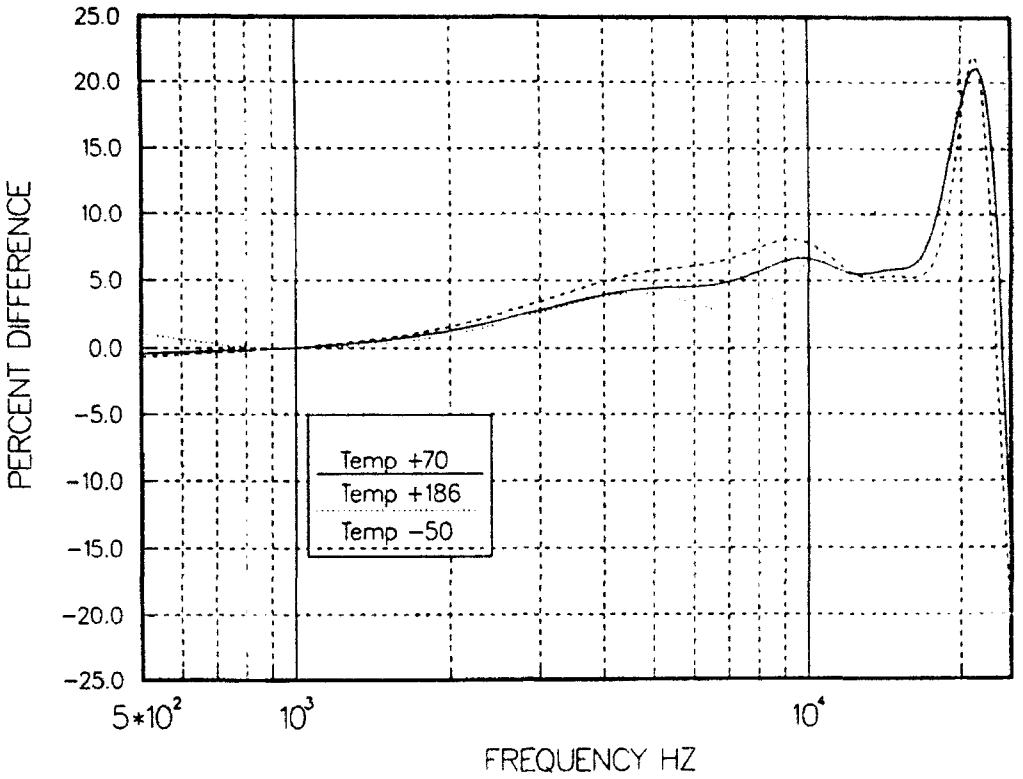

Figure 5: Frequency Response Function Magnitude for the Uniaxial Isolation Technique at -50°F, Ambient (70°F), and +186°F with a 5000 g, 100 μs Input Pulse.

The data from the strain gages and the accelerometers were digitally filtered at 25 kHz prior to the calculations. Sensitivity changes were calculated for the ten pulses applied to each accelerometer and averaged. The changes range from -0.05 %/°F to -0.11 %/°F and are generally higher than the -0.06%/°F quoted in the manufacturer's specifications. At this point, the calculated change is applied to each individual accelerometer until more data can be accumulated for an average sensitivity change calculation.

Frequency response function magnitudes for the triax at ambient are shown in Figure 6 for both the normal input and the transverse input. Frequency response functions for the triax at -50°F are shown in Figure 7 for both the normal input and the transverse input. Phase and coherence functions were also calculated but are not shown. The phase is approximately linear over the 10 kHz bandwidth, and the coherence is one until about 20 kHz which causes the large deviations in the magnitudes shown in Figures 6-7. The phase changes more for the transverse input than for the normal input over the 10 kHz bandwidth.

The triaxial isolation technique with a 7075 aluminum block has also been tested but generally has acceptable performance over a more limited frequency bandwidth, about 4 kHz, than the beryllium. Additionally, the screws in the

aluminum blocks loosen more easily, and there is more out-of-axis response for the aluminum triax. The out-of-axis response is increased in the aluminum block because it has a resonance at about the same frequency as the resonance of the 20,000 g piezoresistive accelerometers mounted in the triax, 350 kHz. The beryllium is stiffer and less dense, so its first resonance is in excess of 400 kHz and does not excite the accelerometer's resonance.

The attachment of the triax to the bar was critical with the Hopkinson bar configuration for a transverse input. The triax was bolted to the Hopkinson bar at the lower acceleration levels, but at input acceleration levels of about 4000 g and above, the triax had to be bolted and glued to the bar. With the bolt and the glue, the triax was prevented from moving with respect to the Hopkinson bar surface during the application of the input acceleration pulse. Additionally, there was a difference in the response of the out-of-axis transverse accelerometers that seems to be dependent upon their orientation. As can be seen in Figure 1, the two transverse accelerometers are not oriented the same way; they are oriented at 90° to each other. The out-of-axis response was generally about 10% if the shock passed across the long dimension of the accelerometer. If the shock passed across the short dimension of the accelerometer, the out-of-axis response was somewhat larger (about 50%) and appeared to contain more excitation of the accelerometer's resonance.

Finally, a comparison of the Fourier transforms for a hard mounted accelerometer and one axis of the triaxial isolation technique is shown in Figure 8 for a 5000 g, 70 μs input pulse on the Hopkinson bar. Figure 8 shows that the triaxial isolation technique has attenuated the accelerometer resonance by a factor of three and, therefore, has successfully isolated the accelerometer from high frequency input.

HOPKINSON BAR CALIBRATION RESULTS

Three separate operations were performed to calibrate the Hopkinson bar. First, a calculation of the wave speed for the titanium Hopkinson bar was made at the temperatures of -50°F and +160°F. Secondly, a reference accelerometer, calibrated by NIST traceable standards, was placed on the end of the bar in the same manner as the accelerometers for the calibration tests and was subjected to shock pulses at various amplitudes. The reference accelerometer output was compared to the acceleration calculated from the Hopkinson bar strain gage response. Lastly, a static load test was performed on the Hopkinson bar; and an effective gage factor was calculated from the measured bar sensitivity.

The stress wave speed in the Hopkinson bar is an important quantity because it occurs in the the Hopkinson bar acceleration calculation as shown in (1) and (2). The stress wave speed is calculated from material properties as:

$$c = \sqrt{\frac{E}{\rho}} \qquad (4)$$

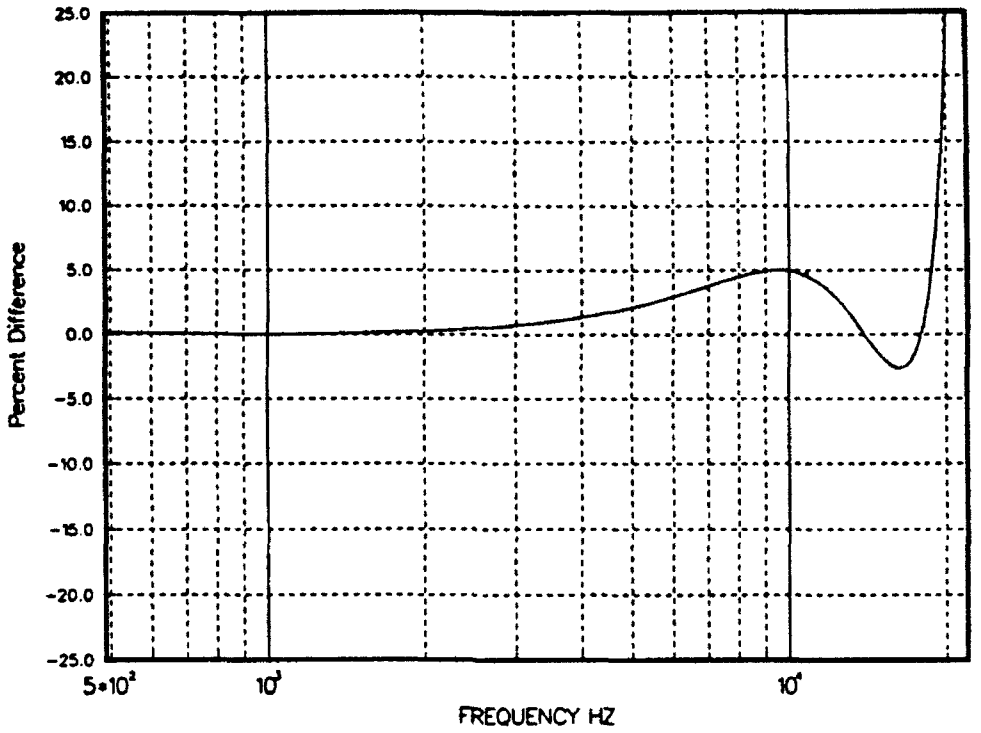

a) Normal Input

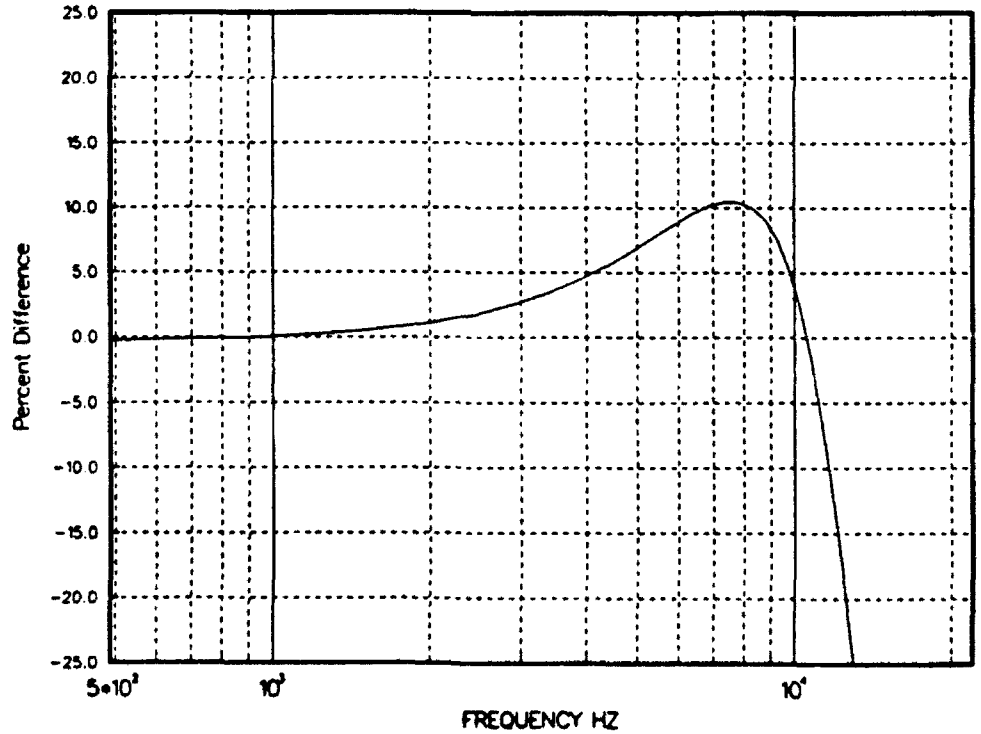

b) Transverse Input

Figure 6: Frequency Response Function Magnitude for the Triaxial Isolation Technique at Ambient (70°F) with a 5000 g, 70 μs Input Pulse.

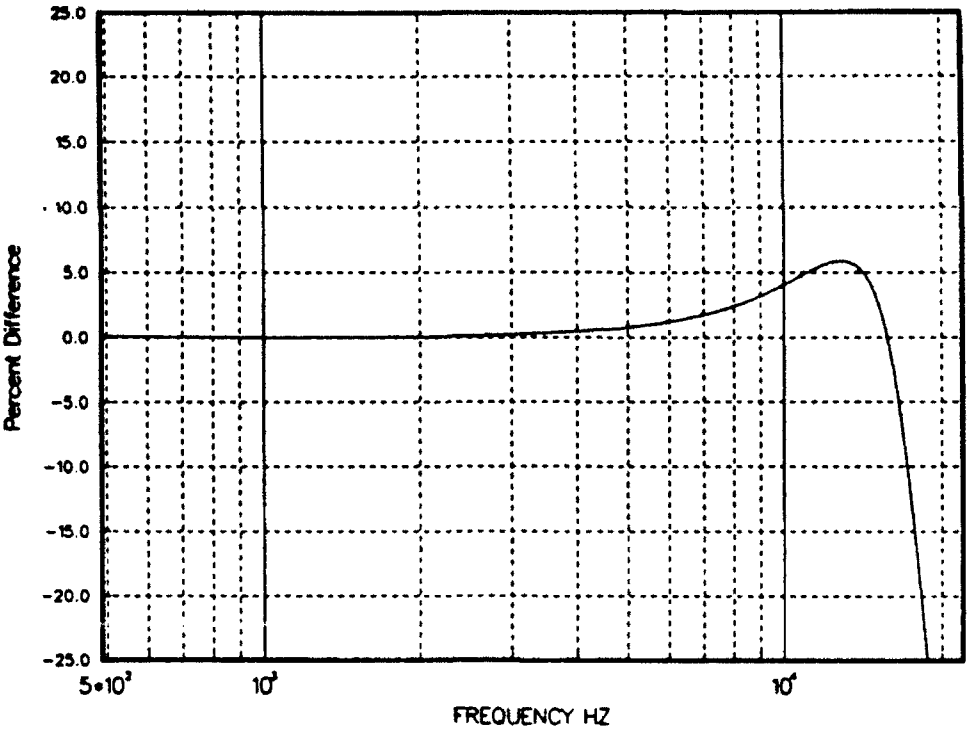

a) Normal Input

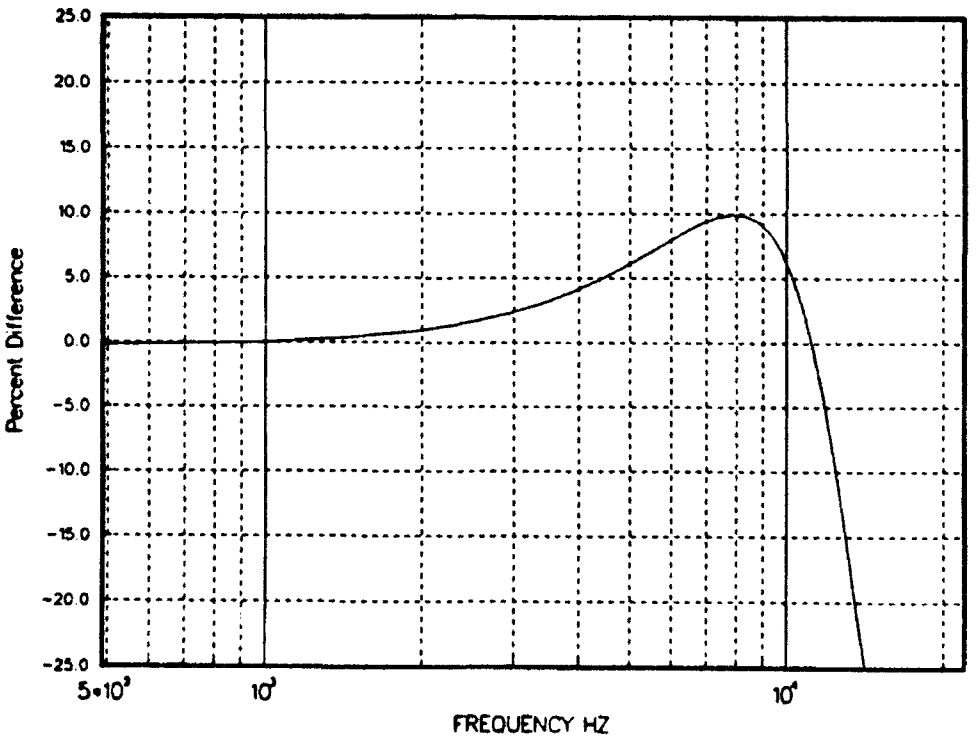

b) Transverse Input

Figure 7: Frequency Response Function Magnitude for the Triaxial Isolation Technique at -50°F with a 5000 g, 70 μs Input Pulse.

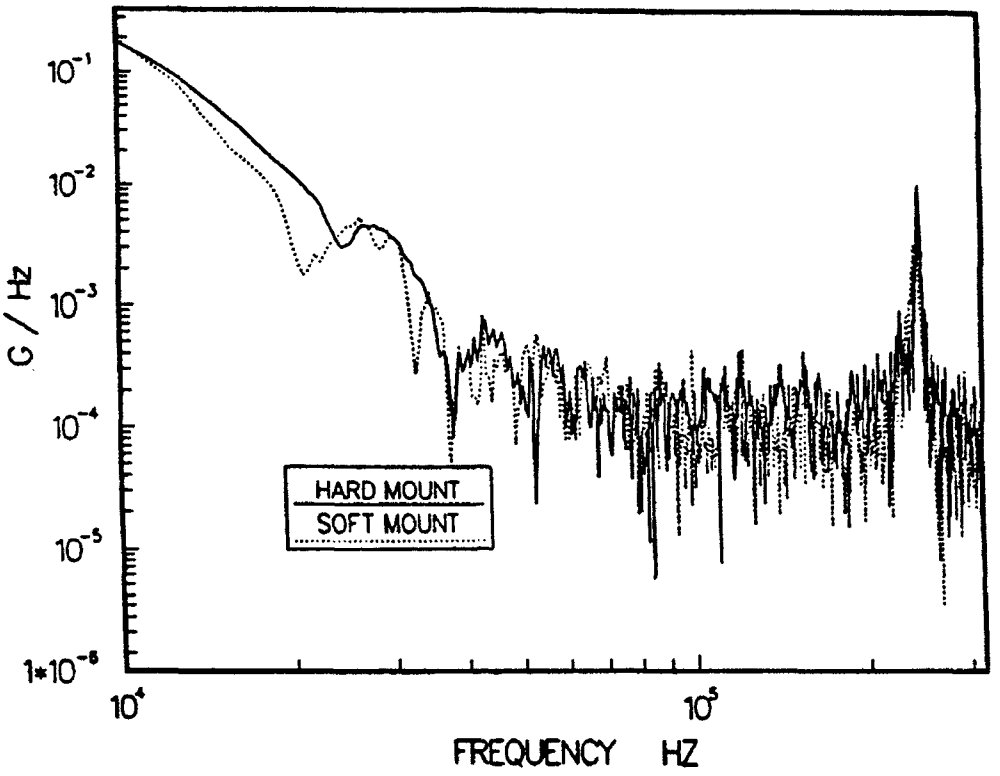

Figure 8: Comparison of Fourier Transforms for a Hard Mounted Accelerometer and One Axis of the Triaxial Isolation Technique with a 5000 g, 70 μs Pulse Input.

where E is the modulus of elasticity and ρ is the density for the Hopkinson bar material. The modulus varies between 102% @-50°F and 97% @+165°F of the nominal value, 16×10^6 psi [16]. The change in density is 0.0015% at either of the temperature extremes and is negligible [16]. The nominal stress wave speed for titanium is $\frac{196,210}{\sqrt{1.02}}$ in/sec. At the cold temperature, the wave speed will increase by $\sqrt{1.02}$ or 1.00995 (1%) in the length of the bar that is inside the temperature chamber, about 2 in. Since the round trip time to the strain gages is measured for the stress wave speed, the stress wave travels twice that distance or 4 in. at about 5 μs/in. It takes 20 μs for the stress wave to traverse this distance. An upper bound for the increase in this time due to the cold temperature is 1% of 20 μs or 0.2 μs. Since the highest resolution available with Shock Laboratory instrumentation is 0.5 μs, this increase in the stress wave speed cannot be measured at -50°F. A similar argument can be made for the decrease in wave speed at the hot temperature; the decrease is about 2% over the 4 in. bar length or 0.4 μs. Again, this change in the wave speed will not be detected with current instrumentation time resolution. These calculations were verified with Hopkinson bar measurements, and consequently, the stress wave speed was not changed for accelerometer calibrations performed at -50°F or +160°F.

A Kistler 805A reference accelerometer (S/N 1886) was used for the second part of the Hopkinson bar evaluation. The 805A has a NIST-traceable

calibration, for both shock and vibration. The 805A was placed on the Hopkinson bar in Figure 3 in the same manner as the accelerometers calibrated. The response of the 805A was compared to the acceleration derived from the strain gages on the bar using a frequency response function. For a nominal pulse duration of 100 μs and three shock levels (4000 g, 10000 g, and 15000 g), an ensemble of five pulses was applied to the reference accelerometer. An example of a shock pulse with its corresponding Fourier transform magnitude measured by the strain gages is shown in Figure 9. Considerable preparation of the Hopkinson Bar data was required before

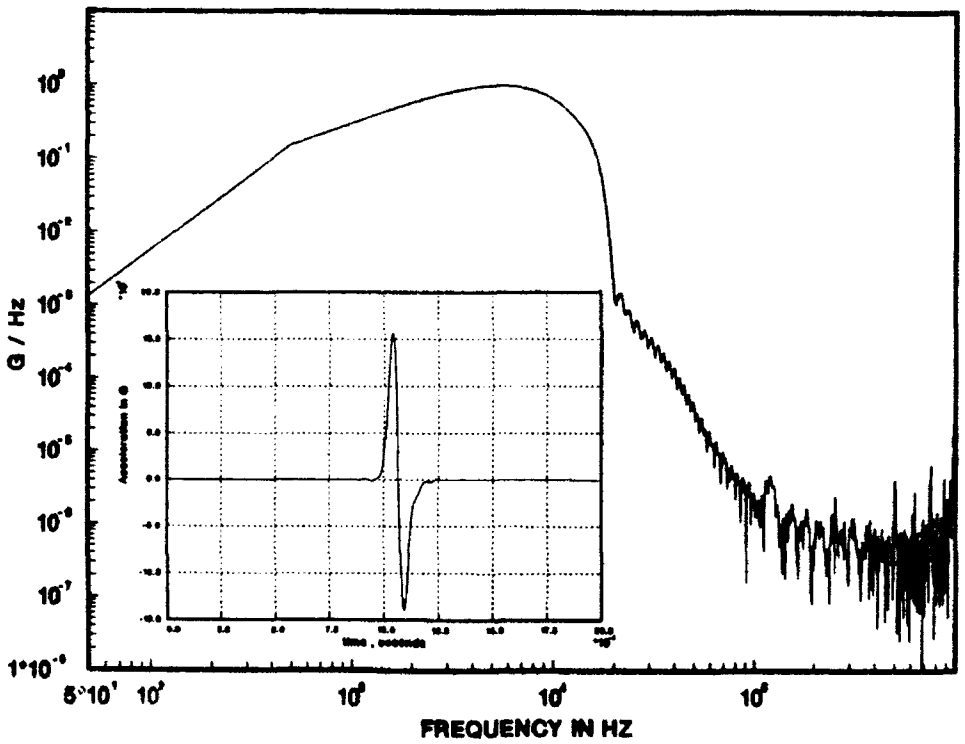

Figure 9: Fourier Transform Magnitude for 15000 G Pulse.

frequency response functions could be calculated. Since an acceleration response to acceleration input frequency response function was desired, the strain data was converted to velocity according to (1). The velocity data were digitally filtered with a ten-pole Butterworth filter whose cutoff frequency of 17 kHz was chosen to reduce the noise created in taking the derivative to obtain the acceleration. The data were filtered in both the forward and backward directions to remove the filter phase shift. The 17 kHz cutoff frequency was determined from an examination of the Fourier transform magnitude. The cutoff frequency for the filter was chosen based on two criteria: 1) the frequency at which the pulse transform becomes noise and 2) the frequency at which the coherence, computed using an ensemble average, between the input and response accelerations deviated from unity. The filter cutoff frequency was chosen higher than the second frequency so that the filter attenuation did not affect the coherent frequency range. Input

acceleration was calculated by taking the derivative of the velocity as described in the previous section. The resultant input acceleration was then shifted in time to account for the wave transit time from the strain gage to the accelerometer assembly. Several tests were performed to determine the correct time shift which was measured as 261 μs. This value is one half the time for the stress wave to travel to the end of the bar and back to the strain gages. The resulting input acceleration data as well as the response data were filtered at 40 kHz with a ten pole Butterworth digital filter in both a forward and backward directions to eliminate filter phase shift and then windowed. A boxcar window tapered with Blackman-Harris cosine functions was applied to prevent leakage errors. The effects of the window and the filter were examined closely to assure that they did not produce any contamination of the data. The magnitude and phase of the frequency response functions, with Hopkinson bar as input and the reference accelerometer as output, were calculated so that a quantitative evaluation could be made of the Hopkinson bar as compared to the reference accelerometer [8]. The frequency response functions for the three different acceleration inputs are shown in Figure 10. Also shown in Figure 10 is the variation of the reference accelerometer sensitivity as a function of frequency for a vibration calibration since the shock calibration data was not available. The senstivity values from the shock calibration and the vibration calibration at 1000 Hz are the same. Each curve is plotted as percent difference from the 1000 Hz value for that curve. The 1000 Hz value was chosen because of noise problems at lower frequencies. The maximum deviations of the Hopkinson bar frequency response functions from the reference accelerometer curve are -1% and +5% at 10 kHz.

A static force calibration, to determine an effective gage factor of the titanium bar, was undertaken as the last part of the certification effort. The bar was placed vertically in a load test machine, manufactured by MTS, and was loaded with a 500 lb compressive load in 50 lb increments. The output of the strain gages was compared to a NIST-traceable calibrated load cell, and a sensitivity for the strain gage, S_{sg}, was calculated in μv/v/lb. The indicated force, F_1, from the bar is then:

$$F_1 = \frac{V_{out}}{S_{sg}\ V_e} \tag{5}$$

where V_{out} is the output voltage from the strain gages as the load is applied and V_e is the excitation voltage on the strain gage bridge. This force, F_1, may be compared to the force measured on the bar, F_2, in response to a shock pulse:

$$F_2 = \frac{2\ E\ A\ V_{out}}{G_f\ V_e} \tag{6}$$

where G_f is the gage factor, E is the modulus of elasticity, and A is the bar cross-sectional area. F_1 and F_2 are set equal to each other in order to

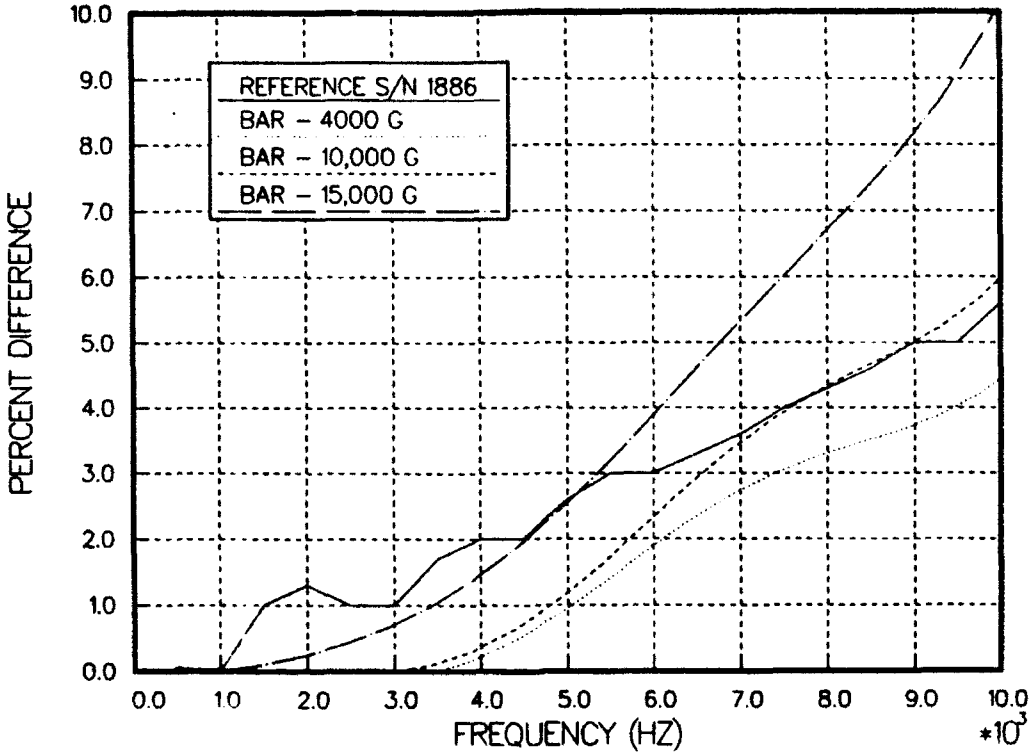

Figure 10: Reference Accelerometer and Hopkinson Bar Frequency Response Functions.

calibrate the output F_2. After common quantities are cancelled, the equality becomes an expression for an equivalent gage factor as:

$$G_f = 2 \cdot E \cdot A \cdot S_{sg} \qquad (7)$$

which has a numerical value of 2.07. This value is 3% lower than the manufacturer's specified value of 2.135. An examination of the numerical values for the frequency response functions, instead of the percent difference shown in Figure 5, reveals that the values at 1000 Hz are ≈1.03 for all three functions. That is, the reference accelerometer is 3% higher than the acceleration derived from the Hopkinson bar which agrees with the 3% lower equivalent gage factor derived from the load test. The peak acceleration values for the Hopkinson bar with a gage factor decreased by 3% and for the reference acclerometer are given in the table below.

The Kistler Model 805A accelerometer, S/N 1886, was calibrated at shock levels of 1000 g, 3000 g, and 10,000 g using traceable, fundamental length and time measurements and certified by the Sandia Primary Standards Laboratory. Their estimate of the uncertainty is +5% of reading (File #4092F). Peak acceleration calculated from the bar data agreed with the peak calculated from the reference accelerometer, 1000 Hz, sensitivity within the +5% uncertainty. The differences averaged 4.3% (three standard deviations = 0.6%) at 4000 g and 1.6% (three standard deviations = 1%) at 10,000 g and

COMPARISON OF CORRECTED HOPKINSON BAR ACCELERATION VALUES WITH REFERENCE ACCELEROMETER

Nominal Peak Value	Corrected Hopkinson Bar Peak Acceleration	Reference Peak Acceleration	Percent Difference
4000 g	4016 g	4189 g	4.1%
	4233 g	4425 g	4.3%
	4044 g	4220 g	4.2%
	4207 g	4402 g	4.4%
	4042 g	4237 g	4.6%
10000 g	10100 g	10240 g	1.4%
	10180 g	10380 g	1.9%
	10370 g	10530 g	1.5%
	10150 g	10360 g	2.0%
	9825 g	9977 g	1.5%
15000 g	16050 g	16320 g	1.7%
	15680 g	15930 g	1.6%
	16590 g	16920 g	2.0%
	14900 g	15080 g	1.2%
	15860 g	16040 g	1.1%

15,000 g. The sum of the reference uncertainty and the maximum of the three standard deviations were added to obtain the estimated uncertainty of 6%. It is felt that the uncertainty should not change as long as the bar suffers no physical damage and the strain gages are not changed.

CONCLUSIONS AND FUTURE WORK

Uniaxial and triaxial isolation techniques for a piezoresistive accelerometer have been characterized over a bandwidth of DC to 10 kHz with a Hopkinson bar. The uniaxial shock isolation technique has demonstrated acceptable characteristics for a temperature range of -50°F to +186°F, and the triaxial shock isolation technique has demonstrated acceptable results for a temperature range of -50°F to 70°F for this bandwidth of DC to 10 kHz. The Hopkinson bar has been certified with a transfer standard with an uncertainty of 6%. The frequency bandwidth for these characterizations and certifications will be extended to 30-50 kHz by the use of a beryllium Hopkinson bar instead of the titanium bar used in these studies. Additionally, characterization of the piezoresistive accelerometer's cross-axis sensitivity, with and without a mechanical isolator, will be studied using the beryllium bar. The low Poisson's ratio and the high stress wave speed for the beryllium will allow these studies.

REFERENCES

1. V. I. Bateman, T. G. Carne, D. L. Gregory, S. W. Attaway, H. R. Yoshimura, "Force Reconstruction for the Slapdown Test of a Nuclear Transportation Cask," ASME Journal of Vibration and Acoustics, Vol. 113, No. 2, 4/91.
2. V. I. Bateman, T. G. Carne, and D. M. McCall, "Force Reconstruction for Impact Tests of an Energy-Absorbing Nose," The International Journal of Analytical and Experimental Modal Analysis, Vol. 7, No. 1, January 1992.
3. D. K. Overmier and M. J. Forrestal, "Experiment for Evaluation of Acceleration Measurement Capability," AIAA Journal, Vol. 13, No. 9, pp.1234-1236, September 1975.
4. D. K. Overmier and P. L. Walter, "A Shock-Isolated Package for an Earth Penetrator Instrumentation System: Design Analysis and Test Results," SAND80-1197, Sandia National Laboratories, October 1980.
5. V. I. Bateman and O. M. Solomon, Jr., "Characterization of Accelerometer Mountings in Shock Environments," SAND86-1606, August 1986.
6. Bateman, V. I., R. G. Bell, and N. T. Davie, "Evaluation of Shock Isolation Techniques for a Piezoresistive Accelerometer," Proceedings of the 60th Shock and Vibration Symposium, David Taylor Research Center, Portsmouth, VA, November 1989.
7. V. I. Bateman, R. G. Bell, F. A. Brown, N. T. Davie, and M. A. Nusser, "Evaluation of Uniaxial and Triaxial Shock Isolation Techniques for a Piezoresistive Accelerometer," Proceedings of the 61st Shock and Vibration Symposium, Vol. IV, October 1990, pp. 161-170.
8. V. I. Bateman, W. B. Leisher, F. A. Brown, and N. T. Davie, "Calibration of a Hopkinson Bar With a Transfer Standard," Proceedings of the 62nd Shock and Vibration Symposium, Vol. III, October 1991, pp. 568-577.
9. R. Davies, "A Critical Study of the Hopkinson Pressure Bar," Philosophical Transactions, Series A, Royal Society of London, Vol. 240, pp. 352-375, January 8, 1948.
10. H. Kolsky, Stress Waves in Solids, Oxford University Press, 1953.
11. J. Cannon and D. Rimbey, "Transient Method of Calibrating a Piezoelectric Accelerometer for the High g-level Range," American Society of Mechanical Engineers No. 71-Vibr-43, ASME Vibrations Conference and the International Design Automation Conference, September 1971, Toronto, Canada.
12. G. Brown, "Accelerometer Calibration with the Hopkinson Pressure Bar," Instrument Society of America preprint No. 49.3.63, 18th Annual ISA Conference and Exhibit, September 1963, Chicago, Illinois.
13. R. D. Sill, "Shock Calibration of Accelerometers at Amplitudes to 100,000 g Using Compression Waves," Proceedings of the 29th International Instrument Symposium, Albuquerque, NM, May 2-6, 1983, pp. 503-516.
14. S. D. Stearns, "Integration and Interpolation of Sampled Waveforms," SAND77-1643, Sandia National Laboratories, January 1978.
15. S. D. Stearns, Digital Signal Analysis, Hayden Book Company Inc., 1975, pp. 37-40.
16. Metallic Materials and Elements for Aerospace Vehicle Structures, MIL-HDBK-5E, June 1987, Section 5.4.1.18.

DYNAMIC PRESSURE CALIBRATION INSTRUMENTS AND SENSOR TRANSIENT RESPONSE

J.F. Lally
PCB Piezotronics, Inc.
Depew, N.Y.

June 22-24, 1993

ABSTRACT:

The NIST recently (4-91) held a workshop which focused on transient pressure and temperature measurement. Based on the papers presented and discussions that followed, the age old question relative to static vs dynamic response of a pressure sensor, is alive and well.

According to the NIST workshop summary report, "Because there is no traceability to NIST for transient pressure or temperature measurements, laboratories that need to make such measurements are left to their own resources to develop calibration and testing programs". As a result, PCB and other companies have developed for in-house needs, calibration instruments to validate the transient response characteristics of their pressure sensors and provide NIST traceability. Transient pressure calibration is generally accomplished by rapidly venting to the sensors diaphragm an accurately known NIST traceable static reference pressure, in milliseconds or tens of microseconds.

Several companies offer commercial hydraulic and pneumatic pulse, step, sine, and shock pressure generators for transient response testing and calibration of pressure sensors over limited amplitude and frequency ranges. To the author's knowledge, no calibration instrument exists to calibrate any pressure, force, shock or vibration sensor at all amplitudes and all frequencies, let alone under all environmental conditions.

This paper surveys commercially available dynamic calibration instruments. It traces transient response testing of a quartz pressure sensor through five different calibration techniques, including static, step, pulse, and shock tube methods over a wide amplitude and frequency range. Test results include sensor sensitivity for each calibration method, calculation of "mean" sensitivity and standard deviation for all five methods.

New "Ultima"
Dynamic Pressure Calibrator

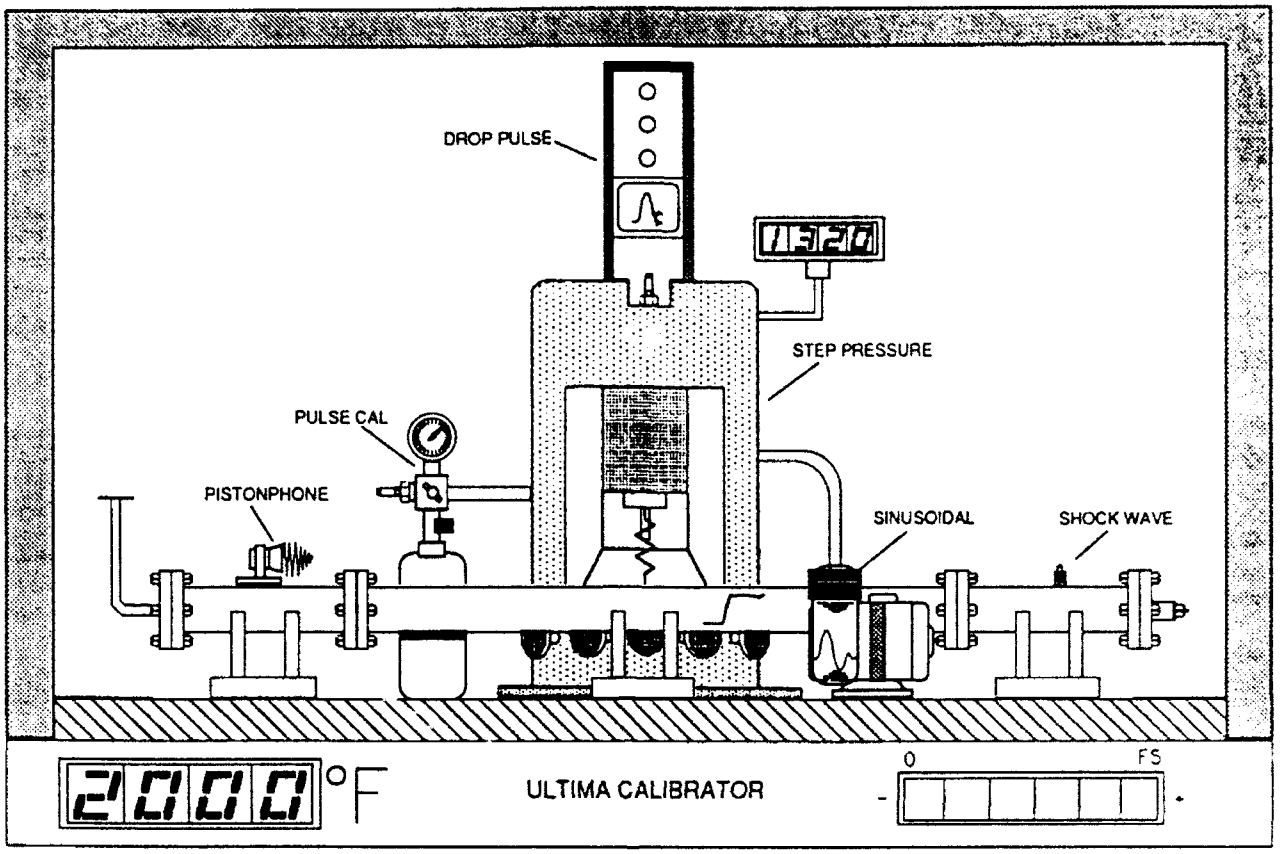

Provides a continuously adjustable step, pulse or sine wave pressure of known amplitude from:

0.00001 psi to 500,000 psi
DC to 10 MHz
Absolute 0 to +2,000 °F

- Computer Controlled
- Automatic, Self Compensating
- Complete with all the Bells and Whistles
- Economically Priced at $99.95
- Delivery from Stock
- NIST Traceable

Manufactured by
"VISIONARY" Calibrator Co.
UTOPIA, USA

Obviously, it would be nice if the "ULTIMA" dynamic calibration device existed. Even if it did exist, I'm not sure how it could be "calibrated". If the "ULTIMA" calibrator were dismantled, you would find it is made up of several individual special purpose calibration devices - each designed to dynamically calibrate pressure transducers over a limited pressure, frequency or temperature range. Each calibrator would pretty much represent the current state-of-the-art for dynamic calibration over the specific operating range of the device.

In 1972, the American Society of Mechanical Engineers established "A Guide for the Dynamic Calibration of Pressure Transducers". The guide was originally published as American National Standard ANSI B88.1-1972;
however, the current number is ANSI MC88.1-1972 (see page 3).

The ANSI calibration guide defines calibration as follows:

> "Calibration means a test during which known values of measurand are applied to a transducer and corresponding output readings are recorded."

The ANSI document then proceeds to qualify expectations for lower accuracy and the somewhat more difficult nature of dynamic calibration;

> "The degree of accuracy associated with these dynamic tests is generally lower, and the manner in which the results are used is generally less rigorous than in the conventional and more easily controllable field of static pressure calibration."

Much of the dynamic pressure calibration equipment used today has evolved out of the transducer manufacturer's necessity to test and calibrate his products, and by the customers' need for in-house capability to test and calibrate transducers more closely to the customers' actual application requirements. A wide variety of calibration devices exist, some of which are offered as commercial products. Several described in the ANSI Dynamic Calibration Guide include:

- PISTONPHONE
- PULSE CALIBRATORS USING FAST-ACTING VALVES
- SINUSOIDAL PRESSURE GENERATORS
- IMPULSE DROP CALIBRATORS
- SHOCK TUBE

Most of the above are traceable to the NIST through an accurate DC reference gage, comparison transfer standard transducer or calculations of physical quantities of mass, gravity, velocity and temperature.

AMERICAN NATIONAL STANDARD

A Guide for the Dynamic Calibration of Pressure Transducers

ANSI B88.1 - 1972

[Note: The current number for this standard is ANSI MC 88.1-1972]

SECRETARIAT

THE AMERICAN SOCIETY OF MECHANICAL ENGINEERS

PUBLISHED BY

THE AMERICAN SOCIETY OF MECHANICAL ENGINEERS

United Engineering Center 345 East 47th Street New York, N. Y. 10017

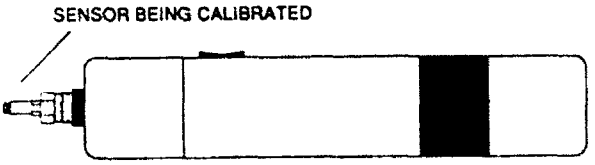

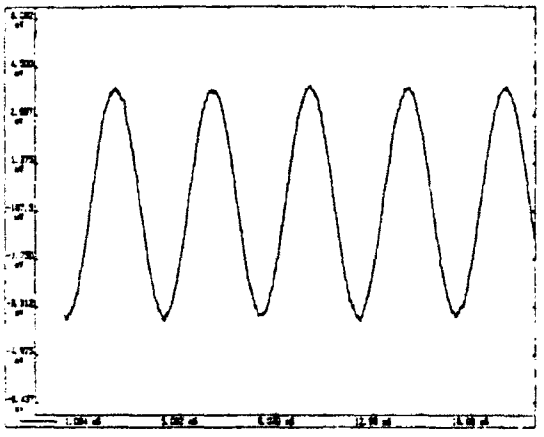

Pistonphone Output 124 dB, 250 Hz

PISTONPHONE

The pistonphone is designed to provide a precision sound reference source at a fixed frequency and amplitude for calibration of low pressure acoustic sensors. It is usually pack aged in a compact, portable battery-powered configuration. Calibration accuracy is claimed to be ± 0.2 dB with certain specified microphones.

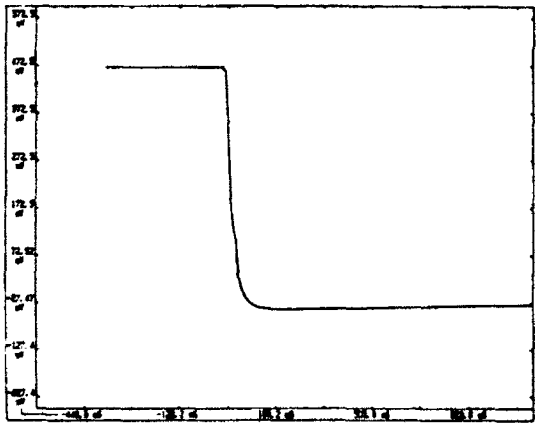

Pressure Release 100 psi
Response Time 60 ms

NIST TRACEABILITY - Dead Weights

DEAD WEIGHT TESTER USED AS A PRESSURE RELEASE CALIBRATOR

The dead weight tester is designed and most commonly used for static calibration of DC type *pressure transducers* such as strain gages, capacitive, piezoresistive, or quartz piezotypes exhibiting long discharge time constants.
The dead weight tester can also be used dynamically in the pressure release mode for transducers whose output characteristics in response to pressure rise and pressure drop have been determined to be the same.

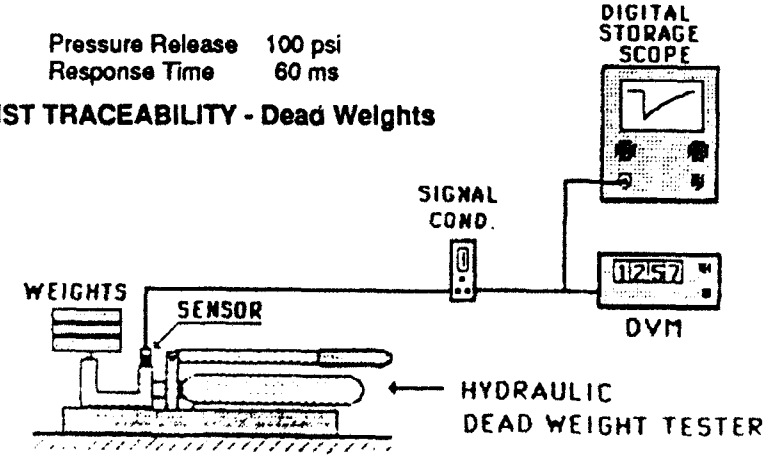

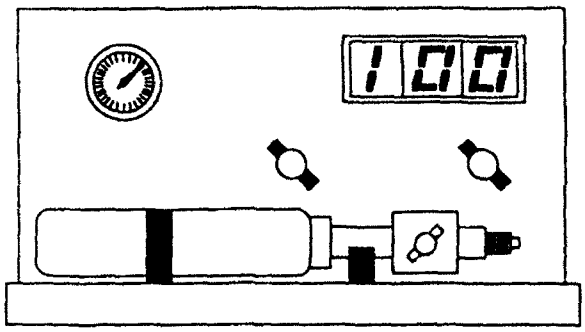

Pneumatic Pulse Calibrator
PCB Model 903A

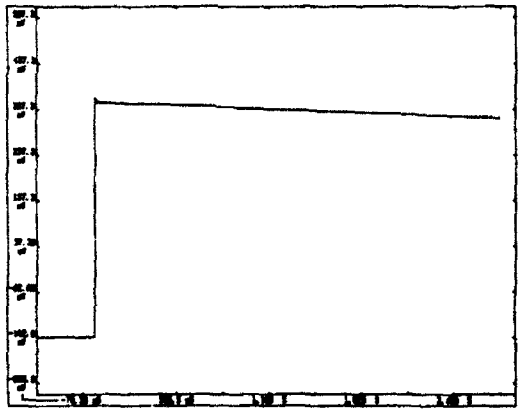

Step Pressure 100 psi
Rise Time 5 ms

NIST TRACEABILITY - DC Reference Gage

PNEUMATIC PULSE CALIBRATOR USING FAST-ACTING VALVES

A number of hydraulic and pneumatic pulse calibration devices have been built using manual or solenoid valves. The device at left uses a digital pressure gage to set an accurate static reference pressure. A manually actuated, fast-acting valve quickly switches the pressure sensor to the reference pressure is produces a positive- going pressure pulse of known amplitude with 5ms rise time. It is more difficult to produce a positive-going step pulse than a negative pressure drop. Major concern with pulse calibrators involves reducing rarefaction waves in the pressure volume associated with the valves.

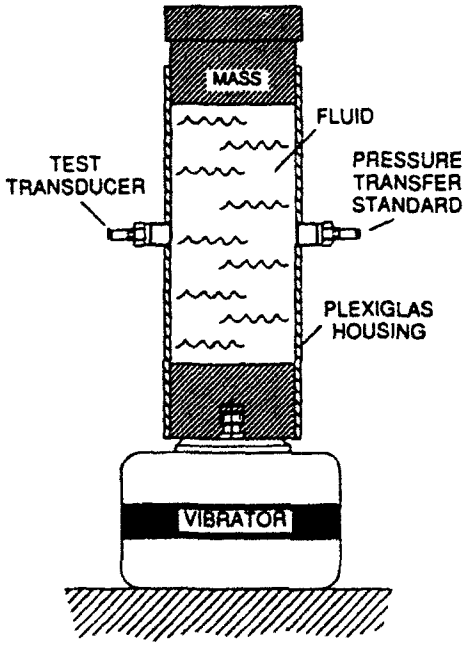

NIST TRACEABILITY - Secondary Pressure Transfer Standard

VIBRATING COLUMN OF LIQUID

This calibration method adapts vibration transfer standard techniques to pressure calibration. An electrodynamic shaker vibrates a column of fluid which generates a sinusoidal pressure wave. Output from sensor being calibrated is compared with transfer standard.

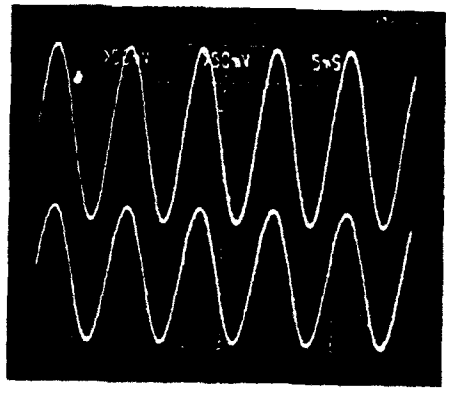

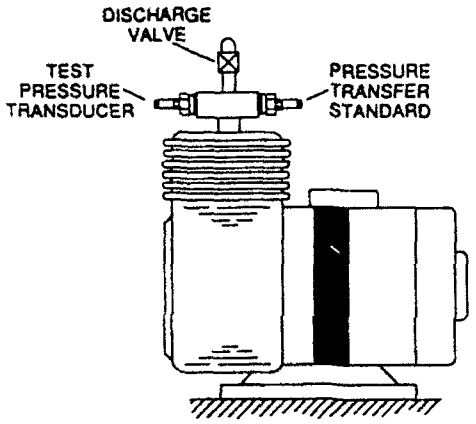

SINUSOIDAL PRESSURE GENERATORS

A small air compressor has been modified to generate a repeatable sine wave output for comparison calibration with a transfer standard. Pressure amplitude can be adjusted by opening or restricting the discharge valve. Frequency is fixed at motor speed. This method of calibration conveniently adapts to temperature coefficient calibration by plumbing test transducer inside oven and transfer standard outside.

Pressure Adjustable	3 to 30 psi
Frequency Fixed	29 Hz

NIST TRACEABILITY - Dynamically Calibrated Secondary Transfer Standard.

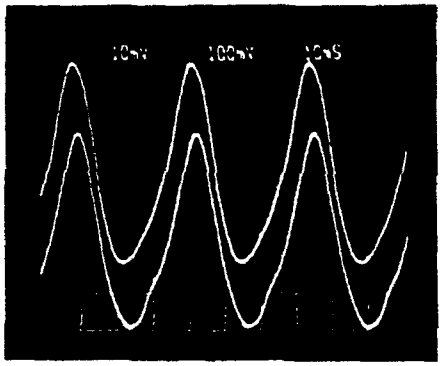

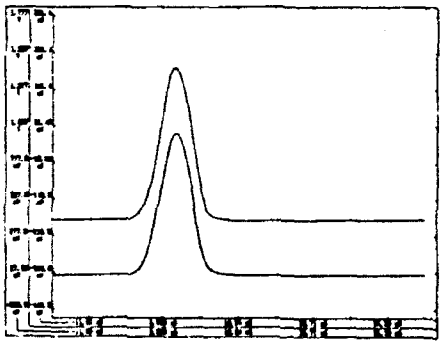

DROP PULSE CALIBRATOR

The drop pulse calibrator uses a tourmaline transfer standard to measure the hydraulic pressure pulse from a mass impacting a piston and cylinder manifold. The drop calibrator has capability to generate a wide range of dynamic pressures from about 100 to 20,000 psi with relative ease. Rise time is about 3ms and pulse duration 6ms. Another manufacturer offers a commercial high pressure version of this type of calibrator which uses calculations of mass based on gravity, velocity, and piston area to determine reference pressure.

Pressure	969.3 psi
Rise Time	3 ms
Duration	6 ms

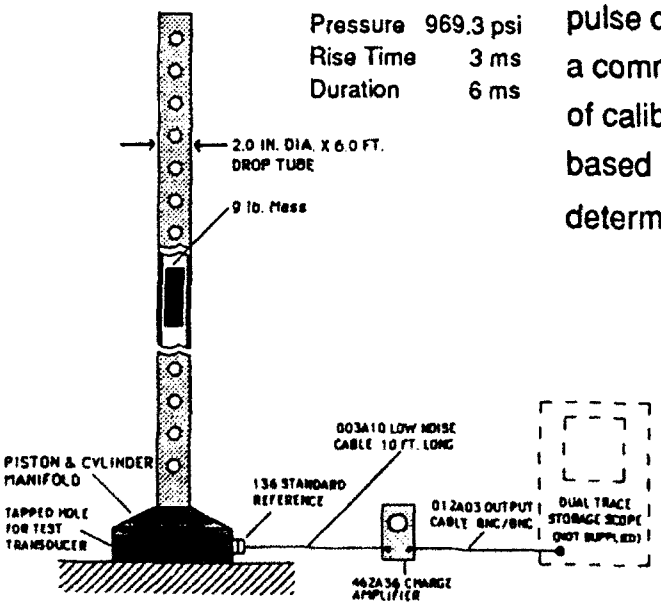

Impulse Calibrator
PCB Model 913A

NIST TRACEABILITY - Through Dynamically Calibrated Model 136A Tourmaline Transfer Standard.

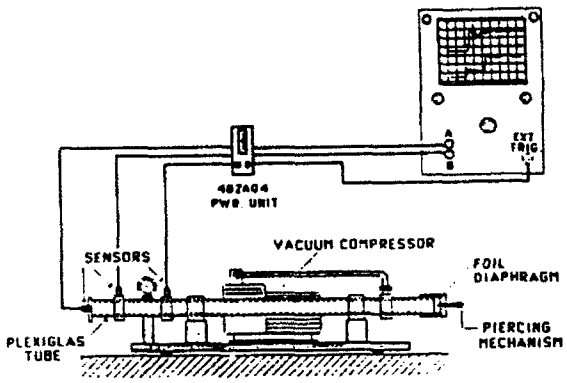

Instrumented Shock Tube, Model 901A02
Atmospheric Driven (3 ft. x 1 1/2 in. diameter)

SHOCK TUBES

Simple atmospheric-driven plexiglas shock tube generates low pressure shock waves for resonant frequency determination of pressure transducers and gas passages associated with recessed diaphragms or recessed mounting. NIST traceability for determination of transducer or passage resonance through electrically calibrated measurement instruments.

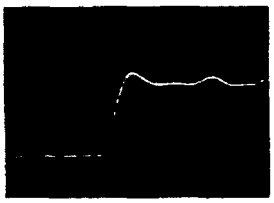

Shock Response from Accel-compensated Transducer

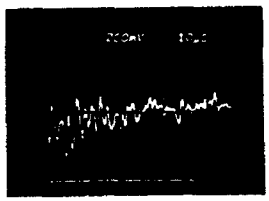

Shock Response from Non-compensated Transducer

CALIBRATION SHOCK TUBE

The helium or air-driven shock tube is capable of producing shock waves with nanosecond rise times at pressures from 3 psi using foil diaphragms to >1,000 psi with sheet aluminum diaphragms. Shock pressure calibration agrees within 3% of other calibration methods. A cone shaped adaptor installed at the end of the shock tube test section amplifies reflected pressures to >10,000 psi. The cone adaptor, although not suited for calibration purposes, is useful for developing high pressure, high temperature shock waves for testing thermal and mechanical shock capability of pressure sensors.

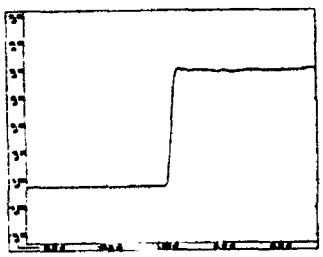

Incident Pressure
134A Pressure Bar
Pressure 123 psi
Rise Time 3 µs

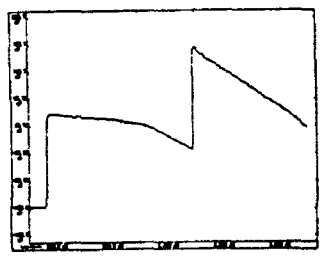

Incident Pressure
113A21 ICP Transduce
Pressure 5 psi
Rise Time 8 µs

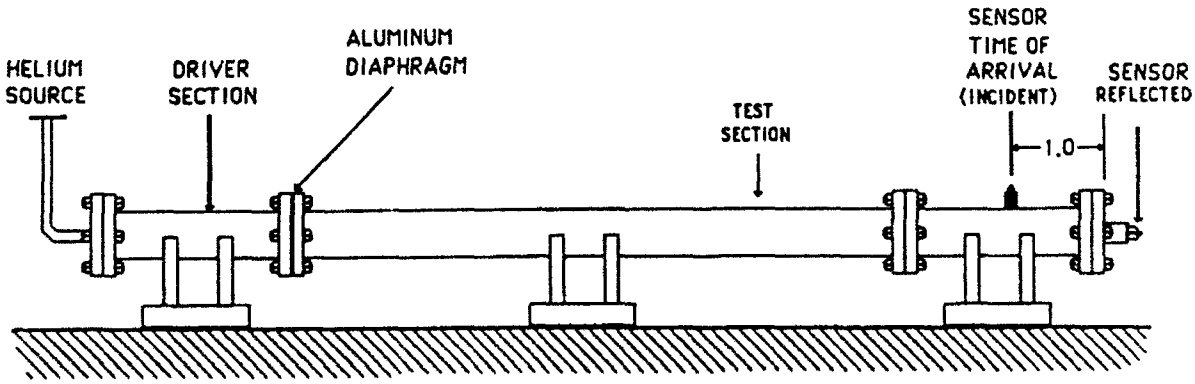

Calibration Shock Tube, Model 901A10
(6 ft. x 3 in. diameter)

Amplitude of shock pressure step is calculated from:
Velocity
Initial absolute pressure
Temperature

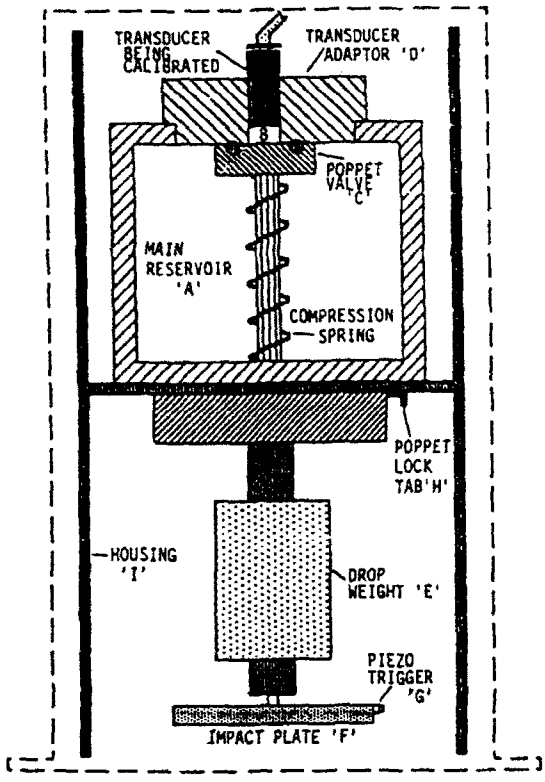

ARONSON SHOCKLESS PRESSURE STEP GENERATOR

The "Aronson" Shockless Pressure Step Generator is a step toward combining capabilities of several of the special purpose calibrators into one device. Capabilities include the use of high accuracy digital reference pressure standards and fast-acting poppet type valves to produce positive or negative step pressures with rise times approaching those of shock tubes.

The Aronson Step Pressure Generator was developed by Phil Aronson and Robert Waser at the U.S. Naval Ordinance Laboratory. Their primary objective was to develop a device capable of performing dynamic step pressure calibration with greater accuracy, speed and ease than was possible with the shock tube. Phil Aronson dedicated much of his professional career to transient pressure measurements and dynamic calibration. After acquiring a license agreement with the Navy, PCB named the calibration device after Phil who passed away in the early 1980's.

The Aronson Step Pressure Generator consists of:

Main Pressure Reservoir "A"
Transducer Adaptor Plug (three sizes)
Spring-loaded poppet valve (three sizes)
A secondary pressure reservoir "B" at poppet valve/diaphragm interface
Impact weight for poppet valve release
Trigger output
Precision Valves for adjusting the gas pressure in both reservoirs
A durable housing and support system
Two each: digital reference pressure gages (optional)
Helium gas pressure source is provided by the customer

The concept and operation of the Aronson Step Pressure Generator is quite fundamental. It simply involves applying to the transducer an accurately known static pressure very quickly. This is accomplished by pressurizing the main reservoir "A" with an accurately measured static pressure and then exposing the transducer to the reference pressure by releasing the quick-opening poppet valve. The pressure drop in the main reservoir due to the added volume between the transducer diaphragm and poppet valve is negligible with flush diaphragm pressure sensors. Any pressure drop would be indicated by the digital pressure gage which monitors pressure in the reservoir.

The "Aronson" Step Pressure Generator has two separate pressure reservoirs (A & B) in which the pressure is controlled by accurate static digital pressure gages. In addition to the main pressure reservoir "A", pressure between the poppet valve and the diaphragm of the transducer (reservoir "B") can be pressurized with a known static pressure. Having control of a known pressure in each reservoir offers unique capability to compare static vs. dynamic response, and provide small incremental pressure steps at higher static levels.

Rise time of a step pressure depends on:

1. type of gas used (helium recommended for fastest rise time)
2. diameter of poppet valve
3. initial pressure difference across the poppet valve
4. design of transducer diaphragm (flush or recess)

Traceability to NIST is through calibration of accurate DC reference gages, used to set the known static pressure level which the transducer under calibration is being rapidly switched to.

ARONSON SHOCKLESS
PRESSURE-STEP GENERATOR
Model 907A

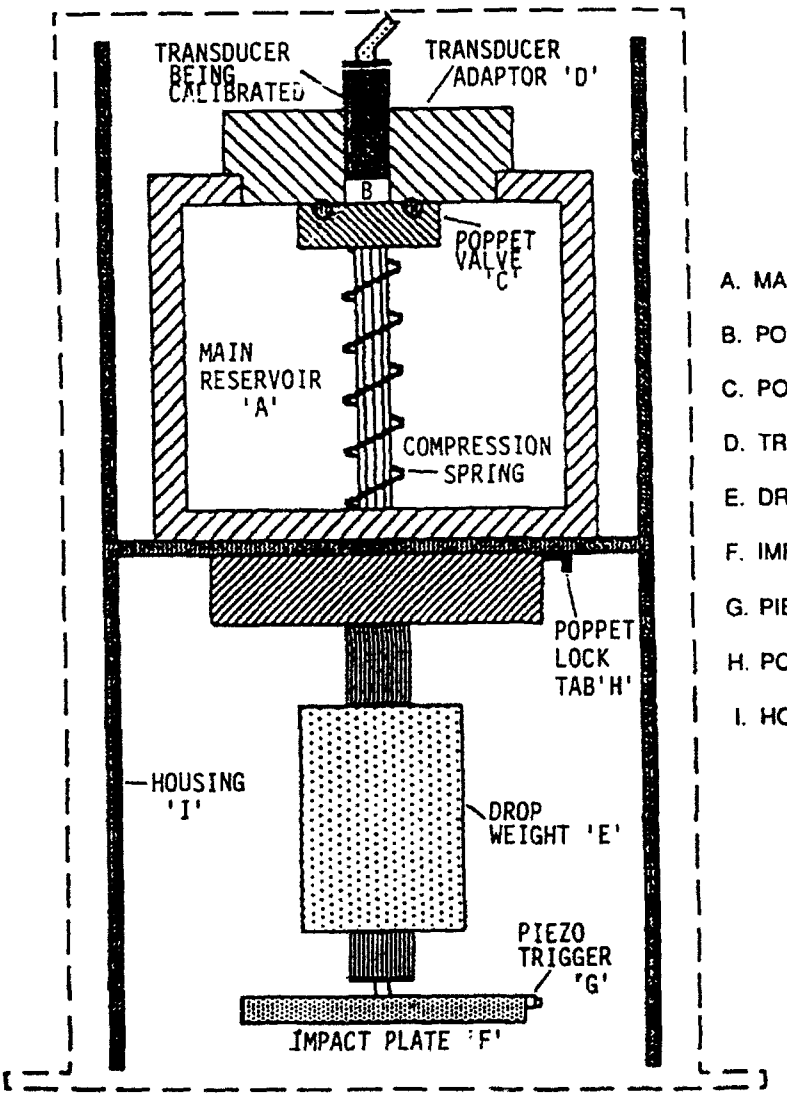

A. MAIN PRESSURE RESEVOIR
B. POPPET VALVE VOLUME
C. POPPET VALVE
D. TRANSDUCER MTG. ADAPTOR
E. DROP WEIGHT
F. IMPACT PLATE
G. PIEZO TRIGGER
H. POPPET LOCK TAB
I. HOUSING

MECHANICAL SYSTEM DIAGRAM

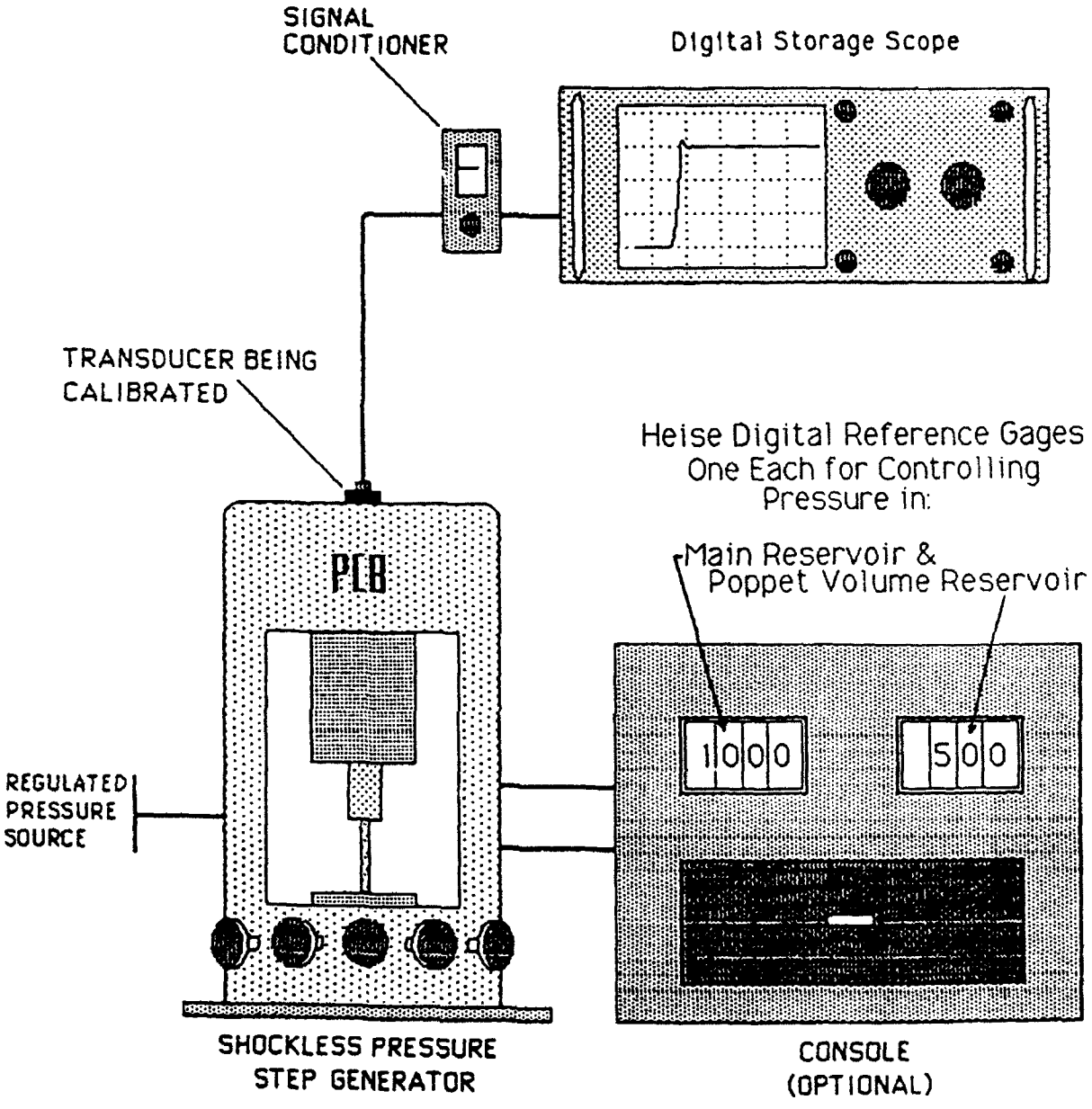

TYPICAL CALIBRATION SYSTEM USING SHOCKLESS PRESSURE-STEP GENERATOR

PCB®
PIEZOTRONICS

NEW SIMPLIFIED MODEL 907A07
ARONSON SHOCKLESS STEP PRESSURE GENERATOR

The standard Model 907A Aronson Step Pressure Generator is a versatile tool capable of performing a wide variety of sensor calibration and test functions. The very nature of its versatility introduces some complexity in operation and slows down basic functions such as generation of positive-going step pressures.

Since many customers use the SPG (Step Pressure Generator) as a single function device, a more simple, faster operating, lower-cost design has been developed. This simplified version maintains the basic structure and operating concept of the 907A. Simplification was achieved through elimination of three, 22-turn, fine-adjust metering-type valves and replacing the other three with two coarser 8-turn control valves with .080" orifices and one 1/4-turn ball-type dump valve. The simplified SPG design uses only one precision Heise digital-type gage for setting a known static reference pressure in the main reservoir.

Elimination of the more costly metering type valves, the Heise reference gage (used to set the poppet valve reference pressure) and reduced labor involved with plumbing the device, has simplified operation and lowered the cost of the Step Pressure Generator with minimum effect on performance characteristics.

PERFORMANCE CHARACTERISTICS:

The simplified SPG (Step Pressure Generator) is designed primarily for quickly and simply generating positive-going known step pressures to 2000 psi with rise times in the order of 30 to 50 microseconds, depending on the type of gas used..

The positive-going, known step pressure can be used for:

* Accurate dynamic calibration of pressure sensors
* Comparison of static vs dynamic calibration
* Determining;
  - Sensor and system discharge time constant
  - Rise time of lower frequency type sensors - strain gages
  - Passage resonances
* Troubleshooting - response, erratic, etc.

The simplified SPG can also be used for vacuum step pressure calibration. The main test function sacrificed by design simplification is the capability to calibrate small pressure changes at higher static levels which may be important for underwater type sensors.

CONVERTING THE STANDARD 907A SPG TO THE SIMPLIFIED DESIGN;

There are two options for converting the PCB Mod 907A to the 907A07 simplified design:

1.) Customer Modification: PCB offers a modification kit complete with high pressure rated, stainless steel valves, plumbing, hardware and instructions for customer modification. The modification kit is priced at $985.00.

2.) Factory Modification: The 907A can be returned to PCB for modification, test and checkout for $1475.00.

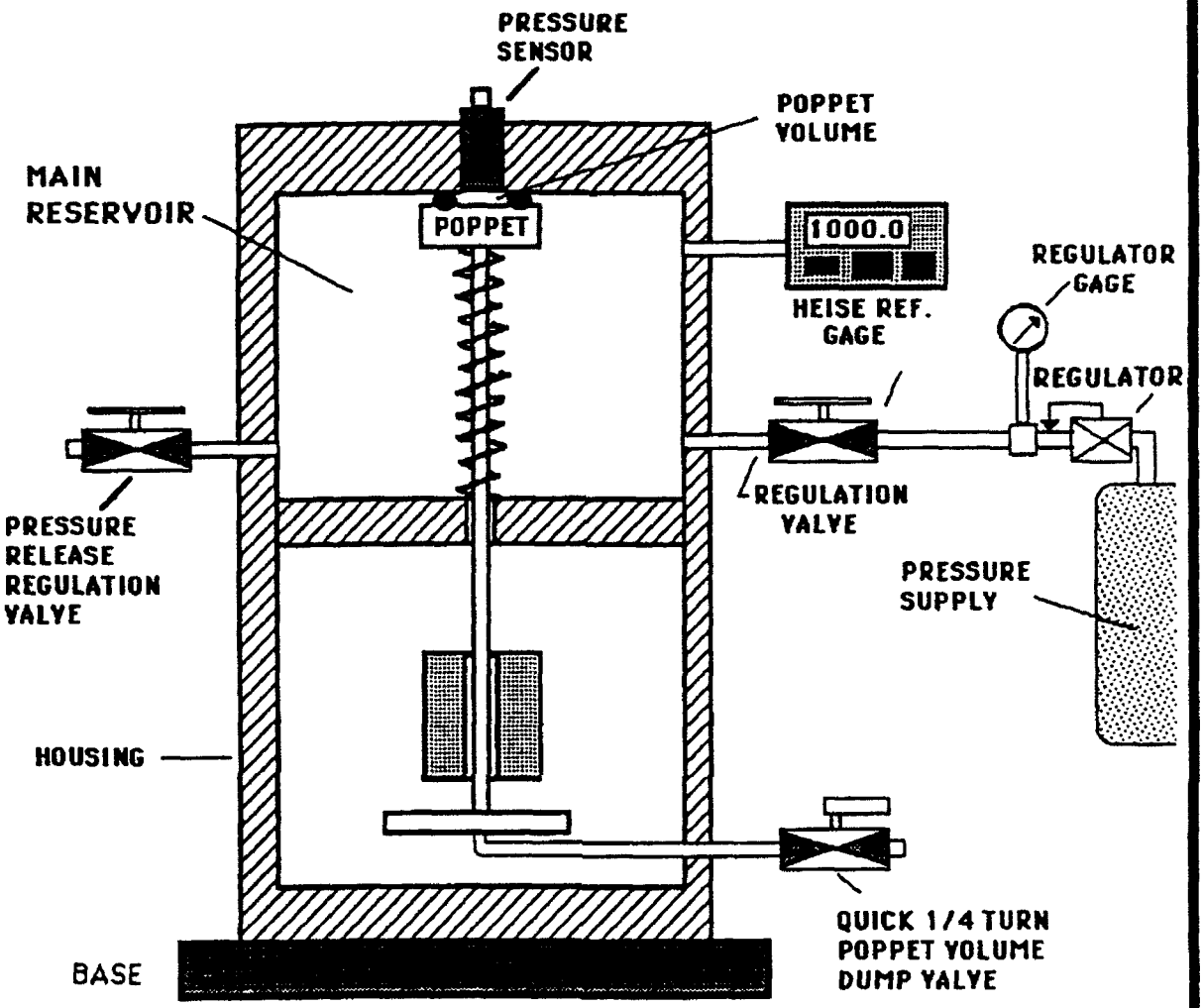

MODEL 907A07
SIMPLIFIED
ARONSON SHOCKLESS PRESSURE STEP GENERATOR
(INCLUDES HEISE DIGITAL REF. GAGE)

PCB®
PIEZOTRONICS

Calibration and test capabilities of the Aronson Step Pressure Generator include:

1. Dynamic calibration of pressure transducers. Oscillations of 71k Hz at peak of the pressure is due to the rarefaction waves at the interface of the poppet valve and transducer diaphragm.

Dynamic calibration of 113A24 ICP Pressure Transducer using Aronson Step Pressure Generator:

Pressure	1000 psi
Transducer Sensitivity	5.3 mV/psi

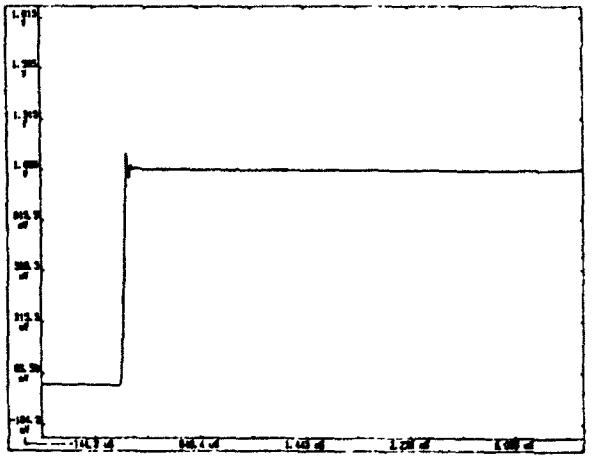

2. Determination of the RC time constant of an entire pressure measurement system including the transducer, signal conditioner and readout.

Discharge Time Constant (DTC)
Time required for a transducer or measurement system to discharge its signal to 37% of the original value from a step change of pressure.

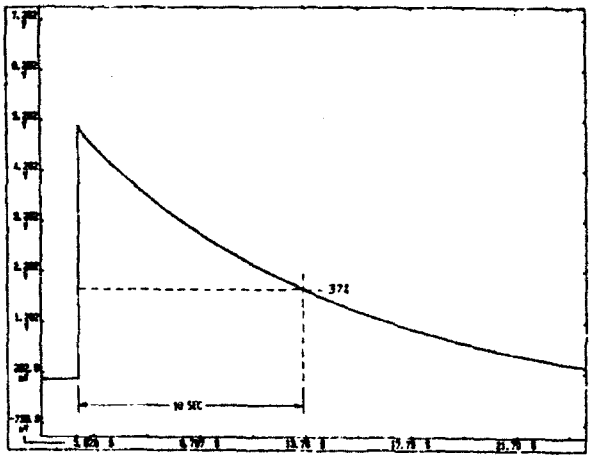

3. Determination of response time and resonance of recessed cavities and passages. Model 113A24, ICP® Pressure Transducer recess mounted 0.050 inch with 150 psi step change in pressure.

Resonant frequency of 0.050 recessed passage

Frequency	24.8k Hz
Rise Time	71 µs
Pressure Step	150 psi

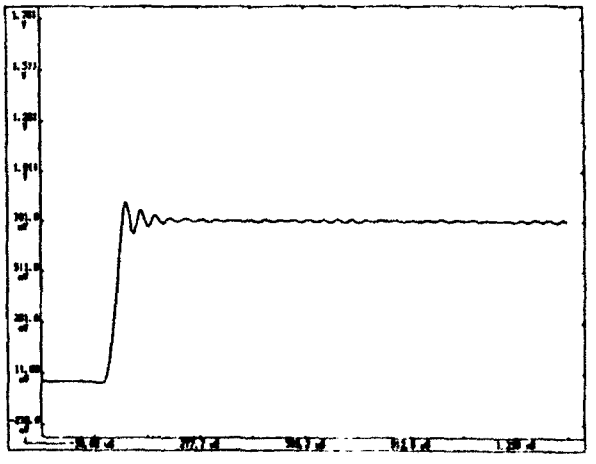

4. Calibration of incremental pressure steps above or below preset static levels. It is possible to simulate the static pressure environment on the sensor diaphragm that might be encountered in an underwater environment while applying a step pressure of known amplitude.

5. Comparison of static and dynamic calibration of a pressure transducer using the same pressure amplitude in the same device without moving the transducer.

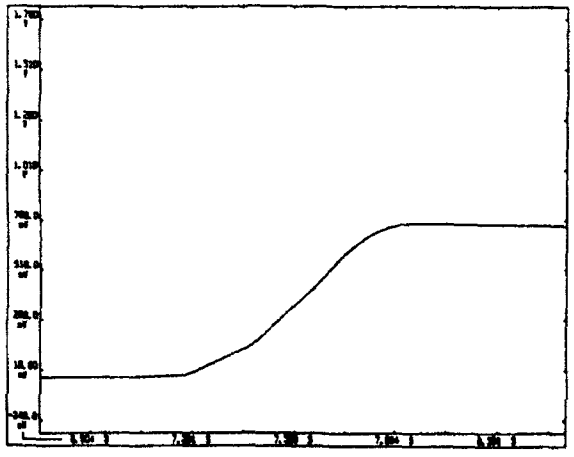

Slowly applied pressure, 150 psi

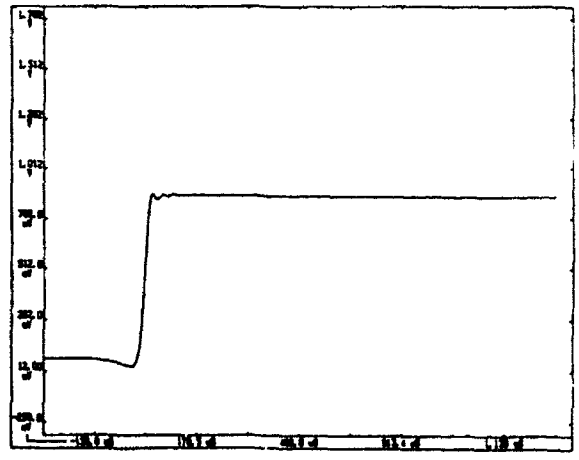

Step pressure of same 150 psi
Rise time < 50 µs

6. Accurate dynamic calibration of pressure transfer standards used in other types of dynamic calibrators, e.g., sinusoidal and drop-pulse calibrators.

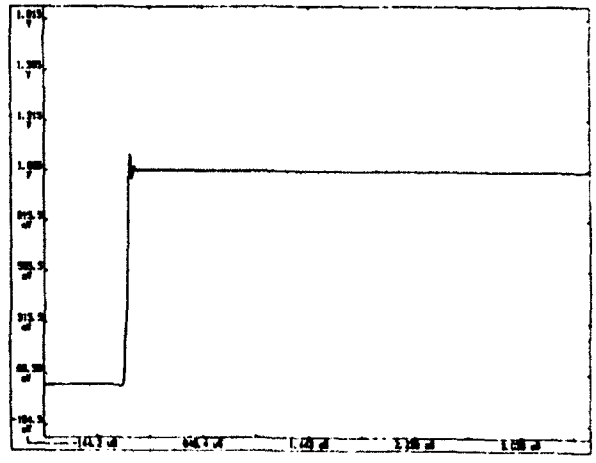

Dynamic calibration of 113A24 ICP Pressure Transducer using Aronson Step Pressure Generator
1000 psi, 5.3 mV/psi

7. Vacuum step pressure calibration.

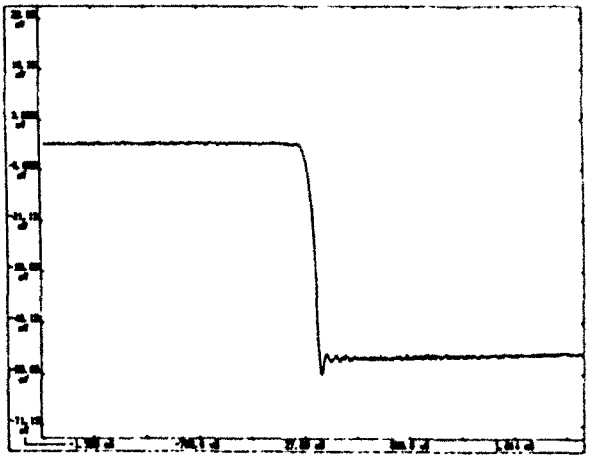

Vacuum step pressure calibration, Model 113A24 ICP Pressure Transducer, -10 psi, 5.34 mV/psi

8. Checkout and troubleshooting of dynamic pressure transducers, expecially those used for shock and blast wave measurements.

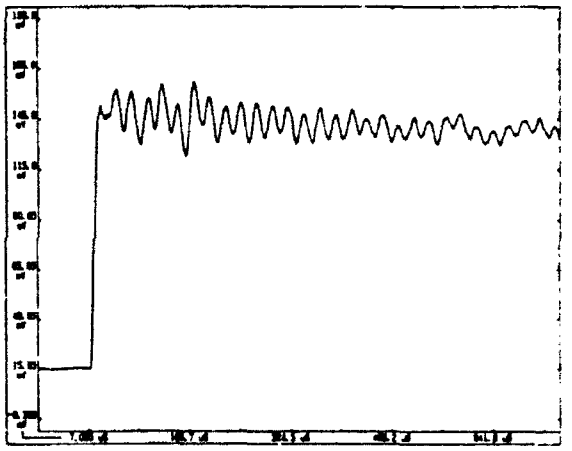

Step pressure calibration detects noise created by defective transducer diaphragm.

9. Pulse calibration detects signal breakup due to erratic connection and resultant zero shift.

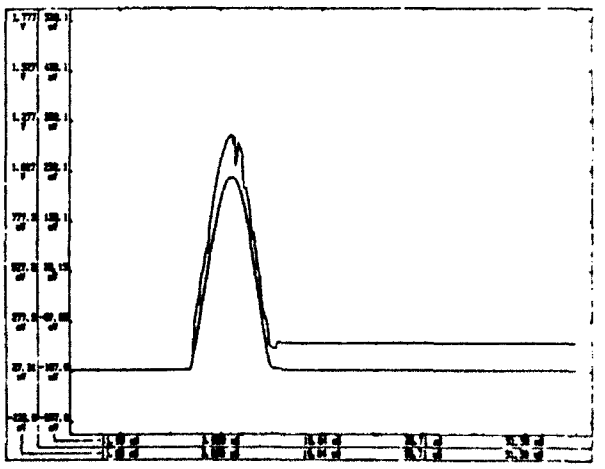

During the process of accumulating calibration data for this report, sensitivity of Model 113A24 ICP Pressure Transducer was recorded and plotted using five different methods of calibration. Sensitivity deviations for the methods was less than ± 1 1/2 %.

Legend:

△ *Dead Weight Test*
□ *Hydraulic Drop Test*
X *Shock Tube Calibrator*
○ *Aronson Shockless Calibrator*
● *Pneumatic Pulse Calibrator*

Mean (y)=5.20942
Standard Deviation (y)=0.06667

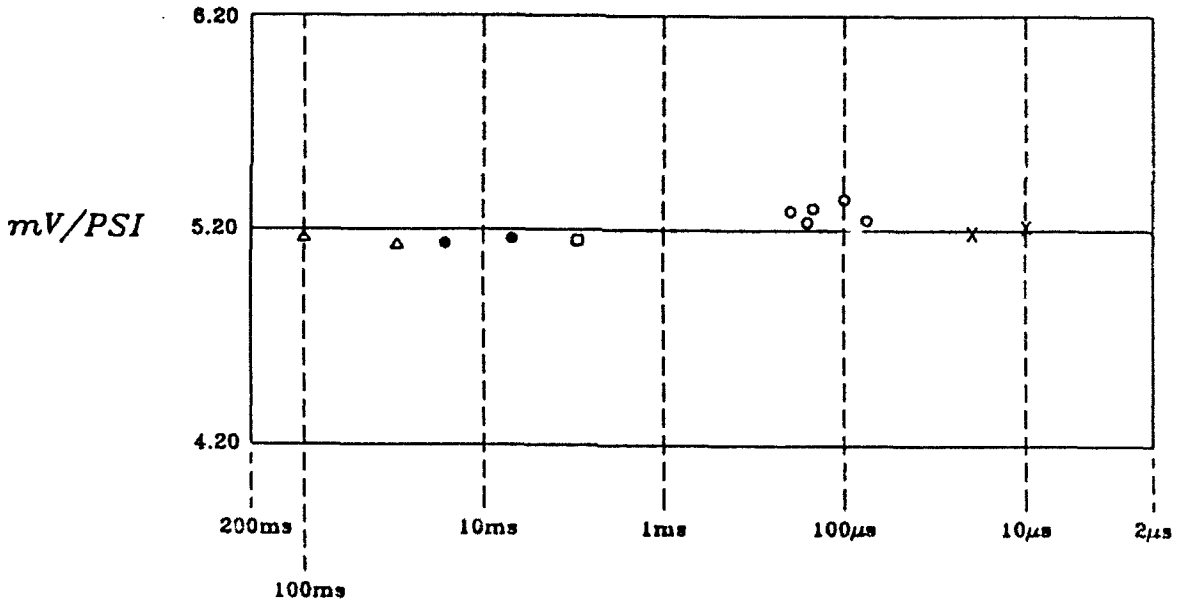

Calibrations of a 113A24 Quartz Pressure Sensor using five different calibrators over a pressure range from 100 to 1000 psi.

A second calibration test program was run on a single ICP pressure sensor over a narrow pressure range from 50 to 100 psi to establish sensitivity correlation by five different calibration methods. The 50 to 100 psi range was selected as the ideal operating range of the shock tube since the pressure wave is well formed at this level.

In order to increase the objectivity and credibility of the test, a pressure sensor with non-standardized sensitivity was selected and each calibration was performed by a different technician without knowledge of previous calibration data.

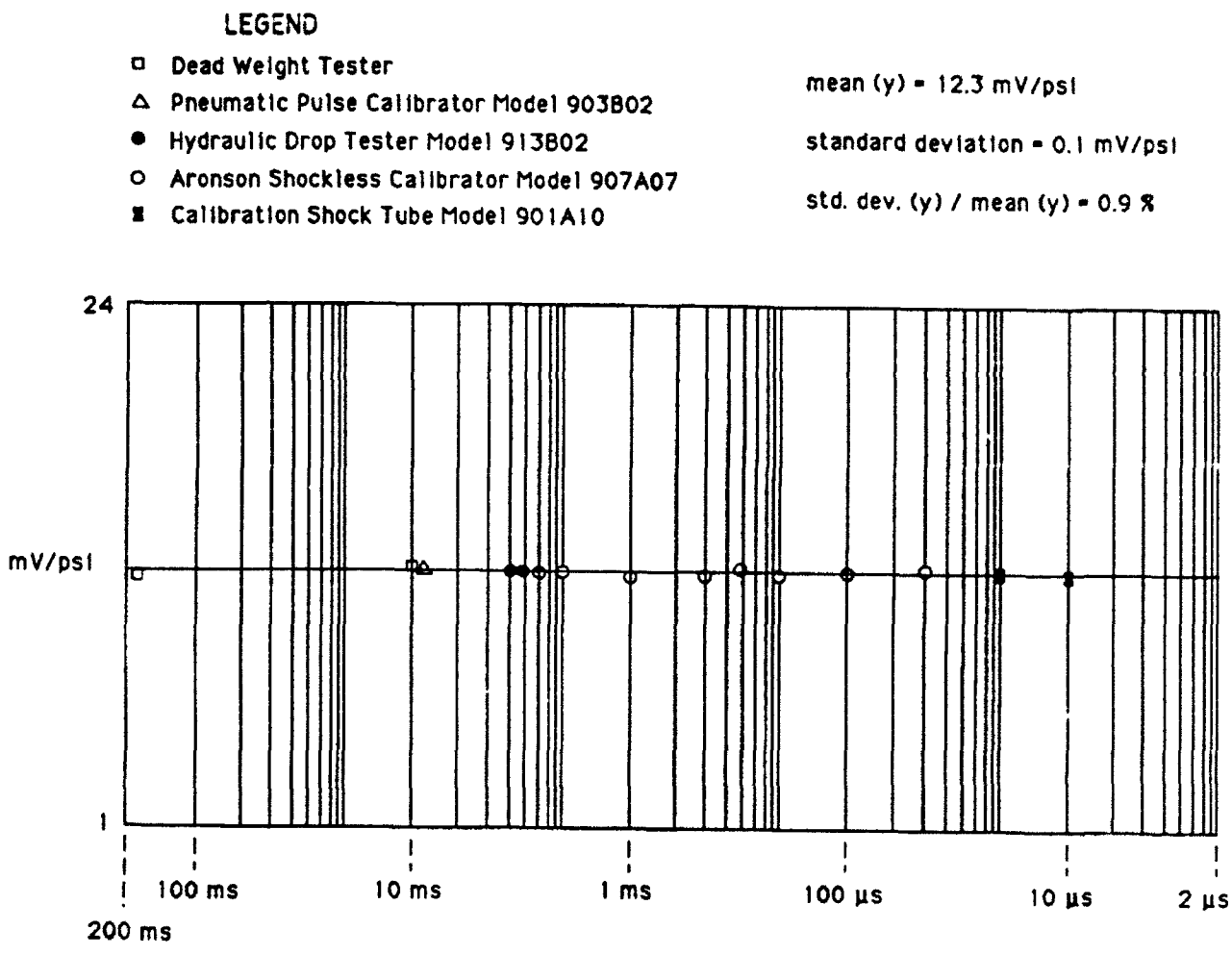

Calibration of a 113A24 Quartz Pressure Sensor
by Five Different Procedures from 50 to 100 psi.

While the Aronson Calibrator has not equaled the performance capability of the "Ultima" calibrator, it is a step in that direction. The digital storage oscilloscope has significantly improved the accuracy of dynamic calibration. Dynamically calibrated pressure transfer standards have also contributed to improving the accuracy of sinusoidal and drop-test impulse calibrations.

◊◊◊◊

Acknowledgement:

The author would like to thank Ben Granath for providing most of the test results used in this paper.

MULTIFUNCTION TRANSDUCER FOR MEASUREMENT OF HEAT FLUX AND PRESSURE TRANSIENTS IN LIVE FIRE TESTS

R. Daniel Ferguson, Edmond Y. Lo, Peter E. Nebolsine
Physical Sciences Inc.
20 New England Business Center
Andover, MA 01810

and

James G. Faller
U.S. Army Combat Systems Test Activity
Aberdeen Proving Ground, MD 21005-5059

ABSTRACT

We describe a transducer which detects and discriminates radiative and convective heat flux transients at its surface, as well as shock waves and blast overpressure. This multifunction device has been developed for the application of hazard evaluation for live fire tests. The transducer sensing elements utilize piezoelectric films which are sensitive to both pressure and temperature changes. The electrical signals are processed to obtain incident heat flux with a thermal response time of order 10 ms, and a total accumulated heat flux capacity of over 100 J/cm^2. Calibration and test results for a prototype transducer are reported.

1. INTRODUCTION

Heat flux gauges are used in live fire testing to characterize events and to assess potential thermal hazards for personnel. Typical gauges are thermocouple-based calorimeters. These conventional devices are limited to measurement of total incident thermal energy, are not well suited to field calibration requirements, and are subject to some ambiguity in data interpretation. To address these issues, a new class of heat flux transducers has been developed under the sponsorship of the U.S. Army SBIR program which meet the requirements specified in Ref. 1.[1]

The transducer is comprised of two layered piezo/pyroelectric polarized polyvinylidine fluoride (PVDF) films on a copper heat sink which are embedded in, and protected by, an epoxy matrix. The difference in the thermal signatures of the films is a direct measure of the thermal gradient, and thus the heat flux. Because the films are below the protective surface, causing a delayed thermal response, these signals must be processed to yield the instantaneous flux at the transducer surface. Pressure signals are common to both films, so that they cancel when the film signals are subtracted to obtain thermal

gradients. Once the thermal signal is known, however, the pressure signal can be extracted.

To fully characterize a thermal event, it is desirable to discriminate the surface-average radiative and convective components of the flux incident on the transducer surface. This is accomplished by dividing each sensor film into two interdigitated sensor patterns, one with an optically absorbing surface coating and the other with an optically broadband infrared/visible reflecting coating. These provide measurements of total incident flux and the purely convective component of heat flux, respectively. Therefore by subtracting these surface average values, the radiative component of heat flux is obtained.

An additional feature of this transducer is a self-contained acoustic calibration/monitoring of proper operation capability. Since the PVDF films are both piezo and pyro active, detection of an acoustic signal can be used at any point prior to, or during, a live fire test to ensure the proper operation.

The transducer concept and design, the data analysis procedure, and some preliminary measurements are described in the following sections. We discuss the development of engineering prototype heat flux transducers suitable for live fire field tests to be performed at Aberdeen Proving Ground. The devices are lightweight, compact, and attachable to clothing. Miniaturized pre-amplifier circuits and a power source will be incorporated into the transducer package. The inexpensive sensing elements have been designed for easy replacement if damaged.

2. HEAT FLUX TRANSDUCER CONCEPT

The highly anisotropic PVDF films in the heat flux sensing elements produce an electric field (or electrode charge accumulation) along the Z-axis as a result of changes in the magnitude and direction of an applied strain or change in temperature. The pyro-activity under conditions of lateral constraint is

$$V_o = \alpha_T(T-T_o)$$

where α_T is the pyroelectric constant and $(T-T_0)$ is the temperature rise due to heating. The heat flux sensor consists of an identical pair of such PVDF films with vacuum-deposited metal electrodes (Cu-Ni) on either face. The prototype design is illustrated in vertical cross section in Figure 1. Films 1 and 2 are embedded in a plastic and are separated by a known thickness, d.

The principle of operation is straightforward. In the presence of an approximately one-dimensional spatial temperature

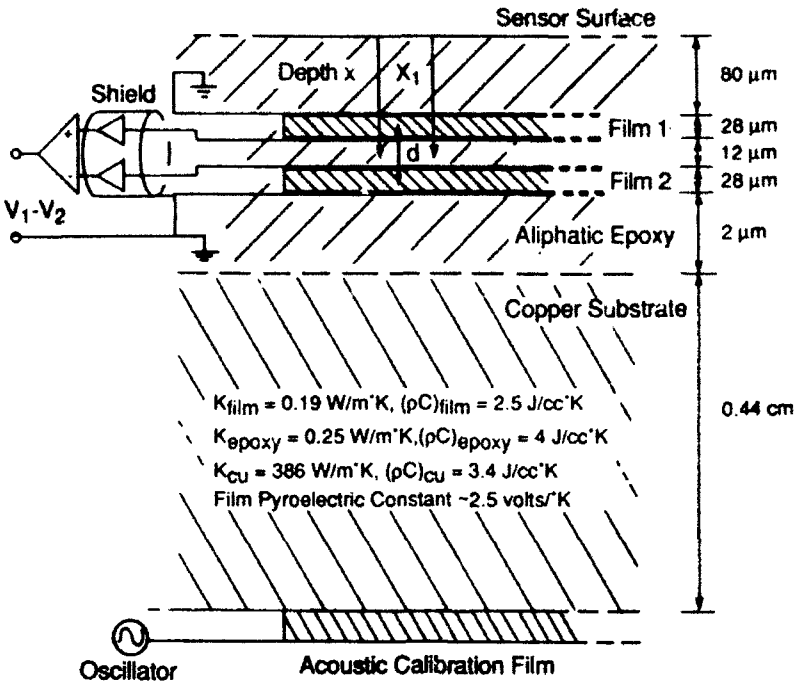

Figure 1. Simple schematic of the prototype transducer shown in vertical cross section. The voltage difference of the plane parallel film pair, measured with a differential amplifier, is proportional to the temperature difference between the films.

gradient, the charge or electrical potential produced by film 1 is dependent on the local mean temperature change, the instantaneous acoustic stress field, and electromagnetic noise. The same is true for film 2 at its local mean temperature. However, acoustic transients are common to both films due to their long wavelengths as compared to film separation distance, and most electromagnetic noise is eliminated by shielding with the exterior ground plane configuration shown in Figure 1. Thus the only signals which are not common to both films are those that reflect differences in mean temperature between the two films. Subtracting the signals, film 2 from film 1, therefore produces a signal directly proportion to ΔT, the temperature difference between the two films. Since the film separation, d, and the thermal conductivity of the embedding material, k, are known, the local instantaneous heat flux is approximately

$$h(x,t) \simeq k \frac{\Delta T}{d} \quad .$$

The exact relationship between this expression for the in-depth heat flux and the true heat flux incident at the transducer surface is described in the theoretical discussion of sensor thermal response provided in Section 3 below.

The thermal response function, and therefore the response time, depends critically upon the depth of film pair. The depth x_1 at which the film pair is embedded is selected to provide the most rapid response time while assuring that the film temperature does not exceed its damage threshold at any time after the onset of heating. Survivability is determined by the film depth and the thermal diffusivity of the embedding material, the proximity and thermal conductivity of the substrate, and the maximum temperature that the PVDF films can withstand.

In addition to these direct means for measuring the heat flux, this configuration offers a unique capability for in-situ testing and calibration by making use of the piezo-electric nature of the PVDF film. The test can be performed by using an auxiliary film as an acoustic transmitter and the sensor films as receivers, as illustrated in Figure 1. By driving the transmitter with a calibrated electrical input and measuring the response of the receivers, proper operation of all films can be verified at any time, including just prior to a live fire test. The operating frequency band limits for pressure measurements are 0.001 Hz to ~1 MHz.

3. THEORY OF SENSOR RESPONSE

The heat flux sensor is comprised of two PVDF films embedded close to the surface of a matrix material with thermal diffusivity comparable to PVDF. However, because it is not located directly on the surface, the sensor output must be processed to obtain the true surface temperature and heat flux histories. The following analysis is provided to demonstrate that the surface heat flux can indeed be easily determined from the output of the embedded sensor. To this end, we consider the response of the film pair to known surface flux conditions.

The instantaneous heat flux at depth x, $h(x,t)$, is conveniently obtained for any arbitrary surface flux, $h_0(x=0,t)$, by convolution with thermal response function at depth x, $R(x,t)$. $R(x,t)$ can be considered to be the response of the sensor to a temporal δ-function heat flux pulse applied at the sensor surface. Note that since the problem is one-dimensional, the response function (and the response time) is independent of sensor area. By convolving the response function with the surface flux, as illustrated symbolically in Figure 2, the expected flux signal at depth x is obtained.

Of course, the ultimate application of the transducer is to determine the surface heat flux from the in-depth measurements, i.e., the inverse of the convolution operation above, or alternately convolution with the inverse response function, $R^{-1}(x,t)$. Fortunately, deconvolution is nearly computationally equivalent to convolution and the calculation is simple, involving little more than a pair of fast Fourier transforms,

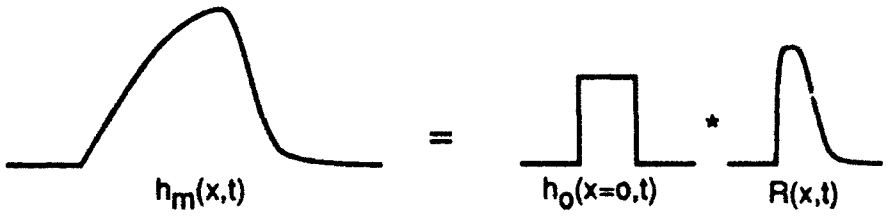

*Is the Convolutional Operator

Figure 2. Symbolic representation of temporal thermal signature at position $x = x_m$.

similar to digital filtering. Again, symbolically, this deconvolution is shown in Figure 3.

The function R is very sensitive to the thermal properties of the materials as well as the layer thicknesses. For the general case of an n-layer transducer consisting of several different materials, a detailed multilayer thermal analysis is required to derive R exactly. Indeed, any arbitrary function of temperatures and fluxes at any point within the structure is easily obtained with the multilayer formalism described below. However, the simple linear deconvolution formalism described above for computing surface flux still applies. Generally, the multilayer thermal analysis consists of straightforward matrix manipulations to determine the (Fourier or Laplace) transformed flux and temperature histories at successive layer interfaces

$$\begin{bmatrix} \tilde{H}_i \\ \tilde{T}_i \end{bmatrix} = A_i \begin{bmatrix} \tilde{H}_{i+1} \\ \tilde{T}_{i+1} \end{bmatrix}$$

where H_i and T_i are heat flux and temperature temporal histories, respectively, with the ~ sign denoting the transform of the heat

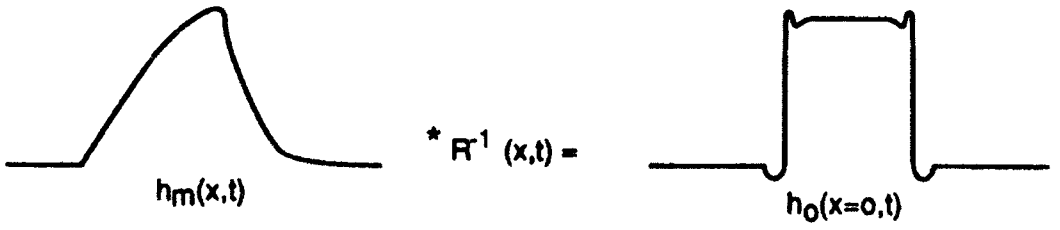

Figure 3. Symbolic representation of the process to obtain the surface heat flux history using the thermal history measured at depth and the inverse of the response function.

flux and temperature temporal histories. A_i is a 2 x 2 matrix which is a function of material properties, thicknesses, and frequency. This multilayer thermal analysis was programmed on a computer and used to compute a response curve for the prototype transducer.

4. PROTOTYPE SENSOR PERFORMANCE

4.1 Calibration

Calibration tests were performed with a short pulse CO_2 laser. Comparisons were made between the calculated and measured temperature difference across the PVDF film pairs in the heat flux sensor at 1 J/cm^2 fluence for calibration. The 1 μm pulses are reasonable representations of a delta-function and are therefore expected to generate the theoretical response curve predicted by the multilayer analysis. This calibration was performed to check predicted against measured response curves, and to measure the actual thermal properties of the materials. A typical comparison is shown in Figure 4.

Deconvolution of the response curve from itself should result in a representation of the input surface heat flux, i.e.,

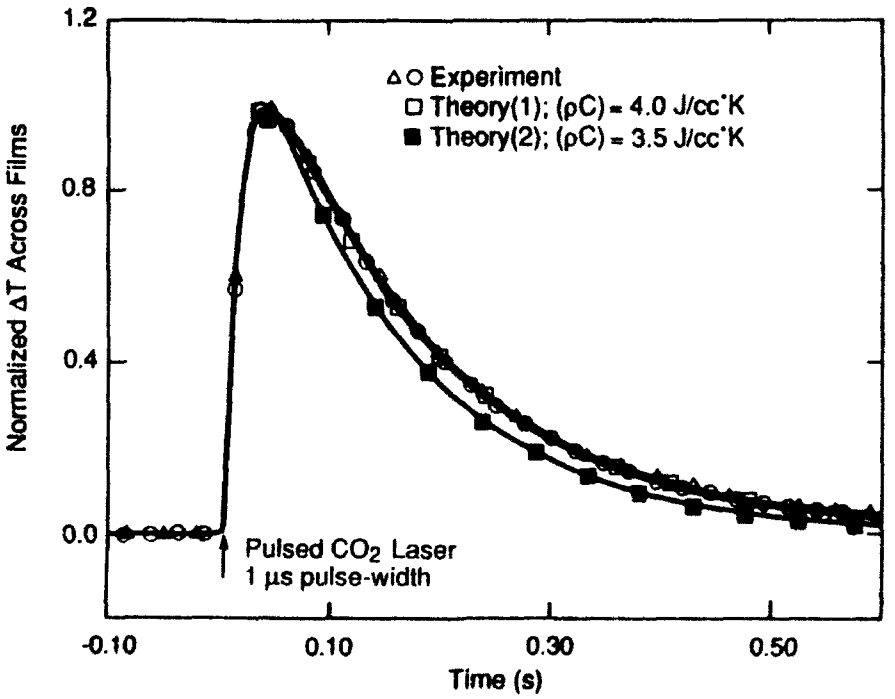

Figure 4. Calibration signals obtained from prototype heat flux transducer using pulsed CO_2 laser as a heat source. Multilayer analysis calculations are also shown.

a delta function. Information is lost to noise and bandwidth limitations, however, which cannot be regained. Thus, deconvolution of the response function from the measurements carries inherent limits. The low frequency limit is determined by either the inverse of the data acquisition period or the limiting low frequency response of the film, (<0.001 Hz), whichever is smaller. The high frequency bandwidth limit is approximately $4D/x^2$, the inverse thermal diffusion time at depth, x. Figure 5a is then the band-limited representation of the laser pulse obtained by deconvolving the response function from the data. The effect of the upper bandwidth limit can be seen in the finite rise and fall times of the estimated surface flux. The ringing is a result of an artificial 60 Hz roll-off introduced to suppress high frequency noise. The rise time is ~10 ms. Figure 5b is the integrated heat flux. The response curve has been scaled by the appropriate calibration constants to produce the known fluence of 1 J/cm^2 determined by conventional laser pulse calorimetry.

This prototype transducer provides fast thermal response, ~10 ms, large signals and robust operation, and a dynamic range spanning from well-below the solar constant (<0.1 W/cm^2) to hundreds of W/cm^2. The maximum (sensor damage level) accumulated heat flux capacity, currently about 100 J/cm^2 (or 88 BTU/ft^2 or 24 cal/cm^2) which corresponds to a severe third-degree burn, is limited only by the size of the heat sink. Combined convective and radiative heat flux tests will now be described.

4.2 Combined Radiative and Convective Heat Flux Tests

Direct measurement of both convective and total (radiative plus convective) flux components can be made with specialized designs, an example of which is shown in Figure 6. This sensor consists of two distinct sets of interdigitated "comb" film pairs. One set of "fingers" with a broadband IR/visible reflecting coating, e.g., aluminum, measures surface average convective flux only, while the other adsorptively coated comb measures both convective plus radiant flux. The difference of these signals thus isolates the radiant flux. The film patterns are etched at PSI using standard photolithography techniques.

As general test of transducer performance, the comb sensor was exposed simultaneously to a blast of purely convective heating (hot air) provided by an ordinary heat gun at close range, and a CO_2 laser pulse. The experimental data for this example case is plotted in Figures 7 through 10. The raw signal voltages from the IR absorbing and reflecting coatings are shown in Figure 7 as the solid and dashed curves respectively. Figure 8 is the corrected data for the total heat flux. A calibration factor is included in the response function to convert voltage to heat flux. Higher frequency features in the

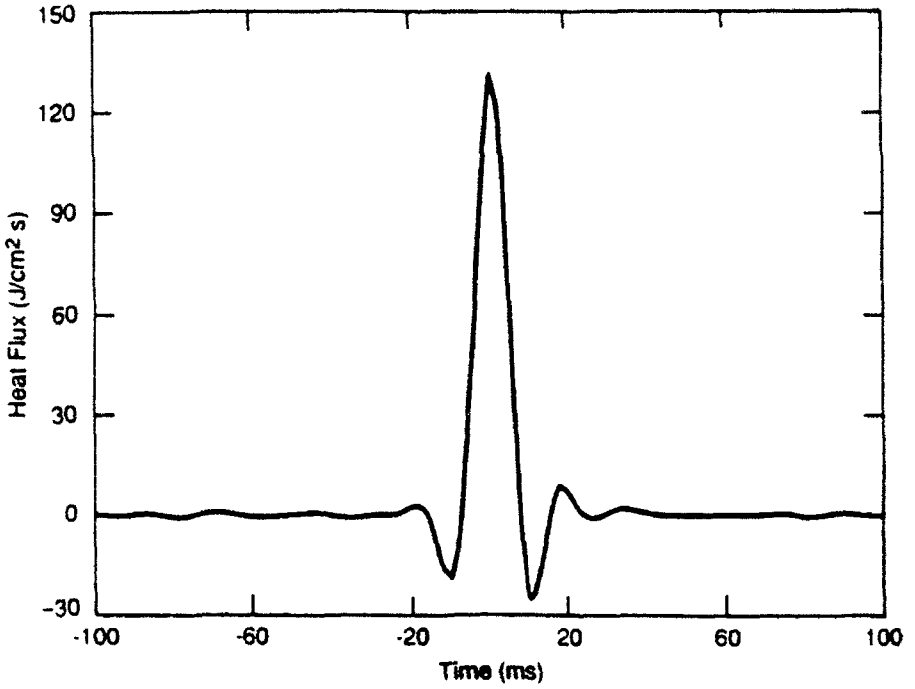

(a)

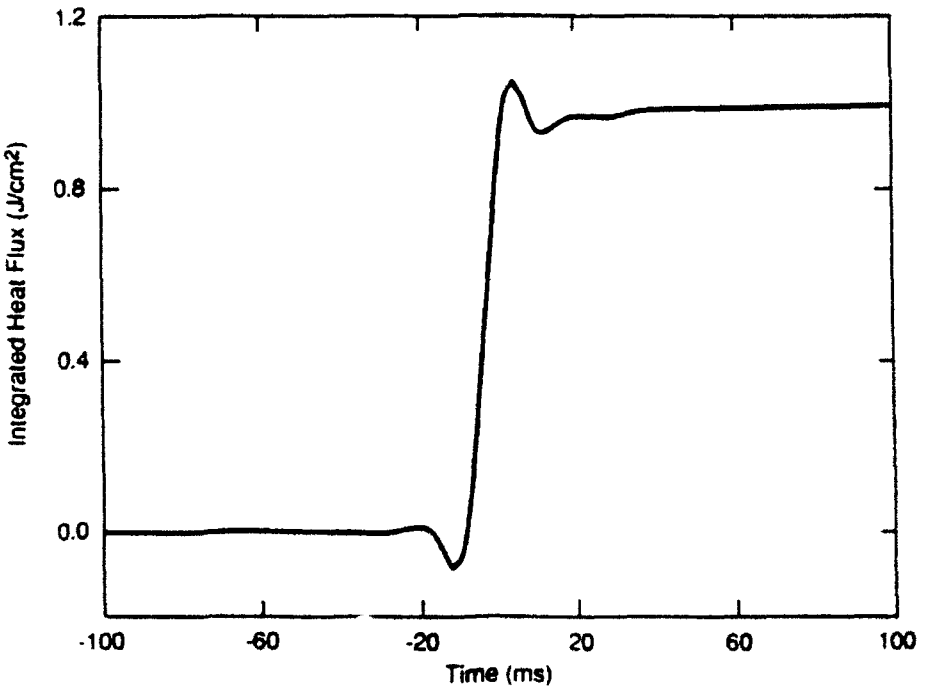

(b)

Figure 5. a) Band-limited instantaneous surface heat flux;
b) integrated heat flux for a 1 J/cm^2 CO_2 laser pulse.

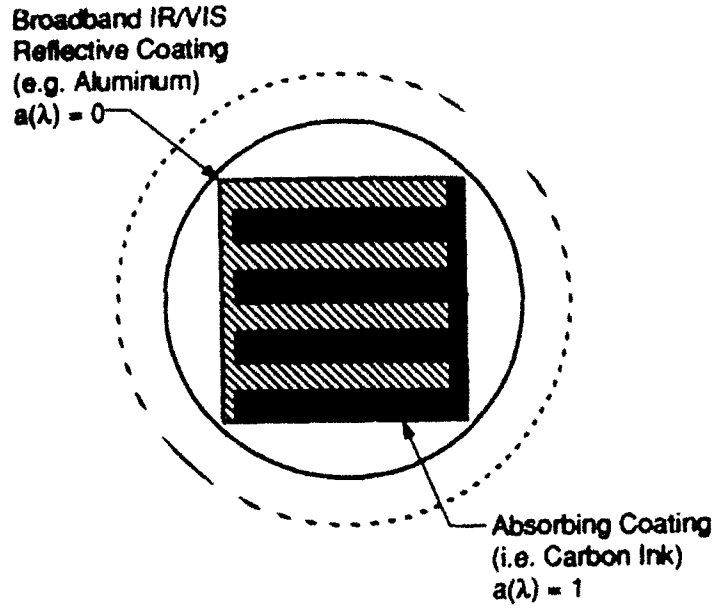

Figure 6. Method for independent measurements of convective and radiant fluxes using interdigitated "comb" sensors on surface coatings.

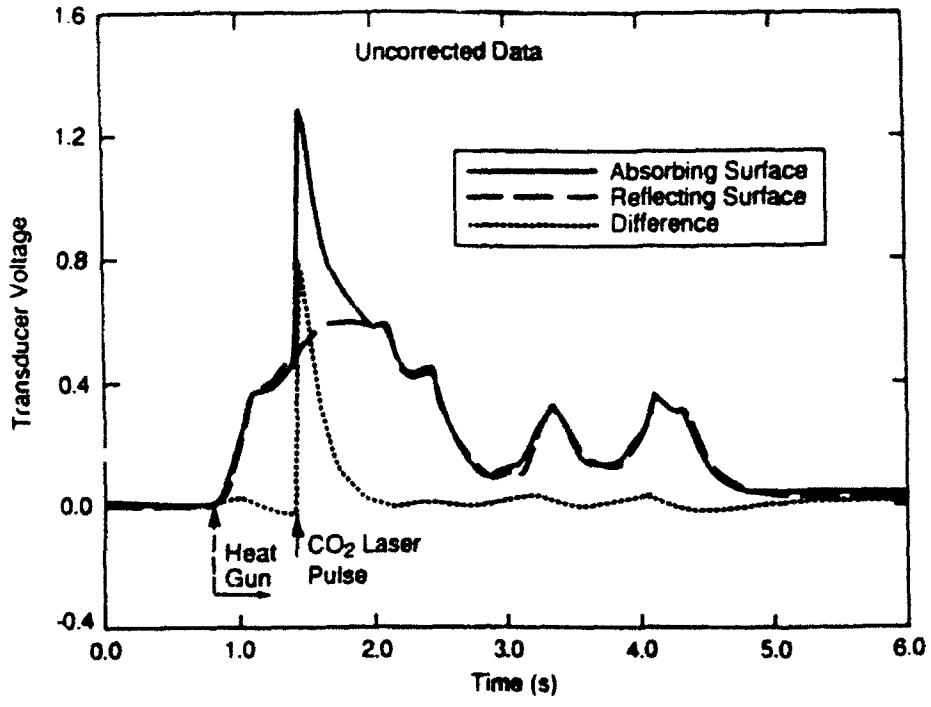

Figure 7. Raw data from comb sensor.

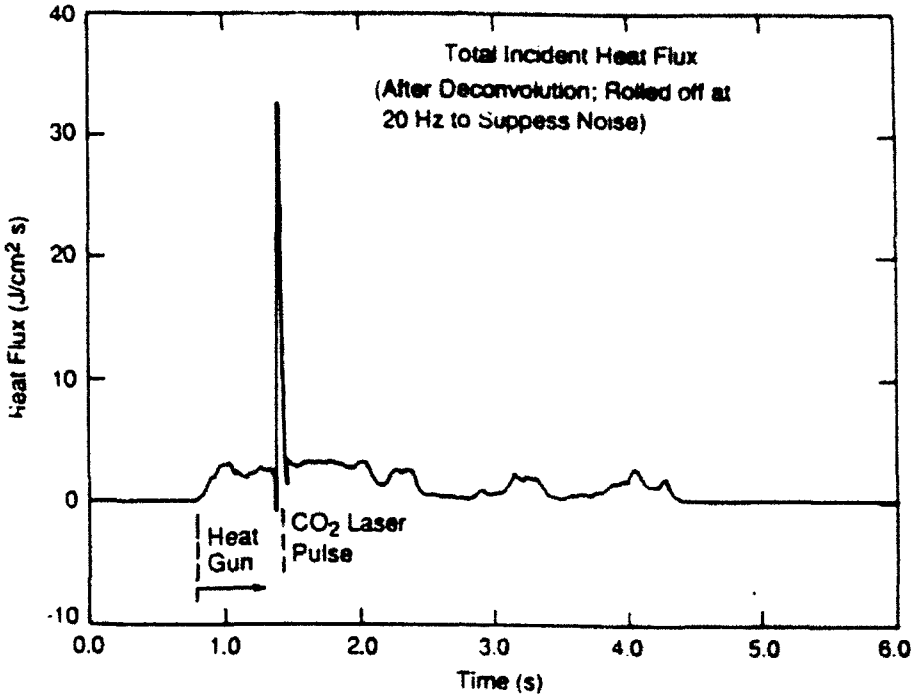

Figure 8. Corrected data for the IR absorbing comb (total flux).

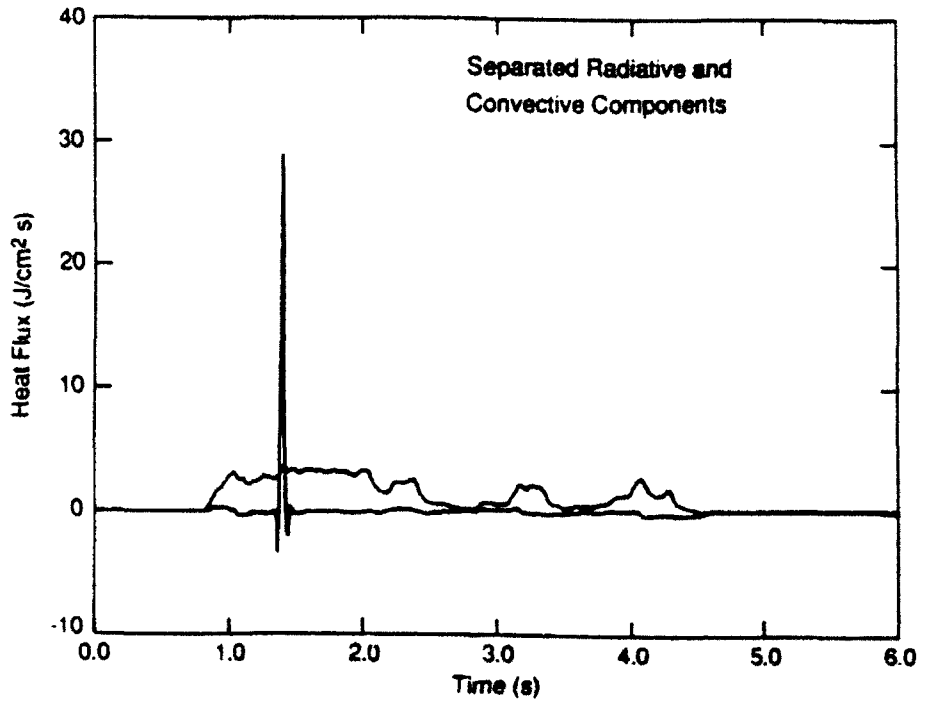

Figure 9. Corrected data for the IR reflecting comb (convective flux) and inferred radiative flux (total - convective).

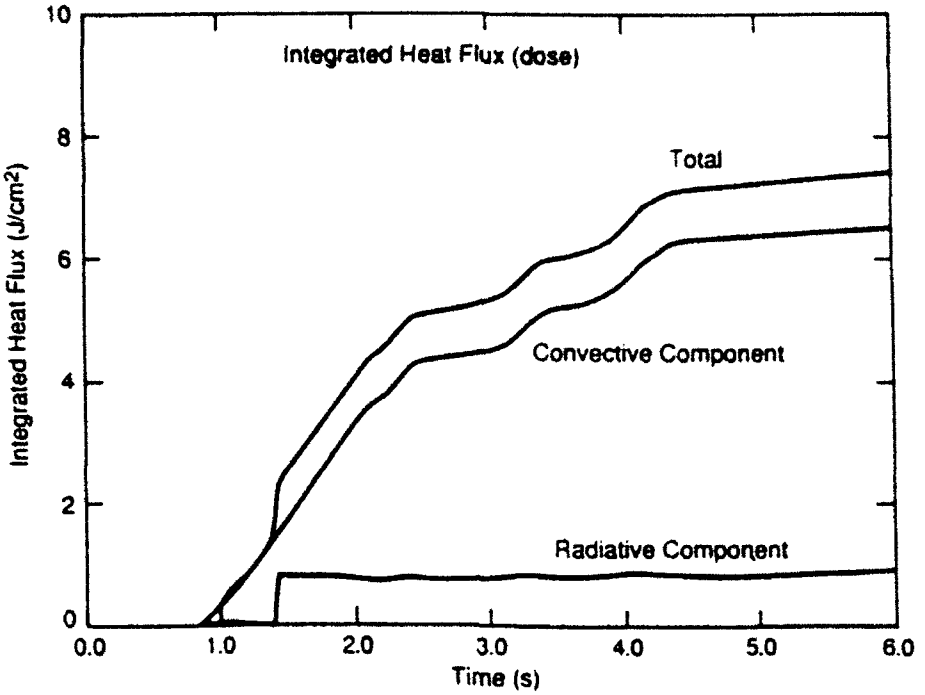

Figure 10. Integrated fluxes (thermal doses to time t).

flux history are clearly observable, reflecting the true bandwidth of the measurement. The location of the laser pulse is evident at once, but in general the radiative component will not be so clearly distinguishable. We must rely upon subtraction of the corrected convective (reflecting comb) flux to isolate the radiative component. This subtraction has been performed in Figure 9, in which the purely convective and inferred radiative heat fluxes are plotted. The component and total flux integrals are plotted in Figure 10. The total radiative fluence is ~1 J/cm^2 as anticipated. The total thermal dose is ~8 J/cm^2 (which is in the second-degree burn range). Thermal doses in this range, and several times greater, were neither observed to stress the transducer, nor to alter the surfaces or calibrations in any visible way.

5. HEAT FLUX TRANSDUCER DESIGNS IN DEVELOPMENT

PSI has assembled the technology needed to manufacture heat flux sensor elements, including established photolithography and spin coating manufacturing techniques. The current PSI heat flux transducer design in development is shown in an exploded view in Figure 11. The interdigitated sensors and substrate are in a rugged, shielded aluminum can with an integral preamplifier that allows the signals to be sent down a cable over 200 ft long. The sensing element is replaceable.

The maximum service temperature of poled PVDF is about 100 C for short periods, so there is the potential damage to the

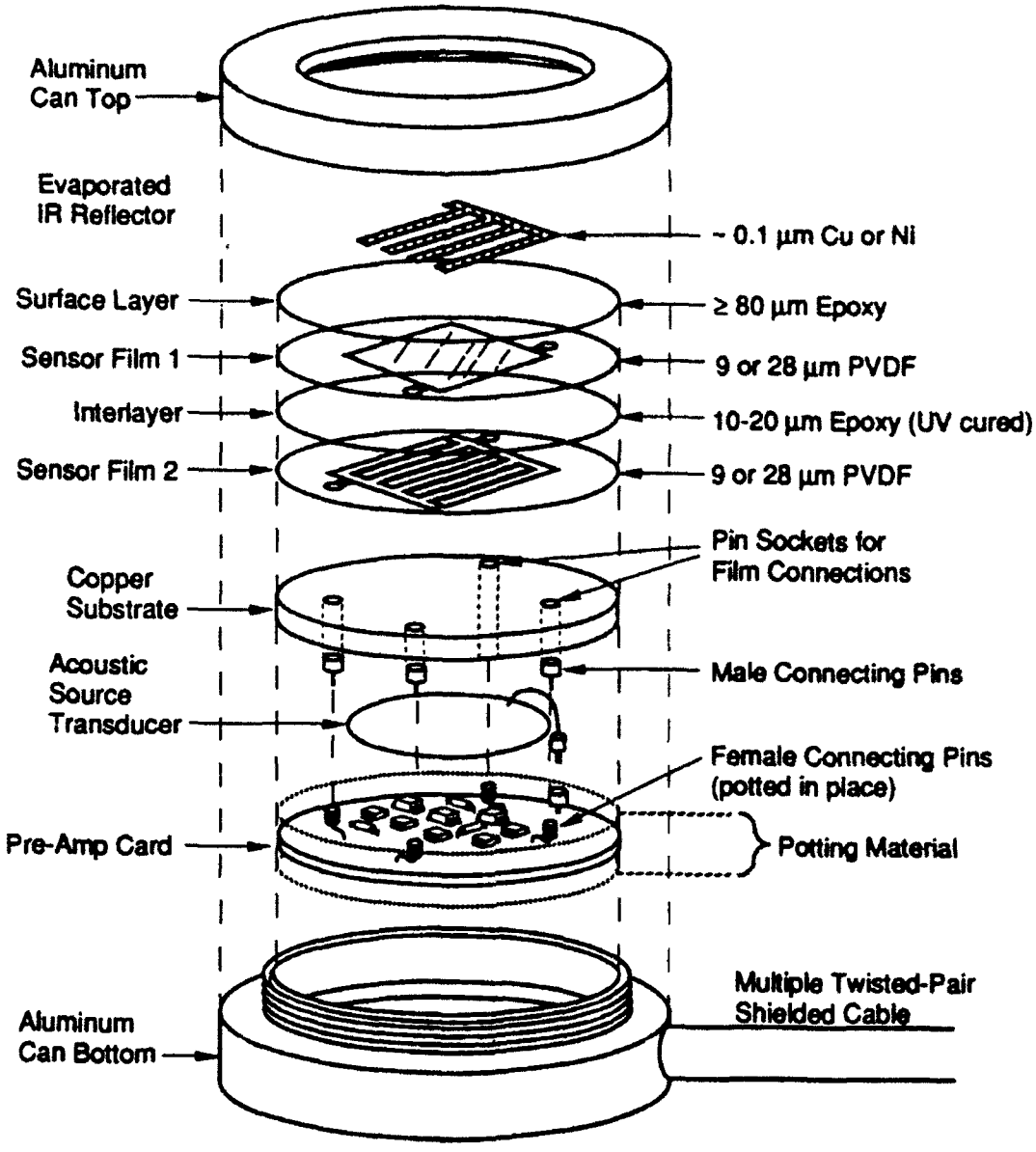

Figure 11. Exploded view of PSI heat flux transducer.

sensing element if the films get too hot. Figure 12 shows the calculated heat flux transducer damage threshold fluence as a function of the duration of the heat flux pulse, for the PVDF film thicknesses indicated. A Gaussian pulse shape was assumed for these computations. The short pulse damage limit is determined by the fluence required to raise the outer film to the damage threshold temperature before the copper heat sink becomes effective. The long pulse damage limit is determined by the total thermal capacity of the heat sink.

Included in Figure 12 is burn data taken by Takata et al.[2] These experiments used a CW CO_2 laser on pig skin at fixed irradiance for various exposure times. The numbers to the side of each symbol provide the burn depth for each of the experiments. Second-degree burns have damage depths of approximately 0.10 to 0.15 mm while a severe third-degree burn has a damage depth of approximately 1 to 2 mm. Note that the damage limit for the heat flux transducer is well beyond this range.

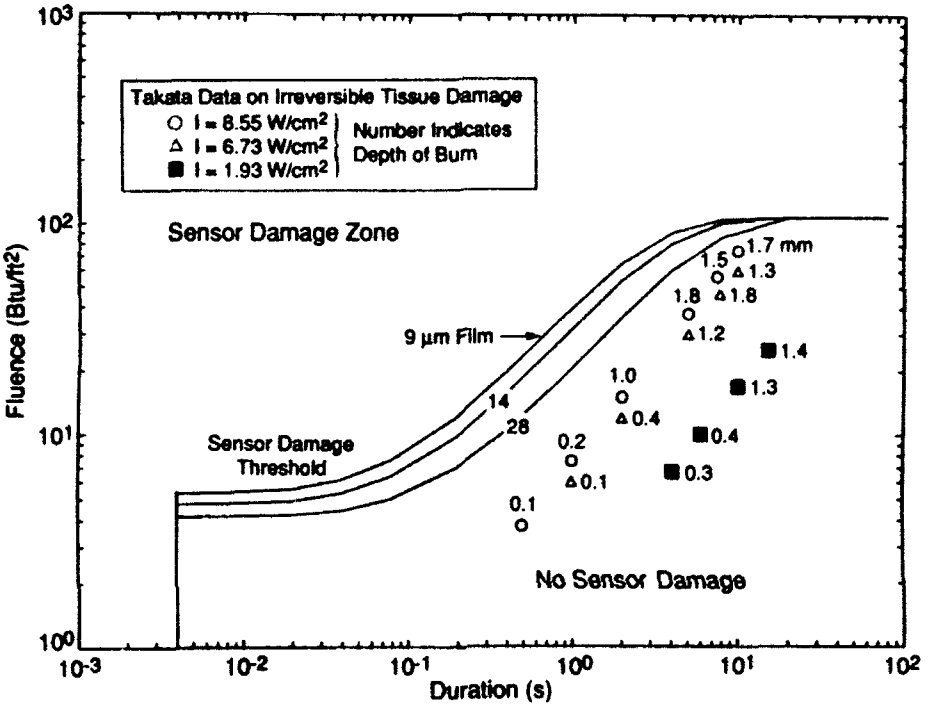

Figure 12. Sensor damage threshold for various PVDF film thicknesses. Also shown is experimental data on tissye damage.

6. SUMMARY

The main features of the prototype transducers are recounted below.

1. Precise measurements of time-integrated heat flux or fluence to at least 100 J/cm^2, and instantaneous heat flux (J/cm^2-sec) within a bandwidth of 0.001 to 100 Hz with excellent noise rejection.

2. Sensor area of more than 10 cm^2 with a capability for surface-average flux measurement over any desired area from a few millimeters square to hundreds of square centimeters, with no loss of response time.

3. Surface preparation and film designs which permit radiant and convective portions of the thermal signatures to be independently characterized.

4. Individual film signals proportional to local temperature changes versus time and containing the acoustic signature of the event (which is generally separated in time and frequency band from the thermal signature).

5. Laboratory calibration of transducer response curves using pulsed CO_2 lasers.

6. Acoustic methods for remote field verification of operation and calibration.

7. A capability to survive live fire events subjecting the transducer to temperature and heat flux levels much greater than those associated with third-degree burns.

Such a transducer will provide detailed data on thermal hazards, and the relationship of these hazards to the events that produce them in live fire testing.

7. ACKNOWLEDGEMENT

This work has been sponsored by the U.S. Army Combat Systems Test Activity, Aberdeen Proving Ground under the U.S. Army's Small Business Innovation Research Program.

8. REFERENCES

1. Faller, J.G., Herud, C., Lukens, L.K. and Walton, W.S., "Methodology Investigation (Final Report) of Evaluation of Crew Vulnerability in Live Fire Testing of Armored Combat Vehicles (Thermal, Toxic Fume, Blast Overpressure, and Acceleration Effects), U.S. Army Combat Systems Test Activity, October 1991.

2. Takata, A.N., Zaneveld, L., and Richter, W., "Laser-Induced Thermal Damage in Skin", USAF School of Aerospace Medicine, Brooks AFB, TX, Report SAM-TR-77-38, 1977

SESSION 2

DATA AQUISITION

A Comparison of Various Video Compression Methods for Use in Instrumentation Systems

James L. Rieger, PE/PTBW, and Sherri L. Gattis, SBIC
Naval Air Warfare Center, Weapons Division [NAWCWD], China Lake, CA

May 3, 1993

Abstract

Various forms of 'lossy' and 'lossless' encoding have been implemented or proposed to allow compression of still and motion picture images, with varying degrees of success which in turn depend on how *success* is defined. Proponents of various systems claim 'compression ratios' which by their nature defy comparison between different system types and suggest there actually may be something like a free lunch. This paper compares various compression methods as well as the implications involved in using them and what happens when different systems encounter the problems associated with the uses of the restored picture.

Key Words: video, compression, instrumentation, JPEG/MPEG

1 'Real' Pictures

A picture is a picture *of something* only when objects in the picture can be recognized by the 'ultimate receiver', which may be a human or a machine. As a consequence, a picture consisting only of a series of dots is meaningless unless at least some of the dots form larger blobs of shape, color, and texture. If motion is to be observed, at least two pictures are needed with the object(s) in motion in different positions, and enough detail to show the change is required. That a picture, or series of pictures, contains some order (that is, un-randomness) implies that we can transmit or store and recover all, or at least the important parts, of the picture, without treating the data as if it were completely random. The difficulty is then in describing what is important in a picture, and to what accuracy we need to express it.

1.1 Dimensions

A street address has two *dimensions* to it, one in the North-South direction and one in the East-West direction. That these directions are *orthogonal* is clear when we consider that if we're a block off on one part of the address, we cannot correct for the error by changing the value of the other dimension. A still or motion picture has attributes which are orthogonal dimensions:

Vertical resolution Vertical resolution is often taken to be the number of horizontal lines in a single picture. The lines need not be scanned in any particular order, but they are often

scanned from top to bottom and may be interlaced. In the NTSC '525 line' television system, there are 480 to 483 of them, scanned with odd-numbered lines from top to bottom and then the even-numbered lines between them from top to bottom again. Vertical resolution can never be greater than the total number of lines, but can be—and often is—far lower.

Horizontal resolution In an analog television system, changes along the horizontal scanning line are limited by bandwidth and slew rate of the electronics, and (like the vertical resolution) by the size and shape of the scanning mechanism. Horizontal resolution can be exprssed in a number of ways, with higher numbers used by the manufacturers, giving the user a false sense of security. Digitized scanning systems can have adjacent picture elements—'pixels'—completely independent, something an analog system can't do, and horizontal resolution is then due entirely to the number of pixels in a line and the shape (and 'fill factor') of the dots. In all systems, resolution is limited by the optical system which focuses the photographed scene onto the scanning mechanism.

Grayscale resolution A scene is limited by the the ratio between lightest and darkest element in it, which may be beyond the range of a human observer. Between the darkest and lightest points in a picture there may be a continuous range of gray, or many shades which appear continuous, or no intermediate shades at all, as in the printing process. The brightness range can be considered to be a linear function, but if considered as a logarithmic *density* function instead can be rendered with fewer discrete shades and still appear to be continuous.

Temporal resolution A picture which changes as a function of time has some form of temporal resolution, although the entire picture may be taken at a single instant and then displayed in a single instant or as a swept image, or the time at which the picture is interrogated may vary with the position of its vertical and horizontal position. Interlace of the vertical (and possibly horizontal) elements in presentation, repetition of previous information, and phosphor persistence (a function of brightness and/or color) complicate the definition still further.

Color resolution In color, the reproduced scene is often altered to compensate for the imperfect illumination of the original scene, a subjective adjustment made so that the rendered colors 'look' right, even though they are not. The difference between a color and black-and-white involves two more components nature of which can be *hue* (the difference between red, green, blue, and orange) and *saturation* (the difference between white, pink, and red) or some other combination; the two color components plus the monochrome representation solve three equations in three unknowns, known as a *tristimulus model* of color. In instrumentation, there can be more colors than three or fewer, and 'colors' may be outside the range of human vision. A human eye cannot resolve a red-blue checkerboard at the same distance that a black-white board can be resolved, nor easily discern between two shades when saturation or illumination is low, hence entertainment television diminishes color signal resolutions accordingly, which may be inappropriate for instrumentation television.

For a picture file to contain the maximum amount of information in the mathematical sense, each of the above dimensions would be totally random. No 'real' picture is that chaotic, even a television receiver tuned between channels, yet only a file consisting of random information in each dimension makes full use of its communication channel.

2 The 'Ultimate Receiver'

The ultimate receiver of entertainment television is the human eye, and the intent of the system is to provide the most pleasing representation of whatever the program's producer wants the viewer to see, whether the resulting scene accurately represents what actually occurred or not. The viewer cannot examine the picture frame by frame, blow up parts of the picture, or vary the brightness and color values of parts of the scenes, although to do so would often be quite revealing. The ultimate receiver of an instrumentation television picture may or may not be a human eye, since electronic devices exist which can measure times, distances, speeds, count objects, etc., from a television signal more accurately than a human observer could. A human observer can examine the resulting scene one picture at a time, and examine parts of the picture by changing the grayscale or color values and ranges, limited only by the quality of the camera, the display, and the medium that connects them. The goal of an instrumentation television system is to allow measurement of *something*, and the system should be optimized to allow whatever measurements to be made. Even if the picture were read and displayed 'perfectly' (whatever that means), the electronics between the pickup and display can only degrade system performance, never improve it.

3 The Nature of Compression

While *compression* has meaning in the analog domain (systems such as NTSC color television are analog compressors), the interest in instrumentation is in compression of files that result from an original digital picture or a conversion (assumed perfect) of an analog signal. Compression of such a file depends on removal of *redundancies* from the signal. The nature of redundancies are semi-intuitive--adjacent film frames look much like one another except where the scenes cut; a single dot in a photo is surrounded by many more dots of nearly the same color; the average brightness of a television picture—black-and-white or color—is close to gray. If we use shorter words to describe the common occurrences than those less common, the overall result will be a smaller file. Removal of picture attributes that don't matter to the user is another possibility, but the losses created by dropping information cannot be recovered, and degrade the reconstructed picture in a subtle or not-so-subtle way.

3.0.1 Compression Ratio

When the size of a compressed file is compared to the size of the uncompressed original, the result can be called a *compression ratio*, although the term is misleading if the compression isn't lossless. A way to inflate any system's apparent compression ratio is to start with a file whose resolution is far higher than the data it represents. Consider a standard television picture (or a VGA screen) consisting of 640 pixels in the horizontal direction, 480 pixels in the vertical direction, and three colors each of which has 8-bit resolution. Since the representation has just over 300,000 pixels, with each pixel expressed to 24-bit accuracy, we thus need nearly one megabyte of picture information to describe the picture completely. However, while we have 2^{24}, or approximately 16 million possible colors, we can have only 300,000 possible colors, and only if each pixel were a different color from all others. We could instead tabulate all the colors in the picture, and assign a unique code to each one, reducing the number of bits per pixel to no more than nineteen--with no degradation to the picture whatsoever. We have achieved a 25% lossless compression. There are far less than

2^{18} colors in an 'average' picture, so the 'compression' can be far more dramatic, but the actual amount will vary with picture content.

With any lossless compression system, the amount of compression achieved varies with picture content, and with the match between the real data and the data expected. Any lossless compression method—and most lossy types—decrease file size on the average, but do not produce the same size file for every picture.

3.1 File Size

The reason that we wish to compress a picture file in the first place is that the uncompressed file resulting from even a single picture is huge; the statement that a picture is worth a thousand words is an understatement. A digital representation of an uncompressed single frame of television is the equivalent of several hundred pages of typewritten text. A single television picture displaces around 600 voice circuits in the telephone network under the best of circumstances. A telemetry channel, be it through a radio link or in a recording medium, is more limited in its capability than needed to handle uncompressed pictures. Since the file size produced varies with picture content and the transmission rate is fixed, a method must be used to limit the file size each picture produces to some maximum, trading resolution for consistent file size. Since the resulting compressed file is of unknown size until after compression, the system must adjust resolution to keep the transmission rate constant.

3.2 Overflow/Underflow

The size of the encode buffer should be such that it cannot overflow when fed maximum surprise at its input while the compression process adjusts resolution to servo the buffer back to normal condition. Similarly, when the picture becomes less complex and the buffer tends toward empty, the resolution should increase until the buffer status returns to normal. If the buffer is emptying even at the highest compressor resolution, the channel must send padding to prevent the buffer being emptied entirely, which will result in a malfunction.

3.3 Delay or Latency

If the servos that keep the buffer in normal condition operate properly, the user need not know that a buffer is operating at all, except that the delivered picture is delayed. However, if the encoder stops transmitting (the missile hits the target and explodes, for example), all data in the transmit buffer is lost. Teleconferencing systems have delays leading to the conclusion that the person on the other end is a bit slow-witted; delays in systems where the picture is being used for remote navigation are more serious. The amount and location of the delay that is tolerable depends on the use.

3.4 Error Recovery

Most systems assume that the file is received intact. Computers get upset and stop or lock up when they encounter a single bit error when reading a file. A video decoder must read through errors,

display something or indicate that it can't, and recover thereafter. An instrumentation system starts receiving a signal after transmission has started, so the decoder must operate with what it gets from the time it starts receiving and onward. Errors due to gaussian noise are randomly spaced, but even if the error rate is one per hundred bits, the chances of two bits in a row being received incorrectly is slight; error-correction systems for this type of noise are fairly easily built. Dealing with errors that occur in bursts, however, generally involves transmitting data in a different order than it was created, and reshuffling back into order at the decoder, increasing delay and buffer size, so error correction is seldom used.

3.5 Limiting Conditions

While the 'average' compression, file size, picture degradation, etc., are of some interest, the item of greatest concern might be the performance of the system under the conditions where compression is at its maximum, or when the system is encountering the picture least suited for the system. The portion of the file that holds the most interesting stuff is likely not an 'average' picture.

4 Decimation

The easiest way to 'compress' anything is to leave something out in some arbitrary fashion. Transmitting every other horizontal pixel and every other line reduces the raw file size by a factor of four; the missing lines and dots can either be regenerated by making the remaining dots bigger or by *interpolating* the missing ones from the remaining ones nearby. It's also possible to reduce a picture rate by transmitting fewer pictures per second and repeating them at a faster rate—movie theaters get 72 Hz flicker from film with 24 frames per second. It's also possible to reduce the grayscale resolution significantly without much difference in average picture quality, as shown in Figure 1.

The image here was approximately 800×500 pixels, and is rendered at each pixel represented by about $2\frac{1}{2}$ one-bit dots to render the semblance of a grayscale image using Stucki dither; there are 975 dots on each horizontal line. This could be called '24:1 compression', but it isn't. With color pictures, reduction of color resolution in space, time, and intensity can be quite extreme without being obvious.

5 Delta Coding

Delta coding sends the difference between the pixel under consideration and the level predicted by a mixture of some combination of pixels already known, under the assumption that any pixel's brightness is somehow related to those around it.[1] Since the predicted value is often close to the actual value much of the time, the difference can be encoded in such a way that no difference with the predicted value is transmitted with a short code and progressively larger differences are transmitted with longer codes—a so-called *entropy coding* technique. Another method is to transmit only a single bit per pixel, its polarity being determined by whether the prediction was lower or

[1]The difference between any predicted and actual value is of use only if the starting value is known, so the starting value must either be transmitted occasionally or agreed on prior to transmission.

Figure 1: One-Bit/Pixel B&W Image from 24-Bit Original Super VGA Image/Pixel

higher than the actual value. The transmitted signal will then toggle between a **one** and a **zero** if the predictor is actually correct, so the step size appears on the display as a granularity. Since abrupt changes in brightness cause longer codes if variable-length codes are used, the resulting file size will vary with predictor efficiency; one-bit codes produce the same file size for any picture but cause blur and delay for rapid transitions. *Adaptive* one-bit coding, which varies step size dynamically, can decrease granularity in areas where brightness doesn't change and sharpens the effects at transitions, but reaction time may cause problems. Delta coding can be used on an analog signal without digitizing it first, which simplifies implementation. Best results are obtained when the sampling rate is an integer or an integer-and-a-half multiple of the horizontal sweep rate.

5.1 Vertical and Horizontal Delta Coding

A predictor based on the previous pixel only is the simplest possible *kernel*, and almost universally the kernel used for one-bit coding. Delta codes which use variable-length coding to transmit several possible differences with the predictor may use two previous pixels to change the ordering of the lengths of entropy codes to increase coding efficiency. The HORACE system described in RCC/TCG-210 uses two pixels in the horizontal direction with variable-length multilevel coding; as a consequence of multilevel coding the file size varies with picture content. To prevent overflow, the coding resolution is adjusted on a line-by-line basis, which the decoder follows without operator intervention.

The previous line in a picture can be used as part of the predictor, and even future[2] lines can be used to predict a single point, but the effect is similar to predicting a new line based on the lines around it. Complexity and delay increase with the selection of a more elaborate kernel, and performance may or may not improve as a result. A screen full of lettering, for example, is more accurately predicted with the previous one or two pixels in the horizontal direction than with a more-elaborate kernel.

5.2 Temporal Delta Coding

A delta coding that transmits the difference between an entire picture and previous (and possible future) pictures can be built; the result is in the category of *inter*frame coding as opposed to *intra*frame coding. Interframe coding works best when the scene doesn't change at all, and file size increases rapidly if something actually moves. At least one previous picture must be stored in its entirety, requiring a large memory on both ends of the link, and because the item of interest in most instrumentation television is the item that moved, interframe coding is seldom used for instrumentation systems. However, teleconferencing systems, which usually involve 'talking heads' and limited movement which can be allowed to blur while the motion continues, might be quite acceptable.

[2]The concept of what the future is is negotiable in digital systems, because delays can be introduced so that the future is available as 'now' is being worked on in the past. The delay introduced depends on how far into the 'future' we need to look.

5.3 Color Delta Coding

Delta coding deals with only one dimension—brightness—over whatever other dimensions coding runs. A color image has several (often three) dimensions to it, requiring that the channel carry as many streams of data as the number of color signals, although not necessarily at the same resolution in the other dimensions. In the standard HORACE color, a color separation is sent after each line, and the user can select the grayscale and horizontal resolution to suit the intended use. The color separation sent can be alternated from one line to the next or several sent each time, and there's no restriction on the size of the separation component data, allowing colors which don't resemble the brightness image much (such as a radar, infrared, X-ray, etc., image), an anaglyphic 3-D pair, or two or three entirely different pictures to be sent, as long as they are in synchronization with one another.

6 Bit Plane Coding

A technique called *run-length* coding is useful when the value of brightness does not change rapidly in the coding direction, since the code is transmitted as a number which represents how many of what level is often shorter than repeating the slowly- or non-changing level over and over. However, in an analog picture the run lengths encountered often have small changes from pixel to pixel, which makes the system inefficient. On the other hand, run-length coding of the individual bits often is efficient, especially in the most-significant bits. Using a zig-zag coding direction rather than a simple horizontal or vertical motion often increases the sizes of the groups encoded. An encoding system based on run-length coding of the individual bit planes can be truncated to a maximum file length resulting in grayscale resolution being the variable dimension, and signals coded in this way can be displayed while being decoded, allowing the user to step between frames quickly until the picture of interest is located.

7 Transform Coding

A television signal is periodic, or nearly so, in the horizontal, vertical, and temporal dimensions, and when transmitted in serial fashion produces a signal with energy clustered about the horizontal and vertical sweep rates. Hence it's possible to transform the picture into a set of orthonormal functions and then transmit the magnitudes (and possibly phases) of those functions instead of the picture. Systems have been built using Fourier, Walsh-Hadamard, Haar, etc., sets. The coefficients change slowly for the low frequencies and more rapidly for the higher frequencies, but the accuracy at which higher frequencies need to be transmitted is lower than that needed for the lower frequencies. The coefficients can be transmitted differentially. Complexity of any transformation is greater than with other processes, and involves memory at both the encoding and decoding ends of the link. Quality ranges from essentially perfect down to terrible; objects in motion and diagonal features generally fare the worst, and tend to flicker as they move.

8 Vector Coding

Since the vertical and horizontal directions in a picture are dimensions, a combination of pixels taken in a group is a *vector* in the mathematical sense, since a change in the value in any element cannot be corrected by any change in other elements. Visually, these vectors appear as mosaic tiles, and are often referred as *tiles* rather than *vectors* for that reason. A typical vector block used might be a 4×4, 8×8, or 16×16 group of pixels, with each pixel represented by a single luminance value or a vector of color values. Just as it is highly unlikely that each pixel in a large picture is of a different color from all others, so is it unlikely that all the tiles comprising a large picture are different from each other—or, even if not identical, a far smaller selection of tiles might be produced which can be used to rebuild the picture to an acceptable approximation. The tiles themselves are more likely to have pixels all of the same color, or nearly so, than to resemble color confetti, just as while all letters of the alphabet occur in normal text, blocks of three containing `the`, `ing`, or `ses` are more likely than `uum`, and `qqx` never occurs at all. A variable-length code can efficiently send vectors, whose statistics are more widely distributed than the values of each pixel.

The JPEG—for Joint Photographic Expe. Group—coding system uses a combination of the techniques discussed above to provide an efficient coding of most pictures. An input picture is first divided into 8×8 tiles, with one tile representing the luminance value and (if the picture is in color) the next tile representing one of two color separation components corresponding more or less to the U and V components used for European color TV.[3] Each tile is then transform coded with the discrete cosine transform into 64 components, the lowest representing the DC value (average brightness) of the tile and the rest indicating spatial frequencies in the vertical, horizontal, and along diagonals. Not surprisingly, many of the diagonal terms are so near zero in amplitude that they can be safely ignored, and the picture reconstructed 'losslessly'[4] For further compression, the amplitudes of the significant spatial components are transmitted with variable length codes and the amplitude changes are bracketed—with the bracketing level determining how crude the reconstruction will be—and the zeros are run-length coded. The coefficients are read out in zig-zag fashion beginning with the DC term, and for further compression all 64 of them need not be transmitted. Differing amounts of loss can be assigned to the color separations, which can be bracketed more broadly and fewer coefficients sent. For any given compression thresholds, the file size will be variable; scenes with high contrast areas and sharp edges make larger files.

The decoder is told what compression thresholds are used at the start of each picture, and resolution cannot be adjusted during a picture. If a file is too large, the entire picture is not transmitted, with the last rows of tiles at greatest risk. Because coding is adjusted for each picture rather than for each line or row of tiles, the encoder buffer must be longer and the delay consequently greater than with the simpler line by line or bit by bit coding adjustments possible with delta coding alone. The benefit of the increased complexity is that a JPEG file is typically far smaller in size than the files created by other schemes, which are limited to no less than one bit per pixel. In color, the user is limited to the color separation ratios allowed by JPEG and to three colors assumed to all contain essentially the same scene—both limitations which are fully acceptable for some uses and wildly inappropriate for others.

[3] For each tile reconstructed, the luminance value tile uses its corresponding color tile and for the other color separation uses an average of the tiles on either side.

[4] Not counting roundoff and truncation errors and what we did to the color separations.

9 Feature Coding

Feature coding is used to keep track of a countable number of objects in the scene, and stores them with regard to position, size, color, or whatever. The theory is that, for example, a scene containing a bouncing red ball is most easily described by keeping track of the size and position of the ball as it moves, and displaying that information at the receiver with little concern about what else is in the picture. While the complexity of such a system increases as the number of objects and with what attributes and precisions we wish to measure, the amount of data that must be exchanged is minimal. Systems which send teleconferencing data by selecting an appropriate face and keeping track of about twelve points on the face for transmission have been demonstrated, and a similar system is used to make animated cartoons. The parts of the picture that aren't coded may be distorted or missing altogether, but if what is to be measured is miss distance, feature coding might be appropriate.

10 Fractal Coding

Perhaps the strangest coding method is that called *fractal* coding, where shapes, colors, and textures are drawn by a system not unlike 'paint by numbers'. The descriptor list can be quite small, involving things as simple as 'color bars' or 'a field of flowers'. Computer screen scenes often lend themselves well to encoding of this type, in part because most scenes are created from primitive elements and in part because what the screen depicts did not have its origin in nature. In some sense, the picture thus generated is identical to the one described, although the resemblance is tenuous if the description is vague or terse. On the other hand, if a tree-bark pattern is placed where a tree trunk is blocked out, that the tree bark thus reconstructed looks as good as the original but doesn't represent it point by point may not matter. A *fractal* coding system can be efficient, but reducing something down to its fractal descriptors is the most time-consuming and computer-intensive technique of all.

11 Conclusion

While we've said often that the type of coding used for pictures, and how to set the knobs on a given system for best results depends on what is wanted, the statement still seems like a copout. Yet without knowing what attributes are essential, which are 'nice to have', and which are superfluous, there is no simple answer. The method used should be determined on the basis of the needs of the user, channel capacity, channel noise performance, cost, and availability. Even with those limitations, however, there's something available which can do almost anything reasonable for any user.

Distribution of Solar Flare Data Using Available Communications Channels

James L. Rieger, PE/PTBW, and David Rosenthal
Naval Air Warfare Center, Weapons Division [NAWCWD], China Lake, CA

May 5, 1993

Abstract

A system is described for distribution of digitized video, tagged alphanumeric data, and alarm notifications reflecting constantly changing conditions in the solar-terrestrial environment. Data are delivered in near real time to users worldwide via existing transmission facilities. Information on the system is accessible to users anywhere in the world via land-line delivery, conventional satellite receivers, cable TV systems, and other methods, in a format compatible with a desktop home computer equipped with a special low-cost data converter and associated software. The system can be configured to distribute information to all or just certain users and can accommodate a wide variety of data types. Solar images in the visible and X-ray spectrum are sent in the background using the HORACE data protocol, allowing priority text traffic and other images to be inserted as priortity dictates, yet a full picture will be available to most users within thirty seconds or so from system turn-on.

Key Words: solar, video, compression, data, networking

1 The Problem/Challenge

Solar radiation data is of interest to earth-based users for a number of reasons, since it affects long-line transmission of power and pipelines as well as radio propagation. Computer images of the sun in the visible spectrum as well as in the X-ray region, for example, are produced by a variety of sources worldwide (since the sun doesn't stay up all day at any one place), and relayed to Boulder, Colorado in a variety of formats. The format of any incoming picture is converted to a standard format which contains a data header, and the picture is then made available for users through the internet using FTP. There are about four pictures per day, replaced at approximately six-hour intervals. Other data (such as sunspot maps, X-ray data taken every four seconds, etc.) are presently disseminated in a number of ways, including long-distance telephone calls using a live operator, and computer tape summaries distributed monthly.

The organization that gathers the data is known as the International Ursigram and World Days Service [IUWDS], a permanent multinational entity established during the International Geophysical Year, 1957–8. Eleven data collection locations, called Regional Warning Centers, constantly gather information from observing facilities in their portions of the world. The Regional Warning Center, the Space Environment Services Center (part of what used to be the National Bureau of Standards) in Boulder, Colorado is designated the World Warning Agency for the IUWDS. In addition

to reporting existing conditions, the agency makes forecasts and issues warnings of changes in the solar-terrestrial environment that could have adverse effects on technological systems. Analogous to conventional weather reporting, the IUWDS reports 'space weather'—an environment every bit as dynamic as terrestrial weather and one with an increasing impact on the entire planet.

The challenge presented, then, is one of distributing the data gathered from various sources and assembled at Boulder to users throughout the US and worldwide. The pictures, presently 512×512 monochrome images, could be sent through a continuous system which sends the other data as it comes in pauses inserted between the horizontal lines of the main picture. The data signals themselves are 'lines' of arbitrary length each beginning with a tag to identify the nature of the data, so the user can examine or save any data considered pertinent and ignore any that isn't. The data signals may be `ascii` text or even binary images, and since there are two eight-bit tag words at the beginning of each packet, there can be more than 65,000 different tags. The highest priority for transmission is called an *alarm*, which notifies everyone receiving the signal that an urgent message follows; the lowest transmission priority is the solar picture, which, even with a lot of data traffic, is reapeated every two minutes or so.

2 Horace Compression

The protocol, or format, used for the presentation level of the system is the HORACE video compression system developed for instrumentation video. Unlike some systems developed for two-way teleconferencing, the HORACE signal can be adjusted at the sending end to optimize horizontal, temporal, and/or grayscale resolution. The transmitted data contains the information to make the proper decoding adjustments on the receiving end without operator intervention. Moreover, HORACE allows transmitting of picture ID data and timing outside the viewing area, and most important for this application, allows transmission of data not associated with the picture at all to be transmitted between horizontal lines. Hence any data with a priority (and in this particular system, all data has a higher priority), the latency between the transmission request and transmission can never be greater than 10 *m*sec or so, worst case at a 64 kb/s transmission rate.[1]

HORACE compression results in a transmitted stream with approximately two bits per pixel, although the exact number varies with picture complexity. Pictures of higher resolution result in an overall lowering of the number of bits per pixel, so if the solar image is increased from a 512×512 image to a 1024×1024 image, the transmission time would increase by a factor of 2.5–3 rather than the factor of four increase that the picture takes.

3 Distribution Channels

The data network could operate through the telephone distribution network alone, using the 64 kb/s synchronous distribution that is provided by a single DS-0 telephone channel which (if two-way) would otherwise carry a voice circuit. Unlike most computer communications, the 64 kb/s rate is set not by the sending computer but rather by the telephone network itself, a situation encountered

[1] Note the difference between a single binary *bit*, indicated with a small letter b, and an eight-bit *byte*, indicated with a capital letter B. Transmission media usually deal with serial data, so data rates in b/s are appropriate measures; computers deal with bytes, so byte rates and capacity are significant. What is used here is the standard convention, but the distinction doesn't get mentioned as often as it should be.

with the newer subscriber service ISDN as well. In order that the signal can reach as many users as possible at lowest cost, the signal is sent through a leased DS-0 circuit to Washington, DC, where it is sent in the vertical blanking interval on the USIA World Service.

The World Service uses two incompatible television formats, one of which is the NTSC system used in North America and Japan, and the other is the PAL system used in most of Europe, Asia, and Africa except for France and what we used to call the Eastern Block Countries. Use of the vertical blanking interval and of the World Service distribution is arbitrary, but the distribution thus arranged covers most of the planet, although ironically to receive the signal in the CONUS requires fairly large receiving apertures. The signal could, in principle, be applied to any television signal distribution that doesn't have a VBI already, or could be placed on a subcarrier with a picture or on a single channel per carrier [SCPC] satellite transponder instead, and indeed all these possibilities are under consideration.

Use of the vertical blanking interval for data distribution is nothing new, and there are numerous incompatible systems for doing so, many of which are in use even now. The system we propose takes advantage of the bandwidth and stability offered by reception from a satellite source, but does not push the technology so far that the error rate goes up too high. The system necessarily operates at a rate higher than the 64 kb/s rate with which it is fed, so that the drift of either the NTSC or PAL system frequencies with respect to each other and to the telephone network data rate are not an issue.

The television system in use in the US is named after the organization that defined the black and white system in the late 1930s which was accepted by the FCC in 1941, and the compatible color system accepted by the FCC in 1953. In both cases, the organization which defined the standards was the National Television System Committee, or NTSC. The US system has 525 lines, 2:1 interlace, and a vertical repetition rate of 60 Hz (or $\frac{1000}{1001}$ times 60 Hz for color). The European black-and-white systems had 405, 625, or 819 lines, and used 50 Hz scanning; following 'standardization', the European Broadcasting Union settled on a single 625-line, 50 Hz system, but with two different color systems and undefined spacing between sound and picture carriers.

In any event, the systems all are based on vacuum-tube technology from the 1930s, intended to minimize the number of tubes in the receivers, which were thought to outnumber transmitters by a large amount. The standards allowed a significant portion of time to the 'flyback' operation which causes the beam to return to the left side of the screen (sort of a 'carriage return') and to return from the bottom of the screen to the top to begin the next vertical scan. The color systems added in later years took advantage of some of the dead horizontal flyback interval to transmit a color synchronization signal, and more recently the vertical blanking interval has been used to transmit such things as captions for the deaf, test signals, and source information. While the number of 'active' lines has no formal definition, the usual arrangement is to use 21 lines in each scan for blanking and non-picture information, leaving $525 - (2 \times 21) = 483$ lines for active picture. Lines 19 and 20 are used for test signals; line 21 for captions. The actual vertical synchronization pulse has a duration of nine lines, during which color burst is not transmitted, and the lines in blanking not in use are simply transmitted as black. The vertical blanking interval from lines ten through 18 can be used for data transmissions, so long as the horizontal and color synchronization intervals are left undisturbed.

In its most pure sense, the master NTSC oscillator is generated from a 5 MHz crystal, multiplied and divided by the ratio $\frac{63}{22}$ to produce a frequency of $14.3181\overline{818}$ MHz. The color synchronization signal is generated by dividing the master oscillator by four, thus producing $3.5795454\overline{5}$ MHz; the

master oscillator is divided by 910 to produce the horizontal oscillator frequency of 15,734.26...kHz, and by 238,875 to produce the vertical oscillator frequency of 59.94...Hz. The factors of each of the divisors can be determined to be

Divisor	Factors
4	2, 2
910	2, 5, 7, 13
238,875	3, 5, 5, 5, 7, 7, 13

There are a number of arrangements which provide all the desired frequencies with a minimum of divisors, or the synchronization signal can be generated by counting down from the master oscillator directly. One minimum-count arrangement is shown in Figure 1.

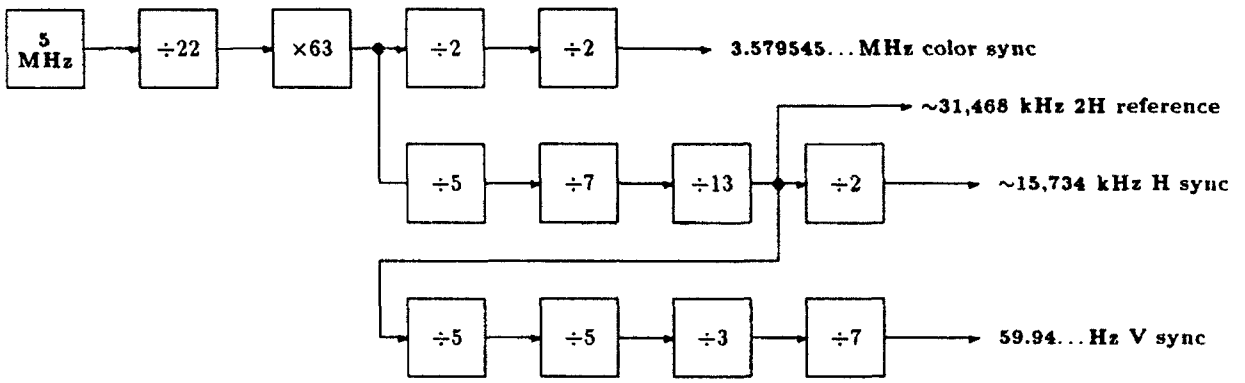

Figure 1: NTSC Reference Frequency Dividers

The data clock for our purposes can be anything as long as it's high enough to get all the data through, but clock is most easily recovered if an integer multiple of the horizontal oscillator is used. Since black-and-white signals start from a master oscillator frequency of two times the horizontal rate, and the 2× rate can be obtained from a color signal as shown in Figure 1, the twice-horizontal rate can be used as a starting point for the data clock multiplier. Maximum frequency for the data clock is limited by the bandwidth of the NTSC distribution system, which is arbitrary but normally taken to be 4.2 MHz, which is 266 times the horizontal rate; we selected 192 times the horizontal rate (96 times the 2H rate), which when used in NRZ data transmission is consequently less than half what it could be and still be useful; the choice of a lower frequency than that limited by bandwidth assures better definition of data transitions.

The synchronization signals are all 'blacker than black' and represent the portion of the brightness scale between zero and −40 on an arbitrary 141-point scale. Video is represented by black, at a level below about $+7\frac{1}{2}$ points on the scale, white is represented by 100 points on the same scale. To be not mistaken for sync, any data sent in the vertical blanking interval (or anywhere else, for that matter), must be in the range of zero to +100. To allow normal functioning of the color and horizontal sync operations, a time duration of 11 microseconds around those functions must be kept clear. Each line thus has about 52.5 microseconds of its 63.5 μsec nominal duration for data insertion. Of the 192 data positions made possible by the multiplier chosen, only 158 are actually available.

The number of levels that each data point can take determine the maximum bit rate possible, with the number of bits per point ('per symbol' in communications argot) being the binary (base two) logarithm of the number of levels. The singal-to-noise ratio of a 'good' television picture is at least 40 dB, but data signals are constrained to $\frac{100}{140}$ of that range, so the signal-to-noise ratio drops to 37 dB, which could allow as many as 70 levels to be transmitted, somewhat more than six bits per symbol. If the range is restricted to four levels, or two bits per symbol, the likelihood of an error is decreased to less than one in a million, so error-correction is likely not required.

To compensate for the fact that the data transmission is synchronized to the television master oscillator and not to the incoming data source, we must allow some of the available lines to be skipped—that is, contain no data—and be recognized as such. To do this, we require that the first bit in any line which actually contains data to be a **1**, **2**, or a **3**, not a **zero**. While this start symbol could still be used for data with that constrain, we ignore that possibility, transmit (and look for) a **three**, and then on a valid line follow with 157 symbols of two-bit data. The maximum bit rate is thus

$$\underbrace{5,000,000 \times \frac{63}{22} \div 238,875}_{V\ rate} \overbrace{\times 8}^{lines/field} \underbrace{\times 157}_{symbols/line} \overbrace{\times 2}^{bits/symbol} = 150,569.4\ldots \text{ b/s} \qquad (1)$$

a number which is sufficient to accept and transmit data rates including 128 kb/s, twice the isosynchronous 64 kb/s DS-0 rate.

The situation in PAL or SECAM is similar, except that since 50 rather than 60 vertical scans are sent per second, the rate drops to 125,474 if only lines 10–18 are used. If the two scans are intended to be closer to identical (so that the highest rate can be used on both, with a minimum of dropped lines), the multiplier used for PAL/SECAM can be slightly higher. If a multiplier of 230 is used for PAL/SECAM, 190 symbols per line could be transmitted, and the communications rate would be 152,125 b/s. A multiplier of 228 or 232 would likely be preferred, however, since a multiple of four times the horizontal rate has some benefits in PAL and SECAM transmissions.

A decoding apparatus looks first for the leading edge of the horizontal synchronization pulse and multiplies by the multiplier number, chosen here to be 192 for NTSC. The leading edge of the sync pulse also zeros a counter which counts from zero to 192. To allow the horizontal and color (if present) pulses to pass, decoding is not engaged until the count reaches 28 (the start point for the 29^{th} symbol). If this symbol is a **three** and line count is between ten and 18, then the line contains data, and data is output as two bits and a strobe for the next 157 symbols. (As an alternative, the data is fed as a single serial stream using a strobe which makes two pulses per symbol.) The output data is sent as a burst, fed to a first-in, first-out buffer [FIFO] which smooths data or allows it to be buffered to an asynchronous data request [DRQ] line in the subsequent equipment.

It should be noted again that there is nothing sacred about the two methods of distribution described, and if the world changes to digital television, for example, the delivery method would change as well (but the major complaint will be in replacing all those television receivers, which can't be easily converted either). All that's necessary is to deliver data to the subscriber at a data rate high enough to work and not so high that the computer can't deal with it, and a separate strobe/clock if the data is not sent at a constant rate.

4 Sender Software

The sending end is a dedicated computer of the desktop size or larger; a desktop IBM PC 'clone' can be used with ease. The function could also be provided along with servicing other users on a larger time-shared machine. The picture to be transmitted is available to the computer in its memory, which could very well have been written to by an external (networked) source. The picture can be stored in compressed form or uncompressed form, and left to the operator to decide. The sending computer may or may not display the picture, but if it does, the picture can be read directly from the display memory and compressed in the process of reading and sending it. Data signals are sent to the computer through one or more serial or parallel lines. The computer sends the data signals out with their respective tags in priority order, where the assigned priorities are under the control of the software. When no data is present, the picture is sent one horizontal line at a time. At the end of each line, the computer checks again for any data signals. If there are any, they're sent, if not, or when data transmission ends, the picture transmission continues from where it left off. The picture transmission carries the picture's source ID and certain other data. The output signal is in strict accordance with the RCC/TCG-210 HORACE format.

5 Uplink Data Drop-'n'-Add

The telephone network sends telephone calls in 64 kb/s channels from one point in the country to another, and calls that need not go coast to coast are removed from the stream in Denver, Omaha, Chicago, or wherever, and others added; thus the data stream at either coast may contain some of the same signals but not all of them. In an analogous fashion, the signal sent from Boulder to Washington, DC, for inclusion into the USIA television signals could have some data packets not sent and replaced with idle channel signals or new tagged data of the same length or shorter than the packets removed. But since the data rate on the television transmissions is greater than that of the Boulder signal, it is also possible to add more tagged data to either the NTSC or PAL feeds without removing anything from the stream at all. Using the numbers used here, the added data could be of an amount greater than that supplied from the Boulder source without overloading the system. The receiving end won't know nor care if this added data is present, and won't get upset with anthing if the data isn't there. The channels can still not be filled to capacity because of the lack of synchronism between the telephone company and the TV master oscillators, and the possibility that an asynchronous cut in the video signal on either system will result in one vertical interval being skipped entirely. If multiple distribution channels are used, it's possible that the non-IUWDS signals added to each stream will be entirely different.

6 Receiving Hardware

The system described here is predicated on the assumption that there are many receiving facilities of varying complexity and sophistication, but only one or two sources and distribution systems. Consequently the system is designed to rquire very little at the receiving end for proper operation, allowing hobbyists to receive and display the solar images "because they're there" much like weather photos are decoded now. On the other hand, serious users of any of the data will have access to what they need in time for it to be of use with very little added effort. A typical receive site would use an IBM PC 'clone' for the decoding, display, alarm, and file-handling functions.

6.1 Data Conversion

The receive site can be served by a DS-0 64 kB/s data line delivered from the telephone network, in which case the signal is an exact duplicate of the signal sent from Colorado, although in principle the drop-'n'-add techniques that might be used on the television system could be applied on the telephone distribution as well. Other sites will use the signal provided in the television vertical interval, which may either involve use of a local subscriber terminal which takes the video signal down to baseband and extracts the VBI signal from it, as shown in Figure 2.

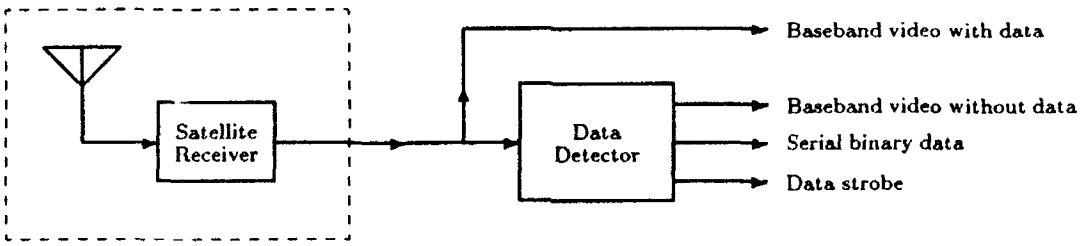

Figure 2: Typical Satellite Receiver Setup

If the subscriber site is served by a cable TV system or over-the-air local broadcast which carries the picture containing the signal. With a television receiver, tuner, or VCR at the subscriber's facility, the baseband signal can be tapped off from the signal without interfering with the normal operation of the device, as shown in Figure 3.

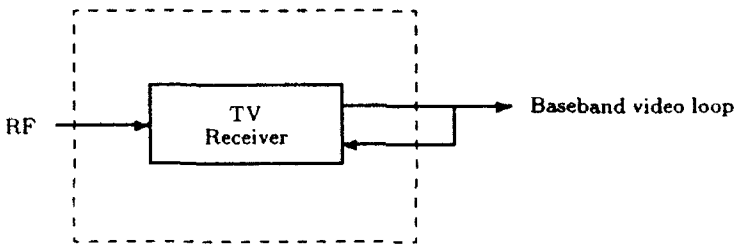

Figure 3: Typical Cable or Broadcast Receiver Setup

In either case, the channel of interest would again be demodulated and the video signal fed into the VBI extractor, similar to the one in Figure 2. The extractor can also provide an output of video with the VBI data removed, to prevent confusion if the video signal is to be taped and broadcast later. It's also possible that a VBI signal could be demodulated once and fed to multiple users through a local distribution system.

Whatever distribution method is used, the interface to the display apparatus consists of two signals, which are the binary digital data itself and a clock or strobe signal, also binary. The data and clock signals will appear to be smooth ('synchronous') from telephone network distribution; from VBI extraction the signals will occur in bursts at intervals determined by the vertical sweep rate of the host television system, with smaller interruptions during TV horizontal synchronization.

6.2 Demultiplexing

Once rendered as a binary signal, a word-alignment box generally external to the computer accepts the data and clock/strobe signals and produces an eight-bit parallel word and a 'data ready' signal to send to the computer, which accepts the word and acknowledges it, allowing the alignment box to prepare to send the next word. The signal can most easily be passed to the computer through a bi-directional parallel port, available at relatively low cost for almost any computer.[2] The word alignment system uses a 24-bit known pattern in the picture line header data and before word tags to establish the word boundary, and works as shown in Figure 4.

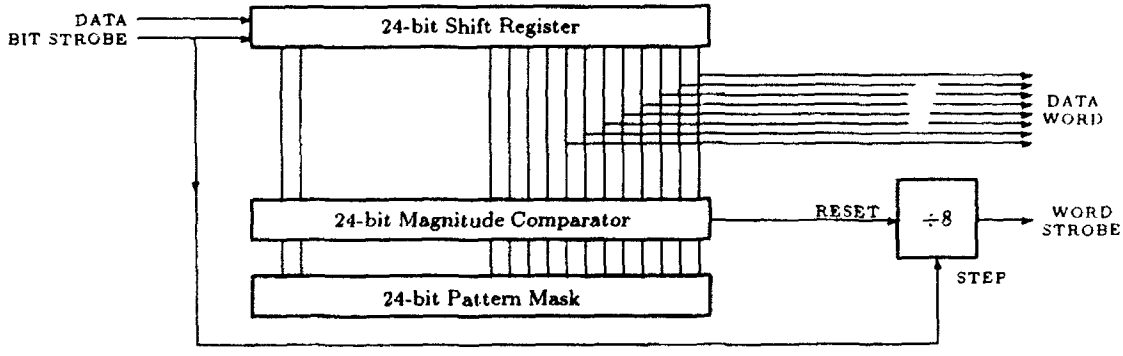

Figure 4: HORACE Framing

The word-framing circuit involves no timers nor oscillators, and can operate at rates far beyond those expected from the computer and the network, hence the circuit can also be used to frame HORACE signals from other sources provided the computer is fast enough to accept them.

Software provided for the computer, written in heavily commented C to allow simple user modification, directs the picture and the data items the user has selected to files, printers, the screen, and the alarm signal to the computer's internal speaker. The computer is not, and need not be, aware of any prioritization of individual messages established on the network.

The picture received is a 512×512 image in a square frame, a size and shape that differ from any current computer display standard. A standard VGA display using a basic 256K memory can display 480 lines of such a picture—essentially all of it, but with only 16 shades of gray representing the 100 or so actual gradations in the original picture. Since the picture is square, there is space to one side of the picture (or on both sides) to display picture source information. The picture can also be displayed in a more limited (possibly much more limited) fashion on EGA, MCGA, CGA, and HGA screens, and the software interrogates the computer to determine the display adapter in use, and to display what it can. Since the limiting item is the display adapter, the full-resolution picture can be captured and fed to a disk or a network for critical viewing if desired. Display adapters with 512K or more memory, required to display the entire picture and grayscale range, are available for less than $150 from practically anywhere that sells computers. If the picture resolution is increased (as sometimes threatened) to 1024×1024, display adapters would require

[2]Not all parallel ports are bidirectional at the data level, although all parallel ports perform some sort of handshake with external equipment. While the implementation shown here uses the full bidirectional port, a somewhat slower implementation which loads data in two four-bit 'nybbles' can also be produced.

more than 1 MB of memory, but most users might opt instead for displaying a decimated image or looking at 25% of the image at a time, either of which can be accommodated in software.

Once the computer is turned on and the software for the distribution system enabled, the user can direct the picture, the picture descriptor information, and each message tag to one or more destinations, including displays, files (local storage devices and networks), printers, as input to other programs, or—as will be the case with most data items—ignore them completely.[3] As soon as the program is directed to accept input, all tagged data is directed as the program dictates, and the picture decoding software begins looking for the start of a picture. Once the beginning of a picture is found, the picture buffer begins to fill; the picture is not displayed until a complete picture has been received starting at its beginning. Since a 512×512 picture at 2 bits/pixel requires 524,288 bits to transmit, and assuming that non-picture data is sent half the time, a complete picture is sent about every 17 seconds. If a system were enabled immediately after the start of a picture, the first picture would be produced within 34 seconds. If tagged data occupies more than 50% of the channel, or if picture complexity causes the average number of bits per pixel to exceed two, the time would be greater, but this estimate is more accurate than one preceded by "...your mileage may vary".

7 Conclusion

The system described here has possibilities beyond those for which it was envisioned, and a similar system can be used to send measurement data from one or more places to one or more places for any desired purpose. By the time this paper is published, we should be able to report further progress on its acceptance by the potential users and the government suppliers of the data.

[3]Encrypted data has its tags sent 'in the clear', so the data in an encrypted packed could be redirected into a file by anyone, but the data itself is unreadable without the key. Different keys may be used for different packets, even if they use the same tag.

Paper for 17th Transducer Workshop
San Diego, CA June 22-24-1993
"Information Capture in Real Time at High Speed"
by: Harry A. Shamir, President

For further information please call:

Harry A. Shamir, Pres.
ColorCode UnLtd. Corp.
100 Inman St.
Cambridge, MA 02139-1206
Tel: (617) 661 3600, Fax: (617) 661 2569 & 876 6468

April 23, 1993

COLORCODE TECHNOLOGY

Table of Contents

ColorCode UnLimited

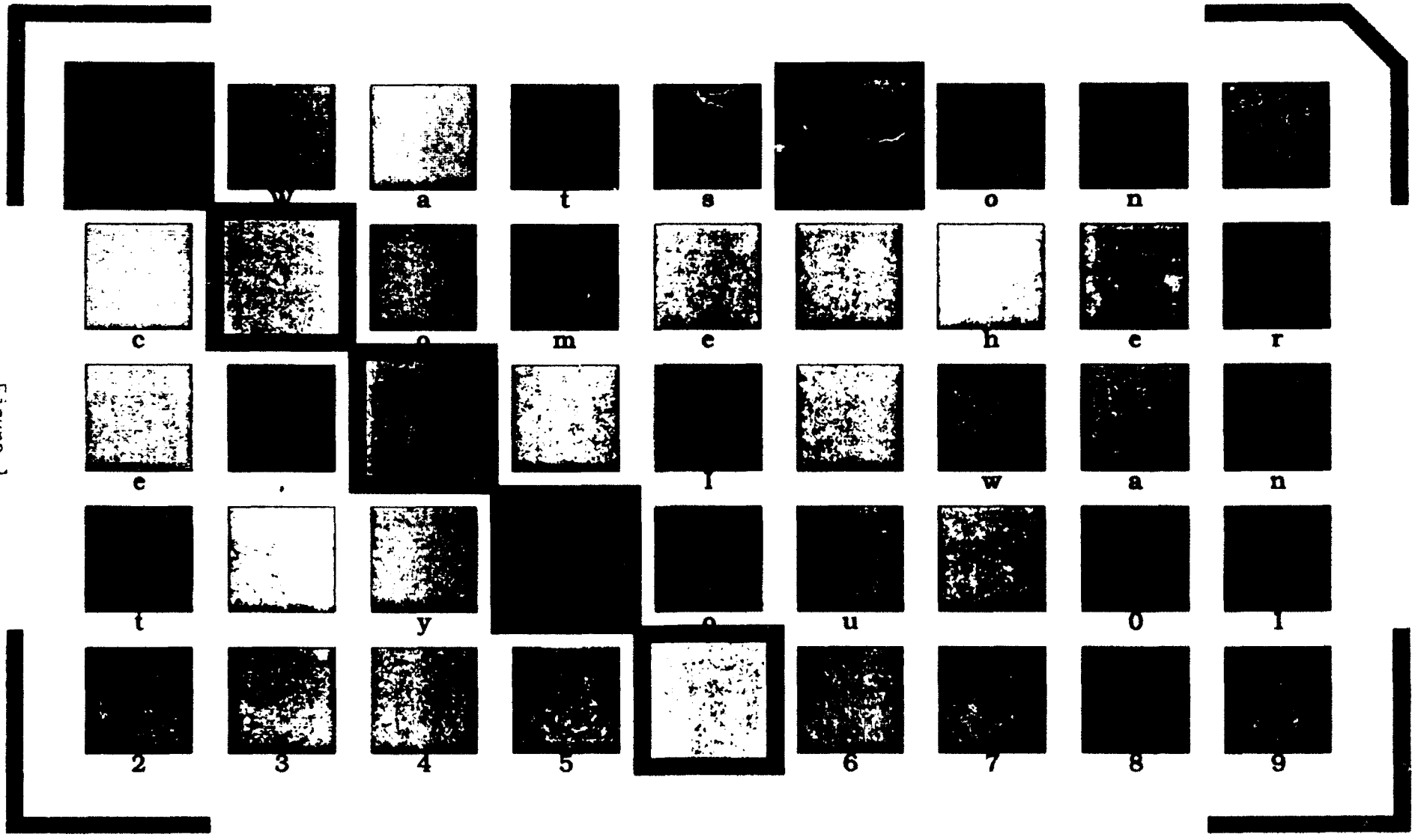

Figure 1

COLORCODE TECHNOLOGY

ABSTRACT PAGE

Technical Abstract

ColorCode UnLtd. Corp. is innovating a method of using shades of colors to store data in a distributed, secure, machine readable, low cost, compressed format. The technique lowers storage cost, and processes all knowledge bases: text, data, images, sound, even olfactory and tactile sensory inputs. The information is encoded using special algorithms into an array of superdots (hueDots™). Decoding algorithms retranslate the information into comprehensible form. The databases and information can be stored on paper, plastic, film, or photopaper. For high speed capture of data from a multitude of bases, storage is on transparancy color or monochrome film.

The methodology hinges on the accuracy of solid state technology in detecting properties of light. Built-in is a mathematical color calibration technique compensating for consistent distortions sourced at printer, reader or media, and from eventual fading of colors.

Key words: Information storage; High Speed data capture; compression.

Potential Commercial Applications:

ColorCode technology has a high potential payoff in several major areas, but in this paper we shall limit ourselves to rapid data capture from a variety of sensors.

INTRODUCTION

Current technology for information exchange and distribution requires either direct interconnection among computers, or transfer of physical storage media, e.g. disks, paper or film. The current highest density of physical information storage repository systems use ablated microdots (optical means) on metallized plastic media, implemented today in CDs, CD-ROMs and optical Tapes.

ColorCode is convinced a market exists for a competing storage technology based on color or monochrome photography. The concept as explained below makes use of commercial film recorders for recording, film scanners for retrieval, and commercial film media for storage.

SUMMARY

Information Capture in Real Time at High Speed is necessary for recording field intelligence information from probe drones. Another application is on testing grounds, where much information is to be transmitted in the very brief time a test is actually under way. Both these devices gather little information for a lengthy period, and may avoid communication emissions until on target. In all applications, when in send mode, the amount of information transmitted is generally much, in a short time. ColorCode's technology will enable receipt of all the data onto one medium, in a non-crash prone manner, for very rapid analysis and use.

Information Capture in Real Time at High Speed is a technology deriving from the basic ColorCode process. The basic process consists of transforming information from the bitstream domain into the color domain. The original information can be text, images, and sensory outputs of any type including sonic, chemical, tactile, pressure, radiative or any other. After Analog to Digital conversion, the resultant bitstream is fed into the software process we call hueCode. In the hueCode process, the bitstream is transformed into color information. The color information, together with printing instructions, are transferred to the printing machine. The printing machine, to which we refer as the huePrinter, then outputs hardcopy on which appear colored dots or bars. We refer to the dots as hueDots, and to the bars as hueBars. The information is now stored on the hardcopy in the form of these colored dots, and is retrievable using standard image capture technology such as CCD or CID cameras. The images thus captured are analysed by the hueReader portion of the hueCode process, and the original bitstream is reproduced. The original bitstream can then be output by the appropriate reproducing means to recreate the text, image, or sensory input.

The speed of information capture obviously depends on the slower of

the speeds of the hueCode process and of the printing process. The hueCode process is rather rapid, thus the bottleneck is actually in the printing, since it includes many mechanical steps, which are notoriously slower than signal processing.

The most rapid medium for accepting color information is film. It is a purely optical imprinting method thus can be well and repeatably controlled. My friends at the film manufacturing companies warn me of the vagaries of the film creation procedure and of the chemistry processes that occur in generating the latent image and in its development. Nevertheless, these vagaries pale in comparison with the variances and non-uniformities of any toner, ink, liquid or dye based technology. Ink printing, electrophotography (xerography), thermal dye transfer (from ribbon or other reservoir), ink jet, are all examples of processes with even greater variability than photography.

In searching for a photographic technique to rapidly capture hueCoded information, one is confronted with the need to make the hueDots very small. Smallness is a significant contributor to speed. However, make too small a hueDot and the ratio between usable information (signal) in the dot area to noise in the same and adjacent area, becomes too low for two reasons: geometrical and color information content. Therefore there are practical limits to the smallness of the hueDots.

The second limit refers to the fact that in a given medium, below a dot size threshold the amount of color information available becomes smaller.

The first limit is the geometrical resolution of the film itself. For instance, a color positive print using standard Polaroid peel-apart media, has a real resolution limit of about 120 micron diameter dot. Wet development positives are a little better, about 30 micron diameter dots. These are reflective media, thus can be used for labels onto parts and documents. They have their application niches. However, if it is speed that is needed, one must seek it in the transmissive media, negative or positive in color. Transmissive media can provide the smallest resolution dot. At least one microphotography film is said to enable a 5 micron diameter resolution dot size.

By the way, to all the above diameters of resolution dots, one must add some inter-dot spacing, to keep the dots from cross-talking. Cross talk would really create more noise than supportable.

Now the problem becomes interesting, since to achieve high information density using many very small dots in a given area, the film resolving power must be high. High film resolution is achieved at the expense of speed. Therefore high information density and the speed inherent in its capture on a small area is offset by the slow speed of the film itself. So the quandary is

how to overcome this slowness, how to expose the film to the available information laden light for sufficient time to generate a solid latent image, yet do all this at the speed of incoming data which can be rapid indeed.

The resolution of this problem is the topic of one of ColorCode's inventions. How we do it cannot be revealed yet, but the result will be a machine categorized as a Film Recorder, enabling use of very slow film at high troughput speeds.

Aside from the pure opto-mechanics, there is a second technology from which ColorCode draws: Data Compression. Many techniques exist, and more are under development at multitudes of sources. The bitstream to be hueCoded may be pre-compressed by any of the appropriate compression techniques.

BACKGROUND

A major current digital 'optical' storage technology uses microdots, implemented today in the forms of Compact Disks (CDs), CD ROMs and digital 'optical' tapes. The microdots are formed by ablating or otherwise altering microspots of material, to record binary digits.

The major players in current optical storage technology are SONY, 3M, and others, that offer large disks, 4" diameter CDs, 3" diameter, and smaller digital 'optical' disks. Each disk size requires its own disk player, which is a relatively large device.

We explored the costs of archiving data by digital microdots stored on spools of tape containing 1 Terabyte (1 million megabytes) of data. These current technology archival costs are $ 250,000 for a Writer/Reader, and $ 10,000 per 1 Terabyte reel (10^{12} Bytes). ColorCode archival technology based on the high density film technology is estimated at half the above costs.

ColorCode is not the first entity to have proposed the concept of storage of information using colors. The coding of resistors using color bands is well known. Photography and films have been suggested and studied to carry information based on their ability to store shades (intensities) of colors[1-12]. However, ColorCode is the first to address the practicality of reducing distortions, recurrent noise, slow drift, and color fading. Such reductions bring the storage of information on color and monochrome film from the realm of interesting possibility to practical and commercial reality.

APPROACH

Any pure color is a specific wavelength of light having an

infinitely narrow bandpass, and its intensity is its signal amplitude. Other than that the concept of color does not exist in nature outside the eye-brain combination. The word **color** as used to describe this phenomenon relative to human observers requires three variables to define its value. The most readily known variables are Hue, Saturation and Intensity. Hue is the perception of what is innocently called 'color' in everyday language, and consists of a multitude of different wavelengths each at its own intensity. Hue can be best understood as being the human sensed blend of the array of wavelengths passing through a given filter. Saturation identifies the breadth of the bandpass around a selected nominal wavelength, and can be understood as the list of wavelengths that "make it" through a given filter. Intensity measures the number of photons impinging on the sensor from the light passing through the filter.
ColorCode deals with Hue and Intensity and is not concerned with Saturation, since the actual list of the wavelengths being analysed in their aggregate for Intensity is unimportant beyond the fact that they pass a particular filter.

A machine reader can recognize the differences between intensities of light. By use of appropriate filters, this translates into the ability to differentiate between various shades of colors within the hues. Thus the machine reader can resolve a colored superdot into primary colors and their intensities. ColorCode's technology is based on this ability of a machine reader to separate the hues and provide constituent color intensities.

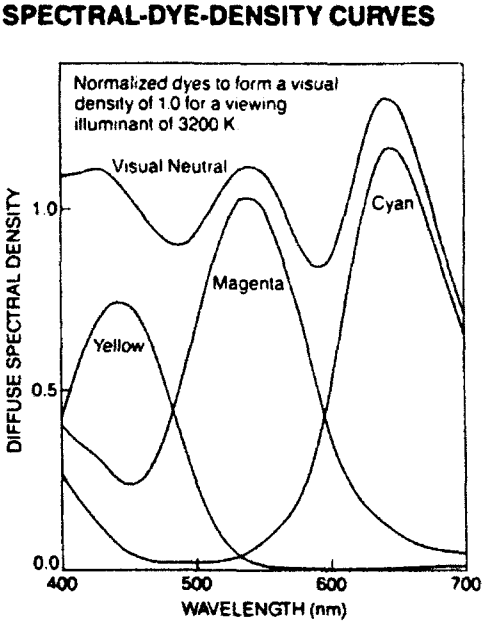

Fig. 2: Kodachrome™ 200 Professional Film, the human eye perceives the blend, the machine distinguishes each component at its own signal amplitude (color intensity):

As is shown by the diagram above, the 3 composite wavelength spans

(bandpasses) used in color photography greatly overlap. However, ColorCode's technology includes a technique for resolving the constituent colors from dots of hue on film. The information is carried in a hueArray™ of superdots or hueDots™ (a dot of composite color). The information is encoded, and optionally encryted, using a special algorithm. A decoding algorithm with optional deciphering, present in the reader machine, translates the information back into a humanly legible form.

Storage Density of hueArrays

The amount of information stored in a hueArray will depend not only on the number of colors but also on the size of the huecode dot (spatial resolution) on the film, the size of the array, the dynamic range (color resolution) of the film at that hueDot size, the arbitrarily chosen factors of redundancy in the system design, and other factors.

As a simple example, an array of 20 x 20 huecodes can represent a string of 2164 base 10 numerals (0 through 9), out of an available population of $(262144)^{400} \approx 2.606 \times 10^{2167}$. In practice, some of the available string of 2164 numerals will be allocated to error checking and other internal data management purposes. We estimate the number of usable numerals will be about 1400.

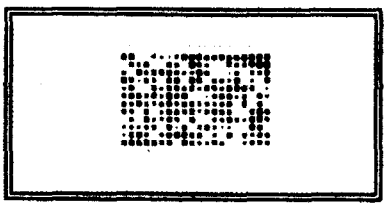

Fig. 3: A much enlarged hueArray, representing 740 ASCII characters

The superdots in the image above are 500 microns x 500 micron. There are 240 dots in this matrix, representing 740 ASCII characters. This is approximately the same information content as one quarter of a single spaced 8 1/2" by 11" page of text, assuming the 2000 characters per page from widely used word-processing systems.

In contrast, if film based huedots were 3 microns in diameter (or square) with 2 micron spacing, each dot-space would occupy an area of approximately 25 square microns. This would yield a dot density of 25 million dots per square inch. At this density, allowing for 2¼ ASCII characters per dot, the information density is 56 megabytes per square inch. **An excess of 28,000 pages of information could be coded and placed in a single square inch.**

Compare this with the information density of a CD (WORM), which on a 4" diameter disk of excellent quality is 725 megabytes, yielding 32 megabytes per square inch, which is only **57% of the** information density of the level G hueArray, (see Table 1 in Appendix).

For maximum information density, the dot sizes (which here include spacings) must be minimized, but optimized so the data encoding accuracy and reliability are not compromised. Table 1 depicts the information storage capacity of an array of hueCodes that would fit onto a 1" by 1" area at various dot size and spacing levels.

Area storage efficiency is offset by the need to have borders around each hueDot that are of relatively large area (a factor of 2 or more). Moreover, below a given dot size, color information is acually lost. Thus each medium and printing technique (film recorder) has its own minimum dot size. Once that size limitation is determined, one can increase information density by increasing the intensity discrimination of each constituent color.

For monochrome films, the size of the minimum hueDot is small. So small indeed that for a higher speed of information capture it may be more practical to use microphotography in monochrome rather than in color. This is currently under investigation.

HueDot Size Reduction, example

On the following page is Fig. 4: 'Superdot size reduction', an example of a test done to explore the minimum superdot size on paper using digital laser printers.

CHARACTERISTIC CURVES

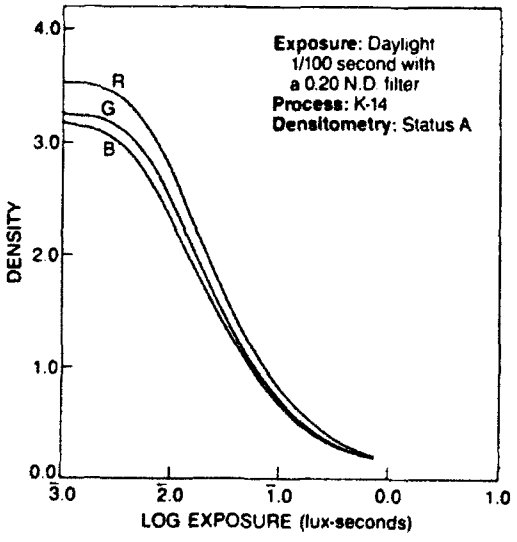

MODULATION-TRANSFER CURVE

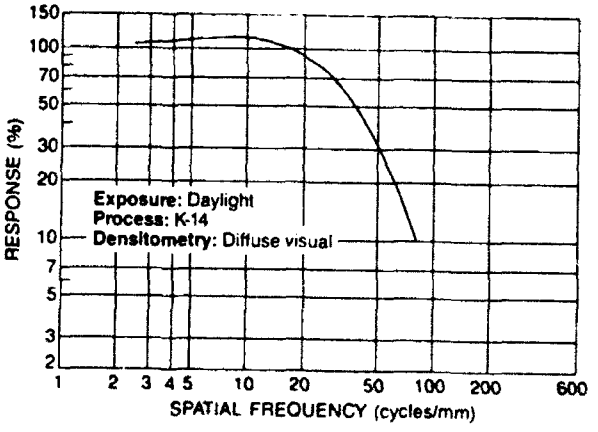

Decrease of Dot Size is Limited Only by Printer Technology

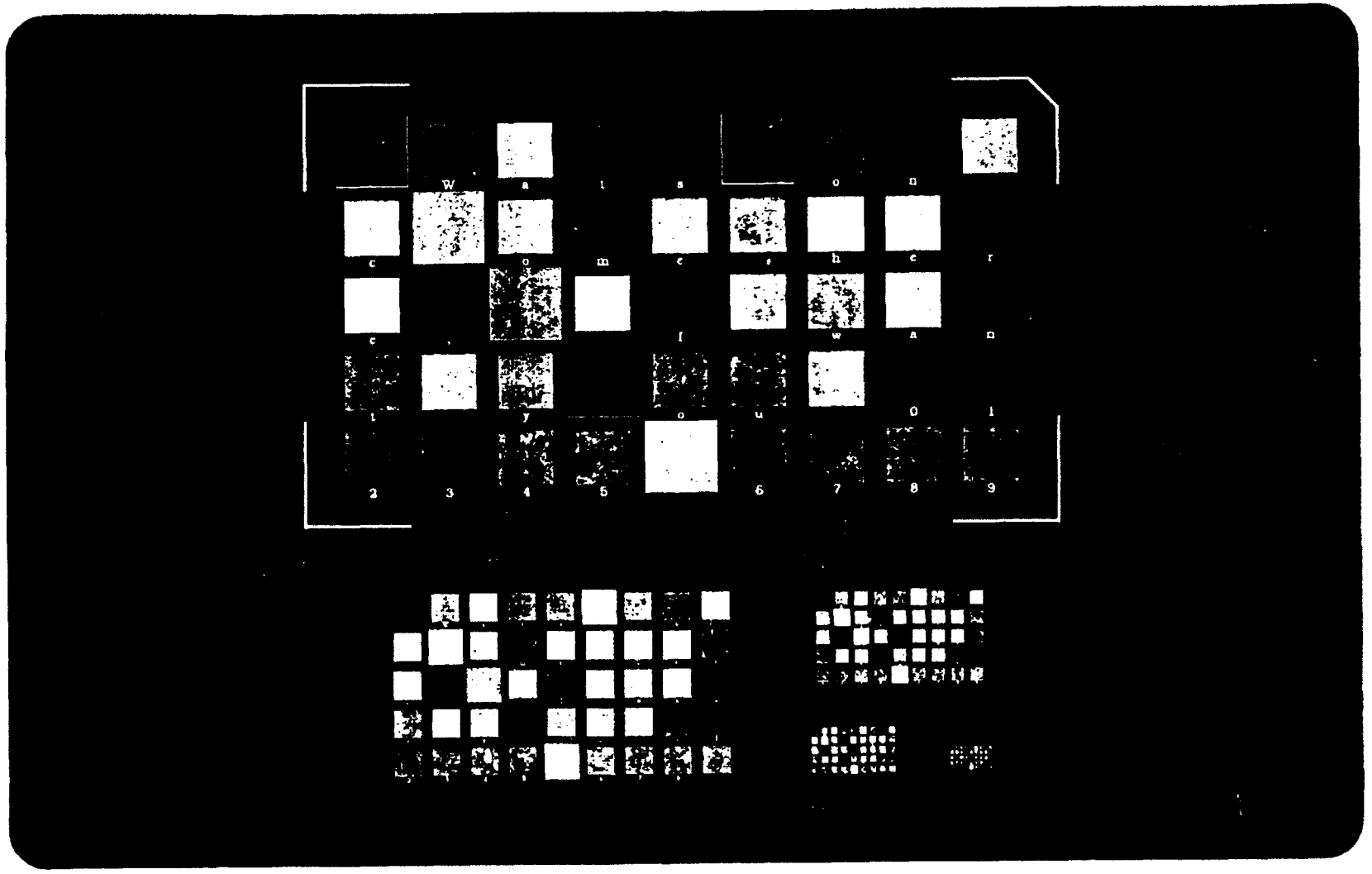

Current Tools

Current Film Recorder technology generates images at rather low thruputs. One image in a minute or two is the norm. The intent of ColorCode is to create a Film Recorder that will overcome this problem.

Currently, storage of information on film at level F occurs using any of the widely available color and shades of gray film recorders. Though not providing the ultimate in dot densities of level G, these machines are acceptable hueArray printers at level F. The conservative estimate for the center to center distance of hueDots using the claimed resolution of the Agfa Matrix Forte (film recorder) of 2742 rows at 4096 pixels per row, is .009 mm (9 micron). The machine issues 24 bits per pixel. This in theory will meet the requirements of level F information density, and even surpass it. However, the machine does create a 25% overlap of dot edges, decreasable by performing repeated shots at lower light intensities. It remains to be seen if these machines can be 'pushed' to a higher information density by using higher resolution ('slower') film and/or improving the lens system on the camera assembled to the machine, and/or altering the software. The goal of ColorCode is to achieve or surpass level G information density on transparent films.

Commercial Readers for films (usually 35 mm transparencies) are also widely available. Some flat bed paper color scanners incorporate transparency readers. To act as hueArray readers, these scanners require only ColorCode software.

Prior Art

As mentioned earlier, ColorCode is not the first to have conceptualized the storage of information using colors. However, prior investigators[1-12] did not have the advantage of modern computerized information analysis. Therefore little if any work was done to separate random and rapid noise from effects of slow drift, and non-linearities in transformations from one medium to another, which are distortions recoverable by calculations. In 'Related Research' below, is listed work performed by the submitters of this Program, indicating the advent of powerful techniques able to correct for signal distortions such as listed above. The incorporation of calibration dots in the hueArrays ensures the applicability of such techniques for recovery of information heretofore deemed irretrievable.

Prior researchers also erred in concluding that storage of information using colors have inherently a low signal to noise ratio. Among the errors were the assumptions of linearity inherent in the use of Fourier transforms in the modelling of photographic information storage[12]. Photographic imaging is well known for its non-linearity, as demonstrated above, taken from a commercial film publication.

Current R&D

ColorCode has demonstrated the general concept of storing information using shades of colors on a variety of media.

Practical limitations to the technology have been determined. The major limiting factor is the non-availability of commercial Printers and films capable of achieving the required Resolutions and recording at speeds practical for information grabbing in real time.

Level F information density is achievable using color film having spatial resolutions of 100 lines per mm, and resolving at least 64 shades per each of the 3 individual colors. This is achievable using current photographic technology.

Level G information density is achievable using color film having spacial resolutions higher than 200 line pairs per mm (lp/mm) and resolving 64 discriminate shades per color. The R&D program will test our assumptions.

Reaching level G allows ColorCode to improve upon currently existing area density of information on CDs by 175%, and improves more than an order of magnitude in its volume density. The volume density is much, much higher since the media carrying the hueArrays is so much thinner than the CD ROM media.

All our explorations in prior art have failed to find work demonstrating either the possibility or impossibility of attaining ColorCode goals at levels G or F. All previous work fell short at not considering the calibration procedures embedded in the ColorCode process, nor did they actually demonstrate empirically any negative conclusions.

ColorCode uses media such as color film available commercially for human eye consumption to store information, thereby ensuring low film cost. Further experimentation will lead to conclusions regarding what can be expected from improved imaging hardware, used with 'slower' (lower ISO number) commmercial color films.

Information Retrieval

The hueArrays on the film are to be read by CCD solid state area or linear arrays in specially built cameras. The basic modules of these devices are commercially available. ColorCode has performed sufficient research to determine that the information retrieval speeds will be satisfactory. Obviously no more can be said at this time.

High Speed Information Capture

There are two constituents to rapid capture of information on film. The first is the rendition of signals from a variety of sources

simultaneusly, into categorized and organized bitstreams. The second is exposure of the rather slow chemistry films, to light modulated by these bitstreams.

The rendition of signals from a variety of sources simultaneusly, into categorized and organized bitstreams is a task ColorCode will not tackle. We leave that to groups specialized in that field. We will take the bitstreams and store them. Then we will retrieve them, also at high speed. But to organize them requires resources we do not have available.

The exposure of the rather slow chemistry films to light modulated by the organized bitstreams will take place in a machine of ColorCode design. It is a novel type of film recorder enabling both long duration exposure on slow, high resolution film, and rapid film motion processing the information stream at high rates.

This machine is as yet subject to secrecy restrictions, thus no details can be given. Until such a time as the ColorCode film recorder shall be ready, the recording will be demonstrated on slower commercial machines.

Currently ColorCode is also concentrating on other applications such as in the medical and pharmaceutical fields. We are always ready to discuss possibilities with potential Strategic Partners.

APPENDIX

References

1. C.S. McCamy, "On the Information in a Microphotograph", Appl. Optics, 4 p. 408 (1965).
2. N. Bar-Chaim, A. Seidman, E. Wiener-Avnear, "A Color Memory Mode Based on the Variable Birefringence in PLZT Ferroelectric Ceramics:, Ferroelectrics, 11, pp. 385-388 (1976).
3. R.A. Bartolini, H.A. Weakliem, B.F. Williams, "Review and Analysis of Optical Recording Media", Opt. Eng., 15, pp 99-105 (1976).
4. F.N. Magee, "Discussion of Electrophotographic Film", Laser Recording and Information Handling, A.A. Jamberdino, Ed., Proc. SPIE 200, pp. 16-19 (1979).
5. S. Masdlowski, "High Density Data Storage on Ultraviolet Sensitive Tape', Optical Storage of Digital Data Technical Digest, Opt. Soc. Am., p WA4-1 (1973).
6. R.G. Zech, "Review of Optical Storage Media", Optical Information Storage, K.G.Lieb, Ed., Proc. SPIE 177, pp. 56-62 (1979).
7. Y. Makunoki, et. al., U.S. Pat. # 4,278,797 (1981).
8. R.C. Jones, "Information Capacity of Photographic Films", J. Opt. Soc. Am., 51, pp. 1159-1171 (1961).
9. R.C. Jones, "On the Point and Line Spread Functions of Photographic Images", J. Opt. Soc. Am., 48, pp. 934-937 (1958).
10. J.H. Altman, H.J. Zweig, "Effect of Spread Function on the Storage of Information on Photographic Emulsions", Photo. Sci.

Eng., 7, pp. 173-177 (1963).
11. R. Shaw, "The Application of Fourier Techniques and Information Theory to the Assessment of Photographic Image Quality", Photo. Sci. Eng., 6, pp. 281-286 (1962).
12. D.R. Lehmbeck, "Experimental Study of the Information Storing Properties of Extended Range Film", Photo. Sci. Eng., 11, pp. 270-278 (1967).

Related Work

J. Schwartz, T. T. Wu, U.S. Pat. # 4,658,286, filed 3/28/83, "Method and Apparatus for Correcting Distortions in Reproducing Systems".
J. Schwartz, T. T. Wu, U.S. Pat. # 4,511,229 filed 6/9/83, "Method and Apparatus for Evaluation of Color Information in Photographic Processes".
J. Schwartz, "Color Equalization", Journal of Imaging Science & Technology, July-Aug. 1992.
H. Shamir, "Multi-Color Information Encoding System", U.S. Pat. Pending.
H. Shamir, "Microlabelling System and Process for Making Microlabels", U.S. Pat. # 5,118,369.

Next page:

Table 1: Storage Capacity for 1 sq. in. Area

STORAGE CAPACITY OF HUECODE ON 1 IN^2

Level	hueDot Size (microns)	hueDot Spacing (Center to Center) (microns)	# hueDots (No./sq.in.)	ASCIIs (bytes capacity) per sq.in.	Text pages per square inch
A*	450	500	2,500	5,600	2.8
B*	230	250	10,000	22,500	11.2
C**	90	100	62,500	140,500	70
D	45	50	250,000	560,000	280
E	22	25	1,000,000	2,250,000	1,125
F	8	10	6,250,000	14,050,000	7,025
G	3	5	25,000,000	56,000,000	28,000

* = On Paper or Film; ** = On Photopaper and Instant Photographs

Example:

At Level G, .103 square inches can store one whole Bible (both Testaments).

This is 175% more than a CD-ROM!

MICRO-PRESSURE SENSORS

Ben Granath
PCB Piezotronics Inc.
Depew, N.Y.

The capability to make certain high frequency pressure measurements is often limited by the size, sensitivity and frequency response characteristics of available commercial pressure sensors.

To meet the needs for such requirements, PCB has developed special purpose ICP type sensors specifically designed for high frequency, short wave length shock and acoustic pressure measurements. The unique performance characteristics of these subminiature sensors with <l mm diameter sensing elements, include high output to 3V/psi and exceptionally fast rise time: 0.5 uS for reflected and <2.0 uS for incident shock wave measurements.

The very high output and fast response of PCB micro-sensors, make them well suited for low pressure projectile shock wave velocity measurements and acoustic pressure wave measurements associated with pyro shock plate motion. A wide range of other high frequency pressure measurements can also be made.

The following plots show some examples.

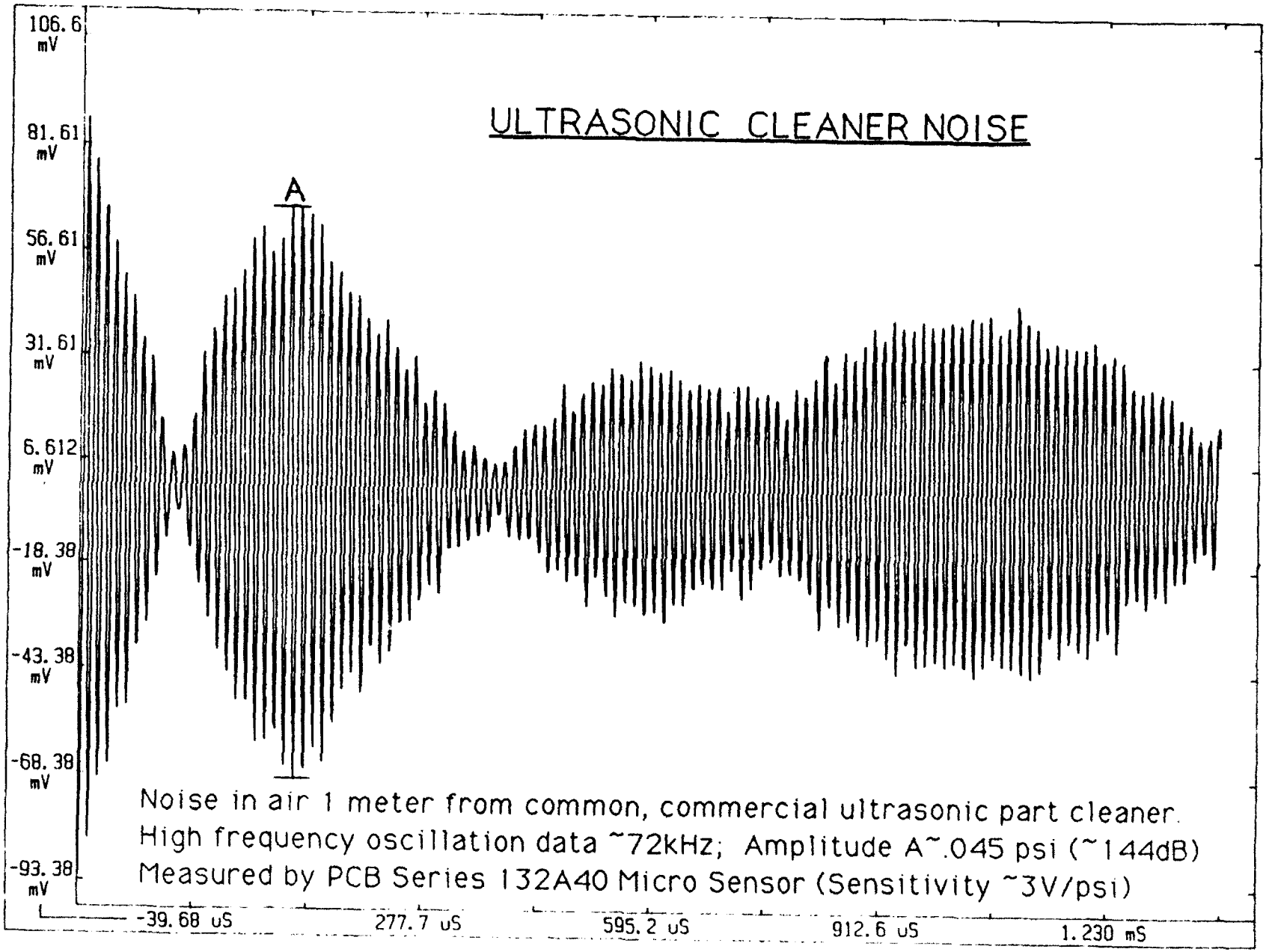
ULTRASONIC CLEANER NOISE
A
106.6 mV
81.61 mV
56.61 mV
31.61 mV
6.612 mV
-18.38 mV
-43.38 mV
-68.38 mV
-93.38 mV
-39.68 uS
277.7 uS
595.2 uS
912.6 uS
1.230 mS
Noise in air 1 meter from common, commercial ultrasonic part cleaner.
High frequency oscillation data ~72kHz; Amplitude A~.045 psi (~144dB)
Measured by PCB Series 132A40 Micro Sensor (Sensitivity ~3V/psi)

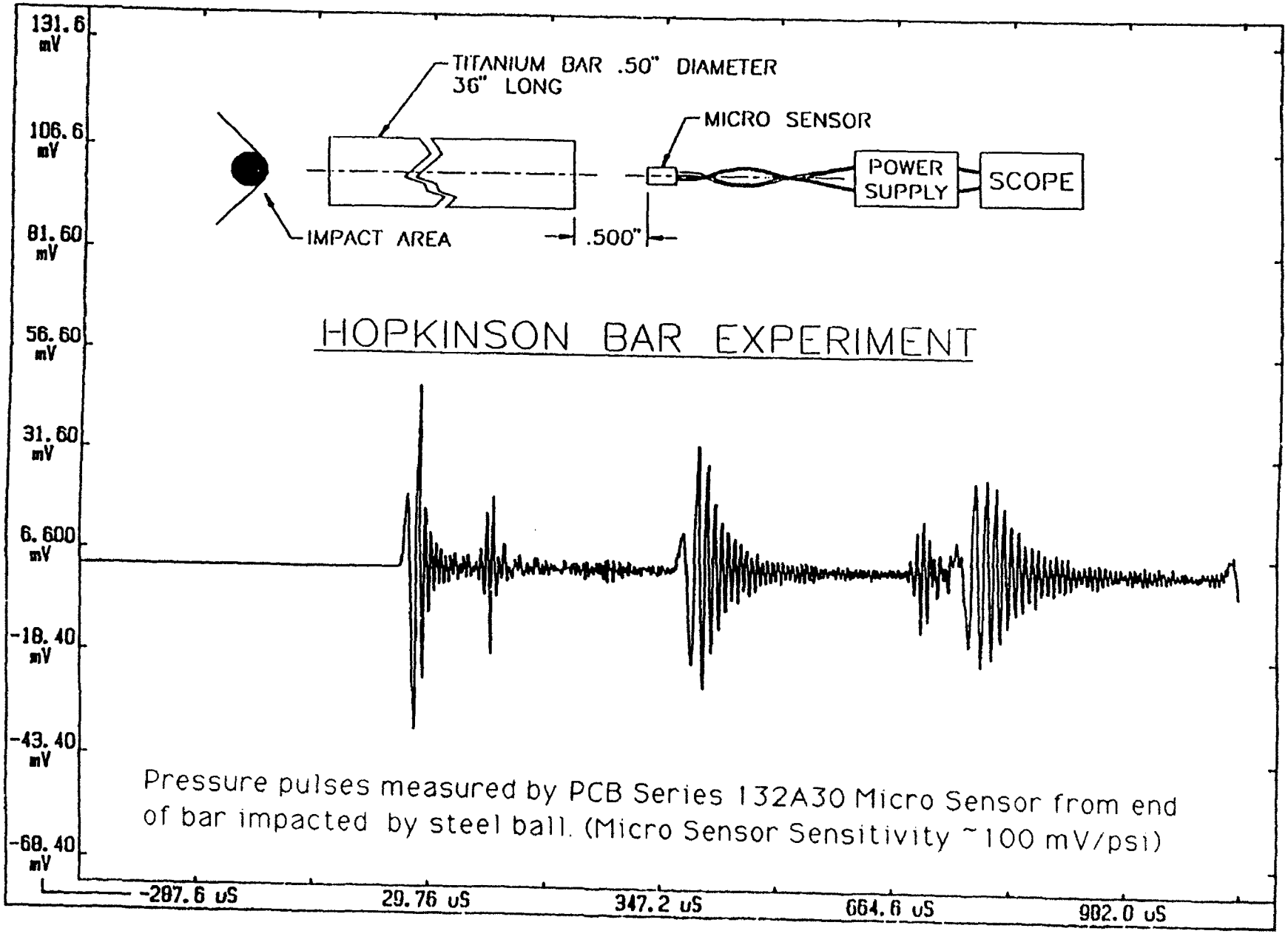
131.6 mV
106.6 mV
81.60 mV
56.60 mV
31.60 mV
6.600 mV
-18.40 mV
-43.40 mV
-68.40 mV
-287.6 uS
29.76 uS
347.2 uS
664.6 uS
982.0 uS
TITANIUM BAR .50" DIAMETER
36" LONG
MICRO SENSOR
POWER SUPPLY
SCOPE
IMPACT AREA
.500"
HOPKINSON BAR EXPERIMENT
Pressure pulses measured by PCB Series 132A30 Micro Sensor from end of bar impacted by steel ball. (Micro Sensor Sensitivity ~100 mV/psi)

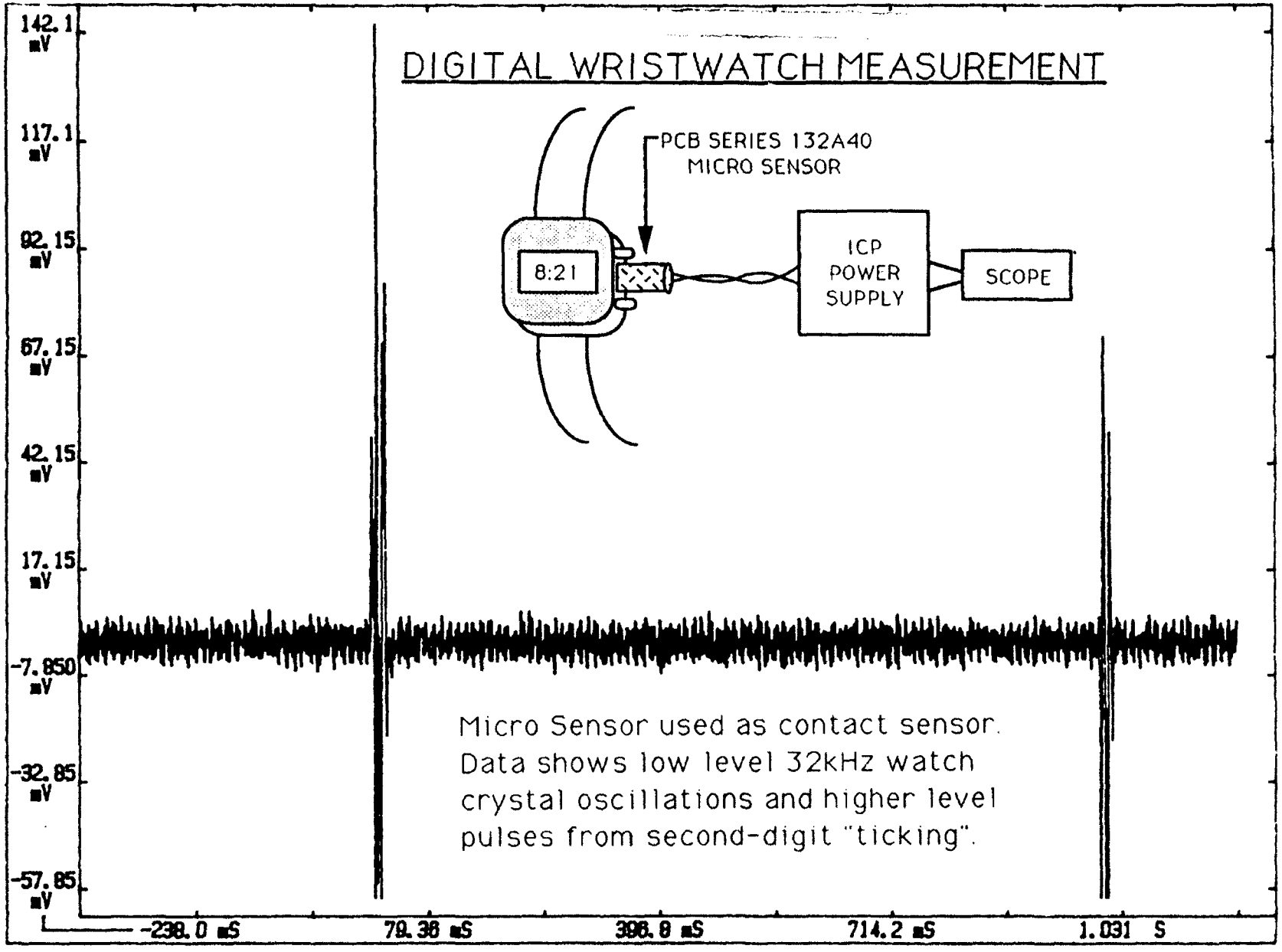
DIGITAL WRISTWATCH MEASUREMENT
PCB SERIES 132A40
MICRO SENSOR
8:21
ICP
POWER
SUPPLY
SCOPE
142.1 mV
117.1 mV
92.15 mV
67.15 mV
42.15 mV
17.15 mV
-7.850 mV
-32.85 mV
-57.85 mV
-238.0 mS
79.38 mS
396.8 mS
714.2 mS
1.031 S
Micro Sensor used as contact sensor.
Data shows low level 32kHz watch
crystal oscillations and higher level
pulses from second-digit "ticking".

132-1320-95

APPLICATION		
NEXT ASS'Y	USED ON	VAR

REVISIONS				
REV	DESCRIPTION	ECN	DATE	APP'D

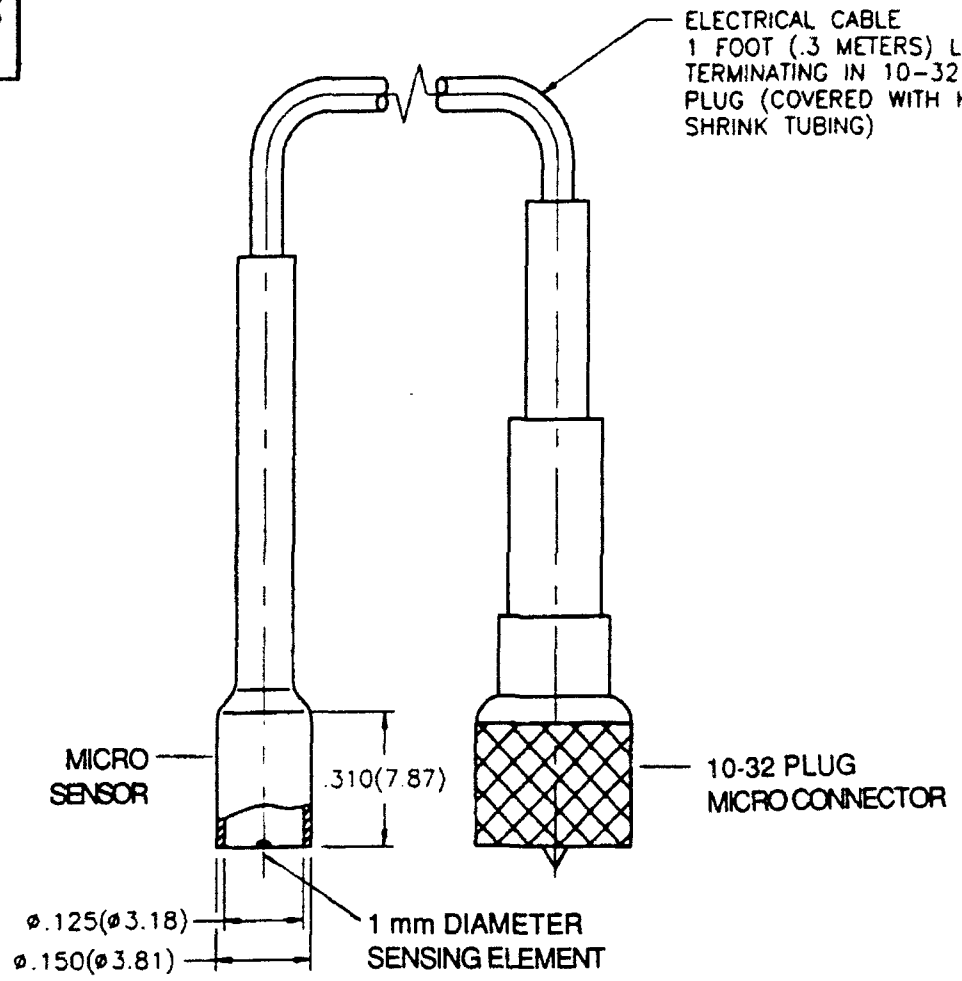

UNLESS SPECIFIED TOLERANCES							
DIMENSIONS IN INCHES: DECIMALS XX ±.01, XXX ±.005; ANGLES ±2 DEGREES	DIMENSIONS IN MILLIMETERS (IN PARENTHESIS): DECIMALS X ±0.3, XX ±0.13; ANGLES ±2 DEGREES	DRAWN	JDH	9/30/92	MFG	RJA	10/14/92
FILLETS AND RADII .003 - .005 (0.07 - 0.13)		CHK'D	DM	10/2/92	ENGR	JF	10/26/92
		APP'D	[signature]	11/5/92	Sales	DJ	11/5/92

TITLE: OUTLINE DRAWING
MODEL 132A32
"MICRO SENSOR"

PCB PIEZOTRONICS, INC.
3425 WALDEN AVE. DEPEW, NEW YORK 14043
PHONE: (716) 684-0001

CODE IDENT. NO.	DWG. NO.
52681	132-1320-95

SCALE: 4X | SHEET 1 OF 1

PCB PIEZOTRONICS

SPECIFICATIONS

ICP Pressure Sensor

Model No.
132A32

Revisions

DYNAMIC PERFORMANCE

Dynamic Amplitude Range (±5V)	psi [Bars]	50 [3.45]
Maximum Pressure	psi [Bars]	50 [3.45]
Resolution	psi [Bars]	0.005 [0.00035]
Sensitivity (nominal)	mV/psi [mV/(Bars)]	100 [1450]
Resonant Frequency	kHz	500
Rise Time (reflected)	µ sec	0.5
Rise Time (incident) (in air)	µ sec	2
Low Frequency Response (-5%)	Hz	8300

ELECTRICAL

Excitation:		
Constant Current	mA	2-20
Voltage	VDC	18-28
Output Impedance	ohms	<100
Output Bias	+ volts	8 to 14
Discharge Time Constant (nominal)	µ sec	60
Polarity		Positive

ENVIRONMENTAL

Temperature Range	°F [°C]	0 to +175 [-17.7 to +79.4]

PHYSICAL

Sensing Element		Ceramic	
Sensing Surface Dimensions	in [mm]	0.02 x 0.03 [0.51 x 0.76]	
Housing Material	st. steel	303	
Dimensions (D x L)	in	0.150 x 0.31	[1]
	[mm]	[3.81 x 7.87]	
Sealing		Epoxy	
Weight	oz [gram]	0.1 [2.98]	[2]
Connector	cable	10-32	[3]

NOTES:
[1] Diameter including heat shrink tubing.
[2] Weight including cable and connector.
[3] Attached 1 ft. twisted pair in heat shrink tubing.

SUPPLIED ACCESSORIES:
None

Approved	[illegible]	[illegible]	Spec No.
Engineer	JACK [illegible]	1-22-93	132-1320-80
Sales	Dave J	1-22-93	Sheet 1 of 1

A PROGRAM TO VALIDATE INSPECTION TECHNOLOGY FOR AGING AIRCRAFT

Patrick L. Walter
Sandia National Laboratories
Albuquerque, NM 87185

Abstract

This paper provides an overview of a program established at Sandia National Laboratories by the Federal Aviation Administration (FAA) to validate nondestructive inspection (NDI) processes for application to aging aircraft. The paper describes an NDI Validation Center, an evolving library of specimens with typical defects, a validation process, ongoing related field experimentation, and current and future work activities.

Introduction

The Aging Aircraft NDI Validation Center (AANC) was established by the Federal Aviation Administration Technical Center (FAATC) at Sandia National Laboratories (SNL) in August of 1991. This Center supports the Inspection portion of the FAA's National Aging Aircraft Program. This national program was mandated by Congress through the 1988 Aviation Safety Act. While the AANC's funding source is the FAA, its ultimate customers include the airframe and engine manufacturers, airlines, and third party maintenance facilities.

The goal of the AANC is to provide independent validation of technologies intended to enhance the structural inspection of aging commuter and transport aircraft. The existing oversupply of passenger capacity and poor airline earnings (1), coupled with defense cutbacks, indicate that technologies validated by the AANC should also attempt to contribute to the financial health of the aviation industry. The deliverables from the AANC's validation activities will be an assessment of the reliability of proposed inspection technologies as well as analyses of the cost benefits to be derived from their implementation.

Center Key Elements and Status

NDI Validation Center-A ribbon cutting ceremony which officially opened the NDI Validation Center was hosted by SNL on February 10, 1993, at the request of the FAATC. The Center is housed in a hangar on the west side of Albuquerque International Airport. This site has close proximity to SNL, ease of access for Center users, and access to airport repair and maintenance facilities. The Center contains 16,875 square feet of aircraft storage space, 7,762 square feet of office and storage space, and 99,988 square feet of outdoor pad space. The Center is intended to replicate a working maintenance environment where human factors which influence inspection reliability can be controlled.

It contains test beds for use by private and government sectors in its growing Sample Defect Library .

Sample Defect Library-This Library contains samples of the major types of damage encountered in aging aircraft for use in validating NDI processes. It presently contains over 100 examples of aircraft repairs; panel, skin and frames sections, and other structural elements. The Sample Defect Library contains representative examples of corrosion, disbonds, and fretting, as well as first and second layer fatigue cracks. A B737-200 with 46,358 cycles, a nonworking JT8D engine, and its complete maintenance records resides in the Center's Library. By using an entire aircraft, the AANC can assess human factor issues such as accessability (e.g., on wing inspection), hangar environmental issues, and inspector-aircraft-NDI equipment interactions. The aircraft can also be used to assess NDI techniques which require fuselage pressurization. Figure 1 illustrates the aircraft/hangar environment. Currently, large sections of DC9 fuselage structure are also being acquired.

Validation Process- The Validation Process (3) consists of an independent, quantitative, and systematic assessment of both the reliability and the implementation costs of an NDI process. An NDI process is defined as the NDI systems and procedures used for inspection; as well as the NDI equipment operator, inspection environment, and the object being inspected. The phases of the Validation Process are Phase 1. Conceptual, Phase 2. Preliminary design, Phase 3. Final design, and Phase 4. Field implementation. Validation activities in Phase 1 are comprised of identification of the interrogated component, flaw, and material type; laboratory verification; initial capability assessment; and initial equipment cost assessments. Phase 2 activities involve laboratory tests, identification and enumeration of preliminary NDI procedures, inspector requirements, and facility requirements. Phase 3 includes assessment of factors affecting reliability, demonstration of feasibility through "blind" procedures, acquisition of inspection time data, and early field trials. Phase 4 involves preparation of validation samples, finalization of procedures, field trials with independent inspectors, field trials with potential users, assessment of inspector training needs, and Beta-site testing.

The AANC becomes progressively more involved through Phases 2, 3, and 4 of the Validation Process. To the extent possible, the environment and conditions affecting inspection will be incorporated into the validation activities that take place in the AANC's Validation Center. If necessary, field trials and experiments to provide input into the reliability and implementation cost assessments will be coordinated at operating airline facilities. The AANC may train airline personnel in the use of a given NDI process and loan them equipment for additional feedback. The first NDI instrument to enter the Validation Process is the Magneto-Optic/Eddy Current Imager (MOI) manufactured by Physical Research, Inc. This instrument uses a magneto-optic sensor to directly view the magnetic field images associated with cracks on the surface of a material.

Field Experimentation-A Principal Structural Element (PSE) is defined as that part of structure whose failure could lead to the loss of the aircraft. All transport aircraft and

some commuters are now designed to Damage Tolerance Analysis (DTA) requirements. DTA is the combination of slow crack growth analysis, residual strength calculations, and NDI procedures (2). FAR 25.571 "Airplane Damage Tolerance Requirements" mandates design requirements for transport aircraft and Figure 2 illustrates the ingredients that make up DTA. Probability of Detection (POD), included in Figure 2 as a function of flaw size, is the fraction of flaws of nominal size, "a", that are expected to be detected in a given inspection. The POD associated with a given NDI process is a key ingredient in setting the inspection interval for a PSE. Airframe manufacturers' determine the POD at their facility for the NDI process they specify to inspect a given PSE. They then apply conservatism (4) to account for differences between the POD they determine and what they expect to exist in the environment of a field maintenance facility. The question unanswered is: what is the actual POD associated with an NDI process at the field maintenance facility?

At the FAATC's request, the AANC designed and is currently implementing an experiment to quantitatively assess the reliability (POD) of high-frequency eddy current inspections of lap splice joints in airline maintenance and inspection facilities. Human factor issues which can degrade inspector performance are encompassed in this experiment (5,6). Specific factors to be studied within the experiment plan include off-angle cracks, unpainted versus painted surfaces, variation of reference standards, accessibility of the task, time into task (boredom), work shifts, and differences in specimen definition. Data will be collected during the experiment on facility conditions such as lighting, noise level, and inspector training and recency of experience. Figure 3 shows the experimental setup which includes approximately 76 feet of lap splice. This experiment is traveling to nine maintenance facilities, three of which are third party (not directly associated with an airline). A human factors expert and an NDI technician are traveling with the experiment. Science Applications International Corporation (SAIC) and AEA Technology, Harwell (UK) participated with SNL in the experiment design. SAIC is fielding the experiment for SNL.

Previously mentioned was that the MOI was the first instrument to enter the Validation Process. The MOI was originally designed to inspect for surface cracks at rivet sites on aircraft skin as a competitive technology to high-frequency eddy current probes. Incorporation of the MOI into this field experiment allows its reliability to be assessed and directly compared to PODs determined for the high-frequency eddy current inspections. The Northwestern University Transportation Center (NUTC) is performing a cost benefit analysis of the MOI.

Current Work Activities-The POD of Eddy Current Lap Splice Experiment has traveled to five maintenance facilities thus far: American Airlines, Dalfort Aviation, Aloha Airlines, Tramco, and Alaska Airlines. The MOI was integrated into this experiment during stops at American and Dalfort. Four more facilities will take part in the experiment through August of 1993.

The FAATC has funded NDI initiatives at Penn State, Wichita State, Carnegie Mellon, and Johns Hopkins Universities; Grumman Aerospace; and Transport Canada. In

addition, its other principal center, Center for Aviation Systems Reliability (CASR: Iowa State, Northwestern, and Wayne State Universities), has many NDI initiatives in progress. Most of these initiatives are in Phase 2 of the Validation Process and will soon be reaching the AANC for demonstrations or early field trials. Wayne State University recently completed one week of demonstrations at the AANC using Thermal Wave Imaging on the B737 aircraft. This imaging is a broad area technique to locate corrosion and disbonds. In addition, the AANC is surveying commercially available manual scanners for eddy current and ultrasonics aircraft inspection as well as commercially available visual inspection aids (e. g., light sources, shadow Moire, structured light). New Mexico State University also is working within the AANC on shearography aided inspection. This laser based inspection technique will be able to map whole strain fields for applications such as quantifying bond degradation in repair applications.

Work is also continuing on acquiring additional blind samples for the Sample Defect Library of the Center. A data base is being established for this Library to electronically catalogue specimen histories and to store inspection results.

Future Work Activities-Experience gained from field experimentation will identify those key human factor elements to replicate in the Validation Center. This will enable a more cost effective assessment of the reliability of NDI processes. A program in visual experimentation will also be initiated. In visual inspection, the human being is the equivalent of the NDI instrument. It is difficult to assign a quantitative reliability to visual flaw inspection. Flaws are detected by many clues such as sight ("smoking rivets"), touch (rough surface), and smell (leaking fuel vapors). Nevertheless, comparative visual inspection experimentation may be performed to assess effects such as directivity, stand-off distance, and inspection aids.

A program will be initiated to baseline the condition of the AANC's B737 aircraft. Dependent on findings, engineered flaws may be placed in the airframe structure against which to assess NDI processes. The Sample Defect Library will continue to be expanded as will its database to accomodate electronic media input as well as to implement data fusion for comparison among multiple inspection techniques. Techniques will be developed to pressurize the B737 to operating cabin levels. This will enable validation of processes associated with NDI techniques such as shearography and acoustic emission which are dependent on a pressurized aircraft. As the funded NDI initiatives within the FAATC's program continue to mature, the AANC will become increasingly involved with field trials and Beta-site testing to interface the FAA's program to the civil aviation industry.

Conclusion

This paper has described the Aging Aircraft NDI Valiation Center established at Sandia National Laboratories by the Federal Aviation Administration Technical Center. The AANC and its Sample Defect Library, integrated into a defined Validation Process, are allowing the reliability and cost effectiveness of NDI processes to be assessed. The

AANC is also conducting a POD experiment which will provide a quantitative assessment of the reliability of existing high frequency eddy current lap splice inspections in airline maintenance facilities. This field experiment will help identify which key human factors to replicate within the Center to provide a more economical and faster assessment of field reliability. A program in visual experimentation will soon be initiated. The AANC will become increasingly involved with field trials and Beta site testing to best interface the FAA's program to the civil aviation industry.

*This work is supported by the FAA Technical Center, Atlantic City International Airport, New Jersey.

Bibliography

1. Dornheim, Michael A., "Cuts, Layoffs Affirm Transport Boom's End", Aviation Week and Space Technology, 22-24 (February 1, 1993).

2. Commercial Product Support (DRAFT), Subdivision Procedure, "Process for Approval of PSE Repairs", Douglas Aircraft Corporation (January 28, 1993).

3. The Role of the Aging Aircraft Development and Demonstration Center in the FAA Validation Process, Aging Aircraft Projects Department 2757, Sandia National Laboratories, Albuquerque, NM, (July 14, 1992).

4. Hagemaier, Donald J., "Reliable Supplemental Inspections of Aging Commercial Aircraft", Douglas Paper 7954, 14pp, and ASNT Fall Conference, Atlanta, GA (October 5-9, 1987).

5. Spencer, Floyd; Borgonovi, Giancarlo; Roach, Dennis; Schurman, Don; Smith, Ron; "Generic Reliability Assessment Programs at Airline Maintenance and Inspection Facilities", Aging Aircraft Projects Department 2757, Sandia National Laboratories, Albuquerque, NM (May 1992).

6. Spencer, Floyd; Borgonovi, Giancarlo; Roach, Dennis; Schurman, Don; Smith, Ron; "Proposed Reliability Assessment Experiment for Eddy Current Inspection of Lap Splice Joints in Airline Maintenance and Inspection Facilities", Aging Aircraft Projects Department 2757, Sandia National Laboratories, Albuquerque, NM (May 1992).

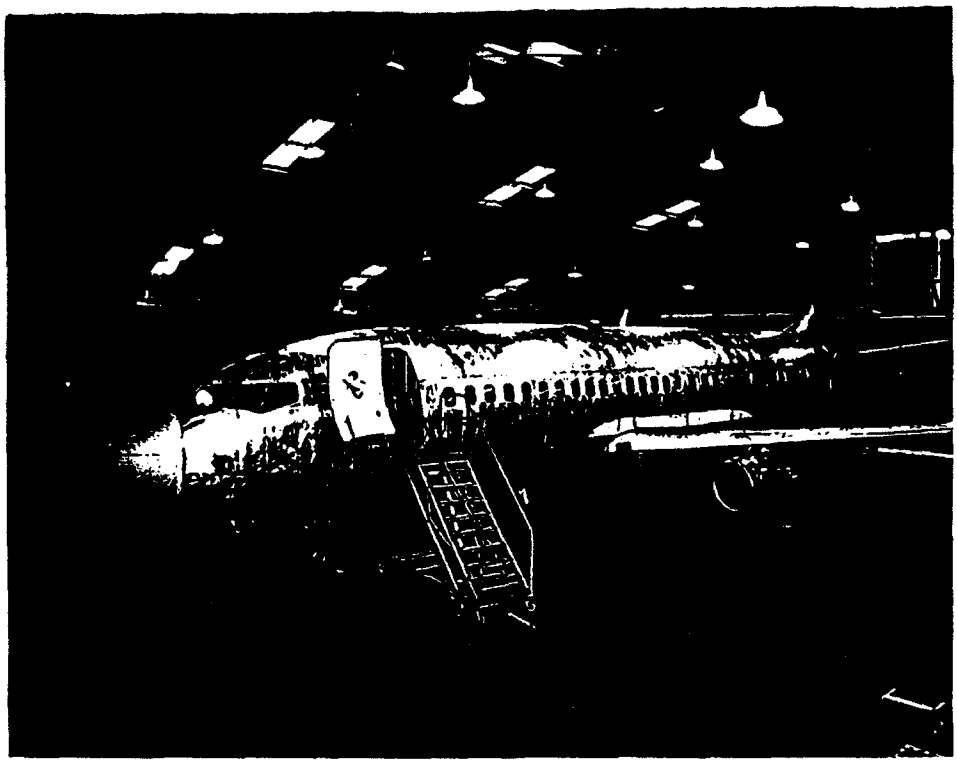

Figure 1. Aging Aircraft Test Specimen in Validation Center

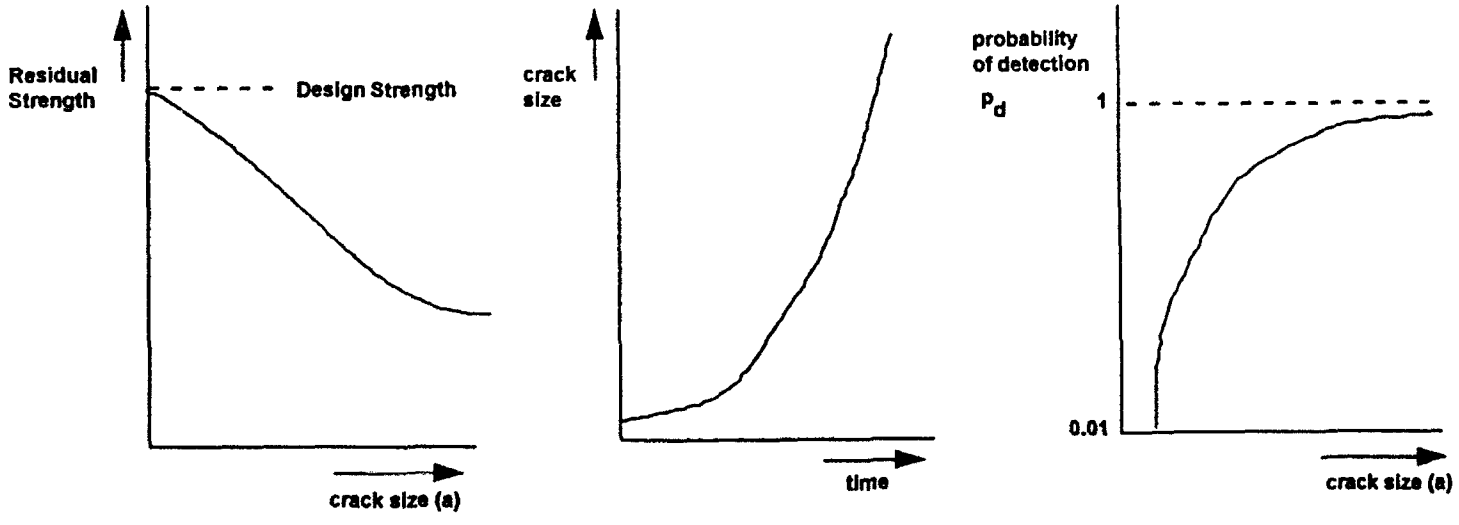

a. Residual strength in a principal structural element

b. Crack growth model

c. Probability of detection for a given inspection technique

Figure 2. Components of Damage Tolerance Analysis

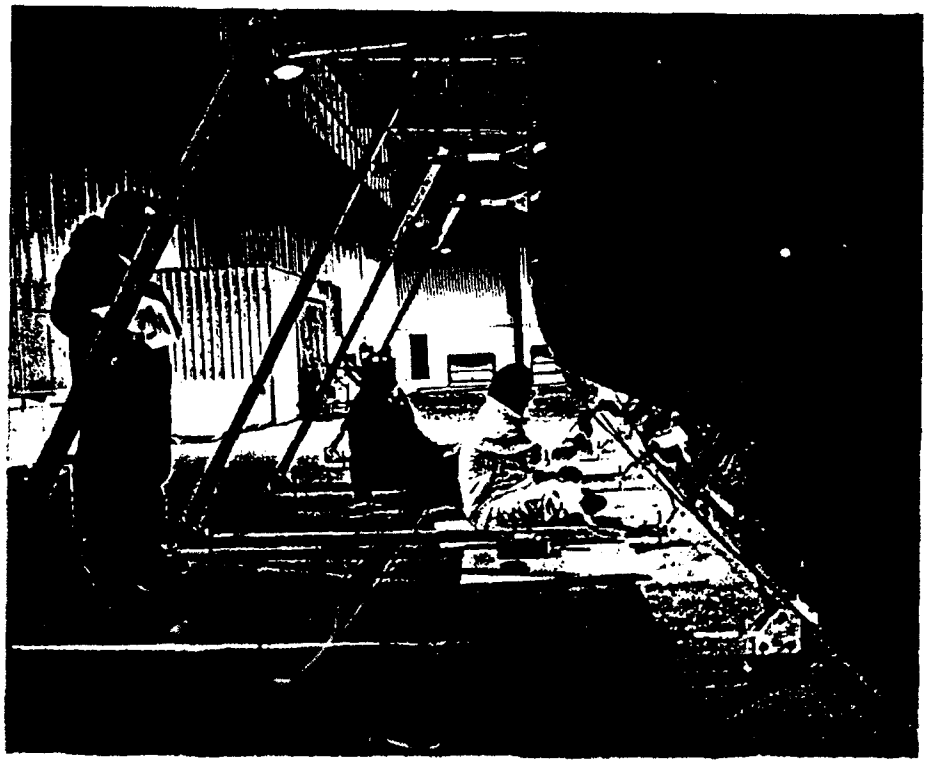

Figure 3. POD of Eddy Current Lap Splice Experiment

A CRYOGENIC PRESSURE SENSOR MODULE FOR SPACE SHUTTLE MAIN ENGINE APPLICATIONS

Seun K. Kahng, Qamar A. Shams, and Vincent B. Cruz
NASA Langley Research Center
Hampton, VA 23681-0001

ABSTRACT

A multichannel cryogenic pressure sensor module has been developed and tested over an extended temperature span from -184 °C to +50 °C and a pressure range of 0 to 5,000 psi. Objectives of this program are to develop a four-channel pressure sensor module with a pressure range of 0 to 5,000 psia and an operating temperature region from -253 °C to 60 °C. Applications of these modules are intended for measurements of hydrogen and oxygen fuel line pressure of the Space Shuttle main engines.

The pressure sensor modules reported in this paper consists of two pressure sensor dice and two differential-input instrument amplifiers, all of which are packaged in a stainless steel pressure vessel with feedthrough pins. The pressure sensor dice are piezoresistive type of silicon-on-silicon structure with an evacuated reference chamber for absolute pressure measurements. The operating pressure range of the sensor dice is from 0 to 5,800 psia with the maximum pressure rated at 8,700 psia. The two instrumentation amplifiers in the module are not exposed to the pressure environment, but they are exposed to the cryogenic environment.

The pressure sensor modules exhibit a typical sensitivity of 0.008 mV/V/psi. Typical offset voltage of these sensors are less than 0.35 percent of full-scale output over a temperature range of -260 °C to 20 °C. Maximum static error and nonrepeatability at -184 °C are 0.31 percent and 0.42 percent of full-scale output, respectively. Vibration and shock tests revealed that no detectable sensor output has been observed up to 80 g's from 20 Hz to 2,000 Hz and 400 g's of a half-wave sinusoidal shock along the three axes. Exposure of the sensor modules in H_2 and O_2 environments at 1800 psi over a period of 31 days showed no sign of sensor performance degradation nor any observable change of the sensor materials.

INTRODUCTION

A two-channel cryogenic pressure sensor unit has been developed for measurements of fuel pressure of Space Shuttle Main Engines (SSME). The pressure sensor unit consists of two piezoresistive silicon pressure sensor dice and two instrument amplifiers; the pressure sensor dice are enclosed in a stainless steel pressure vessel, and the amplifiers are mounted on the outside of the stainless steel pressure vessel. Currently, pressure sensors used for SSME applications are thin-film deposited strain gage types which were primarily constructed for operations outside of the liquid oxygen and hydrogen temperatures, -60 °C to +165 °C.

Desired specifications of the pressure sensor units are:

1) Pressure range: 0 - 5000 psia
2) Temp. range: -253 °C - +60 °C
3) Freq. bandwidth: 0 - 2,000 Hz
4) Vibrations/Shock: 80 g's from 25 Hz to 2,00 Hz and 400 g's impulse
5) Accuracy:
    a) Max. Static Error: Less than 0.25% of FSO

b)	Max. Nonlinearity:	Less than 0.25% of FSO
c)	Max. Thermal Error:	Less than 0.25% of FSO/C at T=-253 °C
		Less than 0.25% of FSO/C at T=+60 °C
6)	Temp. Coeff. of offset Voltage:	Less than 0.05% of FSO/C
7)	Temp. Coeff. of Sensitivity:	Less than 0.25% of FSO/C
8)	Maximum Hysteresis:	Less than 0.5% of FSO
9)	Maximum Over Pressure:	8,700 psia for sensor dice
		12,000 psi for pressure vessel
10)	Long Term Stability:	Less than 1% of FSO/30 days
11)	Materials Compatibility:	High pressure O_2 and H_2 environment

The three most important areas in the development of a cryogenic multichannel SSME pressure sensor unit are silicon pressure sensor dice, cryogenic compatible packaging of the pressure sensor components, and signal conditioning circuit which is integrated next to the pressure sensor dice. High pressure hydrogen and oxygen fuel environments at cryogenic temperatures pose a different set of requirements for the pressure sensors, and they are considered in the following sections.

A cross sectional view of the two channel pressure sensor unit is shown in figure 1. Two silicon pressure sensors are attached on a circular Teflon and alumina substrate with a number of holes which accommodates feedthrough pins of the pressure vessel. The feedthrough pins are soldered to the substrate for the purposes of electrical connection to the silicon sensor dice and structural support of the substrate. Electrical connections between the silicon sensor dice and the substrate are made with ultrasonic bonding of a 0.00075-inch diameter gold wire. Two instrument amplifiers are placed on a Kevlar/epoxy printed circuit board that is mounted to the outside feedthrough pins of the pressure vessel.

When the cryogenic pressure sensor unit is exposed to near the temperatures of liquid hydrogen or oxygen, thermally induced undesirable stress may develop across the bonded interfaces of dissimilar materials of the sensor unit and cause delamination of the bonded interfaces such as silicon pressure sensor dice and a substrate on which the silicon sensors are attached. Any induced stress on the silicon sensor will cause the sensor offset voltage variations that are detrimental to the accuracy of the overall instrument system. Considerable emphasis is given in selection of materials whose temperature coefficients of expansion profile are similar over a wide range of temperatures. Use of an absolute measurement pressure sensor, which does not require a reference pressure port, has eliminated a considerable amount of difficulties associated with introducing a reference port in a high pressure cryogenic system.

The silicon pressure sensor dice in use have an impurity density in the range of 10^{20} atoms per cubic centimeter, which will provide a considerably stable temperature coefficient of offset voltage, with reduced sensitivity, over a cryogenic temperature range. Most of the commercially available silicon pressure sensor dice are lightly doped for a higher sensitivity at room temperatures, however, they may no longer behave as a viable sensor at temperatures below -100 °C. These sensors will show decrease in the bridge resistance values with decreasing temperature from room temperature to roughly -100 °C, due to increase in mobility of the charge carriers. Temperatures below -100 °C, the resistance values will increase with decreasing temperature as an effect of charge carrier freeze-out. These changes in the resistance values cause a considerable variation in offset voltage of the lightly doped silicon pressure sensors.

An instrument amplifier circuit board consists of two instrument amplifiers and other passive components associated with the amplifier circuit. These components are not directly exposed to the cryogenic environment, however, they are located in the outside chamber of the pressure vessel where the temperature is lower than that of ambient. Prototype pressure sensor units have been constructed for cryogenic operations and tested repeatedly at -184 °C with the instrument amplifier circuit board operating for a period of over 4 hours at a time.

Pressure sensor units have been evaluated to determine their sensitivity, long-term stability, offset voltages over a temperature range of -184 °C to +50 °C, maximum static error and nonrepeatability. Vibration and shock tests were conducted up to 80's from 20 Hz to 2,000 Hz and 400 g's of a half wave sinusoidal shock along the three axes. Sensor modules were exposed to gaseous H_2 and O_2 environments at 1,800 psi over a period of 30 days, and the sensors have shown no observable change on their performance characteristics.

TECHNICAL CONSIDERATIONS AND EXPERIMENTAL RESULTS

This section deals with the selection criteria for silicon pressure sensors for cryogenic applications, bonding/adhesive materials, instrument amplifier circuits compatible with cryogenic pressure sensor applications, pressure vessel and its frequency response, and experimental results.

1. Silicon Pressure Sensor Dice for Cryogenic Applications

Silicon pressure sensor dice have four piezoresistance elements forming a Wheatstone bridge configuration on a monolithic silicon substrate. Changes in the values of these resistances are observed as a function of pressure input to the sensor. Properties of these resistors along with mechanical configuration of the sensor play important roles: sensitivity, thermal properties, accuracy, hysteresis, and long-term stability.

These resistors are metalogically diffused into the silicon substrate either by means of thermal diffusion or ion implantation of impurity atoms into a silicon substrate, and the number of these impurities determine the density of charge carriers available in the conduction band of the silicon bridge resistor. As the charge carrier density is increased, piezoresistance and temperature coefficient of resistance decrease [1]. For a lightly doped pressure sensor, a higher value of piezoresistance coefficient is obtained but its offset voltage may become undesirably high at cryogenic temperatures. At temperatures near -200 °C, a lightly doped bridge resistors may increase their resistance values by a factor of three, and offset voltages of silicon pressure sensors may vary unpredictably [2]. It is noted that impurity density of $1x10^{20}/cm^3$ is a reasonable compromise for acceptable sensor stability and sensitivity.

Selected silicon pressure sensor dice for the cryogenic SSME applications have their impurity density near $1x10^{20}/cm^3$, and the pressure sensor dice are micromachined to form a pressure sensing diaphragm with a support rim. The supporting rim is bonded with gold/tin eutectic material to a silicon substrate in vacuum, thus making the sensor an absolute type device. Temperature coefficients of offset voltage of silicon pressure sensors were studied with the sensor dice bonded to a Teflon printed circuit board with cryogenic adhesive and with others free from the board, and it showed that no determinable variations in the offset voltages between these two cases were observed over a temperature span of -184 °C to +50 °C. The maximum offset voltage of these sensors has been less than 0.35 percent of full scale output from -260 °C to 20 °C, see figure 2.

2. Pressure Sensor Board and Pressure Vessel

The pressure sensor boards are either Teflon based printed circuit boards with copper electrode or aluminum nitride wafers with thick-film gold electrode. Electrical connections between the pressure sensor dice and the pressure sensor board were made with 0.00075-inch diameter gold wire using an ultrasonic wedge bonder. In addition to Teflon based printed circuit board and aluminum nitride boards, alumina boards were also evaluated. All of these boards have not shown any sign of degradation or microcracks, after they were exposed to 10 consecutive thermal cycles from room temperature to liquid nitrogen bath dip.

In view of materials compatibility in high pressure hydrogen and oxygen environments, and the differences in temperature coefficients of expansion between silicon with respect to the pressure sensor

board materials, aluminum nitride and alumina show favorable properties. Temperature coefficient of expansion of silicon is known to be in the range of 5 to 6 parts-per-million (ppm) per degree C, while that of aluminum nitride shows 4 ppm/C, Teflon varies from 18 (x-axis) to 13 (y-axis) ppm/C, and alumina with 5.4 ppm/C. Bonding of silicon pressure sensor dice to the boards was made with gold/tin (Au/Sn) eutectic and cryogenic adhesive (Crest-7450) for aluminum nitride and Teflon PCB, respectively.

Use of Au/Sn eutectic sheet requires heating of the silicon sensor dice and the board to 320 °C. It is noted that a fractional surface area of the silicon pressure sensor dice were bonded to the board so as to minimize unwanted stress generated by the difference in coefficients of thermal expansion of two dissimilar materials, a typical bonding area is approximately 2 mm x 2 mm.

Crest-7450 is rated by the manufacturer with elongation factor of 1.5 percent and tensile shear stress of 7,000 psi at -196 °C. Room temperature elongation factor of Crest-7450 is 500 percent. Pull tests conducted in our laboratory showed 3,200 psi tensile shear stress at -184 °C, no attempt has been made to resolve this discrepancy as the pressure sensor dice would be subjected to shear stress well below 3,200 psi, as they are absolute sensors. Pull tests of Au/Sn bond with silicon sensor dice could not be carried out properly as either silicon sensor or aluminum nitride substrate broke off before any bonding failure across the interface took place.

The pressure vessels have been designed and obtained through a commercial concern, the specifications of the vessels are: (1) 12,000 psi maximum operational pressure, (2) operational temperature range from -253 °C to +60 °C, (3) leak rate less than 10^{-9} Torr, (4) shock level of 400 g's half-wave 4 msec. sinusoid and 80 g's from 20 to 2,000 Hz, (5) vessel material of #316 stainless steel, and electrical contacts of MIL-I23011, class 2, with type 3 gold plating. The vessels have shown excellent structural integrity throughout the numerous thermal cycles with no leakage at the glass insulation to metal joints. The vessel has been hydrostatically pressurized to 15,000 psi to evaluate its structural and sealing integrity after a number of thermal cycles from room temperature to -196 °C.

3. Exposure to Hydrogen and Oxygen Fuel Environments

Though actual exposure of the pressure sensor units to oxygen and hydrogen fuel environments is in the order of minutes for each mission of Space Shuttle flight, materials used for the pressure sensor units were selected to assure their compatibility with high pressure gaseous/liquid oxygen and hydrogen. The materials exposed to the fuel environments are pressure vessel of stainless steel #316 with glass insulation and gold plated Kovar electrical feedthrough pins. The pressure vessel contains silicon pressure sensor dice bonded on a copper lined Teflon substrate with a cryogenic adhesive or a thick-film gold electroded aluminum nitride with Au/Sn eutectic material.

Type 300 series stainless steel and copper alloys are known to be compatible for gaseous and liquid oxygen service. Type 300 stainless steel and copper alloys are approved, NHB 8060.1 criteria, for use in gaseous oxygen at 10,000 and 6,700 psig at temperatures less than 72 °C, respectively [3], In liquid oxygen at 1,050 psig, copper alloys and type 300 stainless steel are compatible for service based upon NHB 8060.1A criteria. Compatibility information on the remaining materials in high pressure oxygen environments have not been found. In cryogenic gaseous and liquid hydrogen environments, the materials used for the sensor units are known to be stable.

Upon integration of the pressure sensor units and establishment of the sensor baseline performance, they were exposed to gaseous oxygen and hydrogen at 1,800 psi for a period of 30 days each. Comparison of these sensor units' performance after the 30 days period in each gas has shown no detectable change in sensor characteristics.

4. Thermal Shock

During the course of normal operations, the pressure sensor units will be exposed to gaseous or liquid environment as well as a mixture of both states in some cases. The sensor units may experience a considerable change in temperature when the state of fuel changes from gas to liquid, which may be the case when the Space Shuttle main engines are started. Though this sudden change of temperature and gaseous to liquid state cannot be simulated, a number of substrates with silicon pressure sensor dice were dropped into liquid nitrogen bath and then brought it back to room temperature for three times, which correspond to a severe thermal shock. Visual observation under microscope does not reveal any damages or microcracks of the dice, and simple manual sheer tests of the die to substrate do not indicate any delamination of the die to substrate bond.

5. Instrument Amplifier Circuit Board

The instrument amplifier circuit board consists of two instrumentation amplifiers (AD 524SD) and a set of resistors. All of these electronic components were tested in liquid nitrogen temperature before they were integrated into the board. The cryogenic temperature response shows that the gain variations of these amplifiers were measured to be less than 0.0026 percent of FSO per degree C [2]. Approximately 50 percent of AD 524SDs failed when they were first operated at the liquid nitrogen temperature. Teledyne 911's have been used with the similar results.

6. Vibration Tests

Vibration and mechanical shock tests were conducted at a room temperature and -196 °C. For the vibration tests, acceleration levels were varied up to 80 g's from 20 Hz to 2,000 Hz along the three axes while the sensor outputs were monitored. This vibration test has been repeated twice at room temperatures and also near -196 °C, and no resonant frequency was observed from the sensor outputs. A series of shock tests at room temperatures and near -196 °C have revealed that the sensor units are immune to a quarter-wave sinusoidal shock of 4 msec. period reaching the shock level of 400 g's.

7. Long-Term Stability

A long term stability of the pressure sensor units were observed at room temperatures over a period of 31 days at six pressure set points from 0 to 5,000 psi with an increment of 1,000 psi. On each day the pressure sensor unit was turned on and tested immediately at 11 pressure points from 0 to 5,000 psi and back to 0 psi. A long-term stability of 0.56 percent of full-scale output has been observed over a period of 31day's. Figure 3 shows the 31day long-term stability profile of a pressure sensor unit. No attempt was made to determine hysteresis of the sensors as the pressure settings were not made without over- and under-shooting of the desired pressure settings.

8. Resonance Frequency Estimation of Pressure Vessel

Helmholtz resonance frequencies have been estimated with a final version pressure vessel of 0.7 inch D x 0.75 inch L cylindrical pressure vessel with -184 °C gaseous media, the resonant frequencies varied from 200 Hz to 2,500 Hz for the inlet orifice radius of 0.1 inch to 0.25 inch.

9. Pressure Sensor Performance

A cryogenic two-channel pressure unit was connected to a pressure controller and data acquisition system. The pressure sensor unit was placed in an environmental chamber whose temperature was adjusted from -184 °C to +20 °C. Figure 4 is a typical response of the pressure sensor units with increasing pressure from 0 to 5,000 psi and returning to 0 psi. Maximum static error and nonrepeatability are 0.31 percent and 0.42 percent of full-scale output, respectively.

CONCLUSION AND REMARKS

A cryogenic 2-channel pressure sensor unit for the SSME has been developed and tested over an extended temperature span from -184 °C to +50 °C and a pressure range of 0 to 5,000 psi. The pressure units have a typical sensitivity of 0.008 mV/V/psi. Maximum offset voltages are less than 0.35 percent of full-scale output over a temperature range of -260 °C to 20 °C. Typical maximum static error and non-repeatability at -184 °C are 0.31 percent and 0.42 percent of full scale output, respectively. Long-term stability of this unit is less than 0.56 percent of FSO/31 days. The pressure sensor units are also immune to a sinusoidal shock up to 400 g's and vibration level of 80 g's from 20 Hz to 2,000 Hz.

REFERENCES

[1] Kanda, Y., "Graphical Representation of the Piezoresistance Coefficients in Silicon," IEEE Trans. Electron Devices, Vol. ED-29, No. 1, January 1982, pp. 64-70.

[2] Kahng, Seun. K. and Chapman, John. J, "Piezoresistive Silicon Pressure Sensors in Cryogenic Environment," Proc. 35th International Instrumentation Symposium, Orlando, Florida, May 1989, pp. 663-667.

[3] Document No. 79K09560, "Material Selection List for Liquid Oxygen Service," and Document No. 79K09561, " Materials Selection List for Gaseous Oxygen and Air Service," NASA, John F. Kennedy Space Center, 1977.

Figure 1. Cross Section of 2-Channel Unit

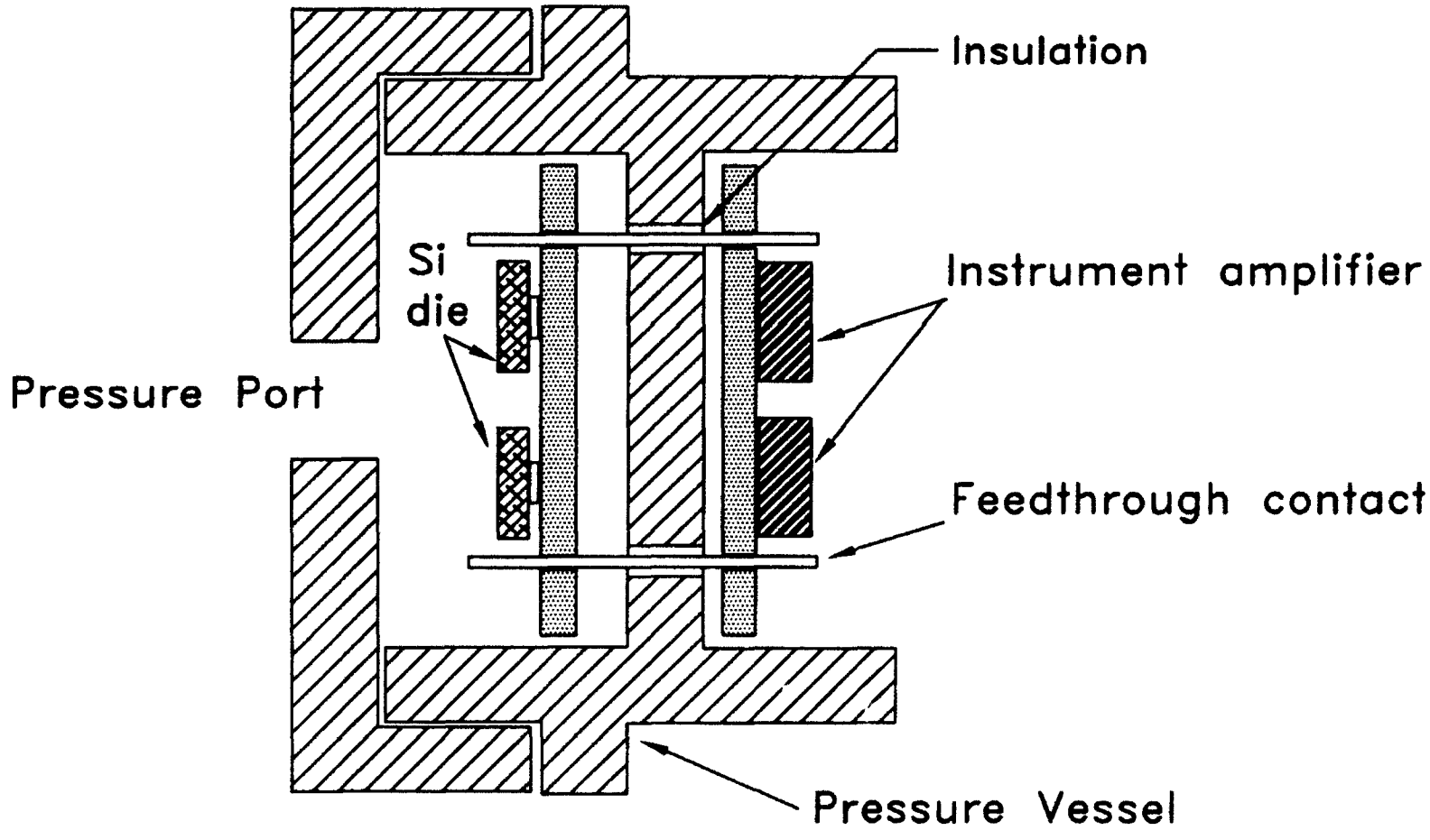

Figure 2. Offset Voltage vs. Temp.

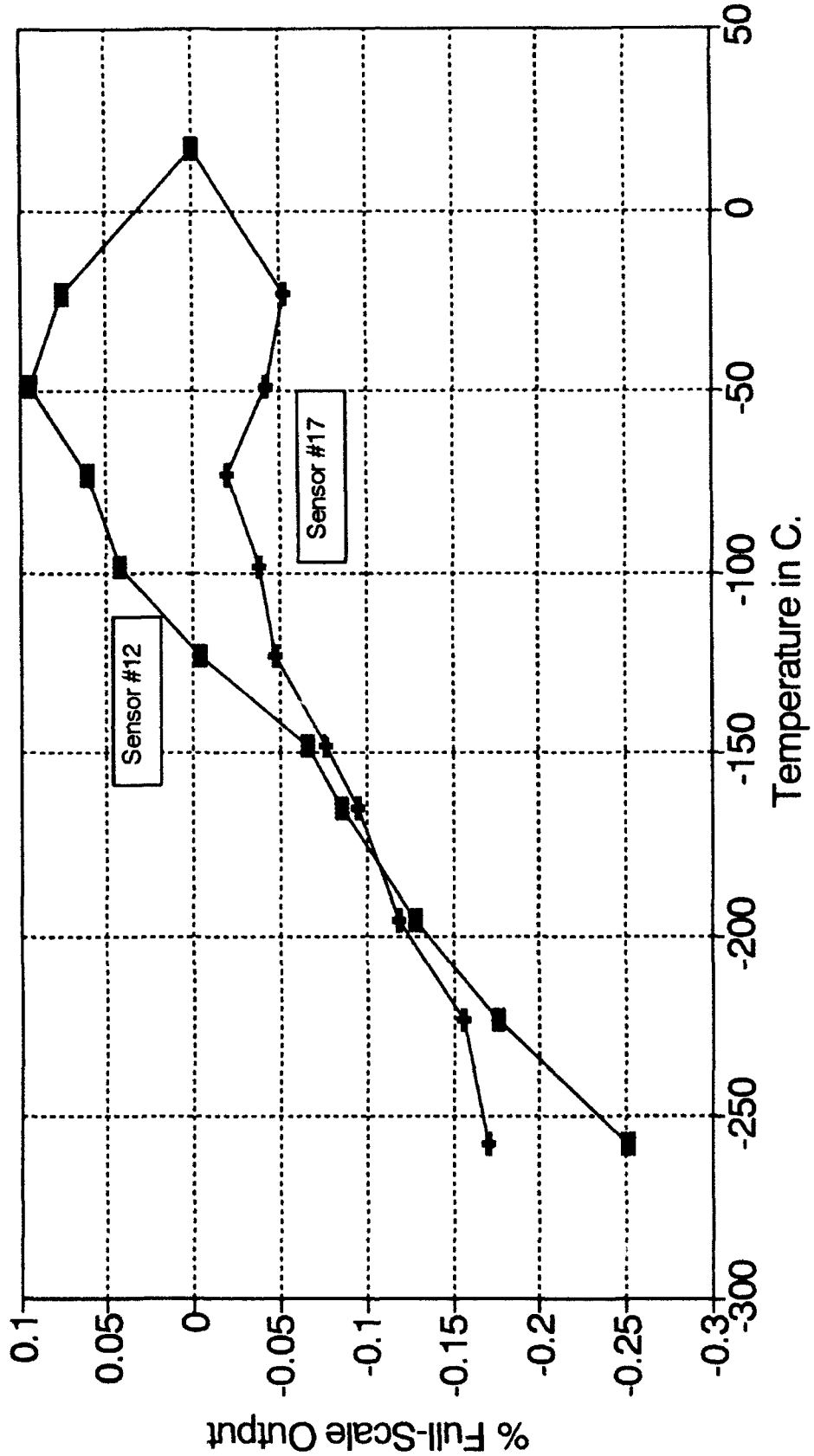

Figure 3. Long Term Stability

(Room Temperature, Gain=10)

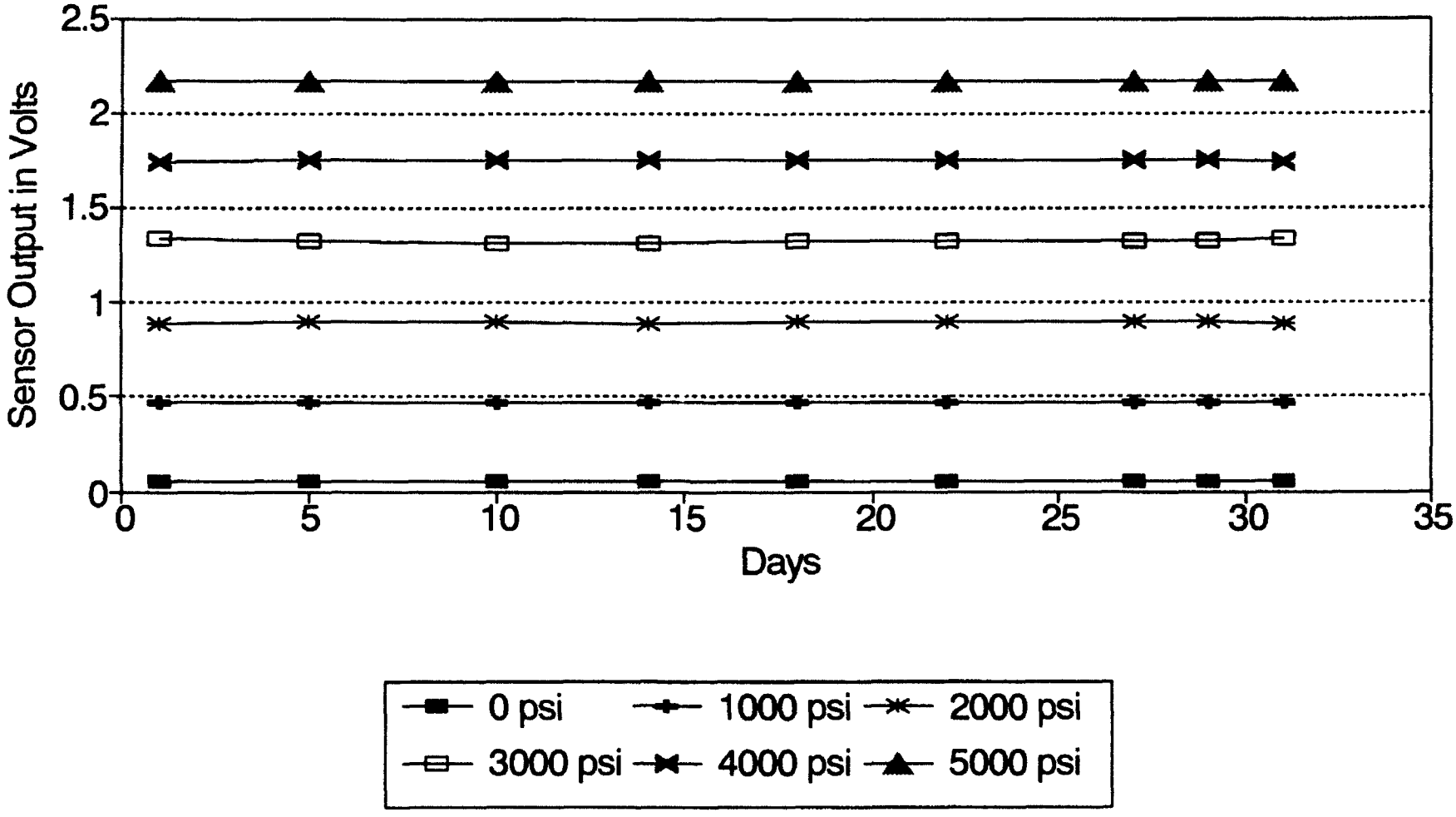

Figure 4. Output vs. Pressure (-184 C)

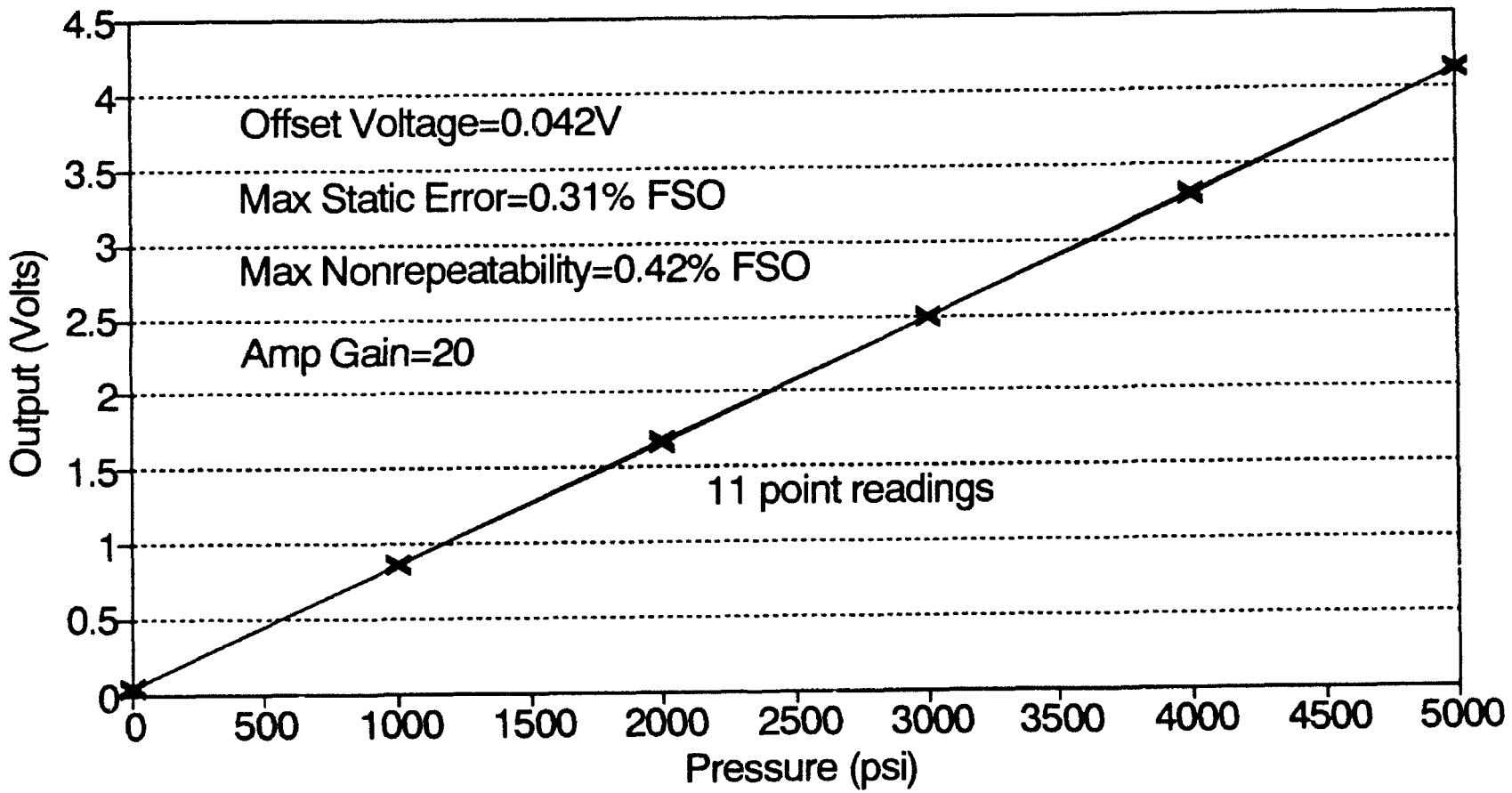

Flight Test Dynamic Data Gathering Using Digital Encoding

by

Paul Villhard
McDonnell Douglas Aerospace
McDonnell Douglas Corporation

Abstract

A family of anti-aliasing dynamic data filters, minimum recommended sampling rates, and a point by point autoranging digital encoding technique have been developed by the McDonnell Douglas Aerospace (MDA) Flight Test Instrumentation Department to replace the Frequency Modulation (FM) analog system. This provides the following advantages to flight test programs: dynamic range of 90 dB; elimination of overscale; optimization of resolution; time correlation of sampled analog data; automated self documenting setup; encryption of analog data; repeatable and quantifiable performance; and uniform support, recording and processing facilities. This paper discusses the dynamic digital data encoding issues, including parameter bandwidth; sample rate selection; and the causes, effects, and elimination of aliasing. It concludes with a description and typical applications of the Digital Data Acquisition System (DDAS) Presample Filter and Dynamic Data modules. Also, as a companion effort to the dynamic data studies we have identified 5 anti-aliasing filters that will accommodate the frequency range of non-dynamic data.

Introduction

A digital data acquisition system converts continuous signals into a series of sampled digital values. The objective is to encode the continuous signal with a finite set of samples which are adequate to preserve both the frequency and amplitude information over a desired bandwidth. To achieve this, the sample rate and presample filter characteristics must be appropriately related and carefully selected. To satisfy these requirements for digital encoding of dynamic data, a family of anti-aliasing filters, minimum recommended sampling rates, and a point by point autoranging digital encoding technique were developed by the McDonnell Douglas Aerospace (MDA) Flight Test Instrumentation Department.

This paper discusses digital dynamic data gathering issues, including parameter bandwidth; sample rate selection; and the causes, effects, and elimination of aliasing. It concludes with a description and typical applications of the Digital Data Acquisition System (DDAS) Presample Filter and Dynamic Data modules. These modules and DDAS are planned for use during the F/A-18E/F flight test program. (DDAS is a high bit rate programmable PCM system developed by the MDA Flight Test Department).

Bandwidth

Requirements for dynamic data start with determining the signal measurement bandwidth. Some of the frequency components will be due to physical phenomena of interest and some due to noise (electrical and environmental). Establishing the band of frequencies of interest is the basis for establishing data sampling parameters, including presample filtering characteristics, sampling rates, and post sampling processes, such as digital filtering. Bandwidth

is established based on measurement objectives, knowledge of the various measurement techniques and their response characteristics.

Sampling & Aliasing

Aliasing is a frequency domain error. It occurs when the replicated signal spectrum caused by the sampling process overlaps the bandwidth of interest. This happens when a continuous signal is periodically sampled and components of the signal are at frequencies higher than half the sample rate. This is called the Nyquist rate. An example of this is typically seen in motion pictures of a rotating spoked wheel or aircraft propeller. As the wheel or propeller rotates faster, it appears to slow down and stop, or even rotate backward. The sampling process produced by the discrete picture frames "aliases" the high rotation speed into the lower frequency interval. Figure 1 is a graphical example of the aliasing process while Figure 2 provides the mathematical basis.

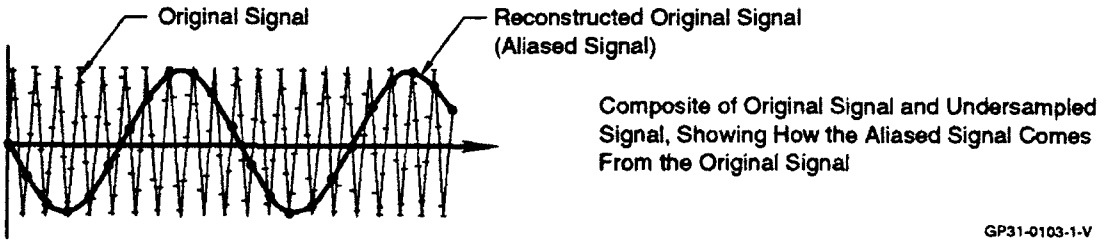

Figure 1.

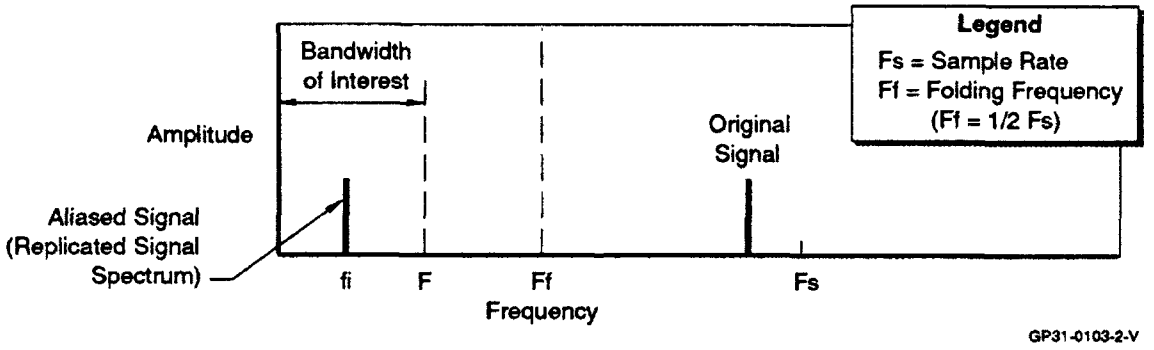

Figure 2.

In Figure 2 the frequency defined as F_f is equal to one half the uniform sample rate, F_s, and is called the folding frequency. It gets its name because all frequencies in the signal are "folded" about F_f. Based on the relationship between frequency and sample rate, the following identifies frequencies with potential for aliasing:

For any frequency of interest, f_i, in the range $0 \leq f_i \leq F$ the higher frequencies aliased with f_i are defined by:

$$(F_s \pm f_i),\ (2F_s \pm f_i),\ \ldots,\ (nF_s \pm f_i)$$

where: F_s = sample rate (1/t)
t = time between sampled points (1/sample rate)
F_f = folding frequency (F_s/2)

For example, if the frequency of interest, f_i, is 2000 Hz and the sample rate chosen is F_s = 8000 samples/second, then data at 2000 Hz is aliased with 6000 Hz, 10000 Hz, 14000 Hz, etc. If there is a component of the sampled signal at 6000 Hz, 10000 Hz, 14000 Hz, etc. it will appear at 2000 Hz. This is true for any frequency components in the interval defined by 0 to 4000 Hz (F_f). To provide the required measurement quality these higher frequency components which alias the lower frequency components in the frequency range of interest must be reduced to an acceptable level. This is done by applying an anti-aliasing filter to the analog signal prior to sampling.

Aliasing is a concern for all data when spectral or time history information is important! Once data is aliased, the true signal cannot be recovered. Aliasing is not detectable in the data but can only be guessed at from knowledge of the phenomena being measured.

Anti-Aliasing Filtering

Anti-aliasing filtering allows sample rate to be reduced while maintaining aliasing at a insignificant level. This is a particular concern during analog to digital conversion of high bandwidth data such as vibration (0 to 2000 Hz bandwidth) and acoustic (0 to 10000 Hz bandwidth).

In analog to digital conversion of high bandwidth data, anti-aliasing filters are applied prior to digital conversion. Ideally, the anti-aliasing filter (see Figure 3) will eliminate all frequency components above the highest desired frequency, allowing the sample rate to be set to two times the highest frequency of interest. This is called the Nyquist rate. Unfortunately, analog filters are not perfect, and exhibit characteristics shown in Figure 4. The actual filter characteristics cause the sample rate requirements to be higher than two times the highest frequency of interest.

The key to selection of a proper filter and sample rate is to ensure that frequencies folded into the frequency range of interest do not compromise the

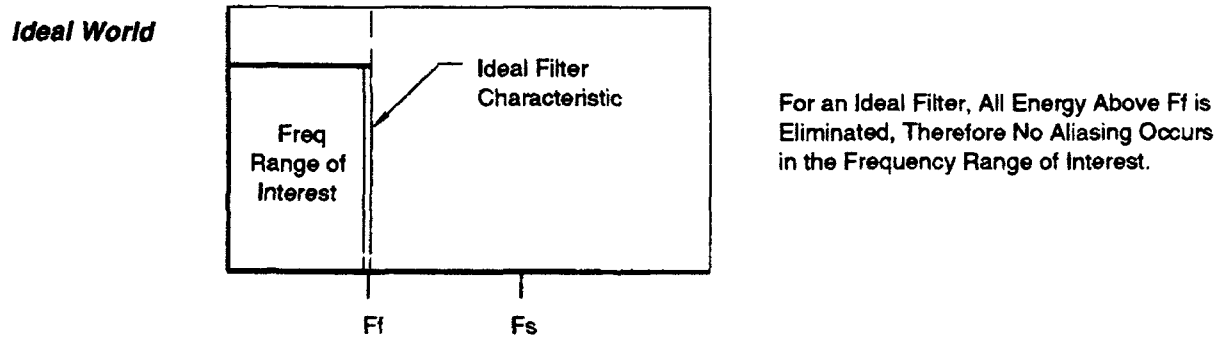

Figure 3.

Real World

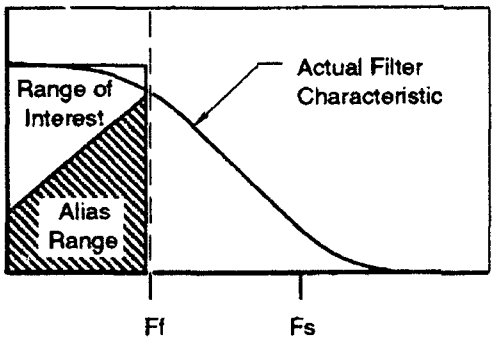

An Actual Filter Does Not Eliminate All Energy Above Ff, Therefore Aliasing Can Occur in the Frequency Range of Interest.

GP31-0103-4-V

Figure 4.

desired quality of data. As shown in Figures 5 and 6, an anti-aliasing filter with more rapid attenuation characteristics reduces the sample rate; while a filter with less rapid attenuation characteristics increases the sample rate. While systems that offer filters with better attenuation characteristics are more expensive and consume more space than lesser filters, they provide advantages which must be considered in design of high frequency data airborne filters. Improved filtering reduces sampling rate, which relaxes aggregate throughput requirements; ground processing input/output bandwidth requirements; storage requirements; and a relaxation of software requirements. All of these were considered when the DDAS Presample Filter module characteristics for vibration and acoustic measurements were chosen.

Basic Filter,
High Sample Rate

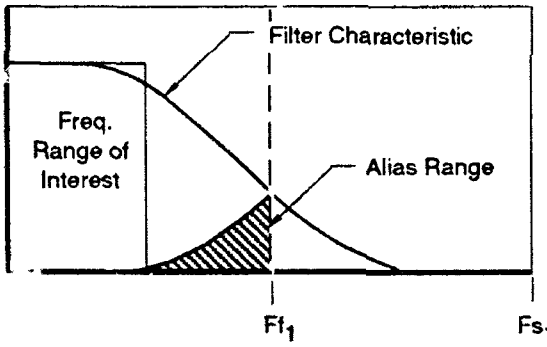

Basic Filter Characteristics Forces Sample Rate to Be Higher to Alleviate Aliasing Effects

GP31-0103-5-V

Figure 5.

More Powerful Filter,
Lower Sample Rate

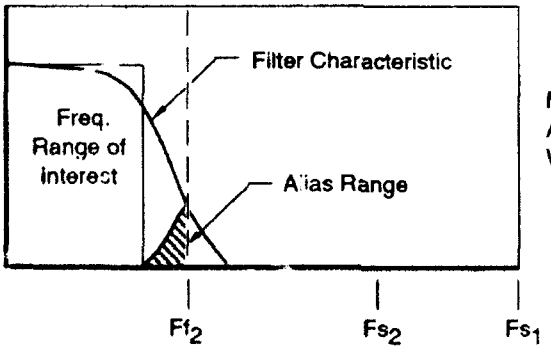

More Powerful Filter Characteristics Allows Sample Rate to be Lowered While Still Alleviating Aliasing Effects

GP31-0103-6-V

Figure 6.

DDAS Presample Filter Module

The anti-aliasing filters and minimum recommended sample rates (see Table 1) chosen for dynamic data measurement applications were the result of a flight test measurement requirements' study made by a committee of McDonnell Douglas Aerospace and General Dynamics instrumentation, data processing, and structural dynamics engineers. The filters are sixth order with a theoretical passband ripple of 5% and aliasing of less than 0.1% of full scale. This specification requires at least 60 dB attenuation at the lowest frequency which aliases into the data frequency range. (See Figures 7 and 8)

Table 1.

Filter Type	Passband	3dB Cut-Off	Minimum Sample Rate
Butterworth	2000 Hz	2390 Hz	9500 samples/sec
Tshebyschev	10000 Hz	11200 Hz	32500 samples/sec

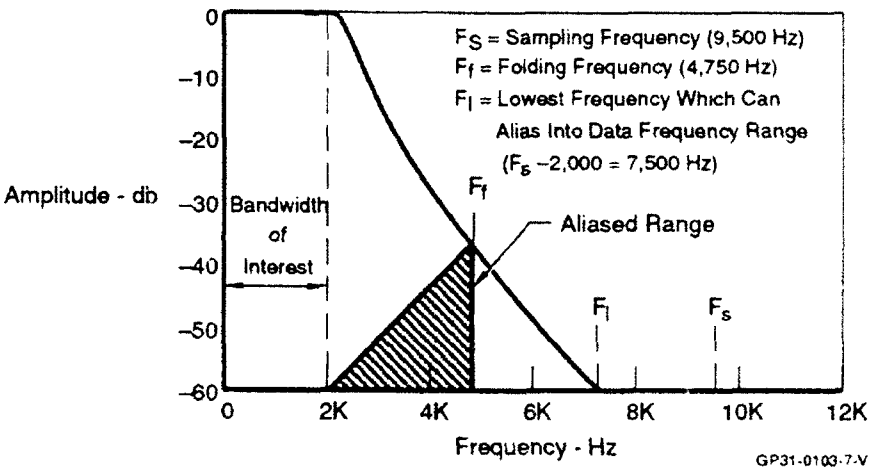

Figure 7. Butterworth 6-Pole Frequency Response

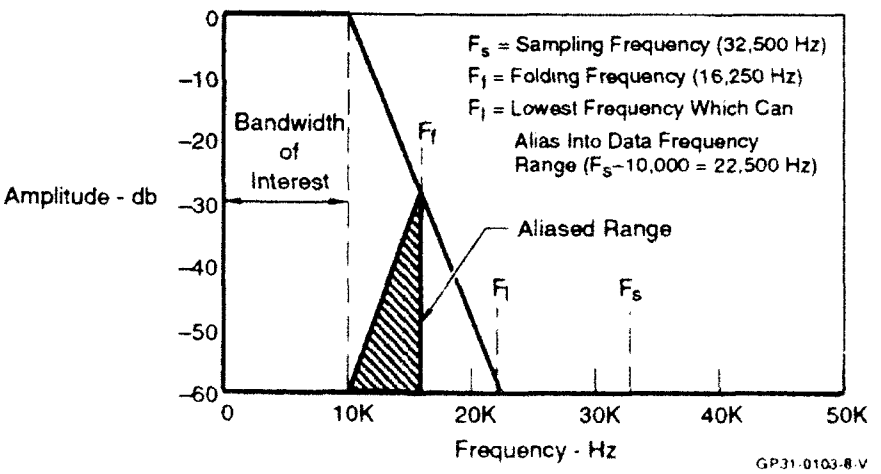

Figure 8. Tshebyschev 6-Pole Frequency Response

The filter design was subcontracted to Aydin Vector. The filters are packaged in a DDAS-compatible module containing 8 channels. They can be adapted to other filter characteristics without redesign because these characteristics are set by plug-in modules but we recommend the standard set described in this paper. Cost is about $1000 per channel.

Presample Filter Module (PSFM)

General: The Presample Filter Module's functional block diagram is given in Figure 9. The module is a signal conditioner for use with the Dynamic Data Module (DDM). The module functions as a differential input amplifier, an anti-aliasing filter, and a simultaneous sampling unit. The buffering function eliminates the sampling spikes commonly generated by the input multiplexers used in encoding units, e.g. the DDM. It also provides the differential input capability which is not available in the DDM. The filter cutoff frequency is selectable for compatibility with the desired signal bandwidth and sample rate. The simultaneous sampling function simplifies the problems of time correlation of parameters in a sampling system. The DDM generates the timing signals needed to control this module's sampling operation. Finally, a constant current source is provided for each channel which eliminates additional hardware when buffered accelerometers are used. It can be selected or deselected by jumper.

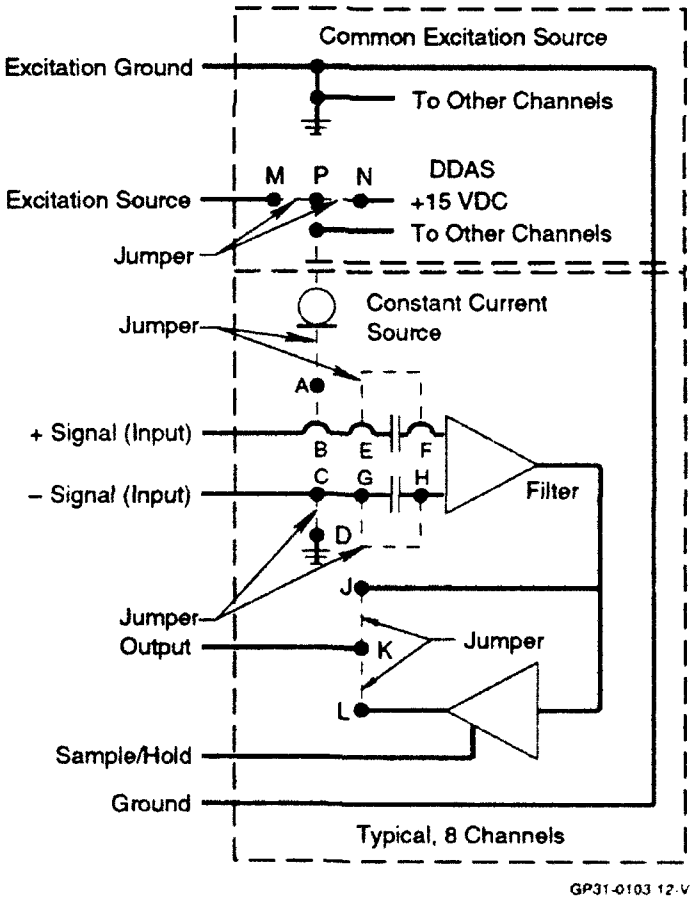

Figure 9. Presample Filter Module Functional Block Diagram

Presample Filter Module Specifications:

Number of Channels:	8
Input Voltage:	±5 mV to ±5 V
Input Overvoltage Protection:	±35 Volts with power on or off
Input Impedance:	10 megohms with power on 100K ohms with power off
Input Coupling:	Direct or capacitive coupling per channel; internal jumper programming
Gain:	1, 16, 32, 64; jumper programmable
Gain Accuracy:	0.5% FS over operating temperature range; better than 0.2% FS over the temperature range of -25°C to +70°C and power variations of up to ±2%
Output Offset Voltage:	10 mV independent of gain selection; 50 microvolts/°C
Filter Characteristics:	
Number of poles:	6
Filter Type/ 3 db Cutoff Frequencies:	Butterworth: 12, 48, 120, 480, 2390 Hz Bessel: 241 Hz Tschebyschev: 11200 Hz
Filter Type determined by:	plug-in modules
Filter Accuracy:	±.15 dB (amplitude) and +3° (phase) of the theoretical response from dc to .9 times the cutoff frequency maintained over the full operating environment
Passband For .5 dB Ripple:	Butterworth: 10, 40, 100, 400, 2000 Hz Bessel: 100 Hz Tschebyschev: 10000 Hz
Output Impedance:	2 ohms max.
Sample Acquisition time:	4 microseconds to 0.1% for a 10 Volt step input or 15 microseconds to 0.03% for a 10 Volt step (jumper selectable)
Output Full Scale	± 5 Volts
Droop Rate:	800 Mv/sec max for 4 microseconds acquisition time; less than 20 Mv/sec for 15 microsecond acquisition time

Track and Hold Control:	compatible with both CMOS and TTL; a logic "1" places the Sample and Hold (S/H) for each channel in the hold mode while a logic "0" places the S/H in the track mode Each channel via jumpering can bypass the S/H mode
Constant Current Excitation Output:	2.2 Ma ± 20% per channel; requires external 14 to 24VDC or will operate off internal DDAS +15VDC; (jumper selectable)
Status Response:	responds over the DDAS Internal Digital Bus (IBUS) with status words indicating the current programming, i.e., cutoff frequency, gain, and jumper configuration for each channel
Operating Environment:	acceleration levels to 15 g's; temperature range of -55°C to +71°C
Physical Size:	1T (.6" x 4" x 5")
Power Dissipation:	3.6 watts (±15VDC, +5VDC)
Weight:	.87 lbs

Dynamic Data Module (DDM)

General: The Dynamic Data Module's functional block diagram is given in Figure 10. The Dynamic Data Module (DDM) is an automatic gain ranging analog-to-digital converter designed to operate in conjunction with the Presample Filter Module (PSFM). The DDM uses an autoranging algorithm (point by point) that selects the optimum gain for each sample rather than time history characteristics. Because of this it is equally applicable to steady state and transient data. The DDM provides a dynamic range of 90 dB, accuracy of 1% full-scale (FS), high speed conversion of over 200K bits/second (uses a ILC Data Device Corp. ADC-00403 successive approximation 12 bit, 2 microsecond A/D converter), and supports simultaneous sampling. Its primary application is analog-to-digital conversion of vibration and acoustic data.

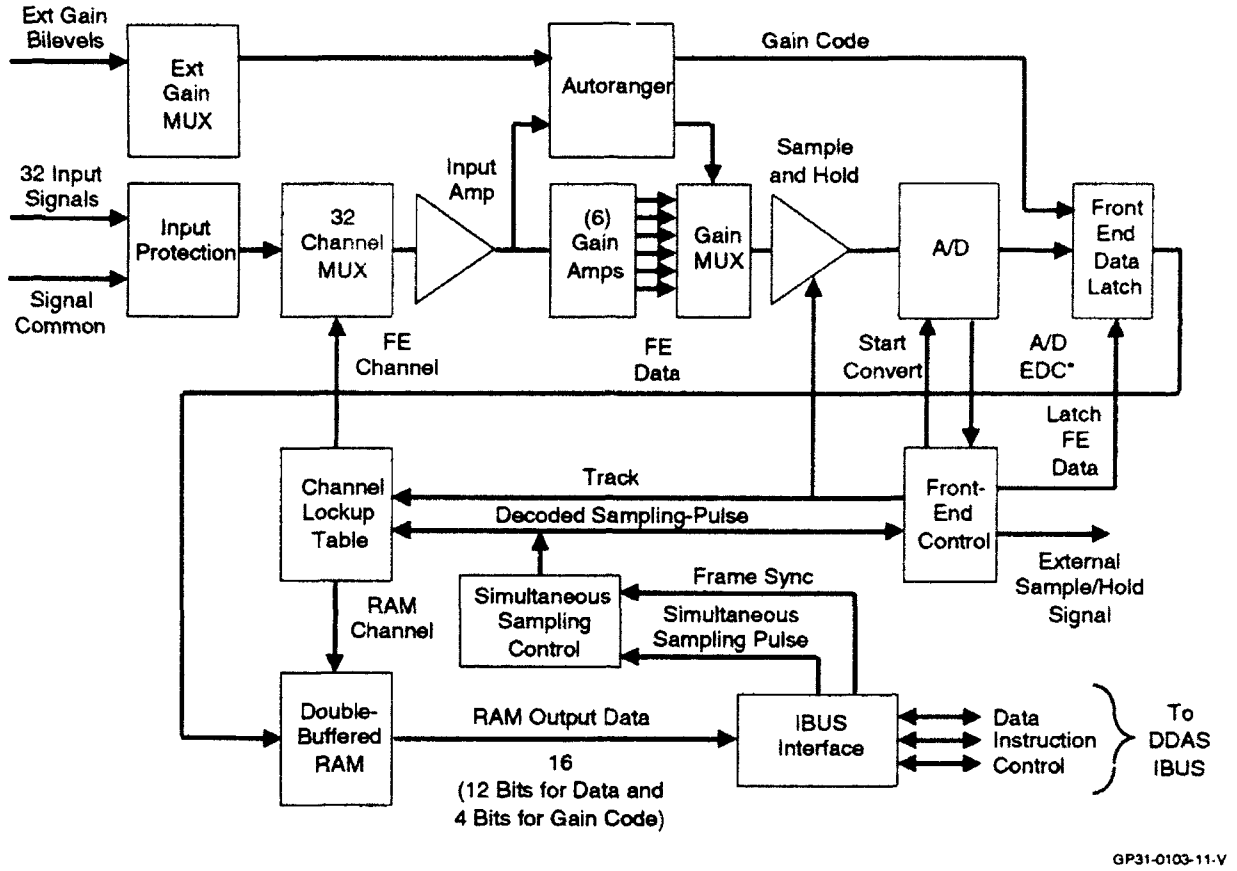

Figure 10. DDM Functional Block Diagram

DDM Specifications:

Inputs:	32 channels, quasi-differential
Signal Range:	±156 Mv to ± 5V (Autoranging)
Accuracy:	± 1% of full scale, ± 1% of reading
Resolution:	10 bits (encoder is 12 bits but due to noise reduces effective resolution)
Dynamic Range:	90 dB
Autoranging Gain:	6 steps 1 to 32 (1, 2, 4, 8, 16, 32)
*** Fixed Gain:**	6 steps 1 to 32 (1, 2, 4, 8, 16, 32)
*** Sample Rate:**	220K sps (aggregate rate for 17 channels or more)
	205K sps (aggregate rate for 5 to 16 channels)
	140K sps (aggregate rate for 1 to 4 channels)
	Note: All channels are sampled at the same rate.

Timing Delay:	1 sample
Simultaneous Sampling:	Provides control pulse to the PSFM. It is derived from the DDAS System Pulse by synchronous division.
Built In Test:	Bit verifies 80% of components
DDAS Interface Data Format:	12 bits for magnitude + 4 bits for gain
Operating Environment:	acceleration levels to 15 g's; temperature range of -55°C to +71°C
Physical Size:	2T (1.2" x 4" x 5")
Power Dissipation:	7.51 watts
Weight:	1.7 lbs

* Fixed Gain and Sample Rate are programmable on a module basis.

Applications

Some typical applications of the Presample Filter Module and the Dynamic Data Module are vibration and acoustic measurements. Examples of these are given below.

Vibration Measurement

A typical vibration measurement data acquisition channel is made up of a piezoelectric linear acceleration transducer, a Presample Filter Module (PSFM), and a Dynamic Data Module (DDM). (See Figure 11.) The combination of the PSFM and DDM provide a flat response within 5% over the frequency range of 0 to 2000 Hz and aliasing of less than 0.1% of full scale at a sampling rate of 10240 samples/second. This sample rate was chosen rather than the minimum sample rate of 9500 samples/second in order to provide a set of sample rates (10 x 2^n samples/second) compatible with multiplex bus data processing.

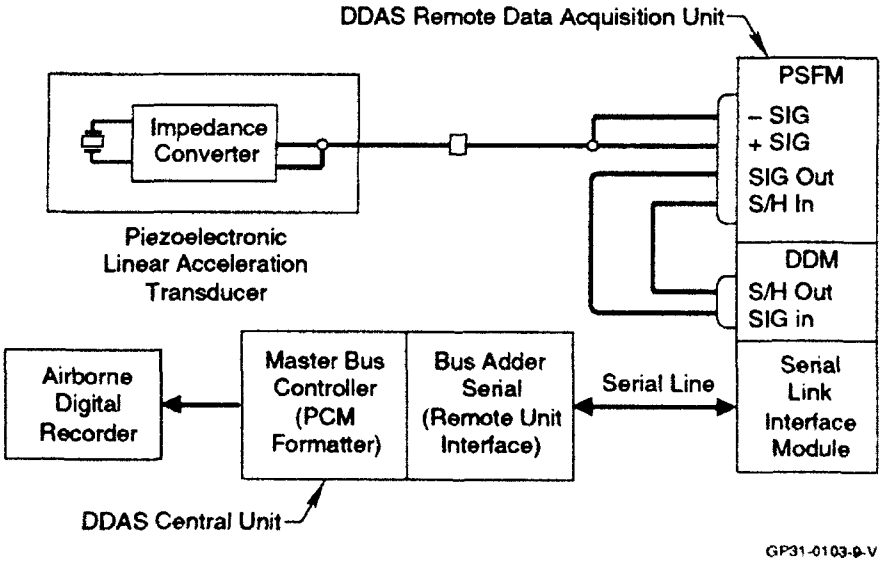

Figure 11. Vibration Measurement Channel

Typically a small, lightweight, piezoelectric linear accelerometer with internal electronics requiring a constant current source is used. It consists of a crystalline quartz element with an internal impedance converter. The quartz element is an effective capacitor which produces a charge across its plates proportional to a force applied to the crystal. The internal impedance converter functions as a charge converter and an emitter-follower and minimizes line capacitive attenuation effects. Typical specifications are listed below.

Range	± 500 g peak, minimum
Sensitivity	10 mv/g ± 5%
Input Bias	9-24 VDC through constant current excitation (2.2 Ma)
Frequency Range	4 Hz to 15K Hz
Amplitude Linearity	± 1%
Output Impedance	100 ohms
Resonant Frequency	80K Hz
Temperature Range	-67°F to 257°F
Weight	10 grams

Transducer signal conditioning is provided by the Presample Filter Module (PSFM). It supplies constant current power to the sensor. The same two lines that provide the constant current power to the sensor are used to bring back the output voltage signal. This type of operation provides benefits in applications involving long connecting cables or high electrical noise environments. The input is capacitively coupled to an input amplifier with selectable gains of 1, 16, 32, or 64. The following filter is a 6-pole Butterworth anti-aliasing filter with its 3 dB cutoff frequency set at 2390 Hz. The output of the filter goes to a sample and hold circuit. The necessary track-and-hold commands come from the Dynamic Data Module. The data is sampled at 10240 times per second by the Dynamic Data Module. It is configured to operate at a conversion rate of 220K samples/second (aggregate rate for 17 channels or more). The combination of the filter characteristics and the sampling rate provides greater than 60 dB attenuation at the lowest frequency component of 8240 Hz which can alias into the data frequency range of 0 to 2000 Hz.

Acoustic Measurement

A typical acoustic measurement data acquisition channel is made up of a piezoelectric sound pressure microphone, a Presample Filter Module (PSFM), and a Dynamic Data Module (DDM). (See Figure 12.) The combination of the PSFM and DDM provide a flat response within 5% over the frequency range of 0 to 10000 Hz and aliasing of less than 0.1% of full scale at the sampling rate of 40960 samples/second. This sample rate was chosen rather than the minimum sample rate of 32,500 samples/second in order to provide a set of sample rates (10 x 2^n samples/second) compatible with multiplex bus data processing.

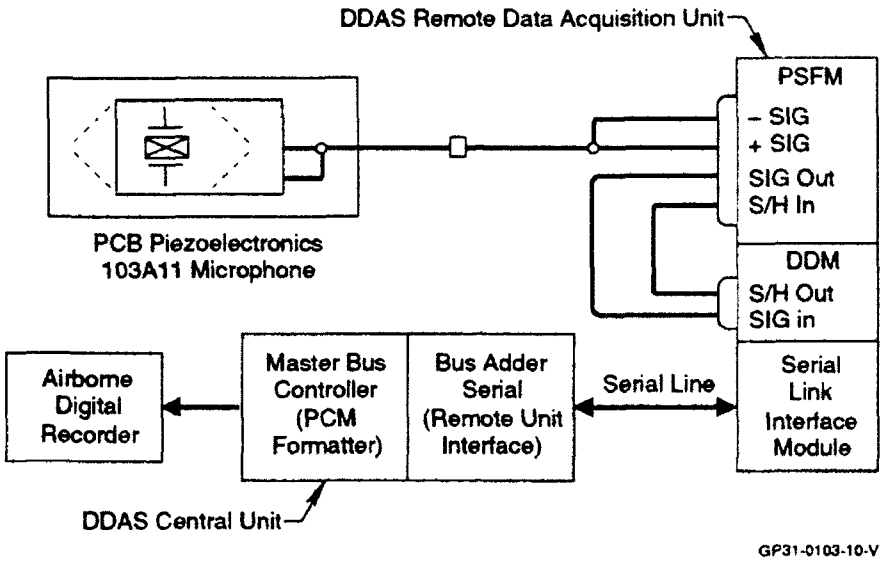

Figure 12. Typical Acoustic Measurement

Typically a small, lightweight, PCB Piezotronics 103A11 microphone with internal electronics requiring a constant current source is used. It is structured with ceramic crystal elements, a microelectronic amplifier, and an accelerometer to cancel out vibration sensitivity. It has a high output sensitivity of 500 mv/psi. Typical specifications are listed below.

Range (3V output)	6 psi (186 dB)
Input Bias	9-24 VDC through constant current excitation (2.2 Ma)
Sensitivity	500 Mv/PSI ± 10%
Resonant Frequency	13K Hz
Linearity	± 2% Full Scale
Output Impedance	100 ohms
Temperature Range	-100°F to 250°F
Weight	2.3 grams

Transducer signal conditioning is provided by the Presample Filter Module (PSFM). It supplies constant current power to the sensor. The same two lines that provide the constant current power to the sensor are used to bring back the output voltage signal. The input is capacitively coupled to an input amplifier with selectable gains of 1, 16, 32, or 64. The following filter is a 6-pole Tshebyschev anti-aliasing filter with its 3 dB cutoff frequency set at 11200 Hz. The output of the filter goes to a sample and hold circuit. The necessary track-and-hold commands come from the Dynamic Data Module. The data is sampled at 40960 times per second by the Dynamic Data Module. It is configured to operate at a conversion rate of 205K samples/second (aggregate rate for 5 to 16 channels). The combination of the filter characteristics and the sampling rate provides greater than 60 dB attenuation at the lowest frequency component of 30960 Hz which can alias into the data frequency range of 0 to 10000 Hz.

DDM vs Non-DDM Vibration Measurement Example

Let's assume that we have a requirement to measure ± 25 g's using a transducer with 10mV/g sensitivity. Further, let's assume that a Non-DDM unit with a 10 bit effective resolution, full scale input of ± 5VDC, and fixed gains the same as the DDM's is used.

For ± 25 g's, The transducer's output will be ± 250 mV. To accommodate this, the gain of the PSFM is set to 16 for both the DDM and the Non-DDM. This results in a ± 4 Volts output for maximum input ± g's. Using the Dynamic Range equation given below

$$\text{Dynamic Range} = 20 \times \text{Log} \left[(Vin/Vin_{FS}) \times Vin_{FS} / Vin_{FS}/(R \times G) \right]$$

Where: Dynamic Range is in dB
- Vin = PSFM output voltage (maximum)
- Vin_{FS} = Allowable Full Scale Voltage Input of Non-DDM or DDM
- R = Resolution of Non-DDM or DDM
- G = Gain of Non-DDM or DDM

and substituting for

- Vin = ± 4 Volts
- Vin_{FS} = ± 5 Volts
- R = 1024
- G = 1

this results in a Non-DDM Dynamic Range of 58 dB. For the DDM example, all the values of the equation variables are the same as the Non-DDM values with the exception of the gain. Due to the DDM's autoranging capabilities, its gain ranges from 1 to 32 compared to the Non-DDM's fixed gain of 1. Substitution of these values into the Dynamic Range equation results in a DDM dynamic range of 88 dB and a 30 dB dynamic improvement when compared to the Non-DDM example.

Conclusion

Anti-aliasing filtering and dynamic data encoding using point by point autoranging developed by the MDA Flight Test Instrumentation Department provides an improvement in data quality of greater than 1000 to 1 when compared to FM encoding systems. The key to this is the correct choice of anti-aliasing filtering and sampling rate. MDA has adopted a standard family of filters and associated minimum sampling (see Table 2 on the following page) to achieve this. The filters are sixth order filters with a theoretical passband ripple of 5% and aliasing of less than 0.1% at the specified sample rate.

*** Table 2.**

Filter Type	Passband	Minimum Sample Rate
Butterworth	10 Hz	48 samples/second
Butterworth	40 Hz	190 samples/second
Butterworth	100 Hz	475 samples/second
Bessel	100 Hz	1575 samples/second
Butterworth	400 Hz	1900 samples/second
Butterworth	2000 Hz	9500 samples/second
Tschebyschev	10000 Hz	32500 samples/second

* As a companion effort to the dynamic data studies, we have identified five (5) additional filters to accommodate the frequency range of non-dynamic data. These filters along with the dynamic data filters cover the entire flight test measurement bandwidth spectrum.

Recommendation

It is recommended that the test community adopt a standard family of filters and sample rates. Those listed in Table 2 are offered for consideration.

Bibliography

1. Derek E. VanPelt. High Frequency Data Gathering Through Digital Data Acquisition Systems. MDA Flight Test Requirements & Analysis Dept 281 Informal Memo, November 26, 1990.

2. Robert Grant. Design and Development Report 9107, Data Filtering in PCM Systems. May 6, 1991.

3. Marc Hoskins. Sample Rate Considerations In Digital Signal Processing. MDA Flight Test Requirements & Analysis Dept 281 Memo, June 19, 1987.

4. MDA Flight Test Instrumentation Dept 283 Design & Development. Design And Development Report No. 8719, DDAS Digital Data Acquisition System. May 1987, rev May 1992.

5. Aydin Vector. Alternate Proposal For An Anti-Aliasing Presample Filter Approach, P-4989. 1989: pp 4-1 - 4-26.

6. John Wegener. MDA Design And Development Report No. 8728, T-048975-1 Dynamic Data Module Maintenance and Use Report. Dec 22, 1989.

SESSION 3

CALIBRATION TECHNIQUES

STATIC VERSUS DYNAMIC CALIBRATION OF MINIATURE PRESSURE TRANSDUCERS

David Banaszak, Electronics Engineer
Gary A. Dale, Instrumentation Engineer

U. S. Air Force, Wright Laboratory
Flight Dynamics Directorate
Wright-Patterson AFB, OH

Abstract

This paper discusses the techniques and results of the Flight Dynamics Directorates' evaluation of dynamic pressure transducers for use during a wind tunnel test of a transport aircraft forebody model. An area of concern was how the static sensitivities of the transducers compared to the dynamic sensitivities. To check this, forty-five transducers were evaluated by two methods. The first method, conducted by the Aeromechanics Division of the Directorate, consisted of a multipoint static calibration to determine the transducer's sensitivity. The second method, conducted by the Structures Division of the Directorate, involved a dynamic calibration of the transducers. The results from the two methods were compared with each other and the manufacturer's sensitivity. Additional static calibrations were done to try to resolve the discrepancies between the static and manufacture's sensitivity. Results, conclusions and recommendations are presented.

Background

The Mechanical Instrumentation Group of the Aeromechanics Division requested dynamic calibration support from the Instrumentation and Acquisition Group of the Structural Dynamics Division for a planned wind tunnel test of a transport aircraft forebody model. The configuration of the test article was such that once the transducers were installed, accessibility was very limited, thereby making in place calibrations impossible. As such, the groups decided to perform both static and dynamic laboratory calibrations on the 45 pressure transducers, prior to installing them in the model. An area of concern was how the static and dynamic sensitivities of the pressure transducers would compare.

Test Item Description

The transducers calibrated were miniature, silicon diaphragm type and cylindrical in shape, nominally .080 inch diameter by .375 inch long. They were differential reference type with ranges of 5 psid, 25 psid and 75 psid. The nominal resonant frequency of the transducers was 125 KHz to 190 KHz, depending on the differential pressure range.

Instrumentation

A block diagram of the static calibration instrumentation is shown in Figure 1. As shown, the physical excitation was applied with a dead weight tester. Transducer excitation voltage was provided by a Kepco power supply and transducer output was read by a HP 3497A Data Acquisition and Control Unit. During the calibration process the excitation voltage was periodically checked to assure stability. The HP 3497A had a 20 channel multiplexer that fed the unamplified transducer output directly into a digital voltmeter. All excitation and transducer electrical leads were shielded. The HP 3497A had an input impedance of greater than 10^{10} ohms, greater than the minimum 10^{6} ohms recommended by the transducer manufacturer. A PC based data system records and reduces the calibration data.

A block diagram of the dynamic calibration instrumentation is shown in Figure 2. As shown in the figure, the instrumentation consisted of a signal generator, power amplifier, high pressure microphone calibrator, instrumentation amplifier, and dual channel FFT analyzer. In addition, a digital X-Y plotter was used to provide hard copy of the FFT analyzer's screen.

Calibration and Data Reduction

The transducers were given 11 point calibrations for the static calibration case. The excitation voltage was equal to that shown on the manufacturer's Certificate of Calibration. After applying excitation power to the transducers they were typically warmed up over night (approximately 16 hours) to assure they were thermally stable. In the rare case a transducer did not receive an over night warm-up, the warm-up was a minimum of 4 hours. The calibration procedure followed was to begin with zero differential pressure on the transducer, then it was loaded to 100 percent of full scale in 20% increments and the loadings repeated, returning to zero differential. The repeat loadings provide the data necessary to check the hysteresis of the transducer. Each pressure load was corrected for the difference between standard and local gravity due to latitude and altitude differences. At each load point the transducer's output voltage was sampled 100 times and averaged to obtain a single calibration point. The exception to this loading procedure was for the 75 psid transducers. Due to the unavailability of a particular dead weight tester, one with a maximum pressure of 1600 in-H_2O (57.808 psi) was used. In this case, the transducer was given a 9 point calibration, zero to 1600 in-H_2O in increments of 400 in-H_2O (14.45 psi). In terms of the 75 psid full scale, this was equivalent to loads of 0%, 19.27%, 38.54%, 57.81% and 77.08% of full scale. For each static calibration, a linear regression was applied to the data giving a slope (pressure/volt) and an intercept. The inverse of the slope gives the sensitivity of the transducer in millivolts per unit pressure, such as mV/psi. Typical results from static calibrations of a 5 psid, 25 psid and 75 psid transducer are show in Figures 3, 4 and 5 respectively.

For the Dynamic calibration, each pressure transducer was inserted into the high pressure microphone calibrator using a specially designed adapter as shown in photo 1. The input signal was adjusted to produce an excitation level of 140 dB Sound Pressure Level (SPL), equivalent to 0.029 psid rms, at a frequency of 150 hertz inside the high pressure microphone calibrator. The calibrator's output signal, proportional to SPL, was connected to Channel A and the transducer output connected to channel B of the analyzer. The voltage corresponding to the calibration frequency was then read from the spectrum analyzer screen. A typical spectrum display used to read off voltages is shown in Figure 6. The calibration spectrums were stored on the analyzer's 3 1/2 inch floppy disk.

Data Analysis

Table 1 shows the results from the static and dynamic calibrations and also gives the manufacturer's sensitivity. As can be seen in the table, there is significant differences in the three sensitivities. For all but 4 (D19, W04, W07 and W13) of the 45 transducers the manufacturer's sensitivity was the highest, followed by the static sensitivity and the dynamic sensitivity, which was the lowest. The average percent difference between the sensitivities is also shown in Table 1. The static sensitivity was on average 3.11% less than the manufacturer's and the dynamic sensitivity was an average of 5.56% less than the manufacture's. Figures 7, 8 and 9 show the sensitivity data from Table 1 by transducer pressure range. The differences between the static and

manufacture's sensitivity are noteworthy in that they were both determined utilizing similar equipment, i.e., dead weight testers and digital voltmeters. The investigators contacted the manufacturer's quality assurance department to determine if procedural differences could explain the differences in sensitivities. It was learned that the manufacturer determines combined non-linearity and hysteresis (CNL&H) by loading the transducer from zero differential to full scale and back to zero differential in increments of 20% of full scale. However, to determine sensitivity, the manufacturer does a straight line fit between zero and full scale.

Due to the difference in methods for determining sensitivity, the manufacturer's 2 point calibration versus the 11 point calibration used by the investigators, it was decided to do some further laboratory investigations. Fortunately there was one spare 5 psid transducer that was never used during the test and three 25 psid transducers that were used, but could be removed from the model, available for further analysis. These transducers were calibrated using both an 11 point and a 2 point load schedule. The 11 point load schedule was the same as previously described, i.e., 20% increments, and the 2 point was a zero and full scale loading. These calibrations were separate and distinct from each other, the zero and full scale loads for the 11 point calibration were *not* used for the 2 point calibration loads. All other aspects of the calibration; transducer warm-up, number of samples taken per calibration point, etc. was as previously described. The results from this phase of the investigation are shown in Table 2. The first 3 columns of sensitivities, 'Manufacturer', '1st Static' and 'Dynamic', are simply the results of the first series of calibrations. The sensitivities labeled '2nd Static' and '2 Pt. Static' are the results from this subsequent laboratory investigation. As shown in Table 2 the sensitivities determined by the two calibration methods, 11 point and 2 point, compare very well. Also, they compare within 1% to the initial static calibrations despite the fact that the calibrations took place 9 *months* apart and that the three 25 psid transducers had been used during the test program. It should be noted that the dead weight testers used for the 5 psid and 25 psid transducer calibrations were returned to the manufacturer for routine recertification between the initial series of calibrations and this second series. The mass of the weights and the mass and area of the piston were certified with traceability to NIST and the values for these which were used for the initial series of calibrations were verified to be correct. The data in Table 2 is plotted in Figure 10.

Additional checks were made of the static calibration instrumentation chain in an attempt to identify any error that could be responsible for the differences between the manufacturer's and the static sensitivities. A voltage standard was connected to the instrumentation chain where the transducer output leads would have normally been connected and 50 millivolts applied. Also, the Kepco power supply was set for 5 volts and it was shorted at the terminal strip where the transducers were ordinarily connected so that it could be read as a signal into the data system. This setup permitted the simulated transducer output of 50 millivolts and the excitation voltage of 5 volts to be measured and recorded. Since a typical transducer static calibration took approximately 15 to 20 minutes it was decided to measure and record the voltage standard and the excitation voltage at 1 minute intervals for 20 minutes. Figure 11 shows the results of one of these series of measurements. As can be seen in the figure the power supply is very stable with the difference between the maximum and minimum voltage during the 20 minutes being 0.000164 volts. The digital voltmeter is also shown to be very accurate, reading the 50 millivolt standard with a maximum error of 0.013 millivolts. Two other checks of the power supply stability and the digital voltmeter accuracy were also done over a period of days to see if there were any longer term trends. The results were essentially identical.

Summary of Results

As shown in Table 1 and Figures 7, 8 and 9 the static sensitivity was always greater than the dynamic sensitivity, by 2.51% on average, but lower than the manufacturer's sensitivity by an average of 3.11%. The average difference between the dynamic and manufacturer's sensitivity was 5.56%. With the exception of transducers D19, W04, W07, and W13 the manufacture's sensitivity was always the greatest followed by the static and then the dynamic sensitivities. The second series of static calibrations, conducted 9 months after the initial calibrations, were well within 1% of the first calibrations. They also showed that there was an insignificant difference between the sensitivities determined using a multipoint and a two point calibration.

Conclusions and Recommendations

Potential reasons for slightly lower dynamic sensitivities compared to static sensitivities may be the different measurement techniques. Since the two calibrations used different setups, there may be slight differences in voltage readouts (a digital voltmeter versus a spectrum analyzer). The dynamic sensitivities may be lower because the static calibrations are accomplished over a period of approximately 20 minutes versus a period of a few seconds for the dynamic calibrations. Another contributing factor may be the effect of combined non-linearity and hysteresis specified for static sensitivities on dynamic sensitivities. Also there may be a slight difference in the transducer frequency response. The output at or near 0 hertz may be higher than the output at 150 hertz. Another contributing factor may be the difference in excitation methods. Given the differences in rms pressure levels applied, .029 psid for the dynamic calibration and 5, 25 or 75 psid for the static calibration, the differences between the static and dynamic sensitivities may not be too surprising. Considering all the potential error sources, the investigators concluded that the dynamic and static sensitivities were reasonably close. The difference between the manufacturer's and the static sensitivity is difficult to explain. The individual components in the measurement chain, the dead weight tester, power supply and digital voltmeter, used for the static calibrations were examined for sources of error. No system errors could be found that would account for the 3.11% average, and as high as 10% for an individual transducer, difference in sensitivities

Assuming similar constrains relative to transducer accessibility exist once the transducers have been installed in the test article, the recommended procedure for using this type of dynamic transducer is as follows. In the laboratory, determine the sensitivity of the transducer by loading it statically with a multipoint calibration. The instrumentation chain used of the laboratory calibrations should be as identical as reasonable possible to the test facility instrumentation chain. Calibrate the transducer dynamically by applying a known sound pressure level at a known frequency to the transducer. The dynamic sensitivity should be reasonably close to the static and, more importantly, the frequency output should be exactly that of the input. After installing the transducers in the test article, an end-to-end check of both the static and dynamic performance of the transducer should be made. For the static check, a known pressure should be applied if possible. The static sensitivity coefficients determined in the laboratory can then be applied to the output voltage to determine if the transducer is performing properly. In addition, a dynamic signal, of known frequency if possible, should be applied to the transducer to verify that it is still operating correctly dynamically.

LIST OF FIGURES, TABLES AND PHOTOGRAPHS

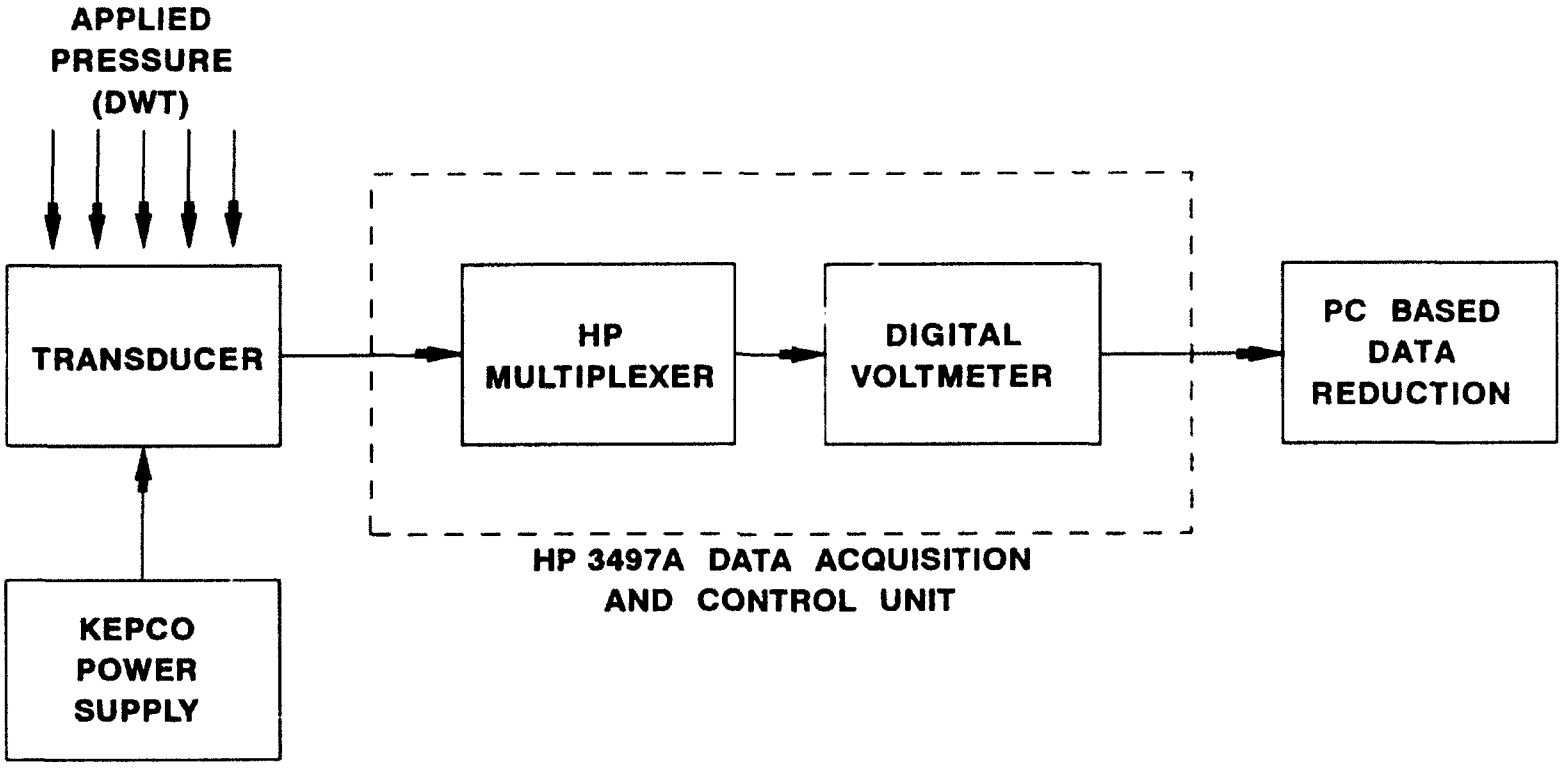

BLOCK DIAGRAM FOR STATIC CALIBRATION

Figure 1

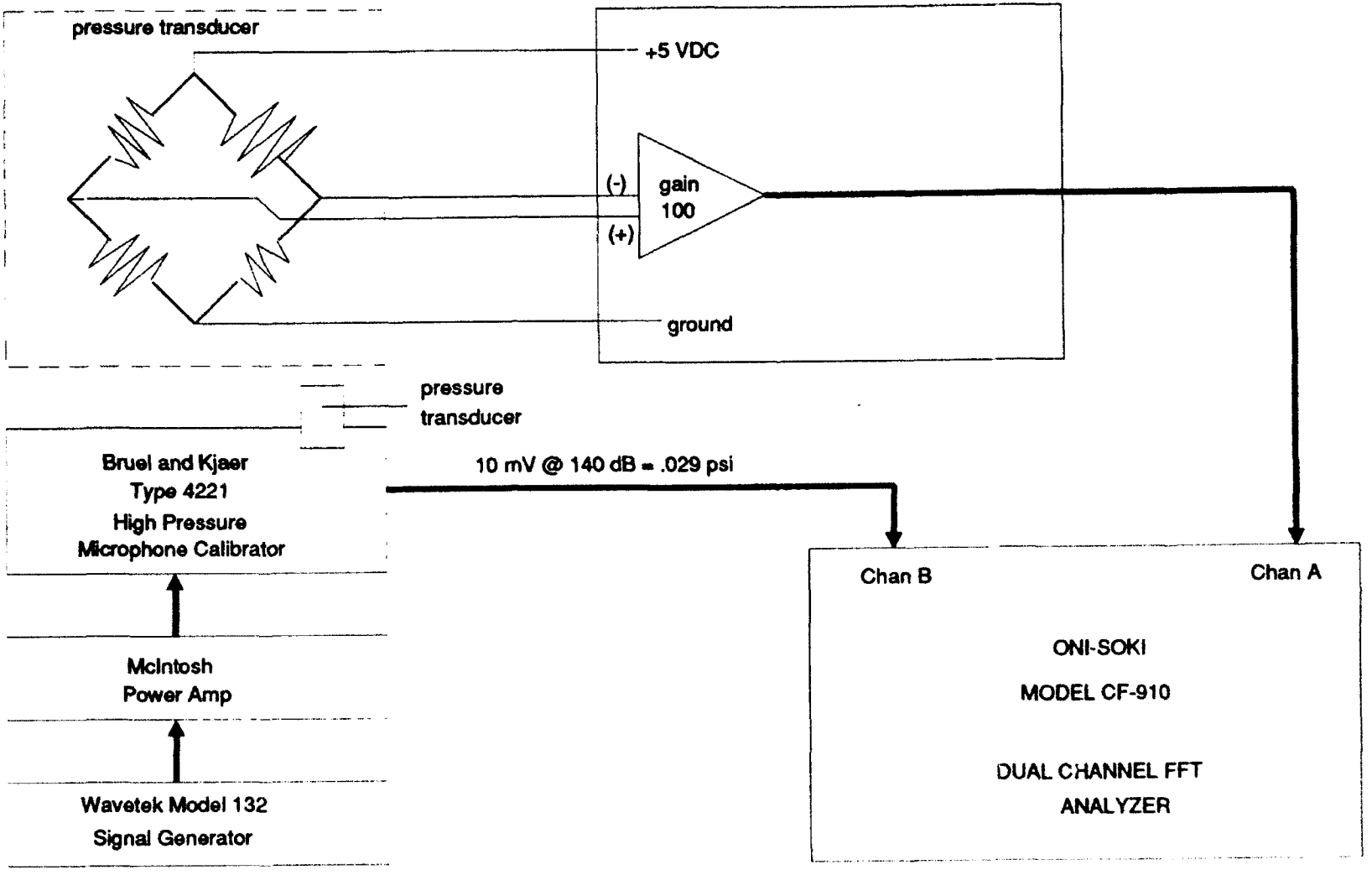

BLOCK DIAGRAM FOR DYNAMIC CALIBRATION

Figure 2

CALIBRATION FOR A 5 PSID TRANSDUCER

SLOPE = 2.41 mV/psi DATE: 6-17-1992

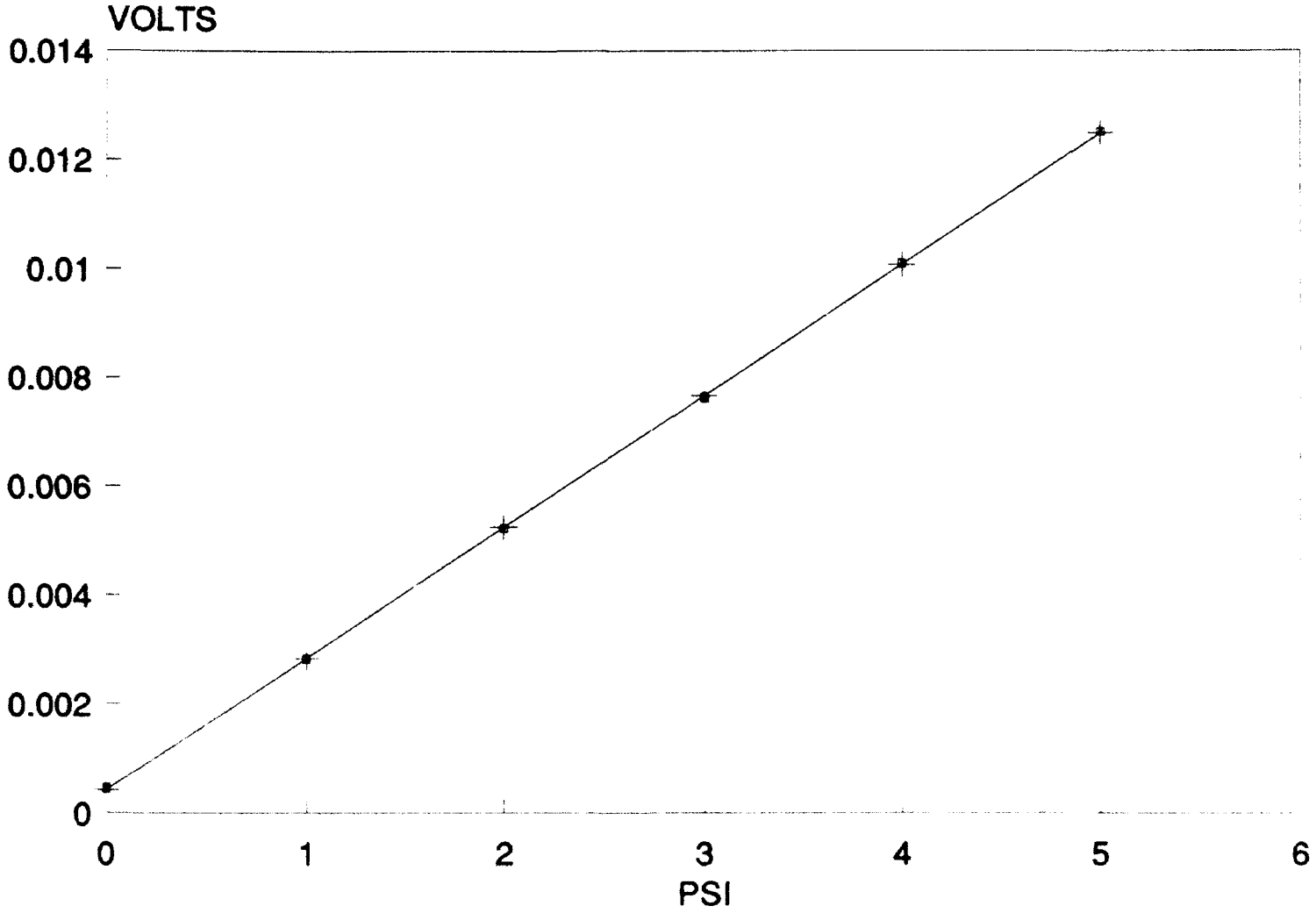

Figure 3

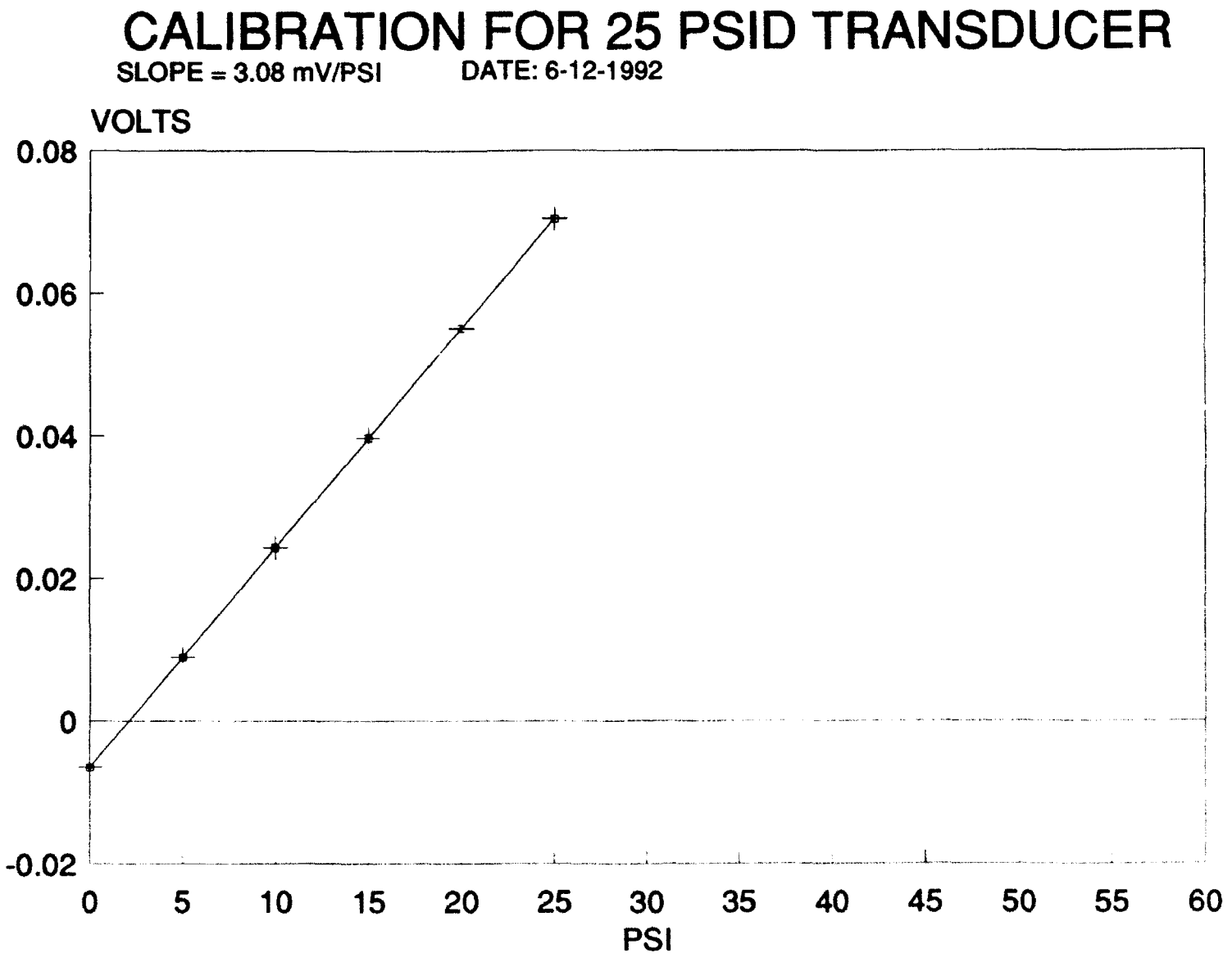
CALIBRATION FOR 25 PSID TRANSDUCER
SLOPE = 3.08 mV/PSI
DATE: 6-12-1992
VOLTS
0.08
0.06
0.04
0.02
0
-0.02
0
5
10
15
20
25
30
35
40
45
50
55
60
PSI

Figure 4

CALIBRATION FOR A 75 PSID TRANSDUCER

SLOPE = 1.13 mV/psi DATE: 6-17-92

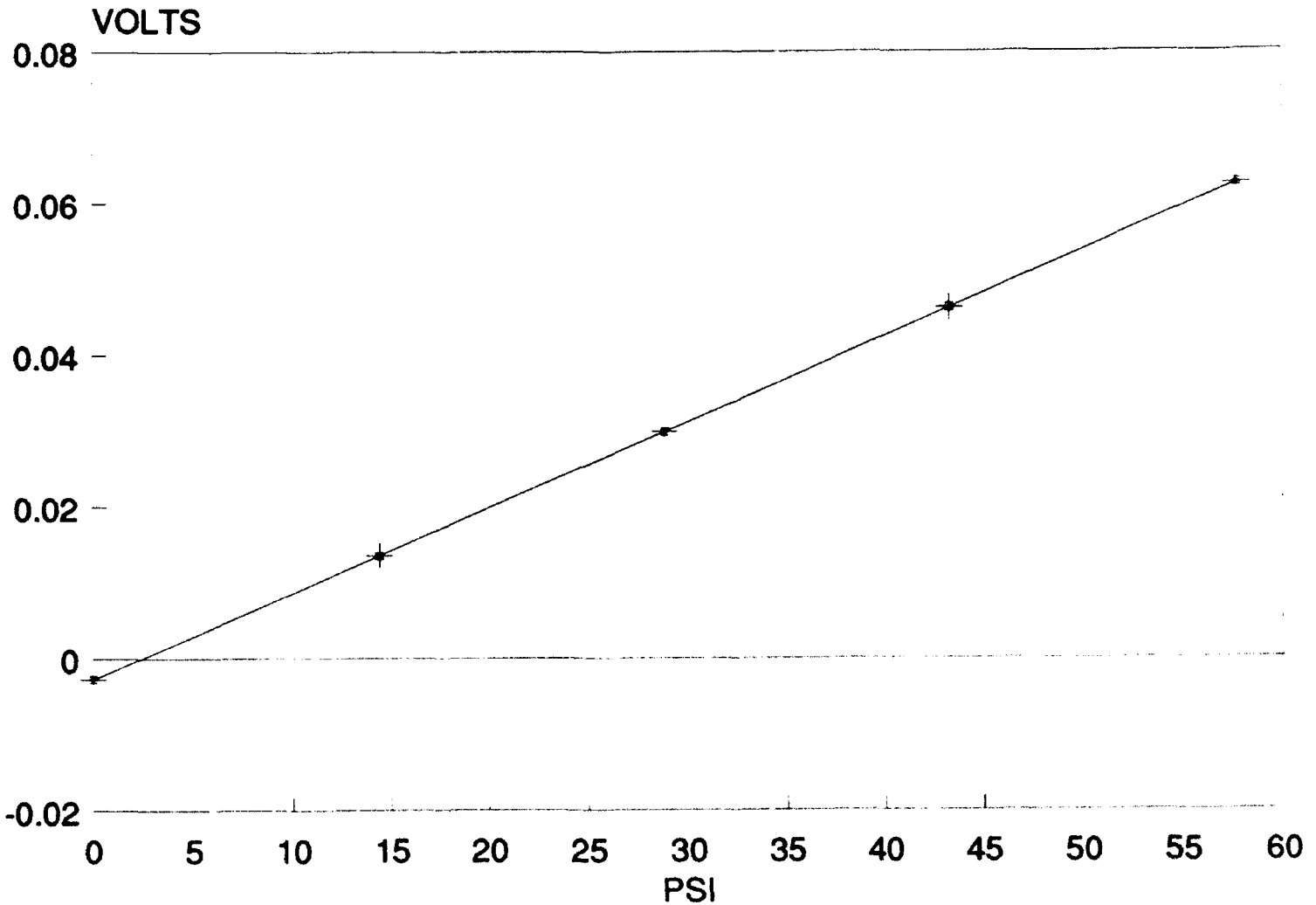

Figure 5

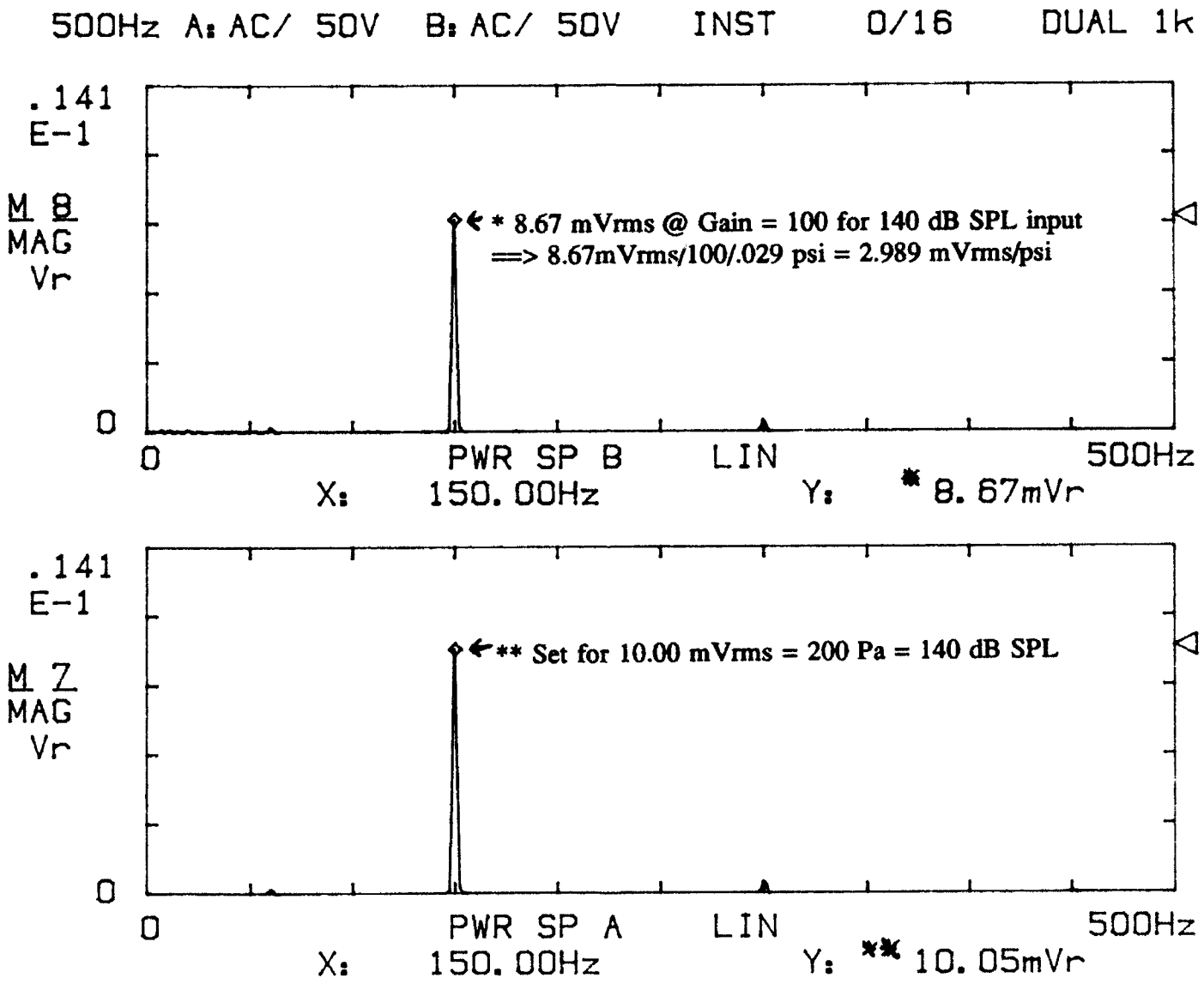

Frequency Spectrum for Dynamic Calibrations
Figure 6

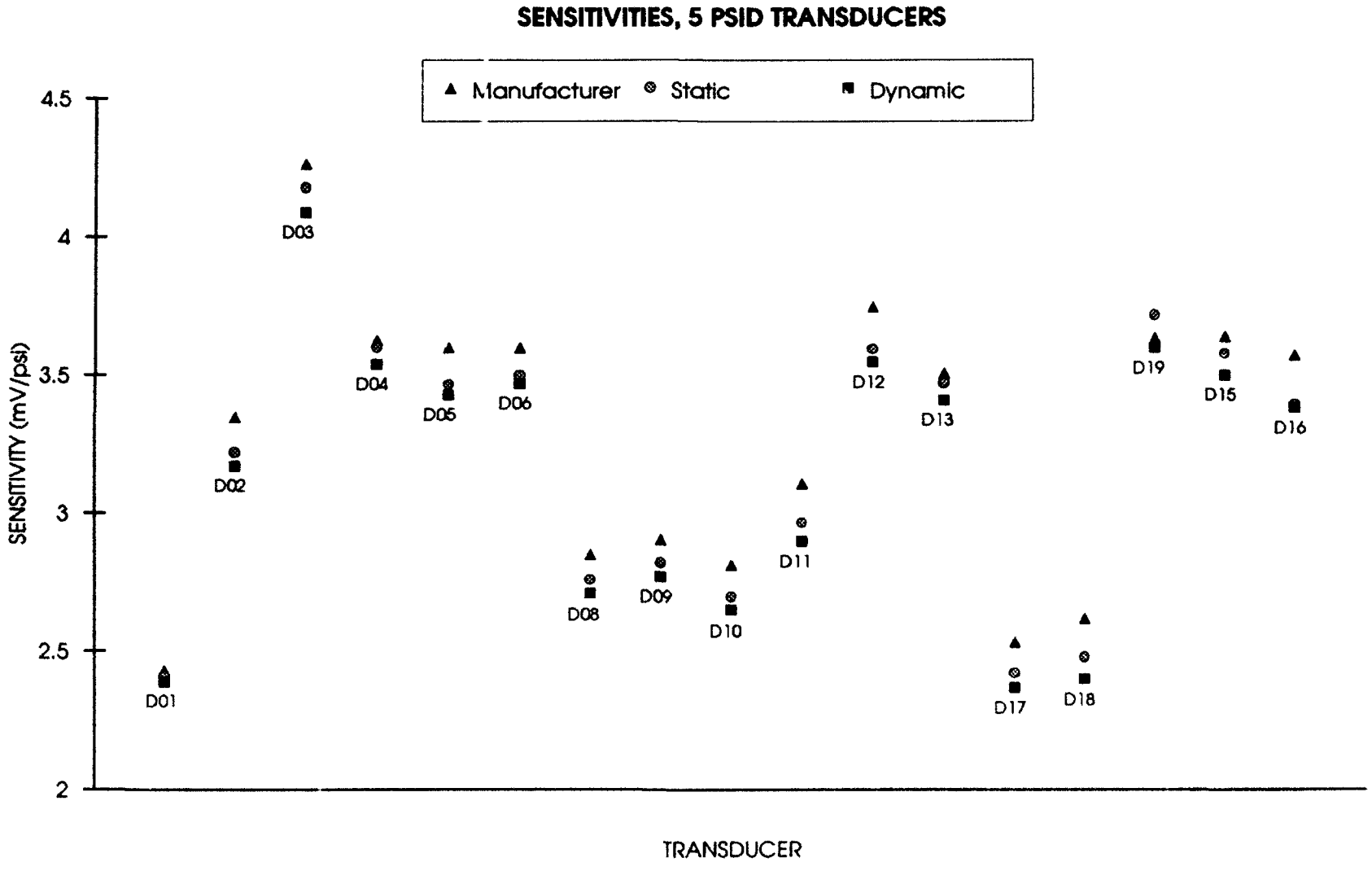
SENSITIVITIES, 5 PSID TRANSDUCERS
Manufacturer
Static
Dynamic
4.5
4
3.5
3
2.5
2
SENSITIVITY (mV/psi)
D01
D02
D03
D04
D05
D06
D08
D09
D10
D11
D12
D13
D17
D18
D19
D15
D16
TRANSDUCER

Figure 7

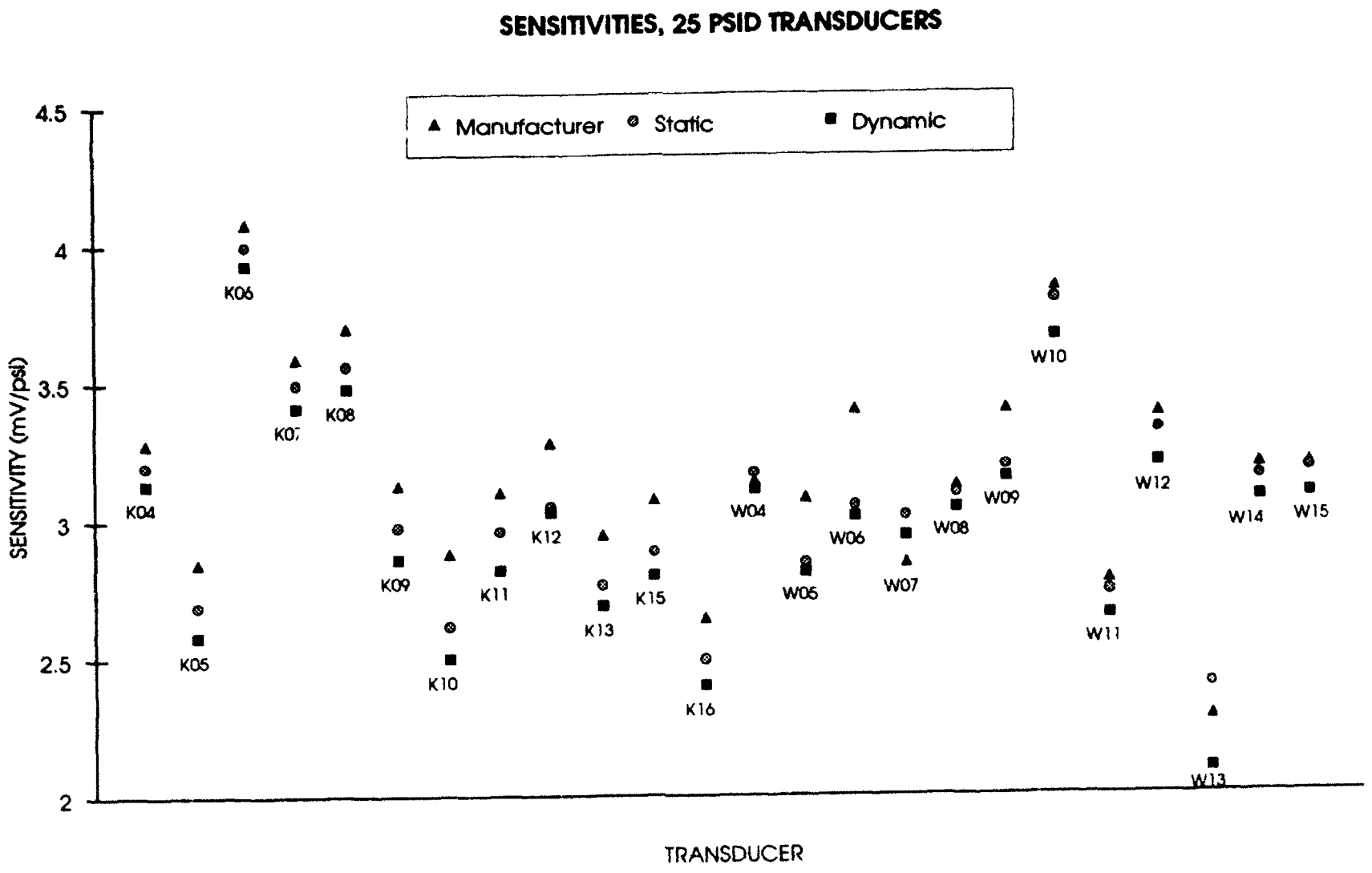
SENSITIVITIES, 25 PSID TRANSDUCERS
Manufacturer
Static
Dynamic
SENSITIVITY (mV/psi)
4.5
4
3.5
3
2.5
2
K04
K05
K06
K07
K08
K09
K10
K11
K12
K13
K15
K16
W04
W05
W06
W07
W08
W09
W10
W11
W12
W13
W14
W15
TRANSDUCER

Figure 8

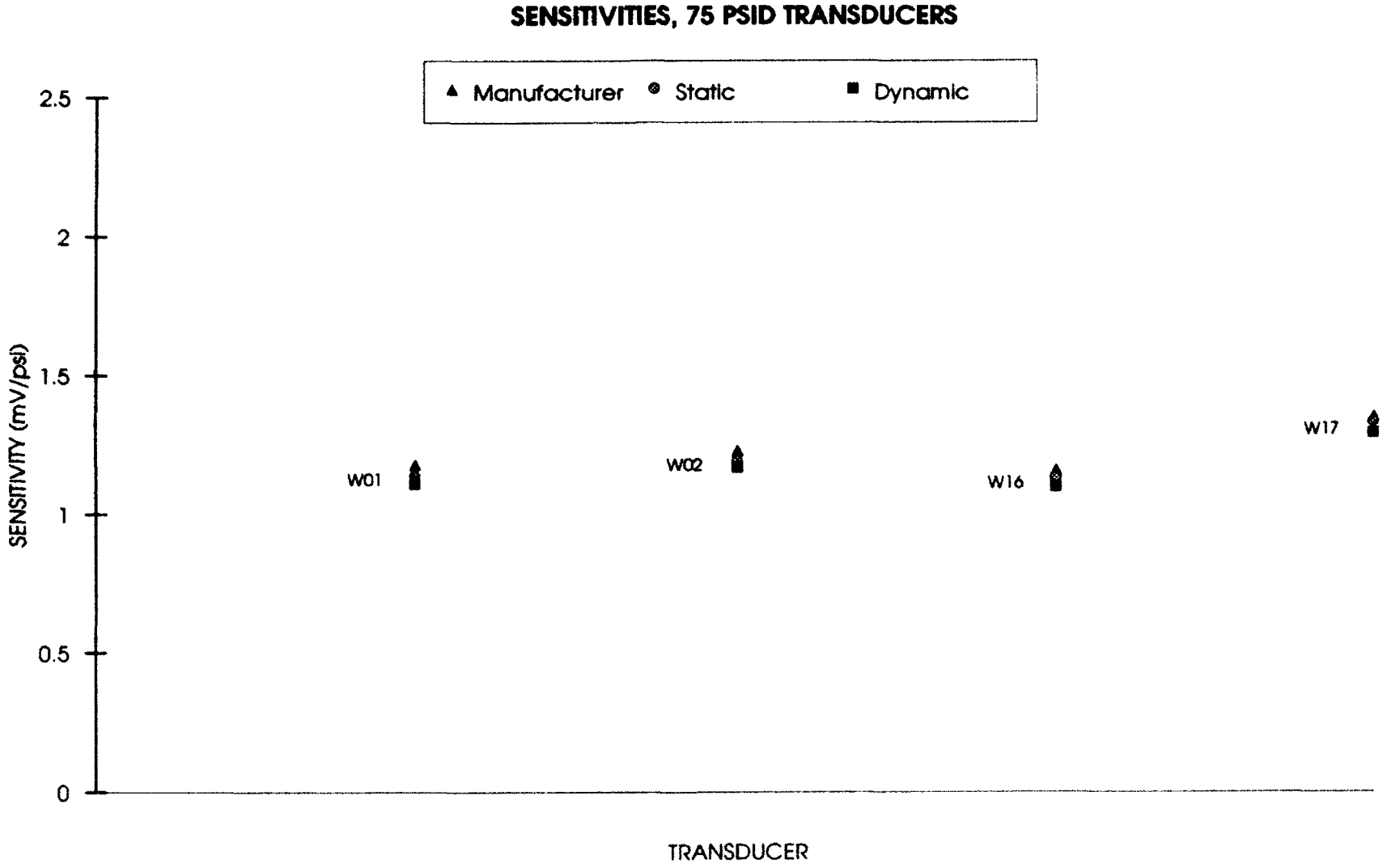
SENSITIVITIES, 75 PSID TRANSDUCERS
Manufacturer
Static
Dynamic
2.5
2
1.5
1
0.5
0
SENSITIVITY (mV/psi)
W01
W02
W16
W17
TRANSDUCER

Figure 9

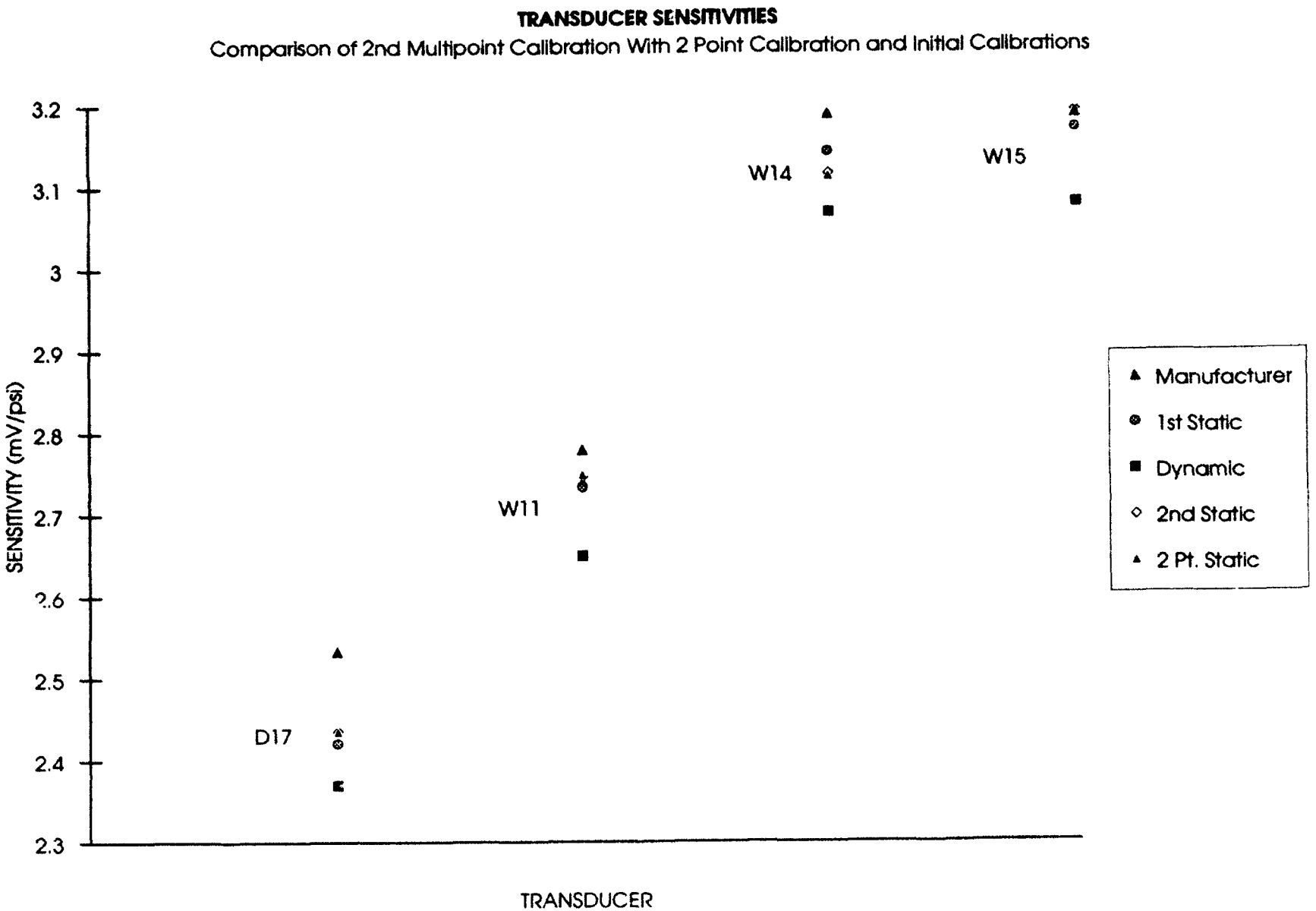
TRANSDUCER SENSITIVITIES
Comparison of 2nd Multipoint Calibration With 2 Point Calibration and Initial Calibrations
SENSITIVITY (mV/psi)
3.2
3.1
3
2.9
2.8
2.7
2.6
2.5
2.4
2.3
D17
W11
W14
W15
TRANSDUCER
Manufacturer
1st Static
Dynamic
2nd Static
2 Pt. Static

Figure 10

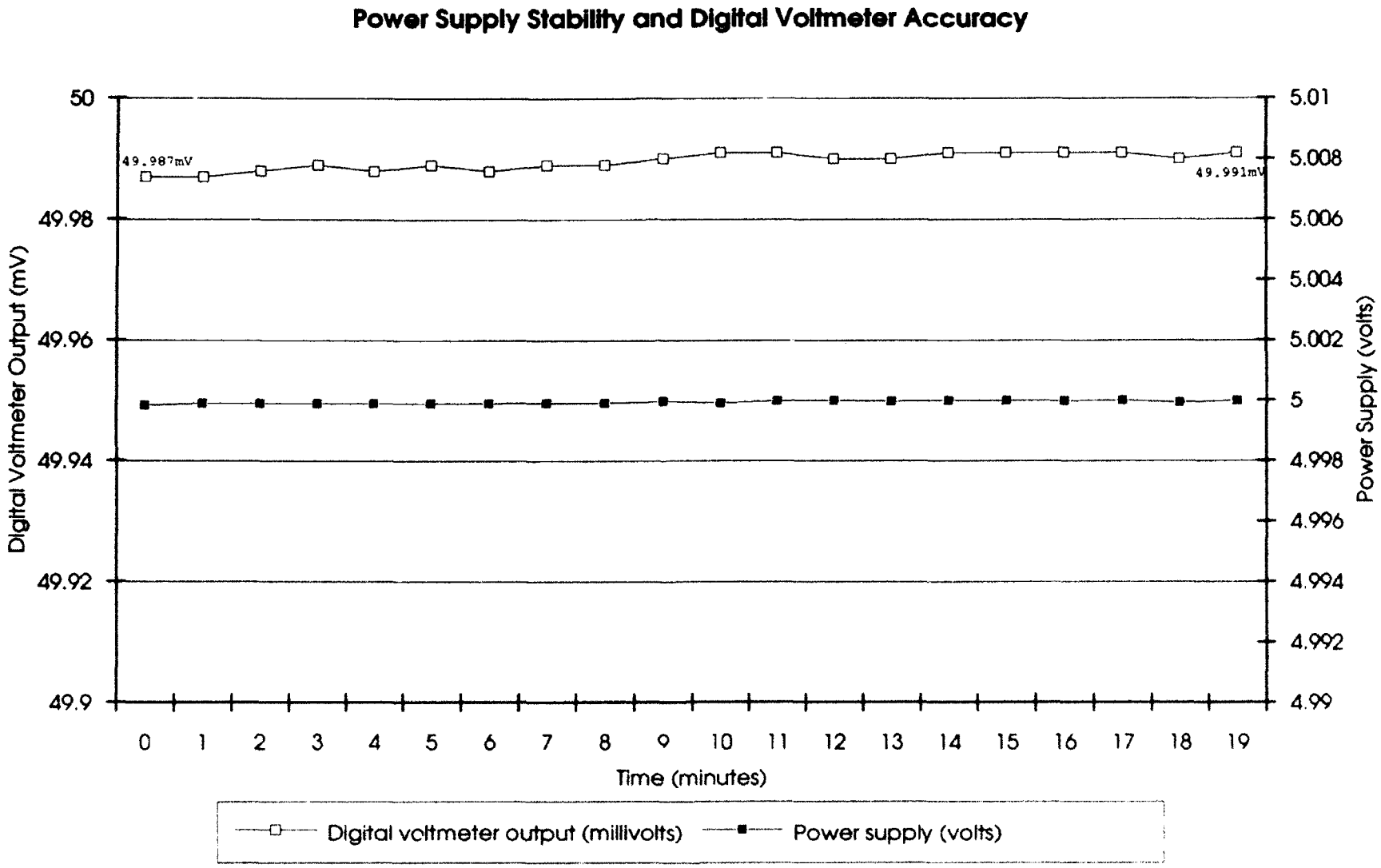
Power Supply Stability and Digital Voltmeter Accuracy
Digital Voltmeter Output (mV)
Power Supply (volts)
50
49.98
49.96
49.94
49.92
49.9
5.01
5.008
5.006
5.004
5.002
5
4.998
4.996
4.994
4.992
4.99
49.987mV
49.991mV
0 1 2 3 4 5 6 7 8 9 10 11 12 13 14 15 16 17 18 19
Time (minutes)
Digital voltmeter output (millivolts)
Power supply (volts)

Figure 11

Differential Pressure	Transducer Identifier	Sensitivity (mV/psi)			Percent Difference		
		Manufacturer	Static	Dynamic	Dynamic-Static	Dynamic-Mfg	Static-Mfg
5 psid	D01	2.430	2.410	2.39	-0.83	-1.65	-0.82
5 psid	D02	3.350	3.220	3.17	-1.55	-5.37	-3.88
5 psid	D03	4.266	4.180	4.09	-2.15	-4.13	-2.02
5 psid	D04	3.628	3.601	3.54	-1.69	-2.43	-0.74
5 psid	D05	3.602	3.466	3.43	-1.04	-4.78	-3.78
5 psid	D06	3.600	3.500	3.47	-0.86	-3.61	-2.78
5 psid	D08	2.850	2.758	2.71	-1.74	-4.91	-3.23
5 psid	D09	2.904	2.820	2.77	-1.77	-4.61	-2.89
5 psid	D10	2.814	2.697	2.65	-1.74	-5.83	-4.16
5 psid	D11	3.108	2.966	2.90	-2.23	-6.69	-4.57
5 psid	D12	3.750	3.595	3.55	-1.25	-5.33	-4.13
5 psid	D13	3.508	3.471	3.41	-1.76	-2.79	-1.05
5 psid	D17	2.534	2.421	2.37	-2.11	-6.47	-4.46
5 psid	D18	2.620	2.479	2.40	-3.19	-8.40	-5.38
5 psid	D19	3.634	3.717	3.60	-3.15	-0.94	2.28
5 psid	D15	3.640	3.577	3.50	-2.15	-3.85	-1.73
5 psid	D16	3.572	3.393	3.38	-0.38	-5.38	-5.01
25 psid	K04	3.281	3.196	3.13	-2.07	-4.60	-2.59
25 psid	K05	2.848	2.688	2.58	-4.02	-9.41	-5.62
25 psid	K06	4.081	3.996	3.93	-1.65	-3.70	-2.08
25 psid	K07	3.591	3.494	3.41	-2.40	-5.04	-2.70
25 psid	K08	3.702	3.561	3.48	-2.27	-6.00	-3.81
25 psid	K09	3.130	2.975	2.86	-3.87	-8.63	-4.95
25 psid	K10	2.881	2.616	2.50	-4.43	-13.22	-9.20
25 psid	K11	3.103	2.959	2.82	-4.70	-9.12	-4.64
25 psid	K12	3.283	3.050	3.03	-0.66	-7.71	-7.10
25 psid	K13	2.948	2.765	2.69	-2.71	-8.75	-6.21
25 psid	K15	3.076	2.885	2.80	-2.95	-8.97	-6.21
25 psid	K16	2.646	2.493	2.40	-3.73	-9.30	-5.78
25 psid	W04	3.142	3.170	3.11	-1.89	-1.02	0.89
25 psid	W05	3.080	2.844	2.81	-1.20	-8.77	-7.66
25 psid	W06	3.399	3.050	3.01	-1.31	-11.44	-10.27
25 psid	W07	2.844	3.012	2.94	-2.39	3.38	5.91
25 psid	W08	3.126	3.091	3.04	-1.65	-2.75	-1.12
25 psid	W09	3.400	3.192	3.15	-1.32	-7.35	-6.12
25 psid	W10	3.840	3.794	3.66	-3.53	-4.69	-1.20
25 psid	W11	2.780	2.734	2.65	-3.07	-4.68	-1.65
25 psid	W12	3.380	3.317	3.20	-3.53	-5.33	-1.86
25 psid	W13	2.280	2.396	2.09	-12.77	-8.33	5.09
25 psid	W14	3.190	3.144	3.07	-2.35	-3.76	-1.44
25 psid	W15	3.190	3.171	3.08	-2.87	-3.45	-0.60
75 psid	W01	1.180	1.138	1.11	-2.46	-5.93	-3.56
75 psid	W02	1.230	1.194	1.17	-2.01	-4.88	-2.93
75 psid	W16	1.160	1.130	1.10	-2.65	-5.17	-2.59
75 psid	W17	1.350	1.329	1.29	-2.93	-4.44	-1.56
				Average=	-2.51	-5.56	-3.11

Table 1. Transducer Sensitivities

TRANSDUCER SENSITIVITIES

Comparison of 2nd Multipoint Calibration With 2 Point Calibration and Initial Calibrations

Differential Pressure	Transducer Identifier	Sensitivity (mV/psi)					Percent Difference	
		Manufacturer	1st Static	Dynamic	2nd Static	2 Pt. Static	1st Static-2nd Static	1st Static-2 Pt. Static
5 psid	D17	2.534	2.421	2.37	2.436	2.436	-0.616	-0.616
25 psid	W11	2.780	2.734	2.65	2.746	2.750	-0.582	-0.582
25 psid	W14	3.190	3.144	3.07	3.118	3.115	0.931	0.931
25 psid	W15	3.190	3.171	3.08	3.193	3.193	-0.689	-0.689

Table 2

High Pressure
Microphone
Calibrator

[redacted]

Photograph 1

Real Time Radiography of Titan IV Booster

M. La Chapell, D. Turner, K. Dolan, D. Perkins and B. Costerus

ABSTRACT

Lawrence Livermore National Laboratory successfully completed a real time radiography of the Titan IV booster motor in February 1993. The success of this project depended on the quick response to Air Force criteria and securing a multi disciplinary team addressing the numerous technical challenges. The team's challenges included large area imager design and fabrication problems; vibrating mitigation obstacles; sound mitigation dilemmas; high levels of fail safe confidence; and operating a fragile, transportable x-ray linear accelerator. The data was viewed real-time and stored utilizing standard video hardware. The data from the test is presently being analyzed.

The multi disciplinary team was presented with many serious technical challenges that needed to be addressed expeditiously. The purpose of this paper is to examine some of the technical issues and how they were executed.

INTRODUCTION

On November 16, 1992, the Air Force requested Lawrence Livermore National Laboratory perform real time radiography for a static test firing of the Titan IV booster. The test was scheduled for December 19, 1992. On December 17, all aspects of the real time radiography system were in place and operational. However, due to other issues, the test was postponed until February of 1993.

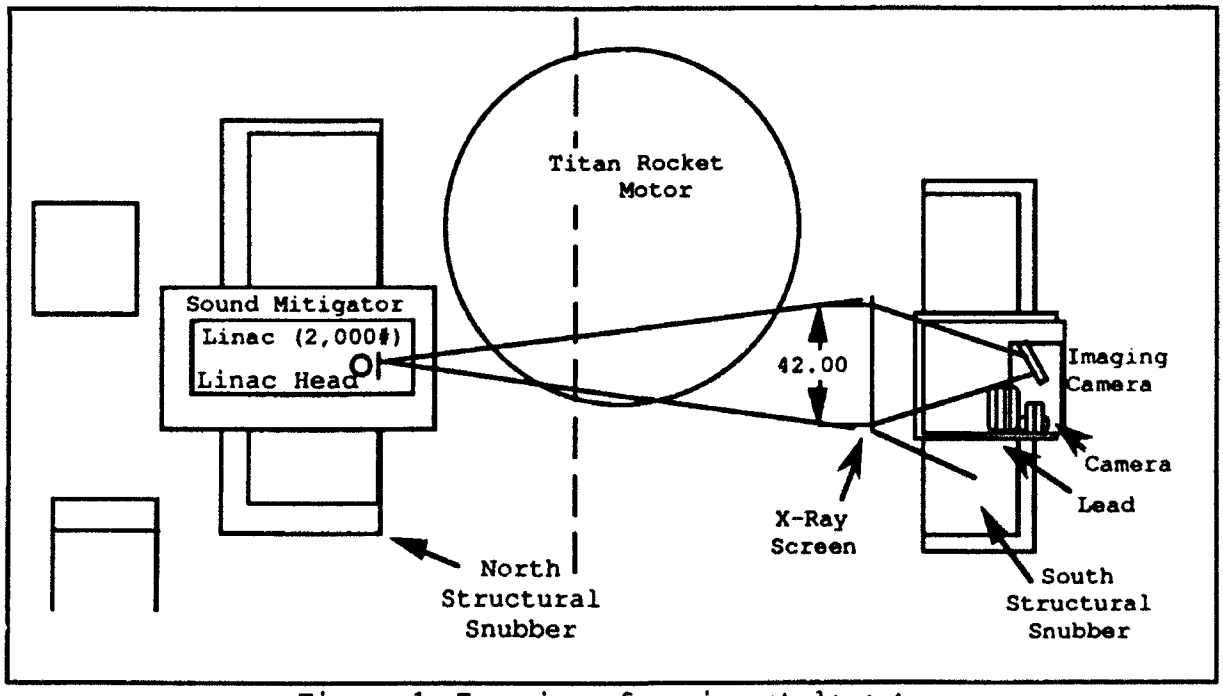

Figure 1. Top view of equipment layout.

THE X-RAY SOURCE

The Linac, a Varian 9 Mev linear accelerator, provided the x-ray source. It was a transportable unit which was contained in a fifty foot trailer. The Linac produced the 3000 rads of x-ray energy that was required to penetrate the 10 foot diameter rocket motor. Even with 3000 rads, the x-rays could not penetrate through the casing and propellant until approximately 20 seconds after motor ignition. The X-ray source was positioned within inches of the aft dome section of the motor as shown in *Figure 1* on the preceding page.

THE X-RAY IMAGING SYSTEM

The x-ray imaging system consists of a fluorescent screen, 42 x 51 inches. This screen is made up of a mosaic of 9 smaller screens arranged in a 3 x 3 format. For redundancy, two solid state micro channel plate intensifier cameras were used to read the image. To protect the cameras from the x-ray environment they were mounted behind lead shielding; consequently, it was necessary to have a 90° front surface turning mirror.

SHOCK AND VIBRATION MITIGATION

Since the Linac head and imager were positioned very close to the aft dome skirt, shock and vibration mitigation became a serious issue. Previous measurements of the motor noise had shown a noise level of 167dB from two motors, and 164dB from just one motor. Exact numbers of the vibration levels were not available but estimates indicate these levels at approximately 1.1g. Noise levels and vibration levels presented serious problems for the Linac head. If the shock and vibration loading to the head was not mitigated, the Linac would be inoperable for the duration of the test. See *Figure 2* for the acceleration data summary.

Unit	Vertical Acceleration (g-pk)	North-South Acceleration (g-pk)	East-West Acceleration (g-pk)
Cameras	0.45	0.4	0.4
Linac	0.95	0.4	0.3
Snubber	5.76	3.2	6.4
Trailer	1.12	1.6	0.8

Figure 2. Peak Accelerations

To mitigate noise on the Linac head, the Linac was placed in a plywood enclosure surrounded by 6 inches of acoustic material. This reduced the noise at the head to approximately 120dB. To mitigate the g shock loading, the Linac and its enclosure were mounted on air springs to the north structural snubber. The imager, positioned on the opposite side of the motor, was mounted on air springs to lessen the vibration and g shock problems.

ELECTRICAL MODIFICATIONS TO INCREASE FAIL SAFE CONFIDENCE

The portable x-ray accelerator is a complex electrical/mechanical system consisting of many components that could be adversely affected by noise and rocket booster vibration. It was important that the Linac produce stable x-rays for the duration of the test. Possible failures could cause machine shutdown or beam instability. Additionally, vibrations in the microwave tuning mechanism could cause extreme fluctuations in the x-ray output. The Linac would shut down if its factory installed protection circuits detected problems with machine integrity such as the vibration of the Linac head, large variations on the pressure, or vacuum and flow switches. Any of these scenarios would result in the failure of the real time radiography portion of this test. Based on this information, a protection bypass system was installed. Prior to firing the booster, the bypass system was activated for the duration of the test.

DATA RECORDING SYSTEM

The output of the video cameras was the standard RS170. This allowed the video data acquisition system to be quite simple. The video data was sent via fiber optic cables to the control room 1300 feet away, and recorded on a standard S-VHS tape and laser disk. Laser disks were used to make the post test data analysis easier. IRIG time was recorded on the audio channels of the video recorders.

TEST RESULTS

During the booster firing, all systems performed quite well. At T+25 seconds the image became well defined and was well formed for the remainder of the test. The vibration mitigation design performed flawlessly, even though the g shock loading was far beyond the original estimates. Except for one period, the Linac was stable for the duration of the test and its output was constant. This exception occurred when radiation output decreased for a short period of time. To date, all data has been recorded and the analysis at LLNL is near completion.

CONCLUSION

This test demonstrates that real time radiography can be successfully implemented and provide meaningful information under adverse test conditions. The issues of extreme g shock and acoustic vibration can be successfully mitigated. High output linear accelerator x-ray generators and large image arrays can be assembled and applied to the diagnosis of rocket booster performance. This type of test can be engineered and assembled in a relatively short period of time.

The Effects of Cable Connections on High Frequency Accelerometer Calibrations

B. F. Payne
National Institute of Standards and Technology
Gaithersburg, MD 20899

ABSTRACT

Accelerometers are widely used in vibration laboratories at frequencies in the range of 10 to 30 kHz. Many problems arise in calibrating accelerometers accurately in this high frequency range. These problems include the geometry of the accelerometer, surface finish of the accelerometer, type of cable used, and type of cable connector. This paper will focus on the effects of cable connectors on accelerometer calibration results. A laser interferometer was used in this testing and measurements were made at 121.1 nm displacement. Changes in the type of connector resulted in significant differences in calibration results for some types of accelerometers. The paper describes the measurement procedure and gives data on some accelerometers that have been tested.

BACKGROUND AND EXPERIMENTAL METHOD

Figure 1 shows schematically a high frequency fringe-disappearance interferometric accelerometer calibration system. This system uses a Michelson interferometer with one of the mirrors attached to the vibrating surface to be measured. The accelerometer is mounted by a screw to the center of the shaker table. The reference mirror of the interferometer is attached to small piezoelectric driver so that the path length difference Δ, of the two arms of the interferometer can be modulated by an oscillator at a low frequency of about 0.5 Hz.

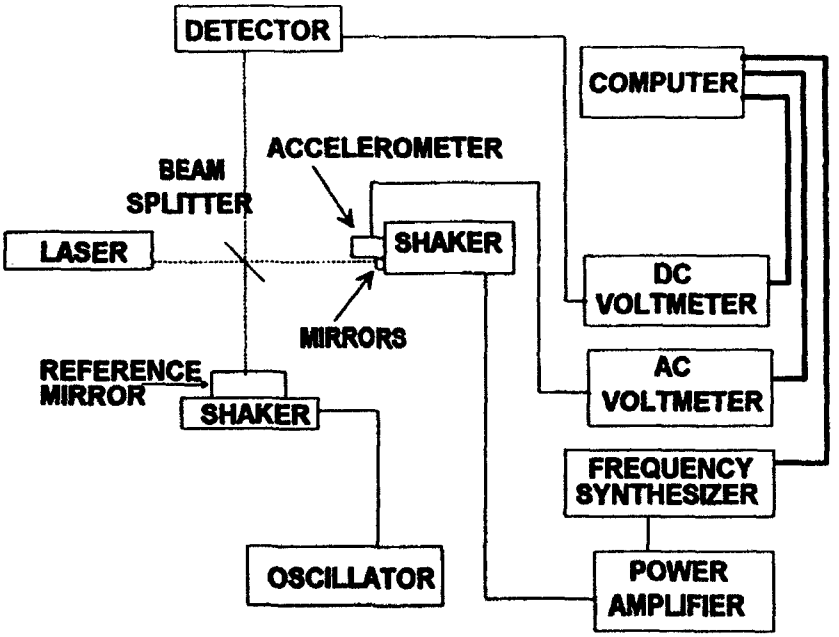

Figure 1. Laser Fringe-Disappearance Interferometer for Accelerometer Calibration

The object of the measurement is to measure the dynamic displacement to which the accelerometer is subjected. The low frequency terms of the photodetector current is given by:

$$I = A + B\ (\cos\ 4\pi\Delta/\lambda)\ J_0(4\pi d/\lambda)$$

where A and B are system constants, d is the displacement amplitude to be measured, λ is the wavelength of the laser light (632.2 nm), Δ is the optical path length difference of the two arms of the interferometer, J_0 is the Bessel function of the first kind of order zero. For any fixed value of d, the range of variation of I is

$$I(max) - I(min) = 2BJ_0(4\pi d/\lambda) = Delta(I)$$

since the cosine function varies from -1 to +1. This difference decreases as d approaches a value which makes

$$J_0(4\pi d/\lambda) = 0.$$

The lowest value of d for which this expression is true is the first fringe disappearance. For a HeNe laser with wavelength λ of 632.2 nm, this value of d is equal to 121.1 nm.

The procedure for automatic displacement measurement is as follows. A computer controlled, programmable digital synthesizer systematically varies d, the amplitude of vibration of the shaker, while a digital DC voltmeter reads Delta(V) from the photo detector circuit (proportional to the Delta(I) in the detector itself) and stores the data. The synthesizer voltage is varied in small increments until Delta(V) reaches its lowest level or Delta(V) = Delta(min). At this condition the amplitude is 121.1 nm, or fringe-disappearance condition. More details of the experimental process are given in (1).

For constant amplitude of 121.1 nm, the following table lists the approximate acceleration values (referenced to the standard acceleration of free fall: 9.80665 m/sec^2) for the frequency range over which the accelerometers were tested.

Frequence kHz	**Acceleration**	**Frequency kHz**	**Acceleration**
10	49	18	158
11	59	19	179
12	70	20	195
13	82	21	215
14	96	22	237
15	110	23	255
16	125	24	281
17	141	25	305

EXPERIMENTAL RESULTS

Three accelerometers were tested for cable connector effects. The first accelerometer was one with a top cable connector and a nominal mounted resonance frequency of 40 kHz. Two cables were used for this test. The first cable was a standard commercial accelerometer cable with a threaded connector for attaching it to the accelerometer. The second cable was a similar cable with one end cut off to remove the threaded connector. A solid pin was attached to the center lead and a fine copper wire to the shield for the ground connection. The tests used three reflecting mirrors attached to the top of the shaker, approximately 120 degrees apart as shown in figure 1. The accelerometer and cables are shown in figure 2. The results of the tests are shown in figure 3. The effect of the threaded connector can be seen in this figure. The data in Figure 3 is the average of the data corresponding to the three mirror positions.

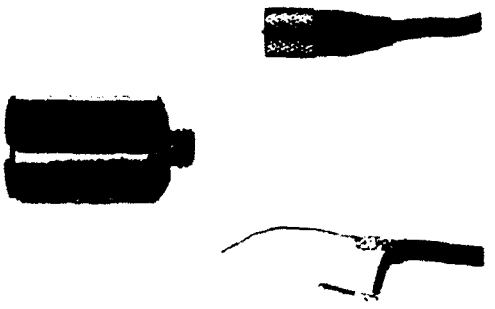

Figure 2. Accelerometer with top mounted cable connector

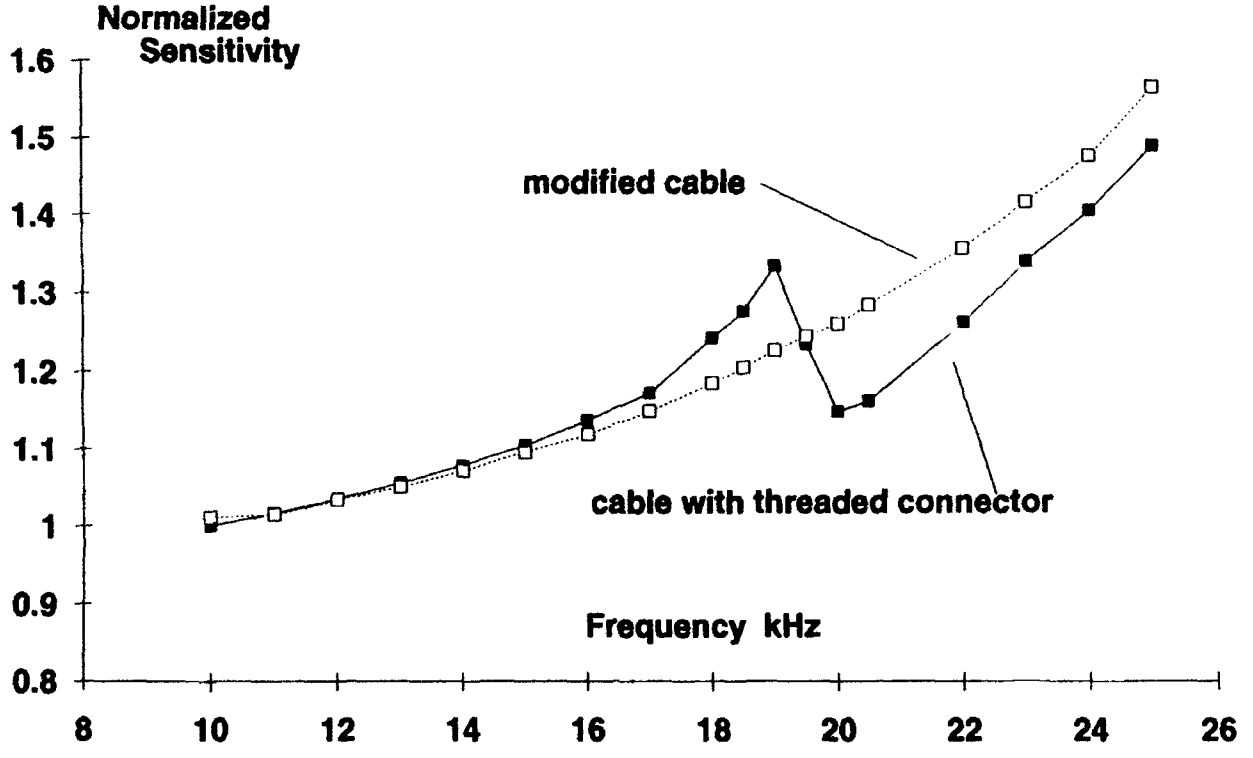

Figure 3. Cable Connector Effects for Accelerometer with Top Mounted Connector

A second accelerometer was tested in a similar manner. This was an accelerometer with a side mounted cable connector and a nominal resonance frequency of 55 kHz. This accelerometer and the same two cables as used for the first accelerometer tested are shown in figure 4. The results of the tests on this accelerometer are shown in figure 5. The effect of the screw connector is similar to that caused in the top mounted accelerometer, except the changes occur at a higher frequency.

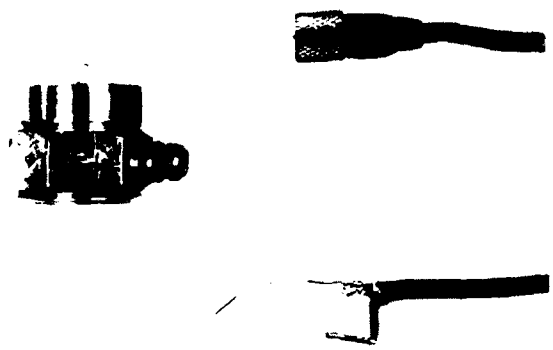

Figure 4. Accelerometer with side mounted connector

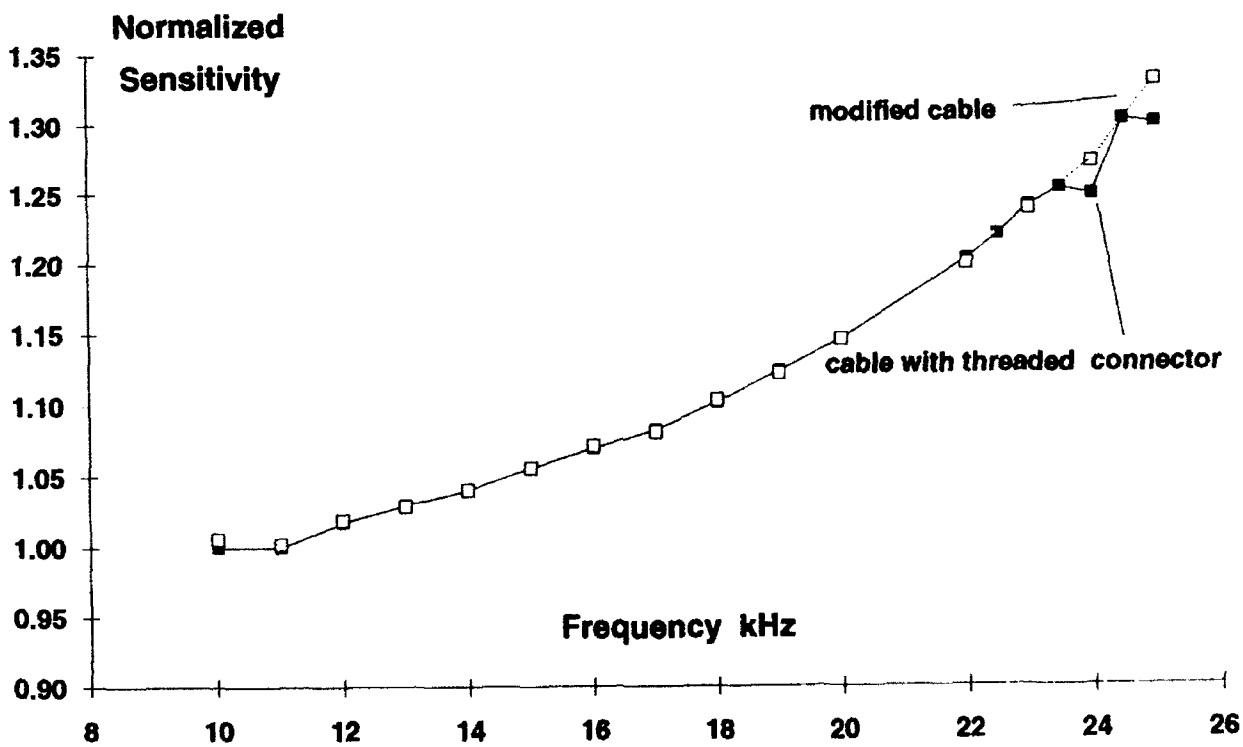

Figure 5. Cable Connector Effects for Accelerometer with Side Mounted Connector

The third accelerometer is a miniature accelerometer with a top mounted connector and a nominal resonance frequency of 90 kHz. The accelerometer and the cables used in the test are shown in figure 6. The cables used were supplied by the manufacturer and are not the same as in the two tests above. However the screw connector is similar. In this case, the integral cable shown in figure 6 was soldered directly to the accelerometer connector to test the effect of the threaded connector on the high frequency sensitivity. The results of the tests on this accelerometer are shown in figure 7.

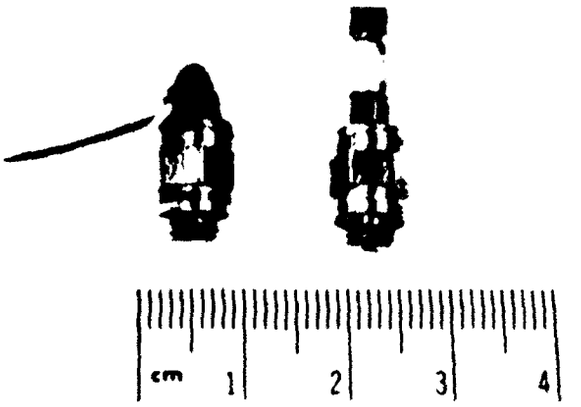

Figure 6. Minature Accelerometer with top mounted cable connector

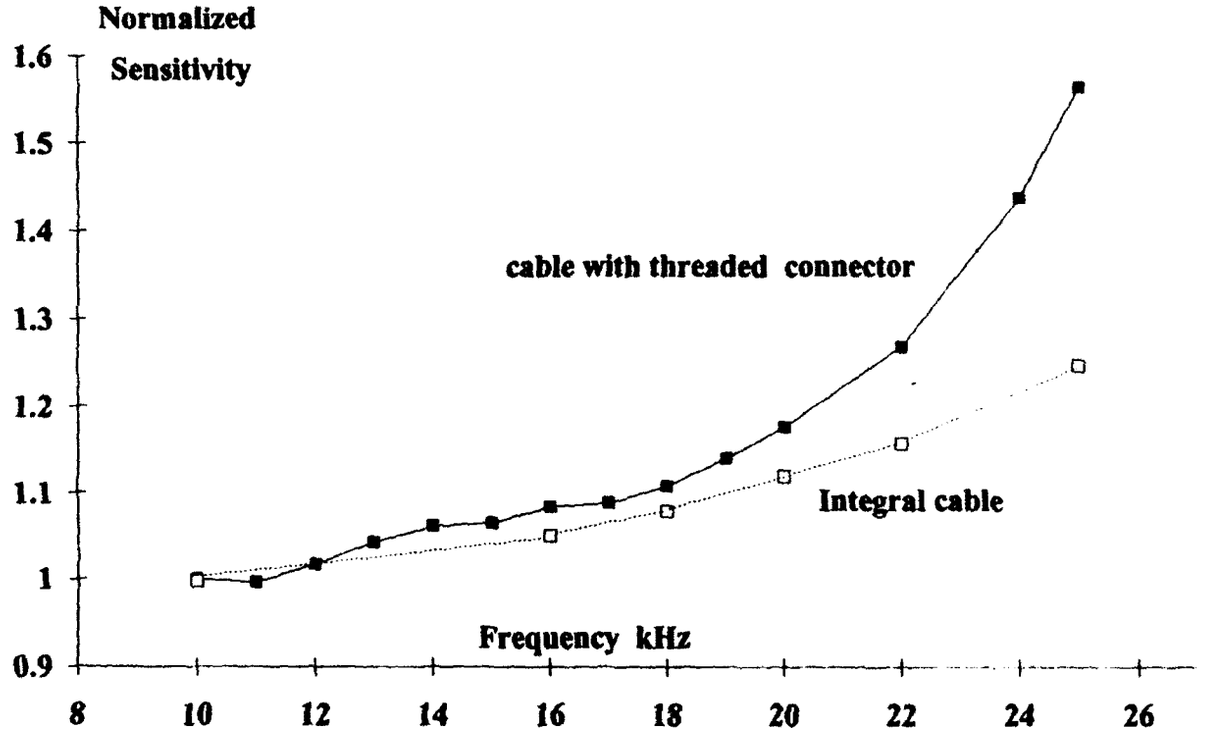

Figure 7. Cable Connector Effects for Minature Accelerometer with Top Mounted Connector

DISCUSSION

Cable connectors can have significant effects on the measured frequency response of accelerometers at high frequencies. More detailed studies need to be performed to determine which cables are best suited to high frequency measurements. Sometimes the connector can produce visible wave form distortion and sometimes the distortion is not evident from the wave form signal. Accelerometers which will be used for high frequency measurements should have cables designed for the specific frequency range over which the accelerometers will be used.

REFERENCES

1. Payne, B.F., ''Automation of Vibration Testing at the National Bureau of Standards'', Proc. IES 30th Annual Tech. Meeting, Orlando, FL.,May 1-3,1984 (IES, Mt.Prospect, IL.),pp. 478-482.

SMART TRANSDUCERS WITH SELF-IDENTIFICATION AND SELF-TEST

Steven C. Chen
PCB Piezotronics, Inc.
Depew, New York

ABSTRACT

Traditional transducers provide an analog output signal to a signal conditioning system for the front-end of a data acquisition system that amplifies, filters, digitizes and reduces the signal. Modern transducers that contain innovative designs such as built-in signal-conditioning electronics are often referred to as "smart transducers". Recent developments in the field of microelectronics has increased the intelligence of the transducers by addition of features such as programmable signal conditioning, self-identification, self-checking and self-calibration into the transducers while providing analog and/or digital output. This paper discusses the implementation of piezoelectric transducers with self-identification and self-test features for large scale applications that use hundreds of transducers. This paper also covers the efforts and technological capability at PCB Piezotronics for intelligent piezoelectric transducer development.

1.0 INTRODUCTION

Piezoelectric transducers have been widely utilized for many years in pressure, force and vibration measurements. The ICP™ (Integrated Circuit Piezoelectric) concept eliminates the problems caused by the extremely high output impedance of piezoelectric sensing structures. ICP systems also provide a more cost effective solution for most of the applications that utilize piezoelectric transducers. The temperature range of ICP transducers reaches 200°C, which satisfies the requirement of most piezoelectric transducer applications. With recent improvements in resolution and temperature range, ICP systems no longer chase the shadow of the charge-mode alternatives and are exploring new grounds of their own.

With the continuing progress in microelectronics technology, today's ICP systems are more than just analog signal conditioning circuitry. ICP systems now support smart features that can make piezoelectric transducers smarter. The smart features improve the accuracy of the output signal, reduce the effect and probability of human errors, integrate the transducers with the readout devices more closely, make the ICP piezoelectric transducer even more easy-to-use, etc.

This paper focuses on smart transducers with self-identification and self-test features. Smart transducer projects developed at PCB Piezotronics since 1985 are reviewed. Hybrid and ASIC (Application Specified Integrated Circuit) implementation technologies are discussed.

2.0 SMART SENSING WITH THE ICP™ CONCEPT

Under the ICP concept, the transducer houses in a single package both a piezoelectric sensing structure and an amplifier for increased performance, and simplified signal and power transmission [1].

ICP instruments operates as 2-wire or 3-wire systems. The internal charge or voltage amplifier provides impedance conversion, amplification and other types of signal conditioning. Both voltage and charge type amplifiers employ a capacitor to convert charge into voltage output. ICP-compatible signal conditioners power the transducer by a constant current through the signal output line [2].

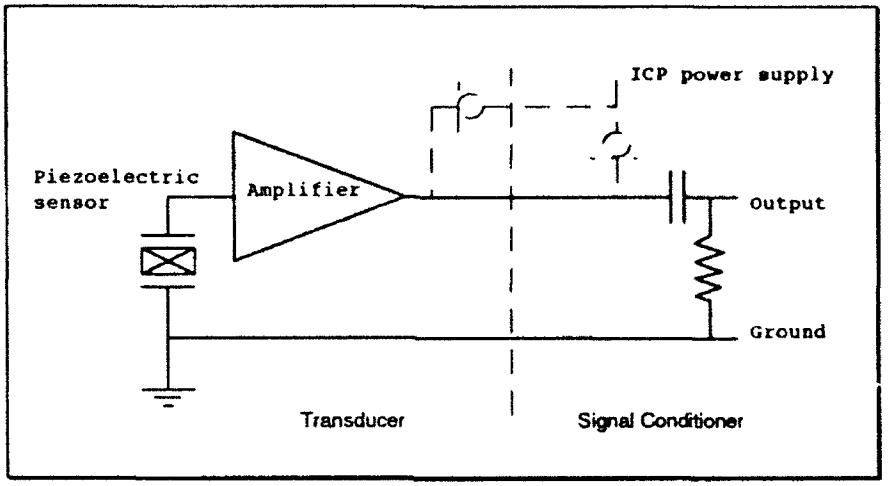

Figure 1. Typical ICP system.

The ICP concept has been promoted in the last 25 years. In general, ICP systems are more cost-effective than charge-mode systems. Original MOSFET ICP amplifiers offered a wide-temperature range with reasonable resolution. Newer JFET ICP amplifiers feature high-resolution with limited temperature range. The latest CMOS ICP amplifiers combine high-resolution and a wide temperature range.

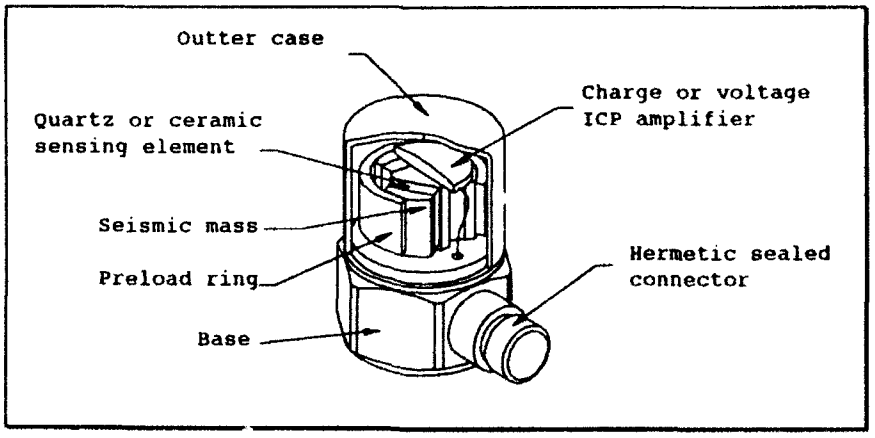

Figure 2. Typical triangular shear ICP accelerometer.

3.0 SMART TRANSDUCER

Significant research efforts have been devoted to the development of products for affordable multi-channel measurement systems. Numerous systems and transducers have developed for cabling management, auto-ranging, bank switching, easy installation, array calibration, etc.[3-7].

Despite the availability of such equipment, testing costs are high, in part because of labor-intensive installation procedures and human errors. To reduce the cost and improve the accuracy of large-scale measurements, customers have indicated the need for accelerometers that can provide the following features:

- automatic transducer and channel identification by serial number broadcasting,
- automatic orientation and location identification with built-in memory or self-detection,
- calibration information storage in built-in memory,
- bi-directional communication between transducers and data acquisition equipment,
- compatibility with existing systems,
- field programmability,
- self-announcing failure monitoring.

With the strong commitment to the ICP concept, smart transducers are a natural extension for the ICP system. In the last few years, several transducers and prototypes have been developed at PCB Piezotronics:

- T-WAM (Transducer With A Memory),
- vibration monitoring transducer # 1,
- vibration monitoring transducer # 2,
- flight transducer,
- vibration monitoring transducer # 3,
- *new general-purpose smart building block.*

Typical ICP systems use 2 or 3 wires. With the addition of built-in intelligence and complex signal conditioning features, there is a need to transmit more data between transducers and signal conditioning equipment. To access all information, the first generation of smart transducers developed at PCB used more connections than the typical ICP system. Nowadays, with the increased density and affordability of microelectronic circuits, the trend is for full compatibility with regular ICP systems. The latest designs use internal multiplexing to transmit analog and digital signals in different time slice.

PCB's newer smart transducers protect the user's investment in existing signal conditioners. In those applications where bi-directional communication is required, existing hardware has to be modified or new equipment has to be added. But, if single-direction communication fulfill the user's needs, the existing data acquisition equipment and system controller can be used with some software changes.

3.1 T-WAM : TRANSDUCER WITH A MEMORY

The first smart transducer designed at PCB Piezotronics was T-WAM (circa 1985). The T-WAM option adds a 128-byte *nonvolatile memory* to standard ICP transducers. The memory chip provides a cost-effective solution for storing archival data (model number, serial number, calibration data, etc.) or other significant data within the sensor unit. In the no-power "sleep" mode, data can be retained up to 10 years. Since T-WAM requires minimal control signals for read/write operations, a six-pin connector is the only physical modification required to convert existing sensors. Data stored in the T-WAM system can be accessed by a host computer through the control unit. Typical applications for the T-WAM option include identifying individual sensor units in an array and providing a nonvolatile storage media for test data.

The T-WAM can also be built in an in-line configuration, so that there is no need for modification of the existing transducers. A thin-film microelectronic circuit was designed and built in PCB Piezotronics' clean room and in-house hybrid facility.

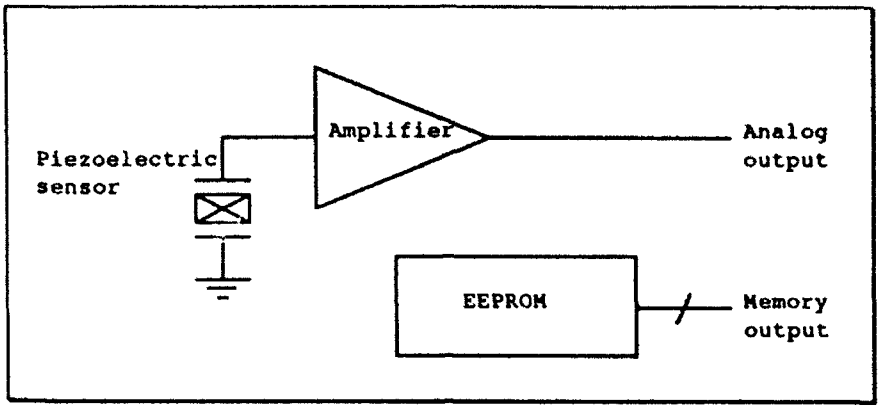

Figure 3. T-WAM (Transducer With A Memory).

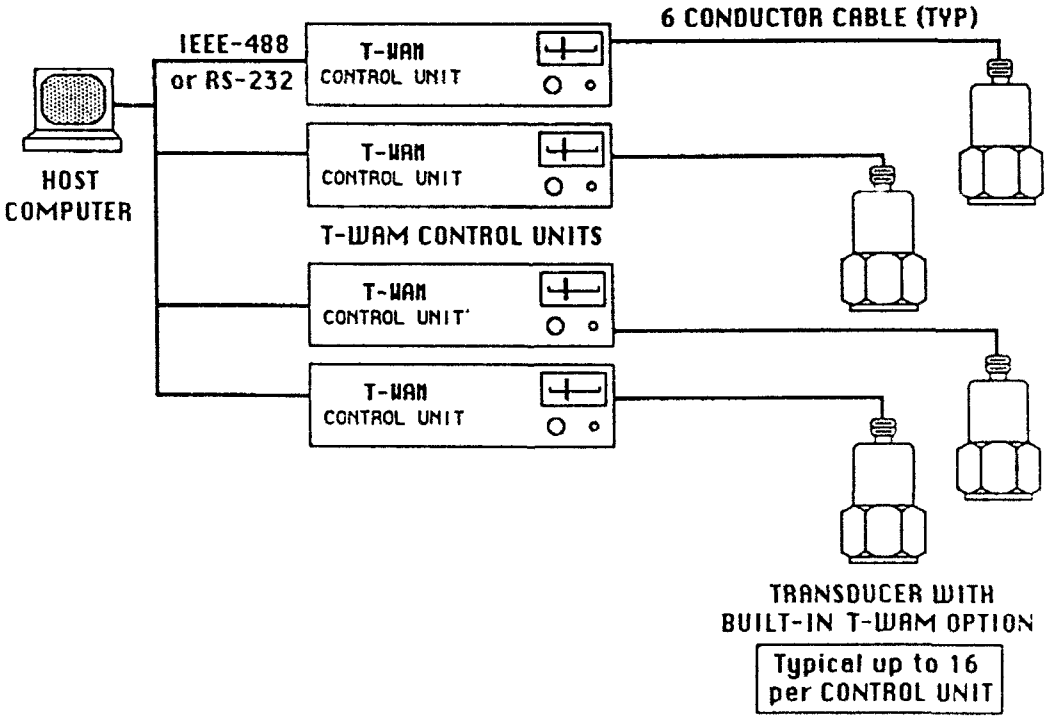

Figure 4. Typical T-WAM System.

3.2 VIBRATION MONITORING TRANSDUCER # 1

PCB transducer model 328M25 is the result of the development of a custom transducer for an application that included permanent installation of the transducer in the hull of a ship. The user required a transducer with bi-directional communication, a 2-wire interface, and self-test / self-calibration capability for fault detection. The transducer designed at PCB comprises a built-in microcomputer and nonvolatile field-programmable memory (E^2PROM).

The content of the E^2PROM is field programmable for quick reconfiguration after installation, for example to store updated calibration data. The system controller can activate the reprogramming mode by sending a predefined pulse train. Since most of the transducers used in the application were mounted in locations which are not easily accessible, this feature is a major advantage.

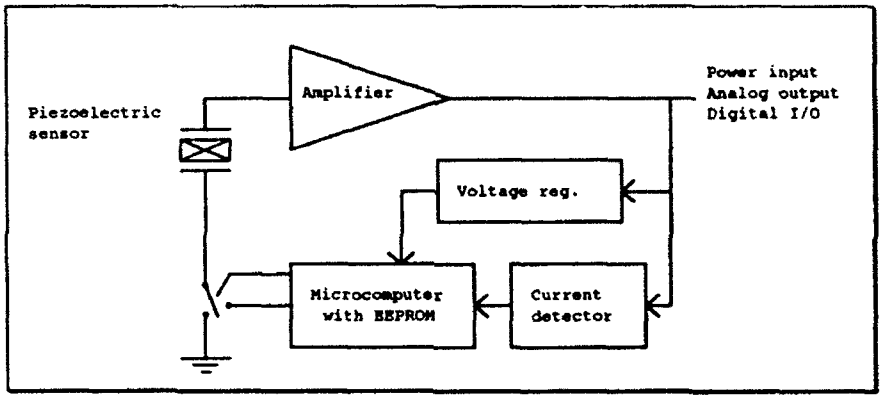

Figure 5. Block Diagram of PCB model 328M25.

3.3 VIBRATION MONITORING TRANSDUCER # 2

This transducer (PCB model 352A02) was custom designed for a structure-borne noise measurement application that required in-flight remote calibration capability. The external calibration input and remote operating mode selection allows the user to test the transducer from remote locations of up to 1000 feet away. Instead of using a fixed frequency pulse train for calibration, this design allows calibration with different types of signals such as fixed sine, random noise, swept sine, etc. In this case, ICP compatibility was not a concern, and a differential output stage was used.

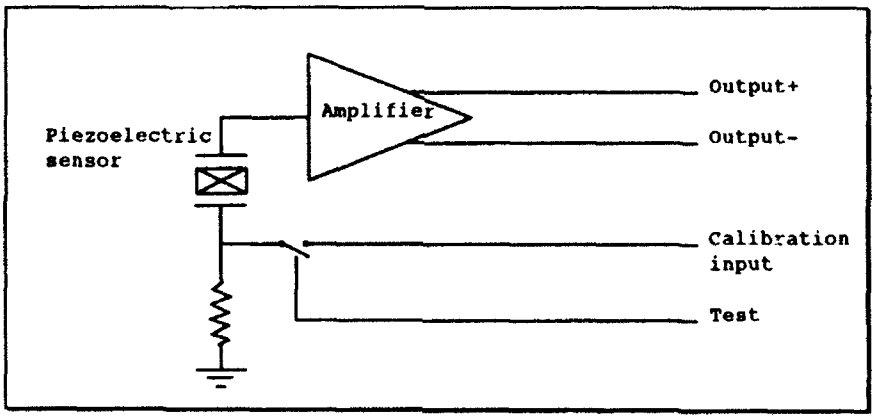

Figure 6. Block diagram of PCB model 352A02.

3.4 FLIGHT TRANSDUCER

The model 353M27 is a shear-mode triaxial accelerometer that was custom designed for a high shock test flight application. To allow remote-controlled test and calibration, the transducer incorporates an internal oscillator that generates a squarewave of known amplitude and frequency for a predefined period of time at turn-on. By examining the square-wave output signal, the user can judge the integrity of the sensing element. This particular design comprises five hybrid circuits per axis inside a triaxial transducer.

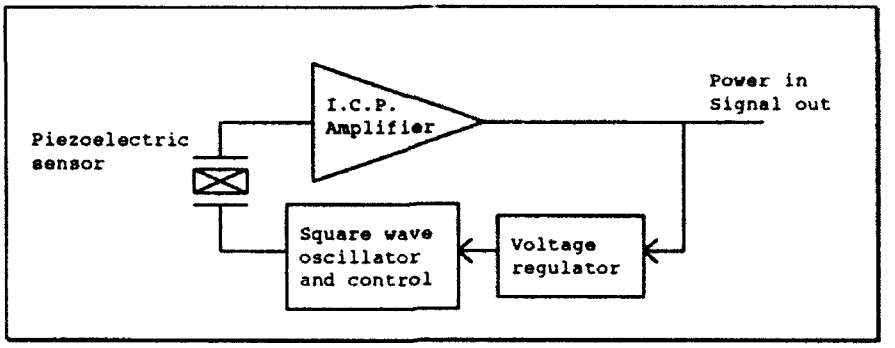

Figure 7. Block diagram of PCB model 353M27.

3.5 VIBRATION MONITORING TRANSDUCER # 3

To reduce the cost of transducers with self-identification, a microelectronic circuit with hard-wired ID code was developed. The circuit may be added to any standard ICP transducer. Upon power up, the transducer transmits the hard-wired ID, then enters the normal analog mode of operation.

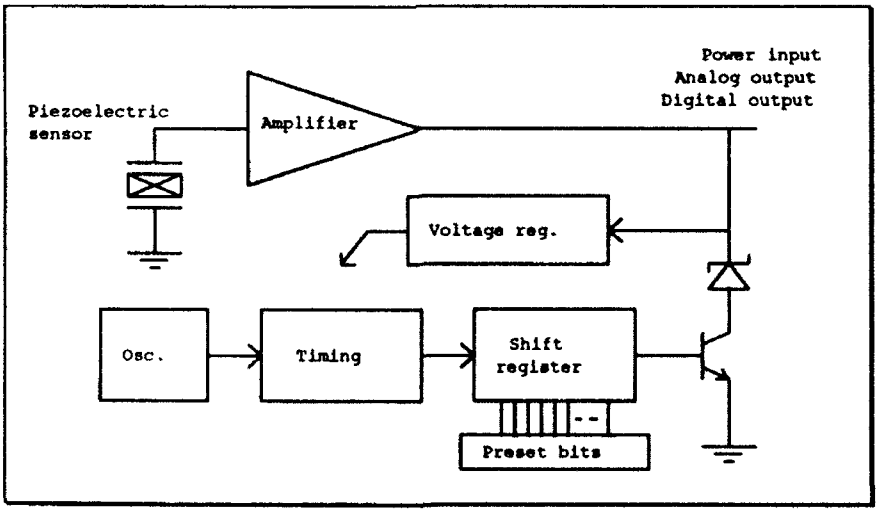

Figure 8. Block diagram of PCB model 308M358.

3.6 General-Purpose Smart Building Block

The latest smart transducer design with self-identification and self-test utilizes high-density programmable logic devices and hybrid analog circuits. Ultimately, the electronics in this transducer is to be implemented on a full-custom mixed-signal ASIC to be utilized as a general-purpose smart building block.

The self-identification and self-test concepts are similar to the ones utilized in previous designs. The primary change is in the system integration stage. This smart transducer and its building block were designed for general users who already have a measurement system, instead of being restricted to one very specific application requiring a particular measurement system. With a simple addition to the existing measurement equipment, a computer can communicate with the transducer bidirectionally. The link between transducers and other measurement systems, such as calibration and field measurement units, shifts the emphasis from smart transducers to smart systems.

The smart building block incorporates a field-programmable E²PROM that contains identification information such as the device's model number, serial number, calibration data (sensitivity and frequency response), as well as 64 user-defined characters that may be used to record the transducer's status, location, orientation, etc. By default, the transducer broadcasts the entire content of its memory upon turn-on, and operates as a regular analog-output ICP sensor thereafter. With added communication equipment, the transducer may be operated in a "programming" mode, which allows the user to read and/or update all data recorded in memory.

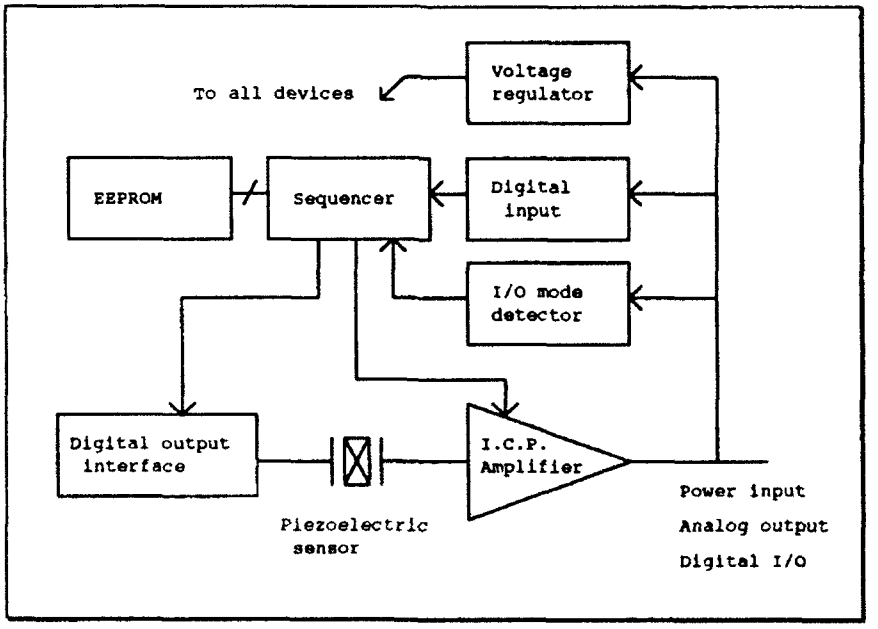

Figure 9. Block diagram of PCB model 326M11.

This smart transducer offers many attractive features to potential users :

- it is usable as a standard analog-output ICP transducer,
- its self-identification message includes calibration data, which opens the possibility for signal conditioning equipment to automatically download and take into account the sensitivity and frequency response of each separate sensor,
- 64 characters of field-programmable user-defined data are available,

- the memory capacity of the smart building block is scalable without affecting compatibility,
- the microelectronic circuit may be used as a standard building block for any ICP transducer,
- the same circuit will be used as part of the control circuitry for ICP transducers with internal user-controlled signal conditioning,
- the smart transducer itself is a building block for larger smart systems, to which PCB is devoting some effort,
- the ASIC standard-cell design approach will enable PCB to develop the smart building block in a short time frame.

4.0 IMPLEMENTATION

As the complexity of electronic circuits increases, the traditional printed circuit board implementation no longer meets size and reliability requirements. For these reasons, the electronics in most modern transducers are fabricated in thin-film or thick-film hybrid technology.

A thin-film circuit consists of wire-bonded IC dies mounted on a ceramic substrate. It offers very small size with low up-front cost and higher unit cost. It is well suited for prototype and low-quantity production. Thick-film technology utilizes surface-mount parts mounted on ceramic substrates. It provides lower unit cost, increased reliability, reworkability and better sealing. It is not well suited for prototype quantity production. Drawbacks of thick-film technology are longer lead time, higher up-front cost, and larger size (see figure 10).

Custom integrated circuits (IC) technology is highly reliable and offers high density. Therefore, it is a good candidate for the implementation of smart transducers. The design of application-specific integrated circuits (ASICs) differs significantly from that of PC-board-based, thin-film, or thick-film circuits. Because of different technological limitations, the electrical design style of ICs has little in common with that of circuits that use discrete parts. Also, since the comparatively high cost of ASIC fabrication often prohibits prototype runs, the design process is highly automated and requires computer-aided design tools to get functional units the first go-around.

Because of high development costs and long manufacturing time, ASICs are only intended for volume production. However, state-of-the-art circuit simulation tools, IC layout computer-aided engineering tools, as well as the wide availability of semiconductor foundry services have made ASICs more affordable and have lowered design time in the last few years.

Several IC fabrication approaches are applicable for smart transducer electronics implementation. Full-custom ICs allow the designer to implement any circuit function, within the limits of the technology, at the price of increased design complexity. Semi-custom ICs based on the use of pre-characterized standard cells offer a more structured, hence faster, design process. Another popular option for fully digital circuits is to use a programmable or erasable/programmable logic array. Such circuits are less expensive and enable fast turnaround. However, they are intrinsically limited to digital circuits, and therefore require extra circuitry to implement a smart transducer.

In addition to many projects which employed hybrid implementation (see chapter 3), both full-custom and standard cell IC design have been actively pursued. A self-identification ASIC similar to the digital circuit described by Eller [9] and with the same functionality as vibration monitoring transducer # 3 (see chapter 3.5) was designed in 1991. Since then, work has begun on a series of full-custom ICs to implement the electronics of a smart transducer on a single chip. As a short-term goal, the digital section of the general-purpose smart building block (see chapter 3.6) is to be fabricated and tested. The approach emphasizes modular design, so as to build a library of IC sub-circuits that can be used several times in order to cut design time and cost.

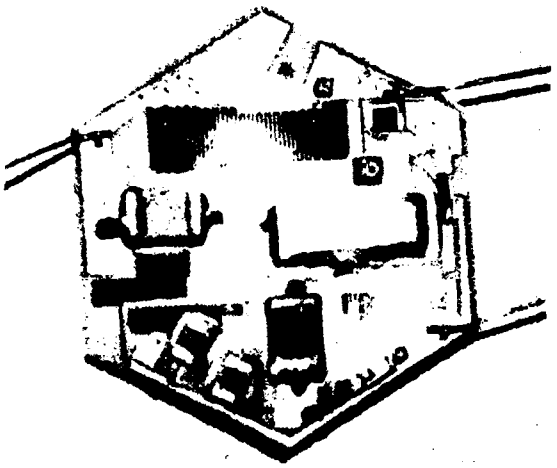

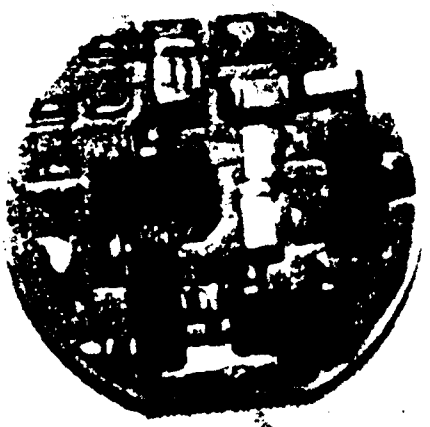

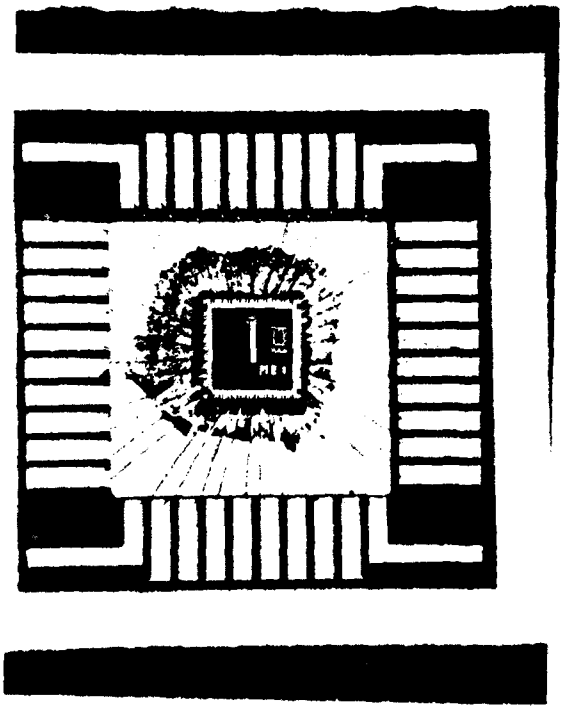

Figure 10. (Top left) Photograph of an ICP amplifier implemented in thin-film technology (370 *mils flat-to-flat*), (Top right) Photograph of an ICP amplifier implemented in thick-film technology (400 *mils diameter*), (Bottom) Photograph of a test ASIC implemented as a MOSIS tinychip (chip size : 90x90 $mils^2$).

5.0 Conclusion

In this paper, we have presented smart transducers designed at PCB Piezotronics since 1985. PCB's goal is to provide test engineers with transducers that are highly reliable and accountable. Smart transducers reduce the cost and time for testing. The end result is higher-quality data and lower overall cost.

Acknowledgment

The author would like to thank Mr. David Guillou for the information and material he provided for this paper.

References

1. PCB Piezotronics, "General Guide to ICP Instrumentation",
2. Lally, R.W., "Application of Integrated-Circuits To Piezoelectric Transducers", Proceedings ISA, 1967
3. Lally, M., Severyn T., "Multichannel Management Concepts for Modal Analysis and Testing", Test Engineering & Management, April 1991
4. Lally, M.J., Brown, D.L., "Structcel - A New Instrumentation System", Proceedings Fourteenth Transducer Workshop, 1987
5. Poland, J.B., Chen, S.C., Hewson, C., Lally, R.W., "Flexible Multichannel Signal Conditioning System", Proceedings IMAC, 1993
6. Chen, S.C., Poland, J., Liang, Z., Lally, R.W., "Smart Transducers", Proceedings IMAC 1993
7. Gierer, J.W., Grant, R.L., "Self Monitoring and Reporting Transducers", Proceedings Fourteenth Transducer Workshop, 1987
8. Talmadge, R., Appley, K.E., "Programmable Transducer Microchip Development", Proceedings Sensors Expo, 1990
9. Eller, E., "An Accelerometer with Internal Self-Test and Identification", Proceedings Sensors Expo West, 1990

SESSION 4

APPLICATIONS

BOA ANGLE-OF-ATTACK SENSOR

Steven J. Meyer
Edmund H. Smith
Naval Air Warfare Center Weapons Division
China Lake, CA 93555

ABSTRACT

This paper documents the design and development of the BOA missile angle-of-attack sensor. The sensor is a four-port hemispherical sensor, and was designed to operate over the range of Mach numbers from 0.5 to 2.5 and for angles-of-attack up to 30 degrees. The design of the sensor and the instrumentation used is described, along with reasons for the design decisions that were made. The methodology used to develop the calibration curves for the sensors is shown. Results are presented for two successful flights, and show good correlation with the predicted angle-of-attack.

BACKGROUND

The Angle-of-Attack (AOA) of a missile refers to angle between the air flow and the missile body. A missile program may find this data very important in analyzing the performance of the missile. This was the case for the BOA missile program. The BOA missile is a Naval Air Warfare Center Weapons Division in-house technology effort to develop a maneuverable air frame. This was done by using small wings and canards, which make the missile less stable and permit greater angles of attack during maneuvering flight. This angle can be found from camera data, but, sometimes there may not be enough camera coverage or no coverage at all. Also, it is desirable to have two data sources. The photo data also takes a long time to reduce and can be costly. Therefore, a method was developed to measure the AOA of the BOA missile directly. The options were to use vanes, hot wire or hot film probes, and pressure ports. The first two are vulnerable to damage and affect the missile's aerodynamic configuration. Probes usually also affect the aerodynamics; but, in the case of the BOA missile, the nose is hemispherical already, so a hemispherical probe can be incorporated with no external configuration change to the missile other than small pressure ports. This type of probe is frequently used, and good

---

Approved for public release; distribution is unlimited.

documentation was available in Reference 1. Hence, this configuration was chosen.

PROBE CONFIGURATION

The probe configuration was chosen to allow use of calibration data contained in Figure 95 of Reference 1 and in Figure 3:13 of Reference 2. These data are for a hemispherical probe with four ports at 45 degrees from the missile centerline and equally spaced circumferentially. The configuration is shown in Figure 1. The data in Reference 1 cover Mach numbers from 0.4 to 2.2, while the data in Reference 2 are for incompressible flow, assumed to be Mach 0.2 or below. It should be noted that the data in Figure 95 of Reference 1 define C_p as being the pressure difference divided by the difference between the free stream total and static pressures rather than being divided by the dynamic pressure, q. The combination of the results is shown in Figure 2, where C_p is referenced to the dynamic pressure. It should also be noted that the data in Reference 1 are for a hemisphere on the end of a probe of the same diameter, while the data in Reference 2 are for a spherical yawhead mounted on a slender sting. Hence, these two sets of data are not totally comparable. In Figure 2, the first point is from Reference 2, while the remainder are from Reference 1. The difference between the points at Mach 0.2 and Mach 0.4 is small, but whether it is due to the change in Mach number or the two different probe configurations is unknown.

Another issue was the difference between the probe configurations assumed in Reference 1 and the actual missile configuration. The portion containing the ports was identical, but the missile nose is not a pure hemisphere, and there are four canards about 7 inches behind the ports. The canards provide the missile control and can deflect up to 20 degrees in either direction. Viewed from the nose, the ports are located between the canards, so that if a pair of ports is vertical, the canards are in the "X" configuration. The lift forces on the canards will have some effect on the flow at the nose, although this diminishes rapidly as the missile velocity becomes supersonic. The amount of upwash caused by the canard lift is unknown, as is the effect of the body contour behind the ports. These effects would have to be determined by wind tunnel testing or possibly by use of computational fluid dynamics (CFD) methods. The testing or calculation would have to be done over a range of Mach numbers and for several different canard deflections.

The two angle-of-attack sensors were fitted with four ports, as discussed above. This allowed determination of the pressure difference between the two pairs of ports, but not the missile velocity or Mach number. The missile velocity was obtained from tracking data and the air density from radiosonde data. These were used to get the dynamic pressure and Mach number. The angle-of-attack data could then be obtained from the probe calibration curve as discussed below.

INSTRUMENTATION

The pressure transducers are selected according to what the flight conditions will be. The maximum pressure and the sensitivity (psi/deg) need to be calculated. Figure 2, which comes from Reference 1, gives the Angle-of-Attack sensitivity and is good for all altitudes. Figure 3 was created from Figure 2 and is good for only one altitude. In this case, it was done for 10,000 feet. The vertical axis is converted to show the needed sensor sensitivity in psi/degree. This is done by the following equations

$$C_p = \frac{P - P_\infty}{q}$$

Where,

P_∞= Atmospheric Pressure at the given altitude

and

$$q = \frac{1}{2}\rho v^2$$

The maximum pressure is then calculated from Figure 1 of Reference 4 and using the above equations. Figure 4 shows the results for an altitude of 10,000 feet.

Once the maximum ranges and the needed sensitivity are known, pressure transducers can be chosen. Two different ranges were selected for the BOA test firings. The first was launched at Mach 0.7 at 10,000 ft. The maximum angle of attack for this test was to be 30° at Mach 2. The maximum pressure was predicted to be about 56 psia, as can be seen in Figure 4; so. 100 psia transducers were chosen. The BOA telemetry system has a 10 bits/word PCM data stream. Using 100 psia transducers, the resolution is 0.1 psia/bit. Looking at Figure 3, this should give enough resolution since all the maneuvers are above Mach 1. The second firing was fired off a sled on the ground going Mach 0.3 with an initial angle of attack of 45°. The most interesting part of the data would be at the lower velocities so the pressure transducers chosen were 50 psia. With 50 psia pressure transducers and a 10 bits/word data stream, the resolution would be 0.05 degrees/bit.

The Endevco Series 8530C piezoresisitive transducers were chosen. The performance characteristics of the pressure transducers are excellent. They have less than 0.5% hysteresis, with typical being about 0.1%. The non-linearity and nonrepeatability are below 0.1%. The units are rated for -65 to 250 °F and have built in temperature compensation so they operate within the stated characteristics over the full temperature range. The stagnation temperate encountered by the missile is above 250 °F for only a few seconds at the peak Mach number. Considering that there is a column of air insulating the sensor and it being mounted in a steel nose that would act as a heat sink, it was determined that the sensors themselves would not be subjected to those temperatures. There was no need to go to a more expensive model that is temperature compensated up to 500 °F.

The resonant frequencies of the two different pressure ranges varied but were on the order of 100,000 Hz, which is far above the missile pitch rate and body bending frequencies. There is a Helmholtz resonance in the ports which needs to be analyzed. Reference 3, which is the instruction manual for the 8530 pressure transducers, has an excellent discussion of how to analyze any Helmholtz resonances you may have. It also explains how the temperature compensation is done as well as other things that need to be considered when using pressure transducers. The Helmholtz resonance was analyzed for probe configuration and was found to be above 1000 Hz. Again, it is above the expected missile frequencies. To be sure these resonances did not corrupt the data, anti-aliasing filters were used. Burr-Brown instrumentation amplifier INA102 were used for signal conditioning. What makes them convenient to use is that they have an optional filtering feature that can be employed that will maintain a balance of impedances. Two capacitors are all that is needed to complete the filter.

The sensors measure the angle of attack in two planes, perpendicular to each other. The sensors were numbered consecutively from 1 to 4 so that the two sensor pairs are 1-3 and 2-4. If the missile is commanded to maneuver in the "plus" direction (i.e., two canards are deflected), then both sensor pairs should show equal angles of attack. If a combined-plane maneuver is commanded, then all four canards are deflected, and one set of sensors will show an angle of attack while the other will not. The first test shot performed combined-plane maneuvers in the plane of sensors 2 and 4 and showed almost no angle of attack on sensors 1-3. The second shot was launched at a 45-degree angle of attack in the "X" position with the sensor pair 2-4 vertical. As expected, this pair showed a large angle of attack, while sensor pair 1-3 showed a maximum of about 6 degrees. The next two maneuvers were in the "plus" planes and showed roughly equal readings from the two transducer pairs, as expected. The last maneuver was in the combined plane, and caused a significant angle of attack in only one pair of sensors, the 1-3 pair, as predicted.

RESULTS

The data from the October 1991 flight were reduced using the calibration curve shown in Figure 2 and the recorded missile flight data. The missile velocity and altitude data were obtained from the trajectory data recorded by optical tracking and reported in Reference 4 . The air density and temperature were obtained from the radiosonde data taken at the time of the test and also reported in Reference 4. These data were combined to give the dynamic pressure and missile Mach number. The pressure data from the four pressure transducers were then used to compute the differential pressures between the two pairs of transducers, and the data in Figure 2 were then used to get the angle of attack in the planes of the two transducer pairs. If there had been a large angle of attack on both sensor pairs simultaneously, it would have been necessary to iterate the results using interaction data similar to that contained in Reference 1, but not provided for a

hemispherical probe. However, the missile maneuvers were almost entirely in the plane of sensors 2-4, so this was not necessary.

The results are shown in Figure 5. The data shown are for the plane of sensors 2-4, since the commanded maneuvers were in this plane, and the angles of attack in the plane of sensor 1-3 never exceeded a few degrees. As can be seen in Figure 5, the agreement between the predicted angle of attack and measured angle of attack is fairly good, but with the measured angle of attack less than the predicted angle of attack for the first maneuver and slightly greater for the second maneuver. The timing of the two maneuvers showed good agreement. The reason for the differences between predicted and measured angles of attack in the first maneuver is that the change in pressure for a given change in angle of attack decreases as the angle of attack increases. Figure 113 of Reference 1 shows a substantial drop in probe sensitivity to angle of attack beyond 20 degrees. A calculation was made using pressure data on a hemispherical nose from Reference 5, and it showed a similar trend. This was used to produce a theoretical non-linearity correction, which is shown in Figure 6 for a Mach number of 2.0. This correction was applied to the data where it exceeded 10 degrees angle of attack, which occurred at about Mach 2.0. This gave considerably better agreement with the predicted angle of attack, as is shown in Figure 7.

The data from the May 1992 BOA-1M ground launch were reduced in the same manner. The flight data were obtained from Reference 6. The missile was launched at a 45-degree angle of attack from a rocket sled on the Supersonic Naval Ordnance Research Track (SNORT), with the sled traveling at about Mach 0.3. The angle of attack quickly diminished as the missile accelerated. The missile was launched in the "X" configuration, so the initial angle of attack was in the combined plane, which is in the plane of sensors 2-4. The missile then performed three commanded maneuvers, one in yaw, one in pitch, and one in the combined plane. For this flight, data are shown for both sensor pairs, and the nonlinear calibration was included. This was needed only during the launch at Mach 0.3 to 0.5, and the calibration curve for this is shown in Figure 8. The results for sensor pair 2-4 are shown in Figure 9, which clearly shows the large launch angle of attack and the first two commanded maneuvers. The third maneuver was programmed to be in the sensor 1-3 plane, and caused only a small disturbance in the angle of attack in the 2-4 plane, as expected. Figure 10 shows the results for the sensor pair 1-3. There is some angle of attack during the launch, but it is small compared to the 2-4 plane. The three commanded maneuvers are clearly shown.

CONCLUSIONS

A hemispherical-type angle of attack sensor has been developed for the BOA missile and successfully flown on two flights. The data obtained agree well with the predicted angles of attack and verify that the two missiles maneuvered as planned. If a wind tunnel calibration

was run, the effects due to nose shape and the canards discussed above could be accounted for, and the accuracy further improved. This would also account for any other differences between this sensor design and those used in References 1 and 2.

NOMENCLATURE

CFD	computational fluid dynamics
NOTS	Naval Ordnance Test Station
NWC	Naval Weapons Center
C_p	pressure coefficient $(P - P_\infty)/q$
q	dynamic pressure, lb/ft^2
P	measured pressure, lb/ft^2
P_∞	static pressure in free stream, lb/ft^2
α	angle of attack, degrees

REFERENCES

1. Air Force Armament Laboratory. *Theory, Performance and Design of Flow Direction and Mach Number Probes*, by G. David Huffman. Eglin Air Force Base, Fla., April 1981. (AFATL-TR-81-44, publication UNCLASSIFIED.)

2. A. Pope and J. Harper. *Low Speed Wind Tunnel Testing*. New York, New York, John Wiley & Sons, 1966.

3. Endevco. "Endevco Piezoresistive Pressure Transducers Instruction Manual," San Juan Capistrano, Calif., July 4,1990. (IM8500.)

4. Naval Weapons Center. "BOA-M Air Launch, Test Plan 91A266," by Scott Mcdowell. China Lake, Calif., NWC, October 1991. (Unnumbered document, publication UNCLASSIFIED.)

5. U.S. Naval Ordnance Test Station. *Pressure and Wave Coefficients for Hemispheres, Hemisphere-Cones, and Hemisphere-Ogives*, by Jerome R. Katz. China Lake, Calif., NOTS, March 1958. (NOTS 1947, publication UNCLASSIFIED.)

6. Naval Weapons Center. "BOA-1M, Test Plan 92T103," by Scott Mcdowell. China Lake, Calif., NWC, May 1992. (Unnumbered document, publication UNCLASSIFIED.)

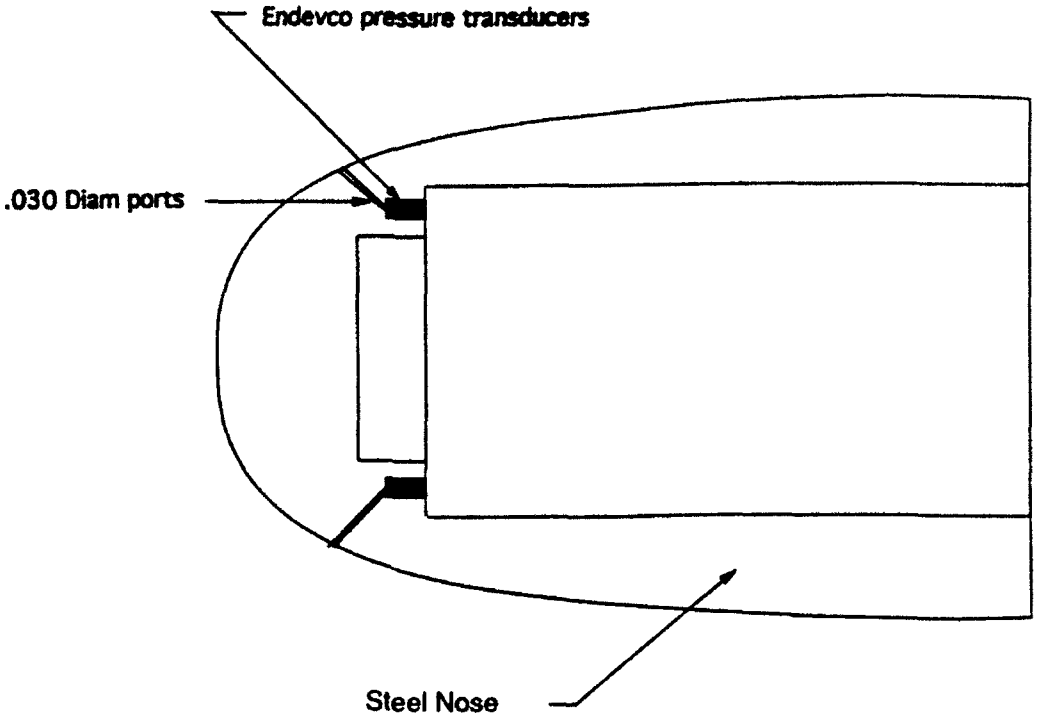

FIGURE 1. Angle-of-Attack Sensor Configuration.

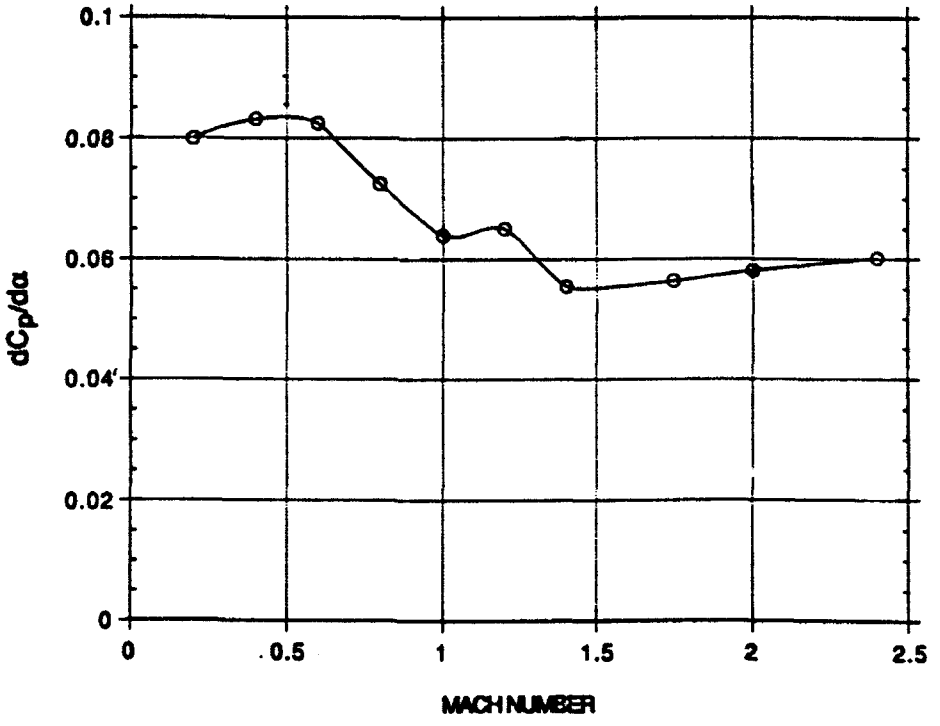

FIGURE 2. Angle-of-Attack Sensor Sensitivity.

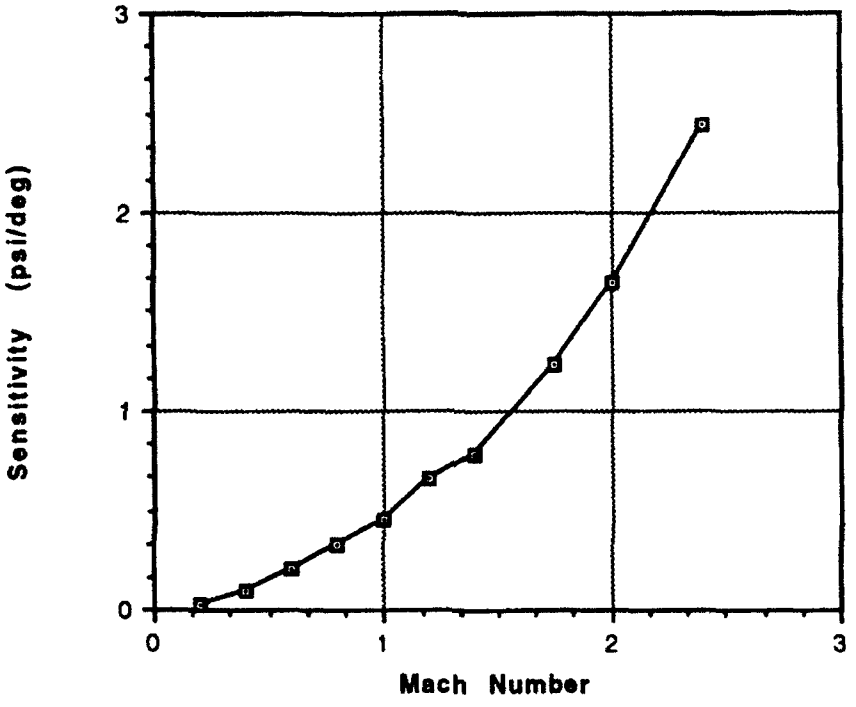

FIGURE 3. Sensitivity for AOA Sensor at 10,000 ft.

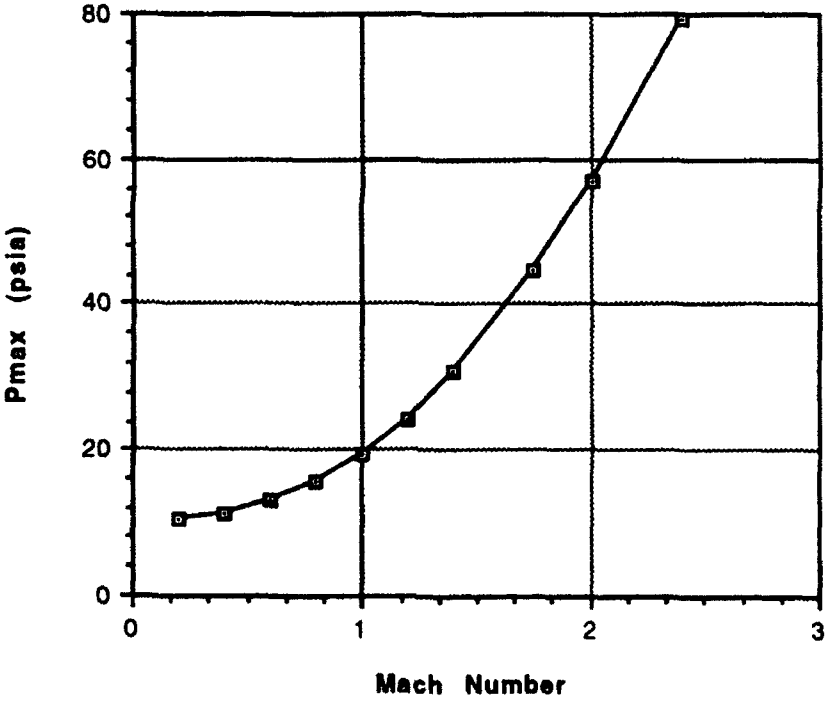

FIGURE 4. Maximum Expected Pressure for AOA Sensor at 10,000 ft.

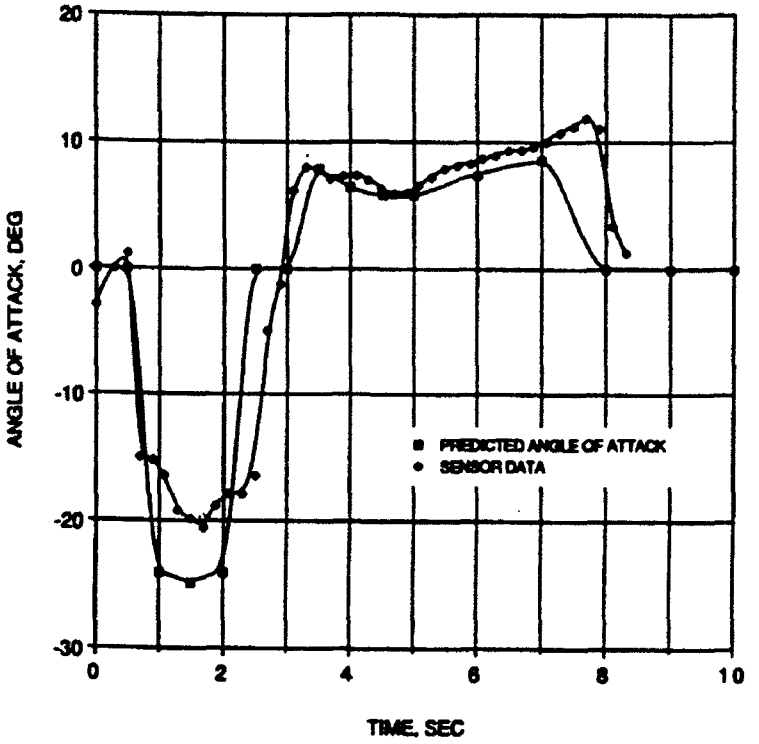

FIGURE 5. Results for BOA-M Flight of Oct. 1991 With Linear Probe Calibration.

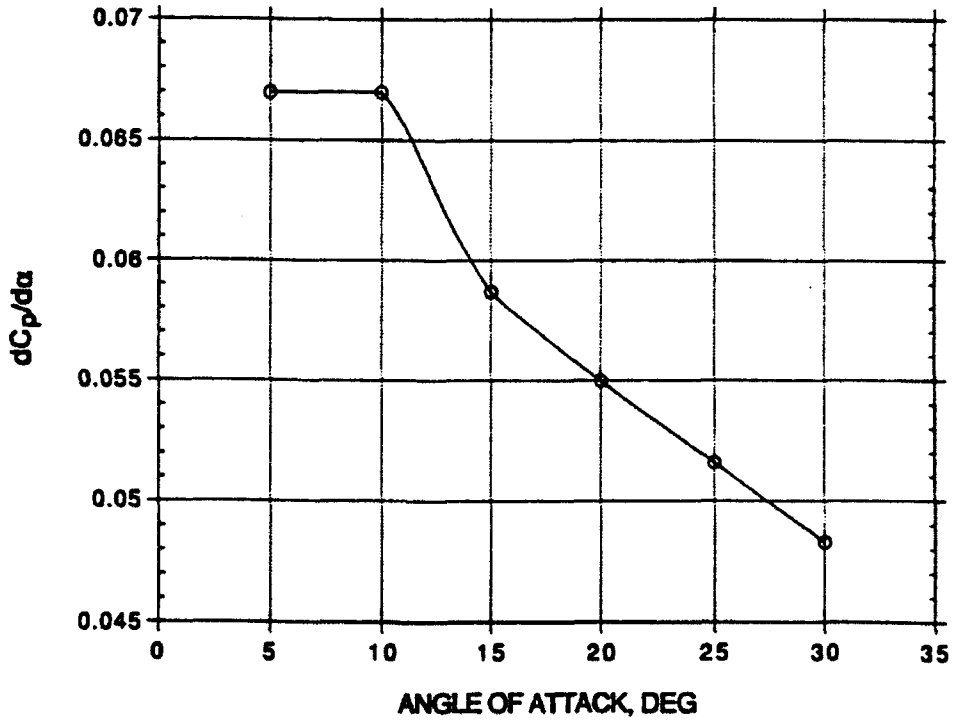

FIGURE 6. Effect of Angle of Attack on Sensor Calibration at M = 2.0.

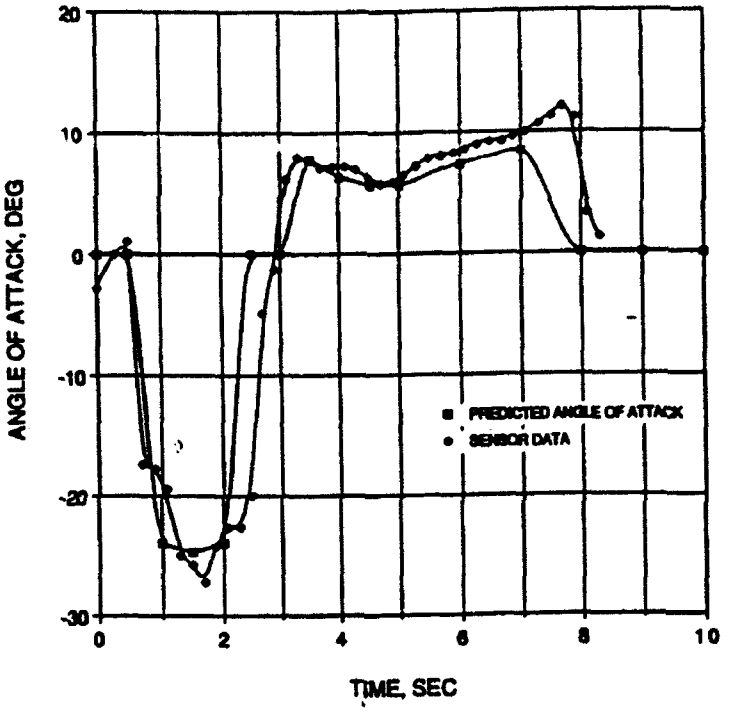

FIGURE 7. Results for BOA-M Flight of Oct. 1991 With Nonlinear Probe Calibration.

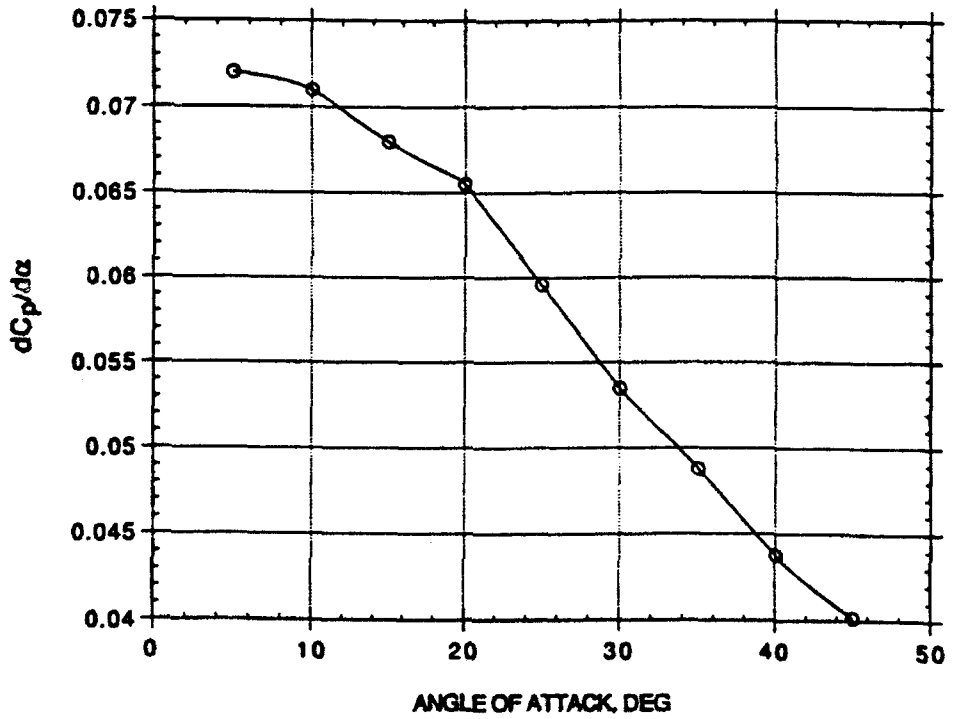

FIGURE 8. Effect of Angle of Attack on Sensor Calibration at M = 0.3 to 0.5.

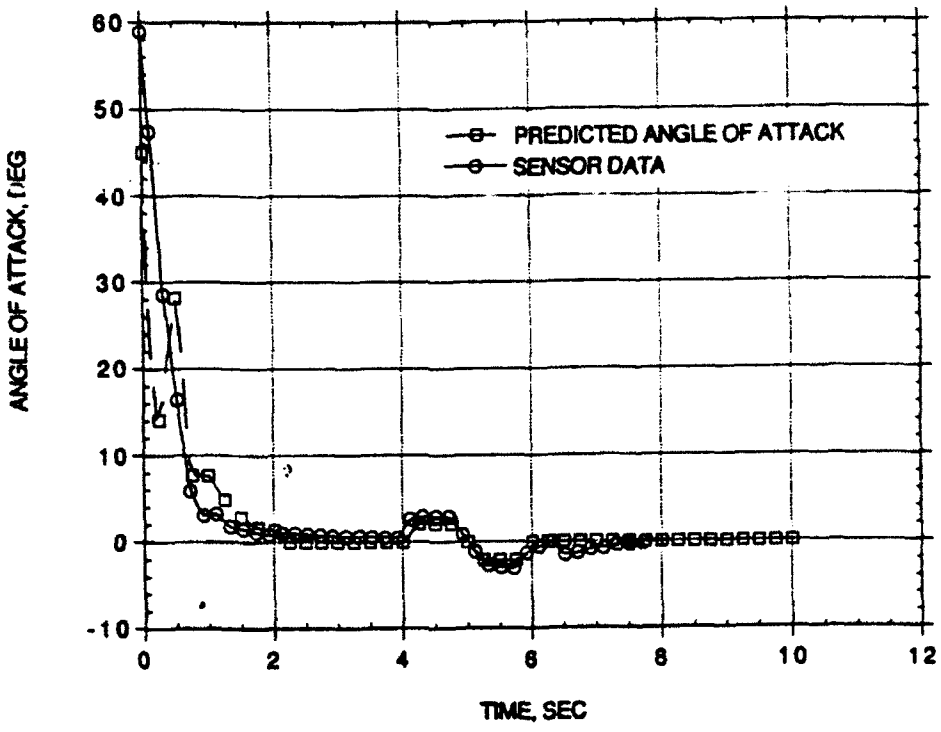

FIGURE 9. Results for BOA-M Flight of May 1992 for Sensor Plane 2-4.

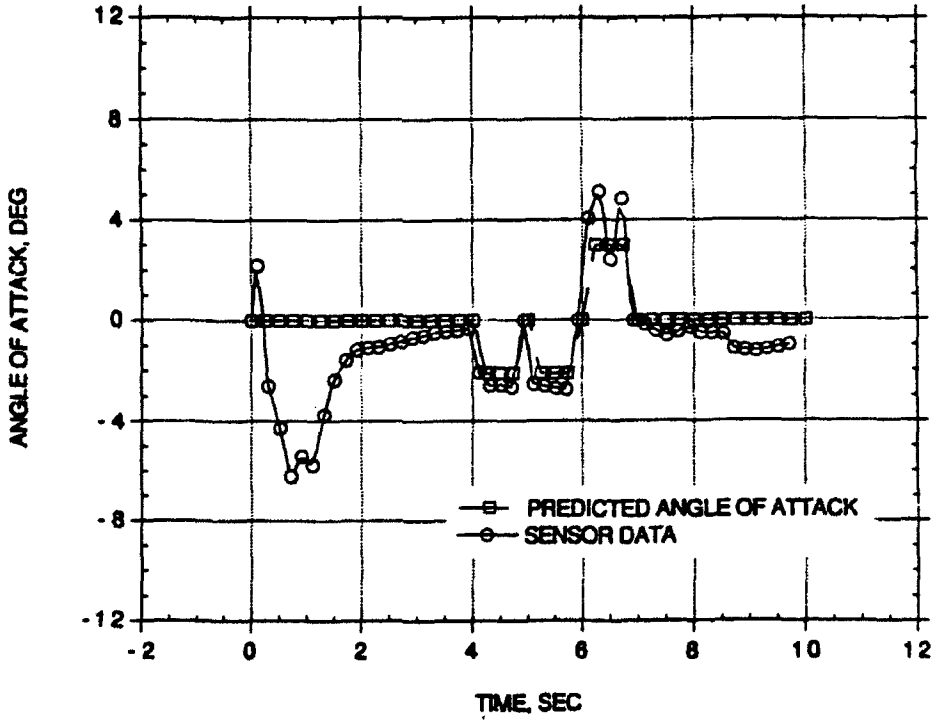

FIGURE 10. Results for BOA-M Flight of May 1992 for Sensor Plane 1-3.

ACCELERATION AND FORCE TRANSDUCER ERRORS

Wayne Tustin
Equipment Reliability Group
340 Calle Lippizana
Santa Barbara, California 93117-9727
805/685-4405

ABSTRACT

This paper is aimed at users of vehicular shock and vibration data who gain that data via telemetry*, alerting them that their shock and vibration transducer errors (as with pressure transducer errors) can be many times greater than their telemetry system errors, often greater than most strain gage and thermocouple errors. The paper calls user attention to sensor "watch out for" items that are seldom mentioned in sensor advertising. Examples include the unwanted sensitivity of sensors to such usage environments as ambient and transient temperature changes, strain in the instrumented structure and lateral motion of the sensor. The paper warns about faulty methods of mounting sensors. Also the effects of exceeding sensor mechanical limits such as upper frequency and of exceeding electrical signal limits. Also triboelectric cable noise when using high-impedance piezoelectric sensors. Also electrical ground loops. Each "watch out for" item is accompanied by one or more recommended practices for minimizing unwanted effects.

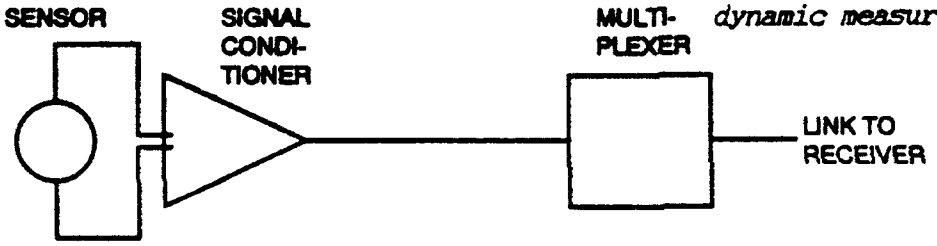

Figure 1 Basic elements needed for dynamic measurements at a distance.

This audience certainly knows that *telemetry means measuring at a distance. Sensor signals pass through "on board" signal conditioning, multiplexing and transmission. The reception/recording station may be a fixed (ground or shore) station, but it can be a chase plane or other vehicle capable of carrying all the receiving, recording (and possibly retransmitting) equipment. The final reception and recording station may provide data processing. Transmission may utilize long wires, telephone (including cellular) links, radio links, infra-red beam optical links, fiber optics, etc.

PARAMETERS TO BE SENSED

Most often, we sense, transmit, receive, store and use motion data in terms of acceleration. (If we later need velocity signals, we obtain them from stored acceleration signals by one electronic integration. We can obtain displacement signals by an additional integration.)[1]

Increasingly, shock and vibration force data[2] is being sought and used. Increasingly, along with accelerometers, we use force sensors. To measure mechanical motion only (ignoring force and mechanical impedance) somewhat resembles measuring electrical voltage only (ignoring current and electrical impedance).

HOW DO ACCELEROMETERS WORK?

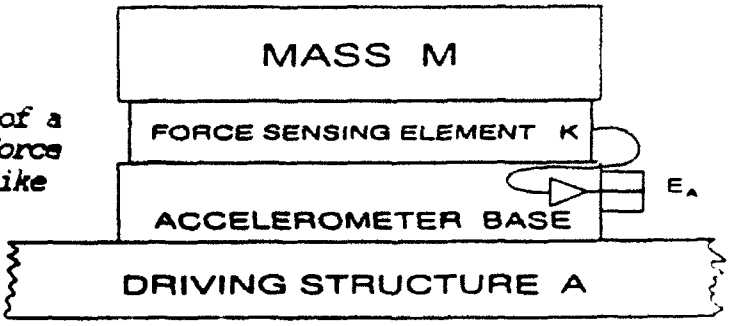

Figure 2 Accelerometers sense motion of a driving structure A by measuring the force applied by a relatively stiff spring-like sensing element K to an inert mass M. Fortunately, F= MA.

Accelerometers deliver a signal E_A proportional to acceleration experienced at the mutual interface between driving structure A and the base. The signal is + when acceleration is directed toward M and K and - when directed away from M and K. Sensitivity is stated in electrical charge or voltage units per unit of acceleration) ms^{-2} or earth gravitational acceleration *g*).

HOW DO FORCE SENSORS WORK?

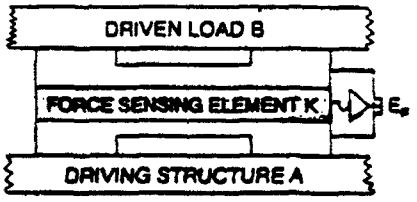

Figure 3 Force from a driving structure A is applied by a relatively stiff spring-like sensing element K to a driven load B, producing a useful electrical signal.

Force sensors (sometimes called load cells) act more directly. They are inserted between some driving structure A (which might be a vehicle or a shaker or shock test machine) and some driven load B. Under some circumstances (*e.g.* at certain frequencies) the roles of A and B may reverse. The sensor delivers a + signal E_F for compressive loads and a - signal for tensile loads. Sensitivity is stated in electrical charge or voltage units per unit of force (newtons or pounds).

SIGNAL CONDITIONING

Figure 1 shows, in addition to the sensor itself, conditioning of the signal to prepare it for multiplexing and transmission. Conditioning is best done close to the sensor, so any high impedance cable is short. See later discussion of cable noise. Increasingly, conditioning employs electronics within the sensor housing (integral electronics); see later section on built-in amplification.

TRANSDUCTION METHODS

This paper focuses on only two of many transduction methods: 1. high electrical impedance crystal or piezoelectric (PE) transduction and 2. relatively low electrical impedance piezoresistive (PR) transduction. In PE units, a self-generating (no power supply needed) crystalline material such as quartz is mechanically loaded in compression or shear or (less commonly) in bending. In PR units, a resistive element is mechanically loaded. PR units always require a power supply (dc or a high-frequency ac "carrier"). Before we had PR units, we used Nichrome wire Wheatstone bridge sensors (very similar to wire strain gages) in which resistance changes produce an electrical signal. In PR units, semiconductor chips (higher sensitivity per unit of strain) substitute for resistance wire.

ACCELEROMETER AND FORCE SENSOR MECHANICAL LIMITS

Select sensors whose axial natural frequency is at least 5 times and whose lowest lateral natural frequency is at least twice the highest frequency present, to avoid sensor resonance[3,4]. Accelerometer resonance involves the inert mass and the transduction element, attached to the base. Force sensor resonance involves the driving and driven structures joined by the transduction element. Never overstress s sensing element beyond its mechanical linearity. And don't allow your sensor to produce such a large signal that "downstream" electronics exceeds <u>its</u> linear behavior. See later section on electrical signal limits.

Avoid violent shock inputs such as dropping onto a concrete floor or striking sensors with any tool. The transduction element may break, and the sensor must be replaced. With "legitimate" inputs less-violent, yet exceeding the linear behavior of the transduction element, sensor sensitivity (electrical output per unit of mechanical input) often changes, yielding faulty data.

On a "first time" measurement, you seldom know what acceleration or force to expect. Even though extra channels and bandwidth are difficult to arrange, consider providing three complete (sensor and signal conditioner) channels, covering a wide dynamic range. <u>One</u> of them will probably be correct.

FORCE SENSORS - AXIAL MASS LOADING

Figure 3 shows that the force sensor elements which connect the driving and driven structures to the high stiffness K force sensing element can themselves be described as two masses. Manufacturers' data sheets[5] give only the unloaded axial natural frequency f_n (resonance) of that combination. For example, Dytran's Model 1051V2 is rated at f_n = 78 kHz, while Kistler's Model 9712A5 is rated at f_n = 70 kHz. The latter has an unstated "sprung mass" of 3 grams. Sensor resonance little (<1%) affects sensor electrical output as long as the user is absolutely certain that the forces acting on his sensor have no frequency components above, respectively, 7.8 and 7 kHz, that is, $0.1 \cdot f_n$.

Users of accelerometers are adequately warned about their sensor's internal resonance effects, between K and M, Figure 1. Accelerometer sensitivity graphs show sensitivity vs. forcing frequency f_f being essentially constant at extremely low forcing frequencies, rising 1% at f_f/f_n = 0.1, 4% at f_f/f_n = 0.2, 12% at f_f/f_n = 0.33, and 33% at f_f/f_n = 0.5 then finally peaking at f_f/f_n = 1. Similar warnings should be given to users of force sensors.

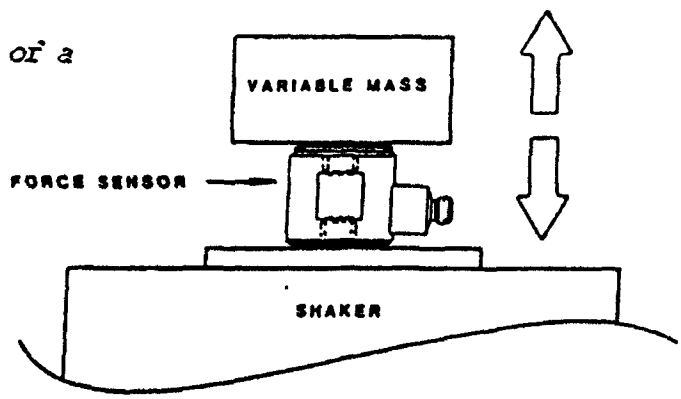

Figure 4 Axial mass inertial loading of a force sensor driven by a shaker.

Zero loading is never encountered. Force sensors are only used to measure force between two structures. How will holding the mass of one structure constant while varying the mass of the other structure affect the force sensor's frequency response? In the absence of published data, an experiment seemed useful.

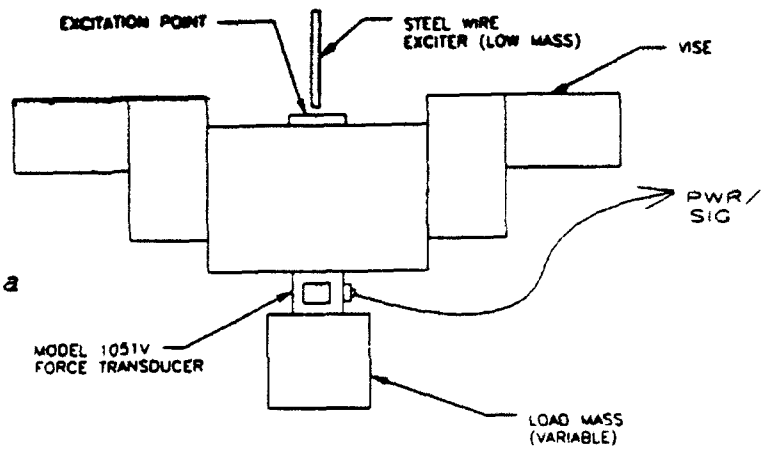

Figure 5 Shock axial excitation of a force sensor.

Hopefully, someone will use a shaker to drive a series of symmetrical mass loads, per Figure 4. Reference 6 describes the physical setup of Figure 5. A Model 1051 axial force sensor drove a series of suspended symmetrical mass loads; experimental results are shown in Table 1. Excitation consisted of single very brief impacts from a short length of steel wire. In lieu of a spectrum analyzer, natural frequency ringing at f_n was estimated by counting cycles on a digital oscilloscope[6].

Table 1

Load, grams	f_n, kHz
0	78
34	48
123	13
301	8.5
510	6.6

What does this experiment indicate to a user of the 1051 force sensor? If he were driving a symmetrical mass load of 510 grams (about one pound), his data from forces above say 3.3 kHz would likely be contaminated by "ringing" at 6.6 kHz. Measurements of shock forces, such as those from explosions, would be irrevocably corrupted beyond what any low pass filtering could rescue.

CALIBRATION

Space does not permit thorough treatment of various calibration methods. Suffice it to say that accelerometers are most often mounted on shakers and vibrated at known acceleration levels and frequencies. Sensitivity is stated as

electrical output/mechanical input in ms^{-2} or g. (1)

Force sensors are calibrated by applying a known vibratory force at known frequencies. Sensitivity is calculated by

electrical output/mechanical input in newtons or pounds. (2)

However, just because a calibration certificate says your sensor has under say ±3% uncertainty does not mean that your end result will have under ±3% uncertainty. Most of this paper is devoted to explaining why your uncertainty might be ±6%, ±16%, ±26% or more.

IGNORE ENVIRONMENTS

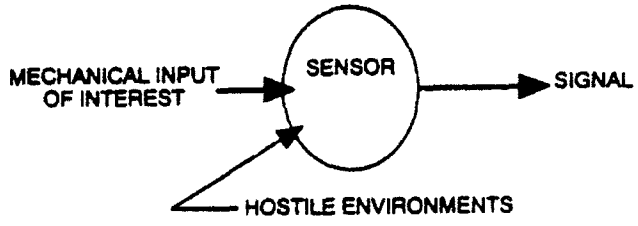

Figure 6 Ideally, only the mechanical input to be measured (motion or force) is converted (transduced) into an electrical signal. Ideally, other "environmental" inputs have zero effect upon the output electrical signal.

Ideally, the electrical signal emanating from the sensor represents only the measurand (acceleration or force) in one direction at the sensor's specific location on the instrumented structure; it does not respond to "environmental" conditions.

Unwanted sensor outputs can be called "noise." Environmental effects on accelerometers are best known, but apply also to force sensors[7]. Multiplexed, transmitted, received, processed, stored and used signals (and resulting data) may be significantly increased or decreased by spurious input. The data user is seldom aware of the error.

Thus we prefer sensors which maximize the "signal/noise" ratio, which give us high sensitivity to axial motion and force, yet low sensitivity to unwanted environmental effects (which are rather arbitrarily grouped below as to mechanical *vs.* electrical).

DELETERIOUS MECHANICAL EFFECTS UPON SENSORS - BASE STRAIN EFFECTS

Bending (or other) strain in the driving (or driven) structure, if it reaches the transduction element within the accelerometer or force sensor, can produce spurious electrical signals in strain-sensitive sensors. A partial solution: between strained structure and sensor, insert a mechanically stiff (could be electrically insulating) washer; this often relieves strain, while transmitting axial forces.

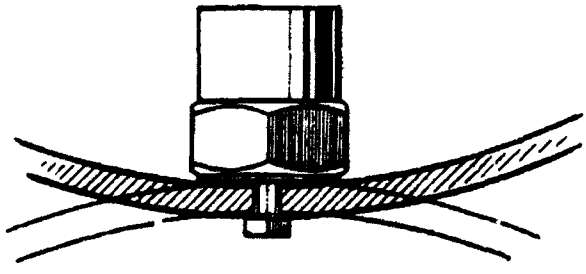

Figure 7 If there is no motion or force normal to the sensor base, there should be no output from the sensor. Strains are usually far more subtle than suggested here, yet can yield faulty data at structural resonant frequencies. Courtesy B&K.

Better, select sensors known (by special checks on a beam undergoing known levels of strain) to be insensitive to strain.

LATERAL MOTION EFFECTS ON ACCELEROMETERS

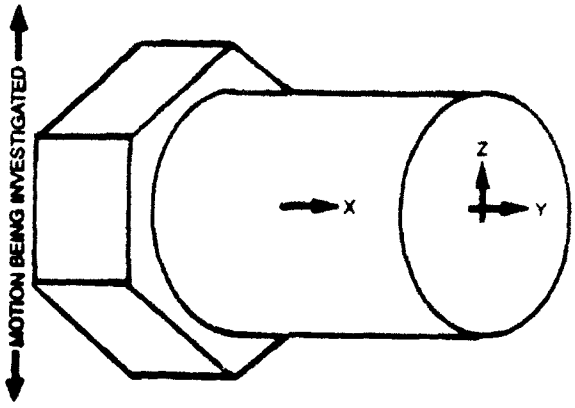

Figure 8 Accelerometer axes are identified for accompanying discussion of lateral sensitivity.

Sensitivity, as was defined in equations (1) and (2), refers to axial loading x of the sensing element. But in the "real world," shock and vibration forces are not uniaxial. What is the electrical response from the transduction element to y and z axis inputs? To torsional inputs? Most literature from most sensor manufacturers implies that their y and z lateral sensitivity is at most a few per cent. Users should ask of their suppliers: at what (usually very low, *e.g.* 12 Hz) single frequency was lateral sensitivity checked? This subject has not been much researched, but some evidence suggests that lateral sensitivity (at say 1,000 Hz) can approach 100%.

Accelerometer sensitivity to lateral motion is difficult to check, because all calibration shakers suffer from some lateral motion[8]. Rather than mount accelerometers directly on a calibration shaker, mount them at the center of a free-free beam. Drive the beam in its first mode, where straight-line motion is available.

ACCELEROMETER MOUNTING METHODS

Sensor manufacturers usually provide threaded mounting studs or threaded mounting holes. When these attachments are used per instructions, good results are usually obtained. Instructions typically call for flatness <700 microinches RMS and roughness <125 microinches RMS. And for mounting torque, *e.g.* 18 lb-in to avoid any chattering between sensor and supporting structure. 1 microinch p-p chatter at say 10,000 Hz can produce 5 equivalent g of "noise." An oil film minimizes chatter.

Suppose that the structure being investigated cannot be drilled and tapped. What then? Consider a temporary mechanical attachment, using adhesive bonding. Indeed, some accelerometers and force sensors are intended only for adhesive mounting. Dental cements, cyanoacrylates and some epoxies work well, even at frequencies to 10 kHz. They also can provide electrical insulation (see GROUND LOOPS, below).

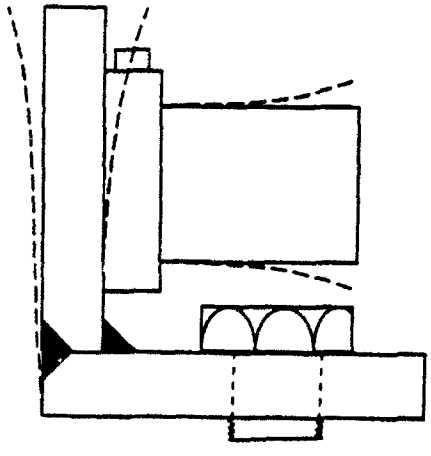

Figure 9 An accelerometer is mounted on a bracket. Bracket flexing (here exaggerated) creates faulty data.

The lowest natural frequency of any needed accelerometer mounting bracket should be at least five times the highest measurement frequency of concern. "Noise" from bracket resonances or looseness can lead to highly erroneous data, "invisible" to users of that data. Bracket design should be approached with the same care as used in vibration test fixture design[9].

NON-SYMMETRICAL LOADING OF FORCE SENSORS

In the "real world," of course, driven loads are never pure masses, but they behave as though they were composed of masses, springs and dampers. Their connection to the force sensor is seldom symmetrical. One could never evaluate all of the possible symmetrical and non-symmetrical loads which force sensors might drive, so Table 1 shows what can happen with symmetrical mass loads. Hopefully, someone will experiment with non-symmetrical, non-pure-mass loads and publish his results.

Another interesting experiment would involve driving through a force sensor into rods of length L terminated with various mass loads.

SHEAR LOADING OF FORCE SENSORS

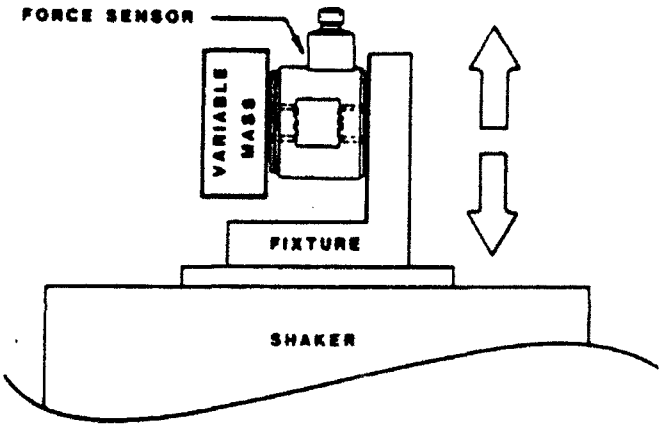

Figure 10 Transverse inertial mass loading of a force sensor.

Figure 10 suggests yet another area of concern: an axial force sensor that is being transversely driven by some structure (here represented by a shaker) and transversely driving some load.. With zero axial force, the sensor's signal should be zero. Inertial forces acting on the mass will laterally load the force sensor.

We trust that in the absence of published data, readers will guard against <u>any</u> lateral excitation in their force measurements. They will, for example, connect a shaker to a load (say for a modal test) only via a length of thin steel wire under tension.

TORSIONAL LOADING OF FORCE SENSORS

Concerned about the absence of published data concerning torsional loading per Figure 11, Kistler experimented with three 12.87 gram loads, having respective outer diameters of 12.7, 18 and 25.4 mm (1 inch), and with heights respectively 12.7 mm (0.5 inch), 6.35 mm and 3.17 mm, such that their moments of inertia were respectively 260, 520 and 1040 gram-mm^2. These were individually mounted atop a 9712A5 force sensor driven by an angular vibration table. Angular acceleration was monitored by two linear accelerometers, and was held constant at 100 rad/second^2 over the frequency range 100-1,000 Hz.

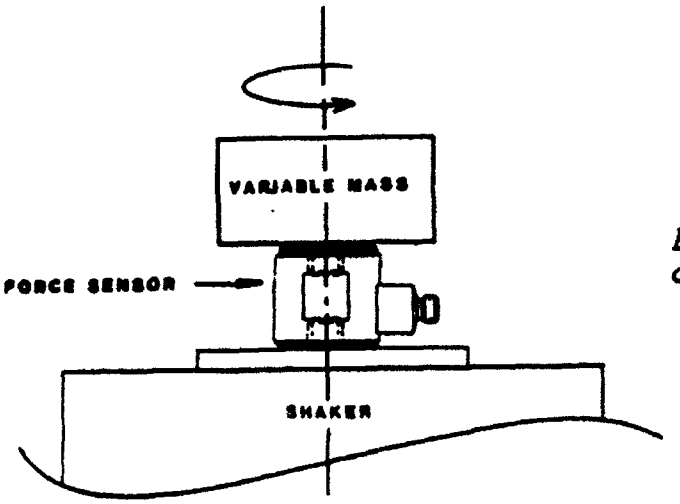

Figure 11 Torsional mass inertial loading of a force sensor atop a torsional shaker.

The Kistler torsional experiment was in one sense a rousing success: nothing happened. The signal produced by the 9712A5 never exceeded the noise level except near a suspected shaker resonance 750 to 800 Hz, even when using a relatively huge 246 gram mass load. It is certainly possible that greater angular accelerations, and over a wider frequency range, would have produced unwanted signals. Further torsional investigations, extending Kistler's work, are hereby encouraged.

SECURING CABLES

Figure 12 Authorities disagree concerning securing cables to instrumented structure.

Watch out for large-displacement, low resonant frequency cable motions, especially troublesome if you use a "strain relief loop" near the sensor. See later discussion of cable noise. To my knowledge, only one experimentor has published his results: I agree with Mangolds[10] who, in 1963, recommended non-restraint. Sensor manufacturers, on the other hand, recommend taping or otherwise securing the cable to the instrumented structure, commencing as close as possible to the sensor's output connector. If they have supporting data, they should publish it.

DELETERIOUS ELECTRICAL EFFECTS - ELECTRICAL SIGNAL LIMITS

In addition to mechanical limits within the sensor, there are upper limits to signals being processed "downstream," before, during or following telemetry transmission. The phenomenon of "clipping" is illustrated, on a sinusoidal signal, in Figure 13. Clipping is far more difficult to see (with an oscilloscope) when viewing other waveforms, especially random vibration and very brief highly oscillatory "real world" shock pulses. Visible or not, clipping always adds additional frequencies to the sensor output signal and (unbeknownst to the user) inserts "noise" into the resulting data.

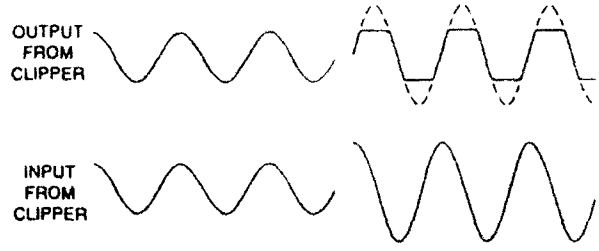

Figure 13 "Clipping" a sine wave creates additional frequencies at multiples (harmonics) of the original frequency.

"Autoranging" is useful for constant or slowly-varying intensities. But definitely not for shock measurements. Better to connect a sensor to say three multiplex channels, adjusted differently such that at least one will be appropriate.

Logarithmic amplification is somethimes employed, with results often expressed in deciBels or dB, rather than in engineering units. Log amplification has the effect of expanding small signals and of compressing large signals. Clipping is less likely. Additional multiplex channels may not be needed.

ELECTRICAL INTERFERENCE - GROUND LOOPS

Electromagnetic and electrostatic fields rarely cause measurement problems. Since high impedance PE sensors and especially their high-impedance cables can pick up unwanted signals from nearby fluorescent lights, from radio, radar, etc. transmitters, such cables should be short. See later discussion of impedance conversion near *vs.* inside the sensor.

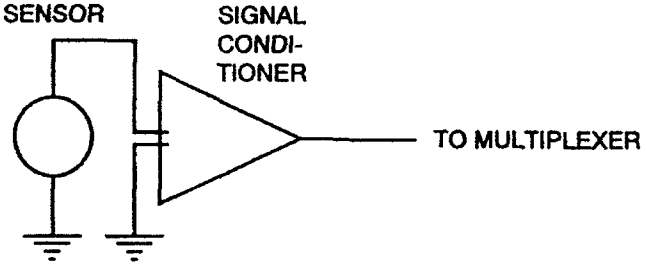

Figure 14 "Ground loops" occur when signal paths are electrically grounded at more than one point, such that a voltage (due to current in other conductors or through the vehicle) exists between these points and finds its way into the signal path.

Electrically conductive "ground loops" (other currents flowing in the vehicle itself) can be exceedingly troublesome. The resulting "noise" signals are injected between the two ground symbols of Figure 14, and are thus added to (may even exceed) the signal being conditioned, multiplexed and transmitted (see Figure 1). These unwanted signals often occur at power line frequency and can exceed the desired signal. Don't use the vehicle frame or chassis as "ground" return on sensor signals, as in Figure 14. Only permit one electrical ground per measurement channel. This can be at the sensor or at the sensor's signal conditioner. If the latter is grounded, you may need to insert a mechanically stiff but electrically insulating stud or washer to mechanically drive each sensor.

Varney[11] has commented upon unsuspected grounding of sensors that were thought to be insulated. Moisture condensed on his sensors, was contaminated, and bridged his insulation.

TRIBOELECTRIC CABLE NOISE (PE)

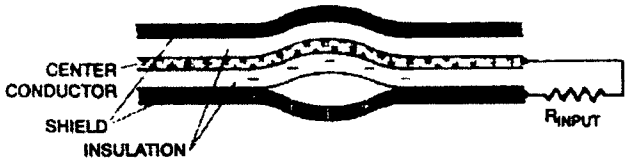

Figure 15 Cross section of coaxial cable which connects high impedance PE accelerometer or force sensor to impedance conversion unit.

Consider Figure 15. Teflon insulation is extruded onto stranded copper wire. Then additional soft copper (functions as both electrical shield and return conductor) is braided onto the Teflon. Finally, plastic (the outer jacket - no electrical function) is extruded onto the copper braid. Miles of cable are fabricated, then cut into short lengths. Connectors are attached. Individual cables are electrically checked, packaged, sold and used. After much use, small areas of Teflon intermittently separate, usually from the outer braid, and rejoin, when the cable is flexed. "Triboelectric noise," often larger than the desired signal, appears at the signal conditioner and on the telemetered signal.

In the laboratory, impedance conversion can be located inside readout meters, spectrum analyzers, etc. On a vehicle, this could be done on a few channels inside the multiplexer. To minimize electrical interference, keep high impedance cables short. Place the impedance converter within a few inches of the sensor; then use a longer, low impedance cable to the telemetry transmitter.

BUILT-IN AMPLIFICATION

Figure 16 Low output impedance of solid-state circuitry inside sensor housing lessens sensitivity to unwanted signals and permits use of twisted-pair leads. Courtesy Kistler.

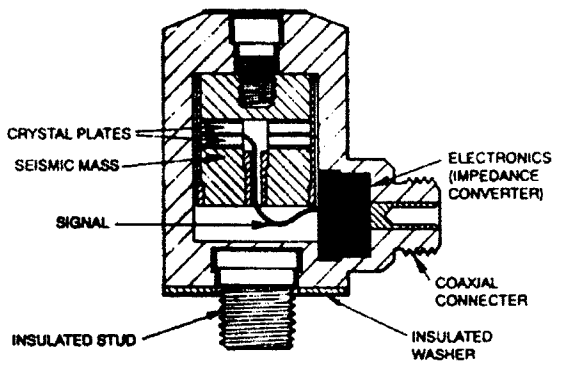

Perhaps the best solution to PE cable noise (from severe mechanical vibration and/or high acoustic pressures), as well as to electrical interference, is to place signal conditioning, impedance reduction to perhaps 100 ohms (and perhaps some amplification and/or digitizing) inside the sensor housing. Then you can normally use inexpensive "twisted pair" wire, less expensive and more rugged than coaxial cable, to the multiplexer.

AMBIENT TEMPERATURE

When an accelerometer or force sensor is used at other than 70°F, its sensitivity will change a few per cent. Manufacturers publish general data on each class of sensor. At considerable expense, you can have individual sensors checked at various ambient temperatures.

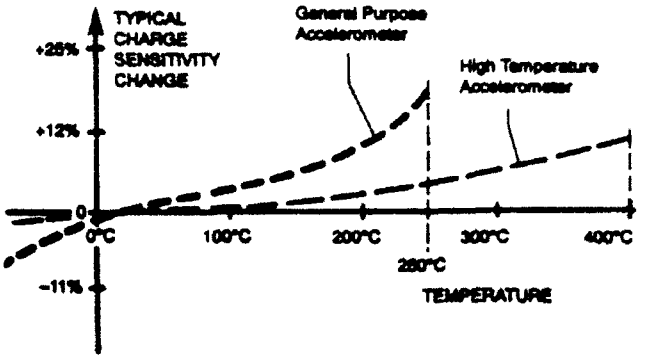

Figure 17 Ambient temperature affects a sensor's sensitivity. Courtesy B&K.

TEMPERATURE TRANSIENTS

Brief exposure to thermal inputs seldom presents problems because the temperature of the transduction element (crystal or resistance bridge) does not have time to change, especially if you thermally protect (insulate) your sensors. Thus there is little or no unwanted electrical signal.

However, infrared radiation (such as pulsed sunlight) on one side of the sensor case can distort the case. On some sensors, this can cause the sensor to produce a large low-frequency electrical surge, "noise." Assuming you only need data above say 5 Hz, consider the use of a 2 Hz high-pass electrical filter.

SUMMARY

This paper alerts those who obtain shock and vibration data via telemetry to transducer errors which can be many times greater than telemetry system errors. The paper points out some sensor "watch out for" items that are seldom mentioned in sensor advertising. Each "watch out for" item is accompanied by one or more recommended practices for minimizing unwanted effects.

The force sensor experiments unfortunately barely scratched the surface. Hopefully, some reader will be interested in conducting further experiments, perhaps for the laboratory portion of an advanced mechanical engineering course.

REFERENCES

1. W. Tustin, "Displacement vs Velocity vs Acceleration vs Jerk," *1992 Proceedings*, Institute of Environmental Sciences

2. W. Tustin, "Control Response rather than Input," *1992 Proceedings*, Institute of Environmental Sciences

3. *Random Vibration in Perspective*, 1984, 200 pp, by W. Tustin and R. Mercado.

4. MIL-HDBK-XXX PROPOSED MILITARY HANDBOOK *Guidelines for Dynamic Data Acquisition and Analysis*, final draft dated 12 March 1993. Contact H. Himelblau, Jet Propulsion Laboratory, m.s.301-456, Pasadena, CA 91109-8099, telephone 818/354-8564.

5. Dytran Catalog and Instrumentation Handbook No. 1192, revised November 1992.

6. Wayne Tustin, David A. Change and John M. Kubler, "Pitfalls in Dynamic Force Measurements" *1993 Proceedings*, Institute of Environmental Sciences, Las Vegas, NV.

7. Tustin, Wayne, "Pitfalls in Shock and Vibration Measurement," *Proceedings, 62nd Shock & Vibration Symposium*, Las Cruces, NM, October 1992.

8. Kinzel, Robert L. and Tustin, Wayne, "Accelerometer Transverse Resonance Effects," *1989 SAE Aerospace Technology Conference*, Anaheim, CA, SAE paper #892380.

9. *Vibration and Shock Test Fixture Design*, 1971, B. Klee, D. Kimball & W. Tustin, , Tustin Technical Institute, Santa Barbara, CA.

10. B. Mangolds, Shock and Vibration Bulletin 33, part 3, 1963

11. B. Varney, Unisys, Salt Lake City, unpublished communication, 1992.

A MINIATURE, DIGITAL ACCELEROMETER FOR REAL-TIME MEASUREMENTS

JOHN C. COLE AND DOUG F. BRAUN
SILICON DESIGNS, INC.
1445 NW MALL STREET
ISSAQUAH, WASHINGTON 98027
PHONE: 206-391-8329

1.0 ABSTRACT

Acceleration measurement is important in a wide range of military, industrial and commercial applications.

Accelerometers for general instrumentation applications are used a few at a time in each unique application. They usually have an analog output that is amplified, filtered, digitized and stored for subsequent, off-line signal processing by a general-purpose computer. Many accelerometers may be multiplexed together for processing by a single general purpose computer. Since the accelerometers are often reused in other instrumentation applications, their cost is not a major driver in their selection.

In contrast, other accelerometer applications require accelerometers that are used for a single application, often permanently mounted on a printed circuit board. The accelerometer and its related subsystem performs a single, dedicated function, usually connected to one microprocessor or application-specific integrated circuit (ASIC) chip in order to make a decision in real-time based on recent acceleration history. Cost of the entire subsystem, its size and power consumption are often the major factors in the design of this class of subsystem. It is this class of subsystem that this paper addresses.

Silicon Designs has developed and is producing the first digital, surface micromachined accelerometer, the Model 1000, for OEM subsystems designed to be produced in large quantities at a low-cost. [1,2] It has a low power consumption (1.0 mA at 5 volts DC) and operates over a wide temperature range (-55 to +125 deg C). The accelerometer is currently available in packages similar to military integrated circuits, leadless chip carriers or J-leaded packages.

In this paper we describe these accelerometers and how they can be used to build low-cost application-specific subsystems. We will show how the accelerometer can be connected to two types of signal processing elements and how the digital output can be used to produce cost-effective acceleration subsystems.

2.0 DIGITAL ACCELEROMETER

The digital accelerometer consists of two dice assembled in a single integrated circuit package: a sense element die and an integrated electronics chip. The sense element die contains two micromachined, capacitive sense elements that respond to acceleration by changing their capacitances. The integrated electronics chip measures the change in capacitance and converts it into a digital pulse output stream.

2.1 Sense Element Structure

Figure 1 shows the basic features of the sense element. It consists of a flat plate of nickel supported above the substrate surface by two torsion bars attached to a central pedestal. The structure is asymmetrically shaped so that one side is heavier than the other, resulting in a center of mass that is offset

from the axis of the torsion bars. When an acceleration produces a moment around the torsion bar axis, the plate is free to rotate around the torsion bar axis, constrained only by the torsional spring constant of the bar.

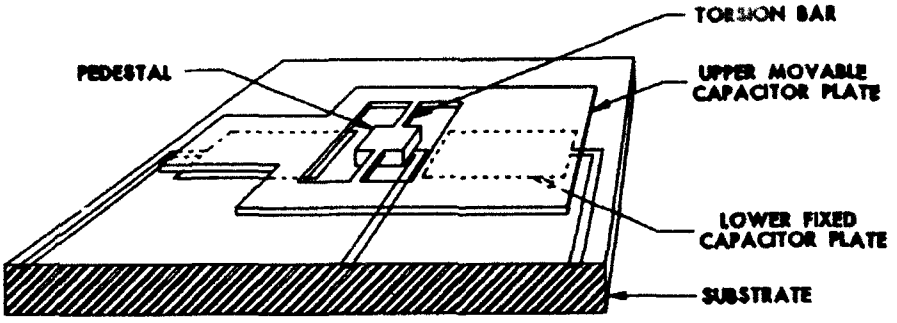

FIGURE 1: SENSE ELEMENT CONCEPT

Symmetrically located on each side of the torsion bar axis on the substrate surface underneath the sense element are two capacitor plates. The sense element structure and the two capacitor plates on the substrate form two air-gap variable capacitors with a common connection. As the sense element rotates around the torsion bar axis, the average distance between the sense element and one surface plate decreases, increasing the capacitance at this end, while the distance to the other plate increases, decreasing this capacitance.

Sense elements are approximately 1000 by 600 microns in size and about 5 microns thick. A spacing of 5 microns results in a capacitance from the sense element to each plate of about 0.15 pF. The sensitivity of the sense elements, the ratio of deflection to acceleration, is determined by the mass of the sense element, distance from the center of mass to the torsion bar axis, and the torsion bar stiffness.

2.2 Integrated Electronics

Small capacitive sense elements require adjacent electronics to measure accurately the small acceleration-caused changes in capacitance in the presence of much larger stray capacitances.

Figure 2 shows a functional block diagram of our basic accelerometer electronics circuit, which converts small sense element capacitance changes into a useable output. Two sense elements form a fully active capacitive bridge. A single IC contains all the transistors and most of the passive components needed to measure the sense element capacitance changes. Fabricated in 3-micron CMOS, it performs the functions of a modulator, demodulator, sense amplifier, sigma-delta A/D converter and clock generator. Thin film resistors on an off-chip substrate provide voltages and currents that are used to calibrate the accelerometer, compensating for bias and scale factor fabrication tolerances of the sense elements. The output pulse frequency is determined by an external digital clock input or optionally by an internal clock generator.

A digital output from the electronics was selected to allow direct connection to an inexpensive microprocessor without requiring a separate analog-to-digital converter, thus minimizing the system cost of applying the accelerometer in a smart sensor application. The digital output also makes it convenient to implement a dedicated signal processing function using digital standard cell or gate array layouts. When going off-chip, it also provides substantial insensitivity to electromagnetic interference (EMI) compared with low-level analog signals.

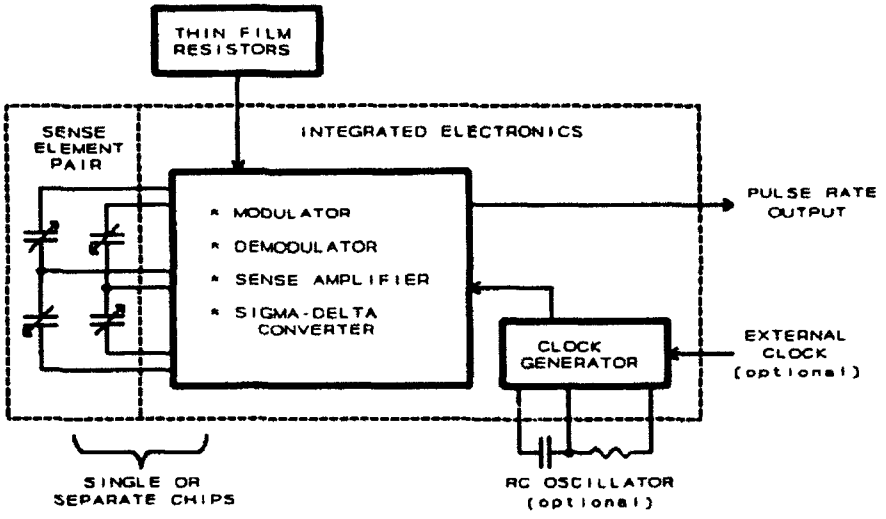

FIGURE 2: FUNCTIONAL BLOCK DIAGRAM OF INTEGRATED ELECTRONICS

2.3 Packaging

Figure 3 shows an exploded view of an accelerometer with a separate sense element and electronic chip mounted in a standard 20-pin lead-less chip carrier LCC. It contains a thin-film substrate, on which is attached the chip containing two sense elements and the integrated electronics IC described earlier. The thin-film substrate is about 6.3 mm square, and the entire package is about 8.9 mm square by 2.8 mm high.

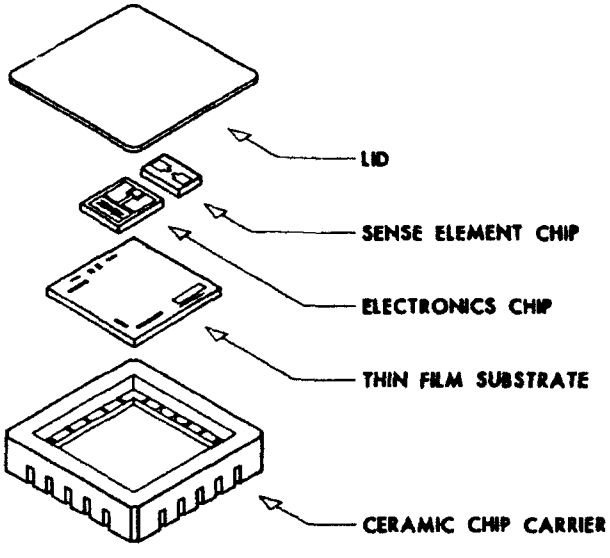

FIGURE 3: EXPLODED VIEW OF ACCELEROMETER

2.4 Digital Output

One pulse stream output of the accelerometer is referred to as the count output or CNT. It consists of a sequence of positive going pulses that are synchronized to the clock input. During each clock period the CNT will either

follow the clock signal or remain at the zero state. The pulse density of CNT, the number of pulses on the CNT output over a period of time divided by the number of clock cycles over that same period of time, is a measure of the average acceleration over that period of time. Figure 4 shows the relationship of the pulse density of the CNT output vs applied acceleration.

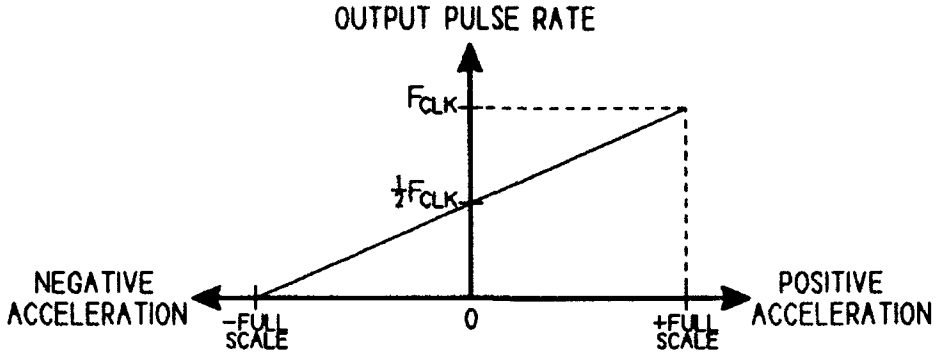

FIGURE 4: OUTPUT PULSE DENSITY OF CNT VS ACCELERATION

Several outputs are available from the accelerometer, examples of which are shown in Figure 5. As described before, the CNT output is a pulse synchronized to the clock. The direction or DIR output is a non-return-to-zero signal that is a logic one during the clock period when the CNT output is a pulse, and it is a logic zero during the clock period when the CNT output stays at a logic zero. The $\overline{DIR}$ output is the complement of the DIR signal.

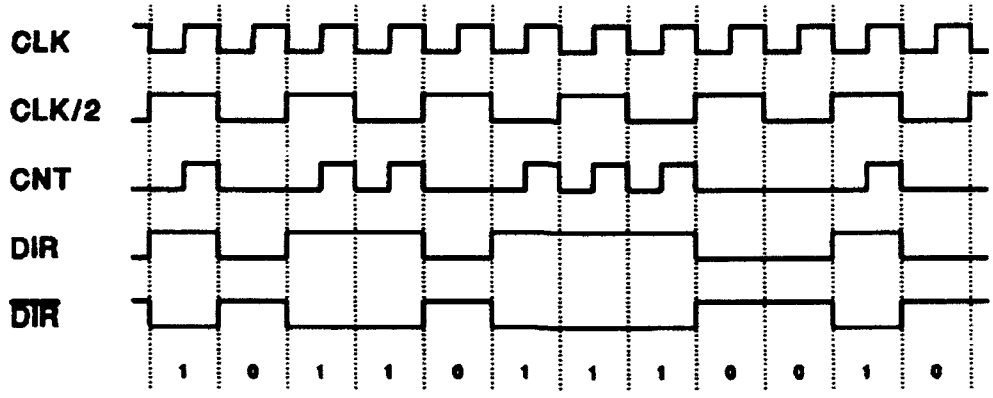

FIGURE 5: EXAMPLE WAVEFORMS OF ACCELEROMETER OUTPUTS

Figure 6 shows the DIR and CNT outputs for various fractions of full-scale acceleration.

3.0 LOW-COST ACCELEROMETER SUBSYSTEMS

Digital counters, much simpler than A/D converters, are the best way to measure the pulse rate or pulse density of a pulse train.

One approach is to connect the CNT output of the accelerometer into the count input of a unidirectional counter which records the number of positive or negative transitions from an initial zero value. Since we are using a unidirectional counter, we can only record a positive number of events. During

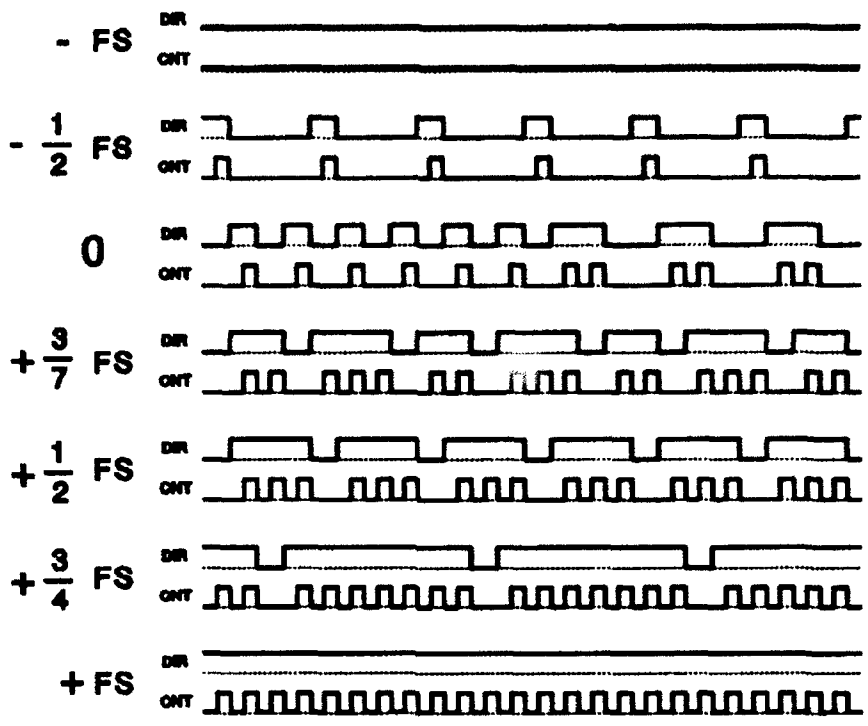

FIGURE 6: ACCELEROMETER OUTPUTS FOR VARIOUS ACCELERATIONS

a time interval, the counter counts the number of pulses output from the accelerometer. The change in the counter value corresponds to the average acceleration over that time interval plus an offset. Since at zero acceleration, the accelerometer puts out half the clock frequency, the offset is equal to half the clock frequency times the length of the time interval.

In the second approach we can connect the DIR accelerometer output to the up/$\overline{\text{down}}$ input of an up/down or bidirectional counter, which can count up and down from an initial zero value. The clock of the up/down counter is connected to same clock as the accelerometer or its complement, depending on the phasing required. This has the advantage over the first approach that the counter reflects the signed value of the average acceleration over the time interval between readings and does not have an offset.

Because the accelerometer puts out a pulse train proportional to acceleration, when the pulse train drives a counter which counts the number of pulses, the counter acts as an integrator. The value stored in the counter is the integral of the acceleration or change in velocity, delta velocity, since the counter was reset. If the counter is read and reset periodically, then the sequence of counter values correspond to the average acceleration over the time period. If the counter is reset when the acceleration is zero, then the counter value each time it is read (without being reset) is proportional to the current velocity.

A minimum accelerometer subsystem is comprised of an accelerometer plus a signal processing element that performs a dedicated function. We will look at two types of signal processing elements:

- a single chip microprocessor or microcomputer, and
- an application-specific integrated circuit (ASIC).

3.1 Embedded Processor-Based Subsystems

The digital accelerometer is well suited for use with processors that include an on-chip counter. Microprocessors having such a counter include the Intel 8051 and similar units from Siemens, Signetics, National, Motorola and Texas Instruments. With these microprocessors no additional interfacing circuitry is required.

Another way of connecting the accelerometer to a microprocessor is through an ASIC which attaches to its data bus. Subsystem designs often use such an ASIC that collects all the interface functions unique to the application into one chip. One or more counters would be only a small part of such a chip in today's technology. This approach has several advantages:

- any microprocessor can be selected,
- the chip can be designed to minimize sampling time jitter, and
- the chip can be designed to eliminate potential software timing problems.

Figure 7 shows a double-buffered design concept for the section of an ASIC needed to interface to a digital accelerometer. The accelerometer drives a counter that can be either unidirectional or bidirectional. The chip also contains a second counter that counts the number of clock cycles for each measurement period. When the second counter reaches the number of counts corresponding to the measurement period, it generates a signal that so indicates and begins counting the next measurement period. The signal from the second counter generates an interrupt to the processor and loads the value of the first counter into a register that can be read by the processor during the interrupt service procedure. This approach requires the processor to service the interrupt only fast enough to avoid overlapping interrupts.

The processor software that reads the accelerometer can be relatively simple. At initialization it needs to set up the measurement period in the second counter, clear the first counter and continue other processing until the interrupt occurs. If the subsystem is at a known acceleration value, the software can measure the accelerometer output after the first measurement period and determine the accelerometer bias at the operating temperature.

When each interrupt occurs, the interrupt routine must read the counter assigned to the accelerometer. Depending on the accuracy requirements of the application, the software can correct for errors in bias, scale factor, and nonlinearity.

3.2 ASIC-Based Subsystems

The advantages of an accelerometer with a digital output show up well when a dedicated ASIC is used to implement the processing algorithms. With analog accelerometers the ASIC would need to have an A/D converter or use analog circuits for processing. When the accelerometer output is already in digital form, special purpose processing can be done with low-cost gate array or standard cell circuits from many digital IC vendors. Use of such chips and available CAD software can cut many months off the development time compared with analog or combined analog/digital ASICs.

Figure 8 shows the generic block diagram of an accelerometer subsystem using an ASIC circuit. The ASIC circuits we show in the following sections make maximum use of counters and a little known but highly useful digital circuit, the binary rate multiplier (BRM), for performing arithmetic on digital pulse data.

A BRM takes a parallel word, which represents a binary fraction, and a clock signal as inputs and produces a digital pulse stream out whose pulse density is equal to the clock frequency multiplied by the binary fraction.

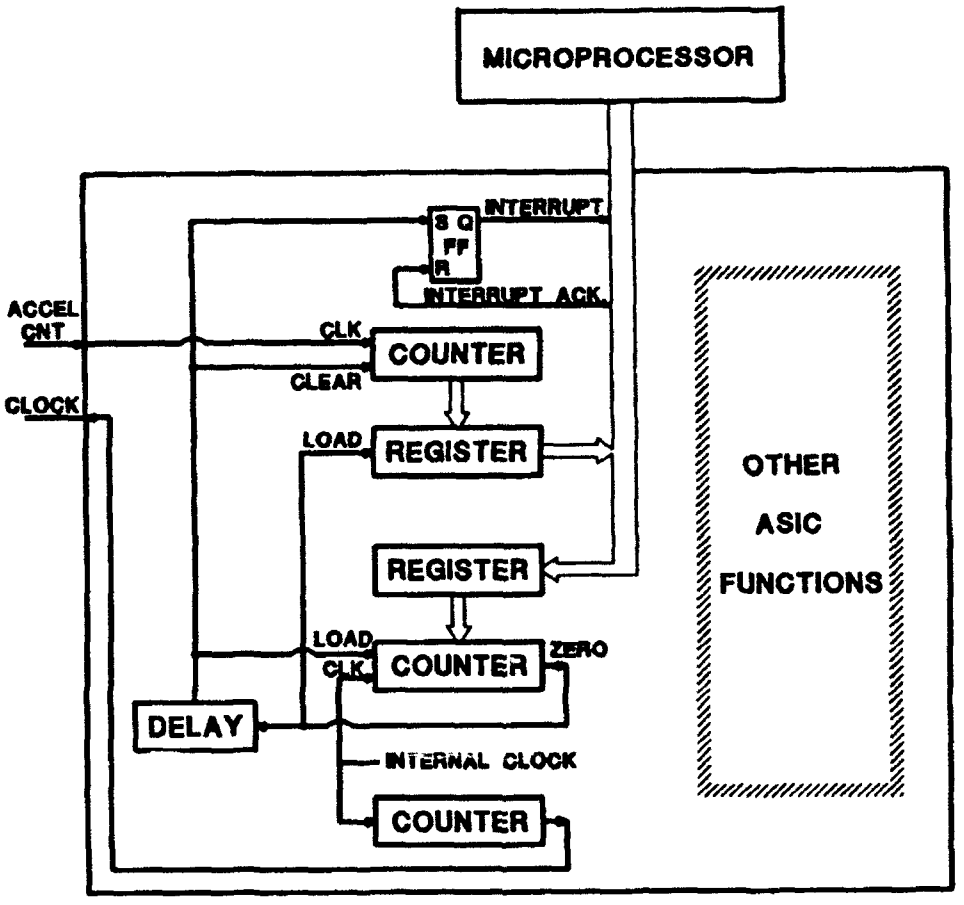

FIGURE 7: DIGITAL ASIC INTERFACE LOGIC TO A MICROPROCESSOR

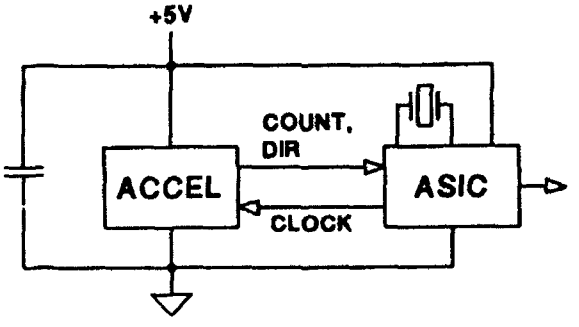

FIGURE 8: BLOCK DIAGRAM OF ASIC SUBSYSTEM

Figure 9 shows by example how a BRM works. The BRM contains a binary counter, a 3-bit counter in this example. The counter is driven by a clock input. The first three columns represent the counter value as it is driven through its eight states counting from 0 to 7.

The next three columns show the clock cycles where the corresponding bit makes a 0 to 1 transition. Note that the least significant bit makes four

COUNTER VALUES			ZERO TO ONE TRANSITION			OUTPUT FOR 5/8 VALUE
0	0	0	0	0	0	0
0	0	1	0	0	1	1
0	1	0	0	1	0	0
0	1	1	0	0	1	1
1	0	0	1	0	0	1
1	0	1	0	0	1	1
1	1	0	0	1	0	0
1	1	1	0	0	1	1

FIGURE 9: EXAMPLE OF A 3-BIT BINARY RATE MULTIPLIER OPERATION

transitions from 0 to 1, the second bit two transitions and the most significant bit one transition; also note that no two bits have 0 to 1 transitions on the same clock cycle. If we were to generate a pulse train for each counter bit, where a pulse occurs when the counter bit makes a 0-to-1 transition, then we have three pulse trains with pulse densities equal to 1/2, 1/4 and 1/8th the clock frequency. If we wanted a pulse train with a density equal to 5/8 of the clock frequency (where 5/8 is the binary fraction 0.101), then we can get such a pulse train by taking the logical OR of those pulse trains where the binary fraction bit is a 1 (the first and third columns for a binary 5 = 101). The last column shows the OR of the first and third columns.

A discrete part that performs this function is the CD4089, made by Harris, National and SGS-Thomson. The 7497 is also a BRM.

3.2.1 Full-Scale Threshold Accelerometer

In looking back at Figure 4, we see that the pulse density of the CNT output increases as the acceleration increases. As we apply an acceleration closer to the full-scale value, we get more and more pulses in a row with only a few intervening periods without pulses. When we are at full-scale acceleration, a pulse occurs during every clock period. Looking at DIR, when we are at full-scale, we see that DIR is always high.

We can build a simple threshold accelerometer with logic that looks for an unbroken string of ones on the DIR output. When more than a defined number of ones in a row occurs, we know that the acceleration is near or above the accelerometer full-scale value. By adjusting the full-scale value of the accelerometer during calibration, we can change the threshold acceleration value to any value within the calibration range. With the present Model 1000 accelerometers, this threshold value can be any value from 5 to 200g. We expect to widen this range with future accelerometer versions.

Figure 10 shows a logic circuit that detects when 15 or more ones are detected on the DIR signal without an intervening zero. When this occurs, it generates a logic one on a threshold output that indicates that the threshold has been reached. The output returns to a logic zero when a zero is detected on the DIR signal. This output can be used to set a latch that generates a signal to a processor that the acceleration has exceeded a threshold until it is cleared by the processor.

The advantages of this approach over using an analog accelerometer together with an analog comparator are its low cost, size and power requirement, since it uses only a fraction of a digital ASIC chip, and its use of digital logic that is not temperature sensitive to set the threshold value. The digital logic could also be integrated into the accelerometer itself, resulting in a threshold

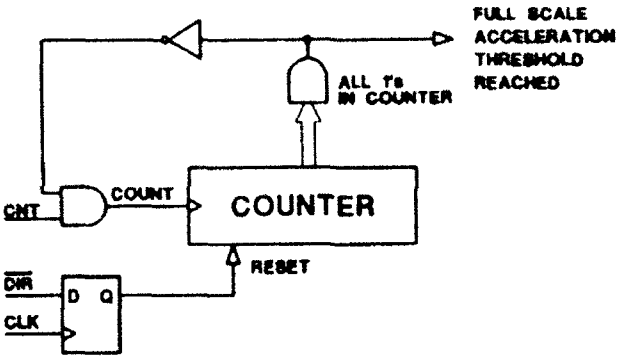

FIGURE 10: BLOCK DIAGRAM OF THRESHOLD DETECTION LOGIC

accelerometer about the same size as the Model 1000.

3.2.2 Multiple Threshold Accelerometer

Suppose that we want to divide the acceleration range up into N non-overlapping regions with N digital outputs that indicate when the acceleration is in the corresponding range. Using analog techniques, this would require (N-1) comparators and some digital logic to combine the comparator outputs.

Figure 11 shows a simple way of performing this function with the digital accelerometer and a small amount of digital logic. Over some time interval we need to count the number of clock periods that have pulses on the CNT output or for which DIR is a logic one. At the end of the time interval, we transfer the value in the counter to a register and zero the counter for the next time period. By decoding several high order bits in the register, we can determine between what two values is the count stored in the register. If we want to combine some ranges, we can do this by combining their respective outputs with an OR gate.

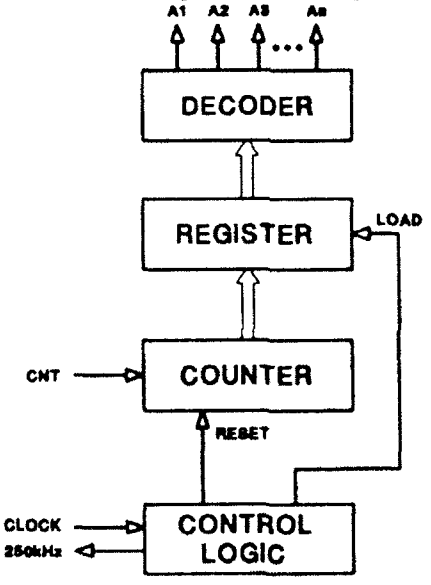

FIGURE 11: BLOCK DIAGRAM OF MULTIPLE THRESHOLD ACCELEROMETER

3.2.3 Distance Measurement Subsystem

A major use of accelerometers in the military is to determine the velocity and/or position of a vehicle by numerically integrating the acceleration. Likewise, by integrating the velocity we can determine the distance travelled.

This function can be done easily in software by a microprocessor; however, it is also possible to perform it in an ASIC using counters and a BRM.

Suppose we have a vehicle that is initially at rest. Suppose we want to know the velocity and distance that a vehicle has travelled in real time as it accelerates along its longitudinal axis, and we want to generate an output when a specified distance has been reached. A digital logic circuit which performs this function is shown in Figure 12.

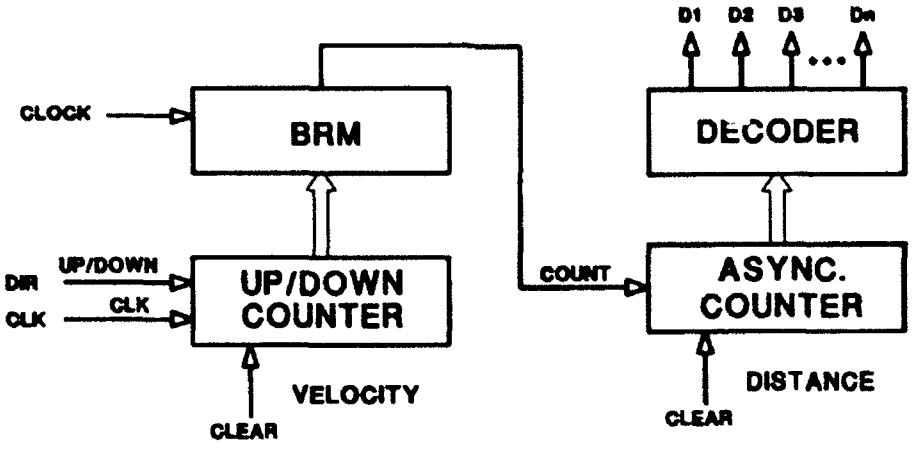

FIGURE 12: BLOCK DIAGRAM OF DISTANCE MEASUREMENT LOGIC

The instantaneous velocity is relatively easy to obtain. As described before, an up/down counter connected to the DIR output of the accelerometer is a way of measuring a change in velocity since the counter value was reset. By resetting the counter value when the vehicle is at rest, the counter value at each instant of time will be a measure of the vehicle velocity. Each bit of the counter corresponds to a velocity of

(Accelerometer Full-Scale) / (Clock Frequency)

If we can produce a pulse train where the pulse density is proportional to velocity, we can use a counter to accumulate distance similar to the velocity counter above. This counter will then accumulate the distance travelled. A BRM with its binary input connected to the velocity counter will produce such a pulse stream. The BRM drives a counter where each bit of the counter corresponds to a distance travelled of about

$$(\text{Accel. Full-Scale}) * 2^{(\text{no. of velocity counter bits})} / (\text{Clock Freq.})$$

3.2.4 Digital Vibration Measurement Subsystem

Some applications require determining the amplitude of vibration measured by an accelerometer. A simple device can be built using a piezoelectric accelerometer combined with several operational amplifiers to amplify, rectify and filter the signal, followed by a A/D converter.

Figure 13 shows a digital circuit that directly rectifies the output of the digital accelerometer, separating its normal outputs into two digital pulse streams corresponding to positive and negative accelerations and a third pulse stream that combines the positive and negative to produce the absolute value of the acceleration. Any of these pulse streams can be processed as described above in an ASIC or FPGA to filter, sample or otherwise process the rectified acceleration. The rectification circuit can be added to the ASIC or FPGA to give a complete vibration processing subsystem in a single low-cost, low-power chip.

DIR PATTERN	POSCNT or POSDIR	NEGCNT or NEGDIR	ABSCNT or ABSDIR
0000	0	1	1
0001	0	1	1
0010	0	1	1
0011	0	0	0
0100	0	0	0
0101	0	0	0
0110	0	0	0
0111	0	0	0
1000	0	0	0
1001	0	0	0
1010	0	0	0
1011	0	0	0
1100	0	0	0
1101	1	0	1
1110	1	0	1
1111	1	0	1

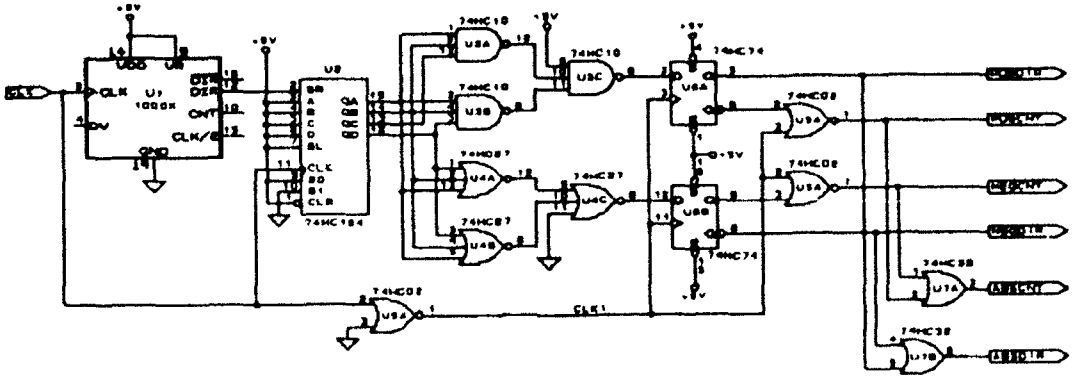

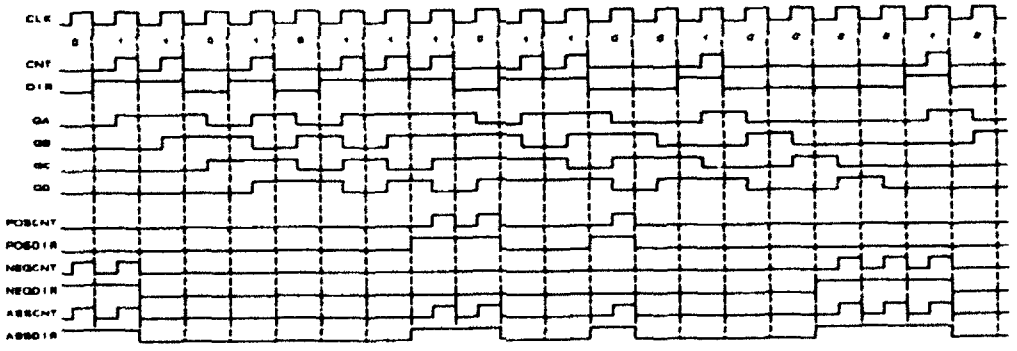

FIGURE 13: ALGORITHM AND CIRCUIT TO RECTIFY MEASURED ACCELERATION

4.0 CONCLUSIONS

In this paper we have shown how to build low-cost digital subsystems using digital accelerometers.

[1] Cole, John C., A New Capacitive Technology for Low-Cost Accelerometer Applications, Proceedings - Sensors Expo 1989, p. 106B.

[2] Cole, John C., A New Sense Element Technology for Accelerometer Subsystems, Proceedings of International Conference on Solid-State Sensors and Actuators (Transducers '91), IEEE, pp 93-96.

AN ULTRASONIC ANGULAR MEASUREMENT SYSTEM

JUSTIN D. REDD
Air Force Flight Test Center
412TW/TSID
Edwards AFB CA

ABSTRACT

An original design is presented for a system capable of measuring the relative angle of a flat surface using reflected ultrasonic wave pulses. No physical contact with the surface is necessary. The measurement range is from 0 to 54 degrees. Theoretical resolution is 5 minutes of arc, with actual measured resolution of approximately 20 minutes of arc. The system has performed successfully in limited flight tests, is capable of rates up to 80 angle measurements per second, and has a solid-state memory recording capacity of 24,000 bytes. The measurements are time-tagged as they are recorded and may be transferred to a personal computer at a later time over a standard RS-232 serial communications link. The system is small (approx. 6 by 4 by 1.5 inches) and uses two standard 9-volt batteries as its power source.

KEY WORDS

Angular Measurement, Ultrasonics, Non-contact Angular Measurement, Inclinometers, Tip-off Angle Measurement

INTRODUCTION

Various methods have been proposed to measure angular displacement at close range using optical or ultrasonic methods. Optical angular measurement devices have been demonstrated involving reflective surfaces, optical code plate sensors, encoded diffraction gratings [1] [2], and photodiode arrays [3]. These optical methods all require modification of the object to be measured (such as attaching mirrors) or contact with the object (such as connection to a shaft). Ultrasonic methods have proven more useful in applications where contact with (or modification of) the object to be measured is not possible [4]. Limitations of non-contact ultrasonic angular measurement systems which have been reported in the past [5] include limited angular range (less than 20 degrees), large size, and complexity. The system described in this paper overcomes many of these limitations.

The original purpose of this project was to find a method to measure the tip-off angle of a cargo pallet as it is being extracted in flight from a C-17 aircraft (Figure 1). The tip-off angle is defined as the angle between the deck of the airplane and the cargo pallet. Some of the requirements for

the system were: minimal modification to the aircraft, accuracy of at least 0.5 degrees, ability to use the system with any arbitrary pallet (no pallet modification allowed), a measurement rate of at least 50 measurements per second, and data recording capability. The system described in this paper was designed to meet these requirements and test results show that, in most cases, it was successful.

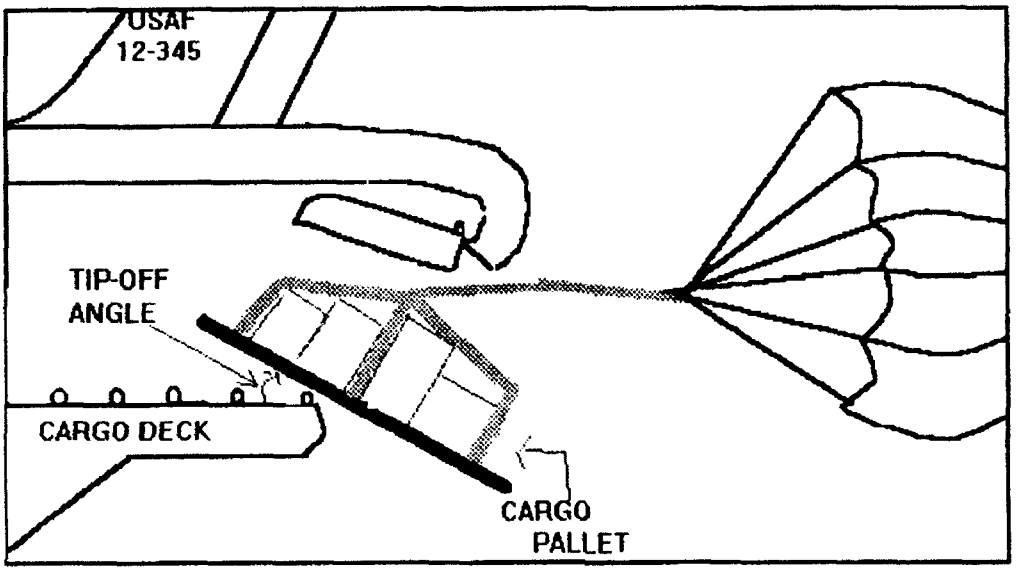

Figure 1. Cargo Pallet Extraction from an Aircraft

SYSTEM DESCRIPTION

The ultrasonic angular measurement system can be divided into three parts: the control box, the ultrasonic transducer, and the reflector block (Figure 2). The system transmits pulses of ultrasound from the transducer which bounce off the cargo pallet, then a reflector block, then back to the pallet, and finally return to the ultrasonic transducer. By measuring the time difference between the transmitted pulse and received echo, the distance that the pulse traveled can be calculated using the speed of sound in air. The system must measure the air temperature since the speed of sound is dependent on temperature. The distance traveled by the pulse of ultrasound is linearly related to the angle in question. Following is a description of each of the three parts of the system.

The control box receives software instructions from a personal computer, provides system control, records the data, and sends the data back to the personal computer. The heart of the control box is a commercially available printed circuit (PC) board which contains a 6303 microprocessor, an analog to digital (A/D) converter, timers, a universal asynchronous receiver/transmitter (UART), read only memory (ROM), and random access memory (RAM). Also included in the control box are RS-232 serial communications driver circuits, power switches, light emitting diode (LED) status indicators, an ultrasonic driver module, a thermistor temperature sensor, and two standard 9-volt batteries. Software is loaded into the control box from a personal computer via the RS-232 serial communications port (after loading the software the personal computer may be disconnected). The two power switches control power on/off and standby/operate modes (standby mode keeps memory active but shuts off all other power in order to save the batteries). The three LEDs indicate low battery power, memory remaining, and data recording mode (stopped, waiting for target, or recording target data). The thermistor temperature sensor puts out an analog voltage proportional to the air temperature and the voltage is then digitized by the A/D converter and used for calculation of the speed of sound. The ultrasonic driver module generates high amplitude electrical pulses of 150 KHz waves which are used to drive the ultrasonic transducer. The ultrasonic driver module also senses the return echo signal from the transducer. One of the 9-volt batteries supplies the ultrasonic driver module and the other supplies the rest of the electronics.

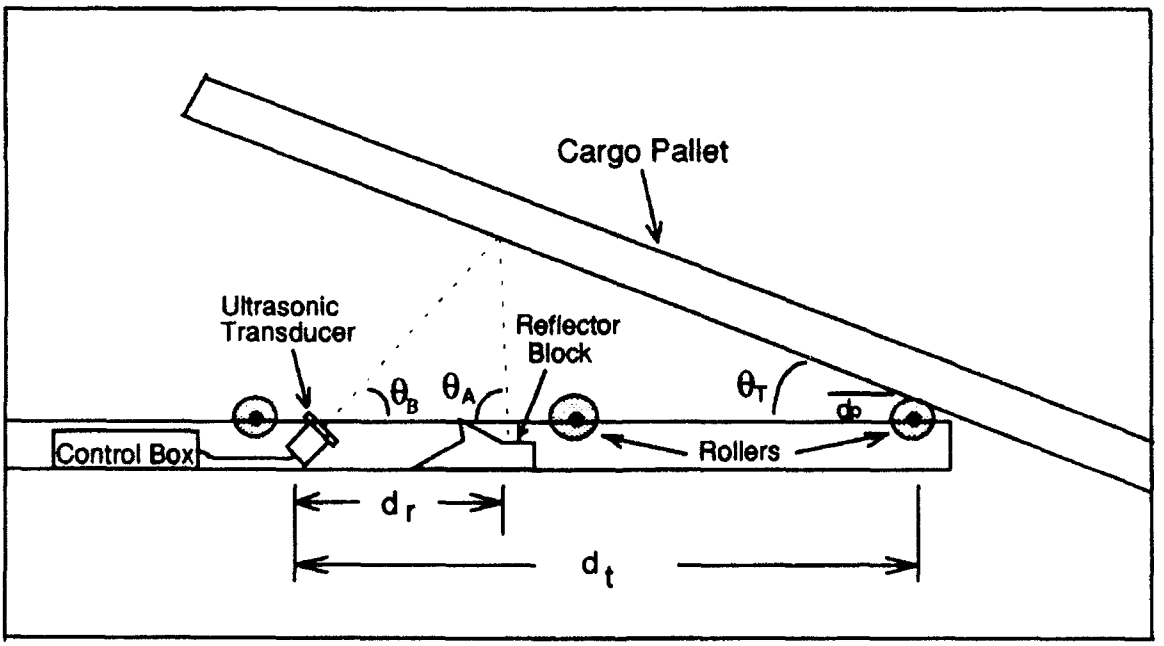

Figure 2. The Ultrasonic Angular Measurement System

The ultrasonic transducer is a piezoelectric device which operates at 150 KHz. It has a beam width of ten degrees and no sidelobes. It converts electrical pulses generated by the control box into ultrasonic waves. It also generates electrical signals when excited by ultrasonic waves (echoes of the transmitted waves).

The reflector block is the most unique part of the system. It enables the measurement of a wide range of angles. The block is machined from a solid piece of aluminum and has various angled surfaces designed to reflect the ultrasonic pulses back in the same direction they came from (see Figure 3). The block is divided into two parallel halves, with each half optimized for a different angular range. The geometry of the system and theory of how the reflector block works are discussed in the following sections.

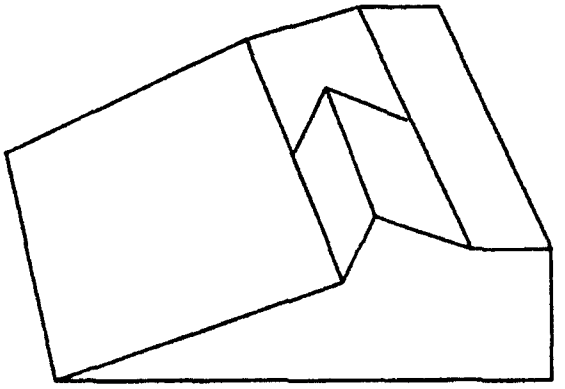

Figure 3. The Reflector Block

SYSTEM OPERATION

In order to understand how the system operates, it is first necessary to understand the geometry. Figure 2 is a side view diagram of the angular measurement system which shows the path of the ultrasonic pulses from the time they leave the transducer until the echoes return to the transducer. This geometry is based on the specific application of measuring the tip-off angle of a cargo pallet being extracted from an airplane, but the method may be generalized to measurement of the relative angle of an arbitrary flat surface. Two assumptions are necessary in order for the system to function: 1) the angle between the plane in which the transducer is mounted and the plane of the surface whose angle is being measured (cargo pallet) may be varied in only one dimension (no twist or tilt except the angle being measured) and 2) The intersection between the two planes must be a fixed line (for example, it would be a violation of this assumption to maintain the relative angle between the two planes while changing the distance between them). These assumptions are valid for the aircraft application since the cargo pallet slides on rollers a fixed distance above, and parallel to, the cargo deck and tips about the constant pivot line at the edge of the cargo deck as it leaves the airplane (see Figure 1). In the tip-off angle application, the angular measurement system is mounted to the cargo deck of the aircraft at a fixed distance from the edge of the deck and the pallet slides on rollers above the system.

The transducer is mounted at a 48-degree angle relative to the aircraft cargo deck. This angle is chosen to optimize angular range, system compactness, and the pulse travel distance versus tip-off angle relationship. The ultrasonic pulses travel at the initial 48-degree angle until they contact the bottom side of the cargo pallet. The pulses are reflected from the bottom of the pallet at an angle determined by the tip-off angle θ_T of the pallet. The pulses arrive at the cargo deck at a distance

d_r from the transducer, and at an angle θ_A relative to the deck. Both d_r and θ_A are functions of the tip-off angle. The reflector block is shaped such that at any given distance d_r, the angular surface of the block will be approximately perpendicular to the angle θ_A. The result is that pulses striking the reflector block are reflected back along the same path that they came from. Pulses returning from the reflector block strike the bottom of the pallet along their original path and are reflected back to the transducer. (Approximations in the angles of the surfaces of the reflector block are compensated for by the fact that the beam width of the ultrasonic pulses is 10 degrees, so that the ultrasonic pulses actually travel at approximately plus or minus 5 degrees from the beam center.) As the pallet tip-off angle increases, the pallet eventually becomes perpendicular to the path of the pulses emitted by the transducer, at which point the pulses are reflected directly back to the transducer instead of to the reflector block. By measuring time difference between the transmitted pulse and the return echo, and with knowledge of the speed of sound, the distance traveled by the ultrasonic pulses can be calculated.

The velocity of sound in air varies with the square root of temperature as shown by the following equation:

$$V_S = 13{,}044\,(273 + T_A)^{1/2} \quad (1)$$

where V_S is the velocity of sound in inches per second, and T_A is the ambient air temperature in degrees centigrade. It is necessary to correct the speed of sound for temperature in order to obtain sufficient measurement accuracy. In the ultrasonic angular measurement system the control box contains a thermistor temperature sensor which is read under software control in order to make this correction.

The distance traveled by the ultrasonic pulses as a function of tip-off angle can be derived mathematically. Neglecting path length changes due to the reflector block (assuming that all pulses are reflected at the level of the cargo deck) the distance equation is given by

$$S = \frac{[d_t \sin\theta_T + d_p \cos\theta_T]}{\sin(\theta_T\,\theta_B)} \times \frac{[1 + \sin\theta_B]}{\sin(2\theta_T + \theta_B)} \quad (2)$$

where S is the distance traveled in inches, θ_T is the tip-off angle in degrees, θ_B is the angle of the transducer relative to the cargo deck in degrees, d_t is the distance of the transducer from the pivot line in inches, and d_p is the vertical distance between the transducer and the bottom of the pallet in inches when θ_T=0. In the application described in this paper, θ_B = 48 degrees, d_t = 22 inches, and d_p = 1 inch. It should be noted that equation (2) applies to angles θ_T of less than 29 degrees. For angles of 29 degrees or greater, the path (as mentioned earlier) is from transducer to pallet and directly back to transducer (bypassing the reflector block).

Operation of the ultrasonic angular measurement system is controlled by the system software. The software is written such that the system is always in one of three modes: waiting for valid

data, recording data, or halted due to a full data buffer. In the waiting for data mode, pulses are sent out and the system waits until valid echoes are detected. Once a valid echo is detected the system changes to the data recording mode. In the data recording mode, time, temperature, and intervals between transmitted pulses and echoes are recorded. New pulses are transmitted at the rate of 80 pulses per second. When non-valid echoes are detected the system reverts back to the wait mode, or, if the data buffer becomes full, the program halts. System mode, data buffer status, and battery status are indicated by light emitting diodes under software control.

TEST RESULTS

Tests performed on the angular measurement system include laboratory calibration and check out as well as limited flight tests. Laboratory calibration was accomplished using a test fixture which simulated the aircraft installation. The fixture included mounting brackets for the control box, transducer, and reflector block. The pallet was simulated by a hinged flat plate with screws that could be tightened in order to hold it at a fixed angle. The angle of the hinged plate was measured visually using a protractor. The plate was moved in one degree increments throughout the entire range of the system and the measured distances corresponding to each angle were recorded. The data measured in this test are plotted in Figure 4.

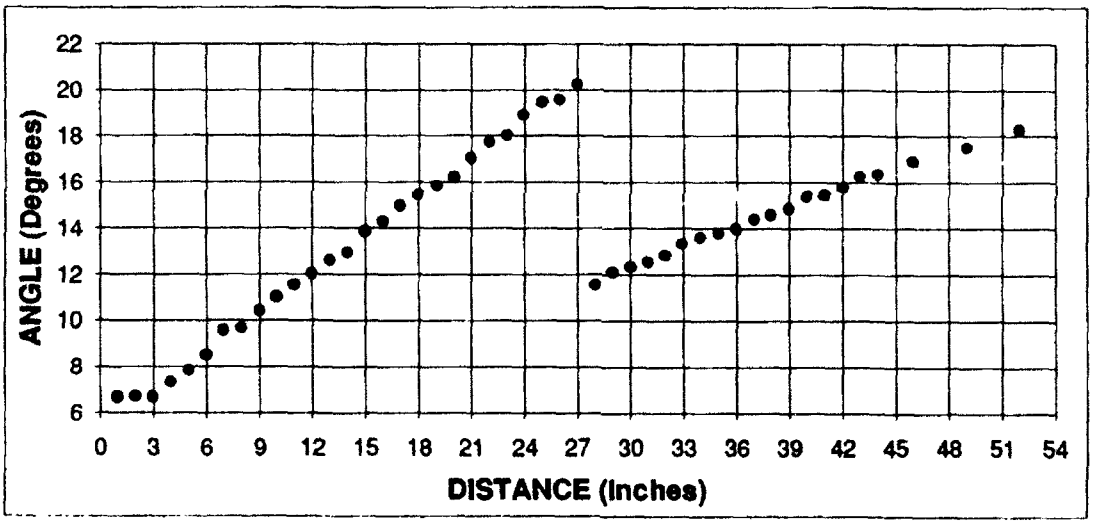

Figure 4. Graph of Distance Versus Angle

The relationship between distance and angle is approximately linear between 4 and 28 degrees and 29 and 54 degrees. The 4 to 28 degree relationship is based on the mode of operation where the ultrasonic pulses travel from the transducer, to the pallet, to the reflector block, and back. The 29 to 54 degree relationship is based on the mode of operation where the ultrasonic pulses are reflected from the bottom of the pallet directly back to the transducer. Linear regression methods show a good linear fit in each of the two angular regions (standard error of 0.32 degrees in the low angle region and 0.49 degrees in the upper angle region). Resulting equations for the two regions are:

$\theta_T(L) = (1.777)S - 8.242$ (3)

$\theta_T(U) = (3.562)S - 12.934$ (4)

where $\theta_T(L)$ is the tip-off angle in the low angle (4 to 28 degree) region, $\theta_T(U)$ is the tip-off angle in the upper angle (29 to 54 degree) region, and S is the measured ultrasonic pulse path distance. Equation (3) agrees approximately with the geometrically derived Equation (2) and differences are attributed mainly to the fact that Equation (2) did not take into account the finite dimensions of the reflector block.

Because of the two distinct linear relationships represented by Equations (3) and (4) in the low angle and upper angle regions, it is necessary to keep track of which angular region the system is operating in. The transition between regions can be determined by noting the abrupt change in the slope of distance versus time (dS/dt) which occurs at the transition.

The theoretical angular resolution of the system can be determined by using Equations (3) and (4) along with the rated distance resolution of the ultrasonic transducer. The transducer resolution is rated at 0.04 inches. Changing S in Equations (3) and (4) by 0.4 inches yields a change in measured angle of 0.07 and 0.14 degrees (4.2 and 8.4 minutes of arc) respectively. The angular measurement equipment used in the laboratory calibration (visual measurement using a protractor) was not accurate enough to verify this resolution.

Limited flight tests have been conducted in a C-141 aircraft in order to determine if the system is effected by possible air turbulence and/or ultrasonic noise generated when the cargo doors are opened in flight. This test was done using the laboratory test fixture (in order to vary measured angles along with an oscilloscope to visually monitor noise received by the transducer.) The system was monitored during opening and closing of the cargo doors. Some noise increase was noted when the cargo doors were just slightly open, but this was not judged important since the system is intended to be operated with the doors fully open. Flight tests of the final system with actual pallets have not yet been completed.

CONCLUSIONS

The ultrasonic angular measurement system described in this paper has proven to be an important improvement in the ability to measure angles in an environment where contact with or modification of the surfaces to be measured is not possible. Compared to other reported ultrasonic angular measurement systems [5], this system uses one transducer instead of three while increasing the measurement range and resolution.

FURTHER INFORMATION

More information on the ultrasonic angular measurement system may be obtained by contacting the author at 416 TS/ENS, 59 N Flightline Road, Edwards AFB, CA 93524-6150, telephone (805) 277-0956 or DSN 527-0956.

ACKNOWLEDGMENTS

This project would not have been possible without tremendous support from the instrumentation division at the Air Force Flight Test Center. Particular thanks go to David Crounse, Kevin Medina, Ted Richardson, Susan Harlow, and Tracy Schaerer.

REFERENCES

1. Spillman, W.B.,el al., "Wavelength Encoded Fiber Optic Angular Displacement Sensor," SPIE Proceedings - Fiber Optic and Laser Sensors VIII, Vol 1367, 1990, Pg 197-202.

2. Ami, M., et al., "Optical Method of Measuring Angular Displacement Using a Diffraction Pattern," Applied Optics, Volume 26, Number 14, October 1987, Pages 4310-4312.

3. Sato, K.,et al., "Optical Method of Measuring Angular Displacement Using Four Photodiode Arrays," Applied Optics, Volume 23, Number 23, December 1984, Pages 4450-4452.

4 Canali, C., et al., "A Temperature Compensated Ultrasonic Sensor Operating in Air for Distance and Proximity Measurements," IEEE Transactions on Industrial Electronics, Volume 1E-29, Number 4, November 1982, Pages 336-341.

5. Marioli, D., et al., "Ultrasonic Distance Measurement for Linear and Angular Position Control," IEEE Transactions on Instrumentation and Measurement, Volume 37, Number 4, December 1988, Pages 578-581.

Commercial Pressure Transducers for Military and Aerospace Applications

Daniel R. Weber
VP of Engineering
Data Instruments Inc.
100 Discovery Way
Acton, MA 01720

William Maitland
Manager Of Sensor Development
Data Instruments Inc.

Abstract

During the past ten years commercial pressure transducers have been priced very competitively, while providing improved performance and reliability. Many industrial and commercial applications have environmental conditions that need transducers to be extremely robust in order to survive; these conditions often rival or exceed military and aerospace requirements, especially for shock, vibration, corrosion resistance and expected number of full-pressure cycles.

To meet the increasing demand for such transducers, some manufacturers have developed designs and processes that allow rugged, high quality devices to be manufactured in high volumes. These transducers typically feature 0.25%-1% accuracy, stainless steel wetted parts with either flush-mount or integral ports, and offer a variety of standard options, including low- or high-level voltage output, 4-20 mA current output, and a selection of excitation voltages or currents. Custom configurations, coatings, special materials, extended temperature ranges, extended testing, and other requirements not cataloged are often available by request. Recently, some of these manufacturers have developed ISO-9001 certified quality management systems, helping ensure that design and manufacturing processes meet many of the requirements of M-I-45208 and M-Q-9858.

A military transducer development project is compared to another project using a modified version of a catalog commercial transducer, and several successful applications are detailed.

Background

The past decade has proven to be a very challenging and competitive period for many pressure transducer manufacturers. Previously, the use of pressure transducers tended to be divided between benign laboratory applications and more demanding applications, such as industrial processes, oil exploration, military and aerospace applications where high prices were a secondary consideration to performance and reliability. With the exception of the process control industry, most of these applications used transducers that were built in low volumes, and tested and calibrated by hand.

The development and rapid acceptance of the microprocessor during the 1970's gave rise to many new applications for pressure transducers. Computers previously had been used only for large scale control systems, but microprocessors allowed computer control of small systems (and household appliances, for that matter). These systems required sensor inputs, but for the applications at which they were targeted the high quality transducers of the time were prohibitively expensive.

One of the new applications was in medical instruments. Although the environmental stress in these applications was low, the requirement for high reliability was crucial, literally a matter of life or death. The corrosive nature of the dialysate in kidney dialysis typically required wetted parts of 316L vac-melt stainless steel that were expensive to machine. As the acceptance of these instruments grew, the quantity of pressure transducers required grew apace; some manufacturers met this demand by investing in numerically-controlled machining equipment and computerized test and trim equipment to increase production volume without compromising quality.

Another new application was the control of commercial refrigeration systems. Driven by the energy shortages of the '70's, users of large refrigeration systems, supermarkets, for example, turned more and more to electronic control in an effort to reduce operating costs. These systems subjected the pressure transducers to a combination of high vibration, low temperatures and high humidity: many of the existing transducers failed, forcing manufacturers to significantly improve the ruggedness of these devices while keeping their prices competitive. Alternatives to expensive machined parts were developed: one very successful design used a combination of a stainless steel machined pressure port, stamped diaphragm, and stamped beam brazed together to form a very robust, yet modestly priced sensor.

The automotive and off-road-vehicle market also started using pressure transducers. Initially, these applications were for engine control to help meet regulations on emissions, but other uses soon developed, including anti-lock braking systems, traction control, load leveling, hydraulic system controls, fuel control and lubrication systems. Automotive applications are extremely demanding in terms of environmental stress, having a typical temperature range of -40 °C to 125 °C, high shock and vibration levels, and exposure to a wide range of corrosive materials. Again, manufacturers responded by increasing the temperature range and ruggedness of their products.

Recently, there has been much talk of a "world market." Behind the hype is a large measure of truth; US and foreign transducer companies are in competition for many of the same customers. One of the most visible aspects of this is the adaptation of ISO 9000 quality standards by US manufacturers. While these standards are not yet equivalent to military requirements, they do help enforce a similar attitude towards properly documented and executed procedures covering the entire process from receipt of order through packaging for shipment. Some commercial transducer manufacturers also produce military products and have

incorporated portions of their military standards manuals into their ISO 9000 programs.

High-volume production has provided commercial manufacturers with an impetus to perform statistical process control and an imperative to design quality in rather than test it in. The result of this has been the development of commercial transducers that perform well under demanding conditions, have high reliability, and are reasonably priced. These are produced in medium to high volumes using highly automated processes where appropriate and generally under stringent quality control guidelines.

Technologies

Although some of the advances have come from new technologies, others involve improved manufacturing methods for traditional ones. Despite several highly touted technological "breakthroughs," virtually all pressure transducers have used the same basic principles for the last 50 or so years: the pressure to be measured is applied to an elastic material and either the strain or deflection of the material is converted to an electrical signal. Traditionally, this has been most commonly done as follows:

Bonded strain gage: A foil or semiconductor gage is bonded to a beam or diaphragm and changes resistance as pressure changes. Usually configured into a Wheatstone bridge circuit.

Capacitive: A diaphragm forms one plate of a capacitor, which changes capacitance as pressure changes. Usually configured into an oscillator circuit.

Potentiometric: A slider moves across a resistive element as pressure changes. Often uses a bellows assembly to generate large deflections.

Some newer technologies include:

Micro-machined: A strain-gage or capacitive sensor is etched onto a silicon die.

Silicon on Sapphire: A micro-machined strain-gage sensor on a sapphire substrate.

Thin film: Metal or semiconductor strain gages are vacuum-deposited or sputtered onto a beam or diaphragm.

Fiber optic: Pressure is either applied directly to a fiber, modulating its optical signal, or to a diaphragm, which deflects and modulates a reflecting signal.

Although several of these technologies have been claimed to be better than the others, each has some strengths and some weaknesses, and often the inherent difference between them is not as important as the execution. Most of these technologies can provide adequate performance in many applications.

A typical sequence of events in manufacturing a pressure transducer is as follows: build the sensor; subject the sensor to extremes of pressure and temperature in excess of those it will see in use; test the sensor to characterize its output over the pressure and temperature range for which it is

intended; trim the sensor to adjust its temperature compensation, zero and full-scale output; re-test to insure that characteristics are correct; do final assembly; and perform a functional check. The care and precision with which each of these steps is performed is usually more critical to the performance of the product than is the underlying technology.

The process of characterizing, testing and trimming sensors has been transformed over the last decade from a predominantly manual operation into a highly automated one. Calibration and test cycles are performed under computer control, with automatic data collection and analysis to calculate appropriate values for trimming. Where trimming used to be done by installing discrete resistors, it is now frequently performed by abrasive- or laser-trimming thick- or thin-film resistors, or in some cases by programming a PROM. The net result is a substantial improvement in the uniformity of the transducers, with a much higher average level of performance in the finished product.

Features

Does the fact that these transducers are manufactured in high volumes mean that they are all the same? While the transducer manufacturers wish that were the case, their customers' differing requirements, even within the same industry, necessitates much flexibility. Transducer lines typically offer a variety of standard and optional features:

Ports: Flush ports have the exposed diaphragm as the front surface and can either be mounted directly into a machined assembly or with the use of an adapter. Integral ports can be female or male. Female ports with internal threads are often used with an adapter to convert them to male ports; while this adds flexibility, it also adds another pressure connection.

Male threaded ports are available in a variety of commonly used US and metric threads; some manufacturers can provide custom threads. Ports are generally attached by brazing or welding. Some technologies use an internal o-ring to seal pressure against a sensor capsule: these o-rings can be a problem over temperature extremes and sometimes interact adversely with the pressure medium, so they need to be carefully matched to the application.

Materials: Wetted materials range from alumina and silicon to plated mild steel through various grades of plated or unplated stainless to titanium. 15-5, 17-4 and 300-series stainless steels are common. Titanium tends to be more expensive, but offers better corrosion resistance, especially to sea water. Iconel-X, Hastelloy and beryllium copper are used for some applications. Teflon or other inert coatings are sometimes used where a non-metallic interface is desired or exotic metals are cost prohibitive.

Electronics: Strain-gage transducers can be either unamplified or amplified. Depending on the underlying technology, unamplified transducers will have a full-scale output voltage of 1 mV to 20 mV per volt of excitation. Unamplified micro-machined transducers may also use constant-current supplies, with a full-scale output of 40-60 mV per mA of excitation.

Amplified transducers can have a wide variety of output voltages, with 0-5 V, 0.5-4.5 V, 1-5 V, 1-6 V, and 0-10 V prevalent. Outputs can be either ratiometric or non-ratiometric to the excitation

voltage. 4-20 mA current output is widely used in industrial process control and is becoming more common in other applications because of its inherent noise immunity and two-wire installation. Logic-level frequency outputs and serial-word digital interfaces are also available.

The excitation will depend on the underlying technology and the associated electronics. Unamplified bridge transducers generally use 5 or 10 Vdc and require either a well-regulated supply or a fully ratiometric system. Note that such transducers are often truly ratiometric over a relatively small excitation voltage range, typically ±1 volt, and may produce drift or span errors if the excitation voltage varies significantly. Constant-current devices generally use 1.5 mAdc. Amplified transducers are often available with internal voltage regulators, which allow them to operate over a typical range of 8-32 Vdc, while 4-20 mA units usually require a range of 12-36 Vdc.

Dielectric breakdown ranges from 25 to 2500 Vdc. Full electrical isolation between excitation and signal output is generally *not* available. Reverse voltage protection for amplified devices is available either standard or as an option on many transducers

Connectors: Cable leadouts or molded connectors are the most common for commercial transducers, but many companies offer optional metal connectors. Cables can always be terminated in a suitable connector without modifying the transducer itself

Commercial pressure transducers offer a wide range of specifications:

Range: 0-5 to 0-20,000 psi in numerous ranges allow matching the transducer to the application. Transducers are often available in bar and kg/cm^2 ranges as well. Gage, sealed, absolute and, to a lesser extent, differential pressure ranges are generally offered.

Overload: Depending on pressure range, 1.5 or 2x full scale, with burst pressures from 5 to 20 x full scale. Extremely high overload capability is generally not available, but higher range transducers can be "turned down" with a proportional improvement in accuracy and reduction in temperature performance.

Accuracy: ±1% of full scale (FS) from best fit straight line (BFSL), including non-linearity, hysteresis and repeatability, is the norm, but many transducers are available with 0.5%, 0.25% or 0.1% either standard or as an option.

It should be noted that some manufacturers offer "typical" rather than "maximum" specifications, especially for accuracy and temperature compensation. Use caution when considering such transducers for critical work, since the ratio of typical to non-typical transducers and the maximum amount by which non-typical units might exceed the specification are rarely indicated or guaranteed.

Temperature range: -40 to 85 °C is the most common industrial temperature range, but automotive applications require -40 to 125

or 150 °C; thus, many transducers are now available to cover this range. Some commercial transducers operate down to -65 °C.

Temperature compensation: The compensated temperature range is usually smaller than the operating temperature range, typically -1 to 54 °C, but extended ranges are available. Thermal effects on span of ±1% FS and on zero of ±2% FS are typical; however, tighter tolerances are optionally available. Automotive transducers often have a stated total error band over the complete operating temperature range; generally ±4% FS including all effects of non-linearity, hysteresis, repeatability, calibration and temperature from -40 to 125 °C.

Shock/vibration: Generally rated from 11.9 to 46.3 g's rms for vibration and 50 to 100 g's rms for shock. Many commercial transducers are tested to various levels of MIL-STD 810C.

Cycle life: Some commercial transducers have been tested for over 100 million full-scale pressure cycles with no degradation in performance.

Selecting transducers

Despite all the available options, using a commercial transducer in a military/aerospace application will probably require some degree of compromise. It is unlikely that a catalog transducer will meet all the requirements that tend to turn up on quote requests (RFQ's) and it is easy to define a transducer so narrowly that a specialty product is required. Consider the specifications that are really important to the mission and be flexible on those that are not. Too often, the pressure transducer is the last item specified in a system, after the error budget has been absorbed by the data collection and processing electronics. This results in specifications that can be met only by an exotic, expensive transducer.

For the most part, commercial transducers trade extreme accuracy against ruggedness and moderate cost. While it is often possible for the transducer manufacturer to improve accuracy or temperature performance, if the application demands 0.1% accuracy and total error bands of better than several percent over a wide temperature range, it is unlikely to be satisfied by this type of sensor. Even so, thoughtful system design can often reduce or eliminate the need for such performance. For example, an automatic zero feature can eliminate the need for extreme long-term zero stability. In a typical software-controlled system, such a feature can be added at no cost if the applied pressure returns to zero (or some known pressure) frequently enough to keep drift within the desired specification. If the system is hardware controlled, the cost of added circuitry to implement this feature will usually be far less than the cost of a high-stability transducer. If the pressure doesn't return to zero with any known regularity, consider adding a solenoid valve to remove pressure from the transducer–this approach may still prove to be a lower cost alternative.

Transducer electrical requirements should be considered early in the design process: it is generally easier and less expensive to design electronics to match a transducer's specifications than the other way around. Being flexible on the excitation supply and full-scale output voltage can save money and improve performance. For example, a bonded foil strain-gage transducer typically has an output of 3 mV/V, while a bonded semiconductor strain-gage transducer has an output of 20 mV/V. This transducer's manufacturer can provide an output equivalent to the foil-gage unit by padding down the output, but a better solution is to lower the gain of the signal conditioning electronics, which can usually be done by changing one or two resistors. This not only makes for a less expensive transducer, but also improves the system signal-to-noise ratio. Frequently, the savings in transducer costs will pay for the electronics change many times over

Physical layout also needs to be considered during system design. Custom sizes and configurations are usually expensive and require long lead-times. Choosing a suitable transducer early in the design process will help ensure that there is adequate room for the transducer, connector and wiring.

Applications

Brief descriptions of applications of commercial pressure transducers in aviation, space and military systems:

Aircraft oxygen/air monitor: Provides cockpit display of the pressure in the cabin emergency tank on jetliners, general aviation and commuter aircraft. A Data Instruments MediaMate 2000 psig transducer is used. This is an unamplified, bonded semiconductor strain-gage model, with a brazed stainless steel port, output of 10mV/V and standard static accuracy of ±0.5% BFSL FS. Special requirements included: a cable leadout instead of molded connector; ±1.3% FS zero and ±2% FS span thermal error from 0 to 130 °F; and an operating temperature range from -65 to 212 °F. The requirements for the jetliner version are similar, with a 3000 psig range and a lower temperature limit of -65 °C.

A related application measures cabin air pressure on jetliners. A standard Data Instruments AB 15 psia transducer is used. This is a bonded strain-gage model with machined stainless steel case, flush-mount port and an unamplified 20 mV/V output.

Portable glide-bomb tester: The bomb's pneumatic system is charged and a pressure transducer is used to detect leaks. The transducer used is a Data Instruments SA 1000 psis. This is an amplified, bonded semiconductor strain-gage unit, with a brazed stainless steel port, standard accuracy of ±0.5% BFSL FS, standard ±1% FS zero and ±1% FS span thermal error over a 100 °F range. The device has to meet the requirements of Mil-T28800 Type I, Class II, Style A for portable equipment used on the flight line; it was submitted to the Defense General Supply Center and received approval. Key requirements for this application were the high level output of 1-6 Vdc and the low temperature operating limit of -40 °C. Military type transducers were generally too large and heavy; those meeting the other requirements did not have internal amplification or were too expensive. The price was less than $200 each.

Hot Water Tank Pressure: Monitors pressure in jetliner lavatory hot water system, and turns off power to heater if pressure rises

above limit. A Data Instruments MediaMate transducer is connected to an amplifier and comparator to form an electronic pressure switch, replacing electromechanical switches that had proved unreliable. Nominal pressure is 25 psig, but 140 psig is applied during system leak testing, so a 100 psig transducer with 2X overload rating is used. A special dual-threaded port allows an extension tube mounted on the port inside the tank to act as an anode to reduce corrosion of critical components. The transducer price is less than $50 each in 1,000-piece quantity.

Engine oil and fuel pressure: One transducer monitors oil pressure, another monitors pressure in the fuel rail of a light aircraft engine. The transducers are both Data Instruments MediaMate models, 100 and 15 psig respectively. The operating environment is similar to that of automotive applications in terms of vibration, heat, and dirt. With 1200 of these systems in use, there has not been a single field failure of the pressure transducers, which are priced around $50 each in these quantities.

An engine oil application for a military hovercraft landing vehicle uses a standard Data Instruments model AB 200 psig, which is supplied with a snubber for high pressure spikes. The transducer is subjected to extreme heat, shock and vibration in this environment.

Coolant system pressure: Monitors pressure of ethylene glycol used to cool on-board computer systems on military aircraft. Data Instruments AB 100 and 200 psig transducers are used. These have been fitted with a threaded male port and a military type connector, but are otherwise catalog products

Project Comparison

Using commercially available transducers has advantages that exceed the obvious one of lower component cost. Overall lead-time is often greatly shortened compared to the typical development of specialty transducers, resulting in reduced project costs and increased time available for system debugging. This last application is an instructive example of the type of savings that can be had by using commercial transducers:

Munitions altimeter: Detonates device at a preset altitude. The transducer is a variation of a Data Instruments AB 50 PSIA. This application requires the transducer to operate properly after experiencing a 3x pressure overload and 385 g's peak shock for 40 milliseconds; however, this only occurs once! The manufacturer provides additional internal potting to ensure the transducer's survival under these conditions. Additional special requirements include constant-current excitation, 0.125% FS BFSL accuracy and printed wiring board connection pins instead of the standard cable leadout.

The commercial transducer selected is produced in annual volumes of many tens of thousands, and has been very successful in a number of high-stress, high-reliability applications. While the modifications require a new outer case, printed wiring board, and rear connector, the basic sensor element is a standard product. Despite all the custom requirements, the time quoted from receipt of order to shipping units for qualification testing was 12 weeks, with production volumes starting to be shipped 8 weeks after qualification. Non-recurring

engineering charges added under $2 to the cost of each transducer for the first year's production volume, with total per copy prices less than 20% higher than the catalog product. A custom-designed military pressure transducer for a similar application had a 26-week design phase, 26-week prototype phase and required 20 weeks after qualification to start small-volume production. Non-recurring engineering charges were hundreds of thousands of dollars and the per copy cost was an order of magnitude higher than the modified commercial product.

Summary

The improved reliability and performance of commercial pressure transducers offer designers of military and aerospace systems an opportunity to reduce costs and development time, especially if the system is designed with the transducer in mind.

Danish Accreditation in the Field of Acoustics.

by

Torben R. Licht

Danish Primary Laboratory of Acoustics (DPLA)

Brüel & Kjær

Denmark

ABSTRACT

Until recently all danish laboratories wanting traceable calibrations had to get traceability by having their standards calibrated abroad, mostly at PTB in Germany or at NIST in Washington DC, USA.

Recently the Danish Primary Laboratory of Acoustics (DPLA) has been established as primary laboratory for calibration of accelerometers and microphones and accredited to perform calibrations and issue calibration certificates as a service to clients.

DPLA is an independent department within the Brüel & Kjær Industries Sound & Vibration division and cooperates with the Acoustics Laboratory at the Technical University of Denmark, Lyngby.

Mutual recognition of calibrations and laboratories is ensured by a multilateral agreement between the following countries: Denmark, Finland, France, Germany, Italy, The Netherlands, Sweden, Switzerland and the United Kingdom. The agreement is made within the framework of WECC (Western European Calibration Cooperation.

A description of the Danish Metrology and Laboratory Accreditation system will be given as well as a brief history of the establishment of DPLA.

INTRODUCTION

Until the end of 1991 no officially recognized laboratory for primary calibrations within the field of acoustics existed in Denmark.

Therefore all laboratories wanting traceable calibrations had to get traceability by having their standards calibrated abroad, mostly at PTB in Germany or at NIST in Washington DC, USA.

Recently the Danish Primary Laboratory of Acoustics (DPLA) has been established as primary laboratory for calibration of accelerometers and microphones and accredited to perform calibrations and issue calibration certificates as a service to clients.

DPLA is an independent department within Brüel & Kjær Industries and cooperates with the Acoustics Laboratory at the Technical University of Denmark, Lyngby.

Mutual recognition of calibrations and laboratories is ensured by a multilateral agreement between the following countries: Denmark, Finland, France, Germany, Italy, The Netherlands, Sweden, Switzerland and the United Kingdom. The agreement is made within the framework of WECC (Western European Calibration Cooperation.

ORGANIZATION IN EUROPE

Until the seventies practically all countries used a national laboratory to maintain reference standards for the most important units, e.g. the meter, the second, the kilogram and the volt.

From these laboratories the industry could get calibrated references valid in that country by traceability.

Due to the increasing international trade and the increasing complexity and accuracy needed for the calibrations a number of european countries started to develop new ways of organizing their calibration services.

Although this followed different paths in the different countries, the increased collaboration, in the EEC and in Europe in general, lead to a common standard EN 45001, "General criteria for the operation of testing laboratories (1989)" ratified by Austria, Belgium, Denmark, Finland, France, Germany, Greece, Iceland, Italy, Luxembourg, The Netherlands, Norway, Portugal, Spain, Sweden, Switzerland and United Kingdom.

This standard is to a large extend based upon the ISO Guide 25, "General requirements for the competence of calibration and testing laboratories" and other ISO guides.

Furthermore a "Multilateral Agreement between the national Calibration services of Denmark, Finland, France, Germany, Italy, The Netherlands, Sweden, Switzerland and United Kingdom" has been signed in December 1990 stating that all recognizes the operation of the other services as equivalent to their own, accept the others' certificates and promotes the acceptance by all users in their own country.

This agreement is made within the framework of the Western European Calibration Cooperation (WECC), which started in 1975 and is based upon a Memorandum of Understanding. It has set up an on-going program of cooperation aimed at establishing mutual confidence between calibration services, so enabling agreements recognizing the technical equivalence of the operation of services to be entered into.

ORGANIZATION IN DENMARK - DANAK

Danish accreditation started its activity in 1975 in accordance with the parliamentary act of 1973 on the formation of the National Testing Board, STP.

The purpose of the scheme was, and to a large extend still is, to verify laboratory performances with reference to their own declarations, rather than reinforcing compulsory national or international requirements. This was natural in the early days when international standards were not available for accreditation. As such standards were developed, they were gradually adopted by STP. Because of its focus on individualism the scheme was highly flexible and well suited for singular accreditation. On the other hand, uniformity in the treatment of similar accreditation was not as good as one might wish, especially in the light of the increasing need for international harmonization.

In January 1990 the practical assessment work in relation to the accreditation scheme was moved to the Danish Institute of Fundamental Metrology (DFM) on a contractual basis with the National Agency of Industry and Trade.

In January 1991 the National Testing Board ceased to exist as a consequence of the new Industry and Trade Promotion Act. A new accreditation scheme DANAK emerged which treats on common ground testing, certification and inspection. The authority to grant accreditation will reside solely with the National Agency of Industry and Trade. This change in the identity of the granting body did not in itself impose changes in the practical accreditation work regarding testing; but changes are being introduced as a result of a project which DFM presently carries out in order to bring the accreditation scheme for testing more in line with international practice.

In order to ensure compatibility between the Danish scheme and international requirements, Denmark has joined multilateral arrangements with WECC and WELAC. During a visit in 1990 by WECC only minor flaws were found and Denmark was accepted as the ninth member of the multilateral European agreement between calibration services.

In order to allocate the resources of the assessment body in the optimum way, the performance of the scheme is regularly compared to the standards EN 45001, 45002 and 45003. In all items of this standard it is found that the Danish scheme formally satisfies the requirements. As a result of such comparisons areas in which improvements would be desirable can be found and thereafter focussed on.

CALIBRATION AT B&K

As the calibration service was established and started to function in 1976 B&K also felt that it might be of value to participate. An application was submitted and some initial contacts with STP showed that the work involved to establish rooms, equipment, procedures etc. was substantial compared to the obtainable benefits, because no mutual recognitions existed and B&K sold 98% of the calibrations/equipment abroad.

It was therefore decided not to pursue the accreditation further, but to continue the work with calibration at an international level.

In the beginning of the eighties calibration requirements came more and more in demand, and B&K started calibration service centers around the world using standardized equipment and written procedures to ensure a high quality on the calibrations.

In 1991 nine centers made more than 4000 calibrations/checks on microphones, accelerometers and calibrators.

HISTORY AND ORGANIZATION OF DPLA

In the autumn 1988 it was discussed again whether it would be practical to have a danish accreditation and whether it would be possible to get an accreditation as a danish primary laboratory.

In January 1989 the application was filed and in the middle of the year an international group of assessors headed by DFM made an audit at B&K. The conclusion was that B&K could be accepted as a primary laboratory, provided a number of requirements were fulfilled. The main requirement was to establish a danish calibration service accredited under DANAK.

In January 1990 the application for an accreditation was filed. This contained also a collaboration agreement with the Acoustics Laboratory at the Technical University of Denmark, Lyngby. This laboratory has been working with calibration for many years, and was therefore a natural partner and would also bring more independence to the laboratory, which became an independent department directly responsible only to B&K top management and not in technical matters. However, after some initial discussions it became clear that it was necessary to change a number of items before an accreditation could be granted.

The main issues were:

A. Calibration rooms with well controlled and described temperature, humidity, air-pressure, acoustic noise, dust particle count, electric and magnetic fields, vibration, voltage regulation and lighting; basically as required in ISA RP52.1 Recommended Practice, Recommended Environments for Standards Laboratories, 1975.

B. Quality manual for the laboratory following the newest methods (mostly referred to as Total Quality Management, TQM).

C. Procedures following the requirement set forth in the Quality manual.

D. Uncertainty budgets following the recommendations from Bureau International de Poids et Mesures. [Ref 1].

E. Statement of impartiality - organizational position.

After some man-years of work the required changes were implemented and the final Quality Manual etc. could be delivered in the summer 1991. During the autumn the assessors audited DPLA, and after a few changes the accreditation was granted in December 1991.

DPLA CAPABILITIES

The calibration capabilities of an accredited laboratory has to be stated in a form suitable to be used in a catalogue of accredited laboratories.

The stated capabilities for accelerometer calibration are:

Measured Quantity / Measurement Unit	Measurement Range	Measurement Capability	Method Used
Vibration Sensitivity: S_v * Volt per meter	≥ 4 V/m (20 Hz - 5 kHz)	$5 \cdot 10^{-3} \cdot S_v$	ISO 5347 Laser Interferometry HeNe Laser
Vibration Sensitivity: S_v * Volt per meter per second	≥ $4 \cdot 10^{-3}$ V/(m/s) (20 Hz - 5 kHz)		
Vibration Sensitivity: S_v * Volt per meter per second squared	≥ $4 \cdot 10^{-6}$ V/(m/s²) (20 Hz - 5 kHz)		
Vibration Sensitivity: S_c ** Coulomb per meter	≥ $1 \cdot 10^{-9}$ C/m (50 Hz - 5 kHz)	$5 \cdot 10^{-3} \cdot S_c$	
Vibration Sensitivity: S_c ** Coulomb per meter per second	≥ $1 \cdot 10^{-12}$ C/(m/s) (50 Hz - 5 kHz)		
Vibration Sensitivity: S_c ** Coulomb per meter per second squared	≥ $1 \cdot 10^{-15}$ C/(m/s²) (50 Hz - 5 kHz)		

* Voltage Output, ** Charge Output.

Transducer Weight: < 500 gram
Transducer Temperature: (24 ± 2) °C
Measurement Conditions: Pressure: (100 ± 5) kPa
Temperature: (23 ± 1) °C
Humidity: (50 ± 25) %RH

A multiplication factor of 2 is used (corresponding to earlier statements of 95 % Confidence Level) according to the requirements from DANAK.

The calibrations are made according to the ISO 5347 standard using a Ratio Counting and a J_1-Minimum Point method. The setup for the Ratio method is shown in fig. 1.

The history of calibration at this level, but not accredited goes back many years. A plot of results on different transfer standards compared to results obtained by NBS/NIST and PTB (Germany) is shown in fig.2.

The capability for microphones is somewhat more complicated to state, and therefore only an extract will be given here:

Measured quantity	Measure-ment range dB re 1V/Pa	Measurement Capability	Method	Remarks
Pressure sensitivity of Laboratory Standard Microphone dB re. 1V/Pa	-26 ± 2dB for Type LS1P (1") IEC 1094-1	31.5 Hz ±0.06dB 63 Hz ±0.04dB 125 Hz ±0.03dB 4000 Hz ±0.03dB 5000 Hz ±0.04dB 6300 Hz ±0.05dB 8000 Hz ±0.06dB 10000Hz ±0.12dB	Pressure Reciprocity Technique	B&K Type 4160
	-37 ± 3dB for Type LS2aP (1/2") IEC 1094-1	31.5 Hz ±0.08dB 63 Hz ±0.05dB 125 Hz ±0.04dB 8000 Hz ±0.04dB 10000Hz ±0.05dB 12500Hz ±0.06dB 16000Hz ±0.08dB 20000Hz ±0.12dB 25000Hz ±0.30dB		B&K Type 4180
	IEC 1094-1 Specifications for Laboratory Standard Microphones	Intermediate values are obtained by interpolation		Measurement conditions: 1013 ±25hPa 23+2-0°C 50 ±20%RH

The procedure used is IEC 1094-2 Primary method for Pressure Calibration of Laboratory Standard Microphones by the Reciprocity Technique.

The multiplication factor used for the uncertainties is 2 (corresponding to the earlier used confidence level of 95%) as required by DANAK.

The setup used is shown in fig. 3

Microphone calibration by B&K has a long history. Instruments for pressure reciprocity calibration has been in the product program for nearly forty years and systematic annual calibrations of internal reference standards can be traced back to the mid sixties.

During this time the uncertainties has been reduced continuously and the frequency range has been extended, partly due to new instruments, partly due to research made in connection with development of new standards. Today most calibrations are based on the IEC 109 standard.

The previously time consuming reciprocity calibrations are today made with automated systems. The software used at DPLA was developed at the Technical University of Denmark, Lyngby.

The history of Primary Standard Microphones and Transfer Standards is shown on fig 4.

An example of the accuracy obtainable is shown in fig. 5, which shows the difference between measurements on the same microphone using different couplers with different volumes.

REFERENCES: 1 Bureau International de Poids et Mesures. Pròces-Verbeaux de séances du CIPM 49, A1 (1981).

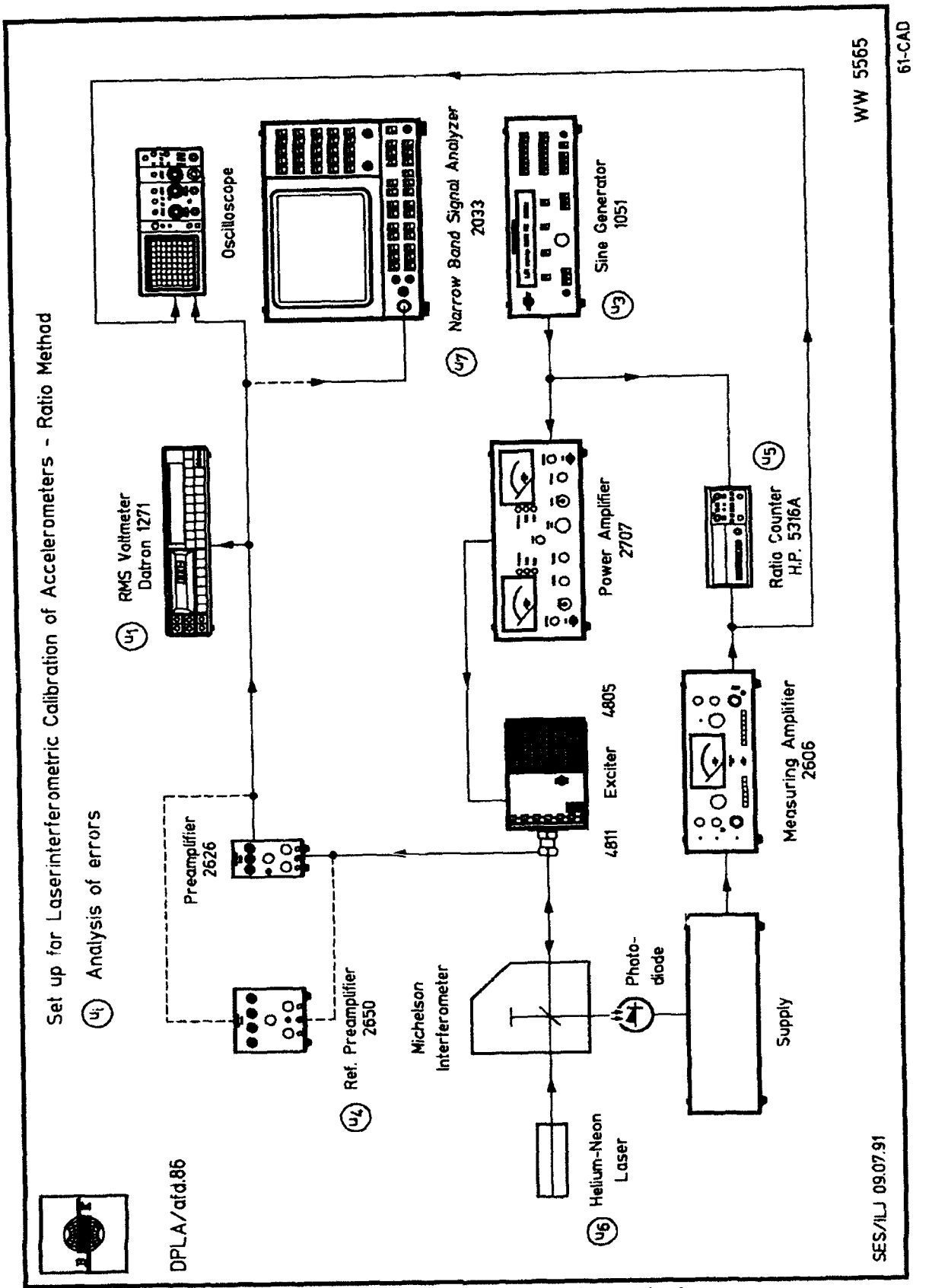

Figure 1. Lasercalibration setup using the Ratio Method.

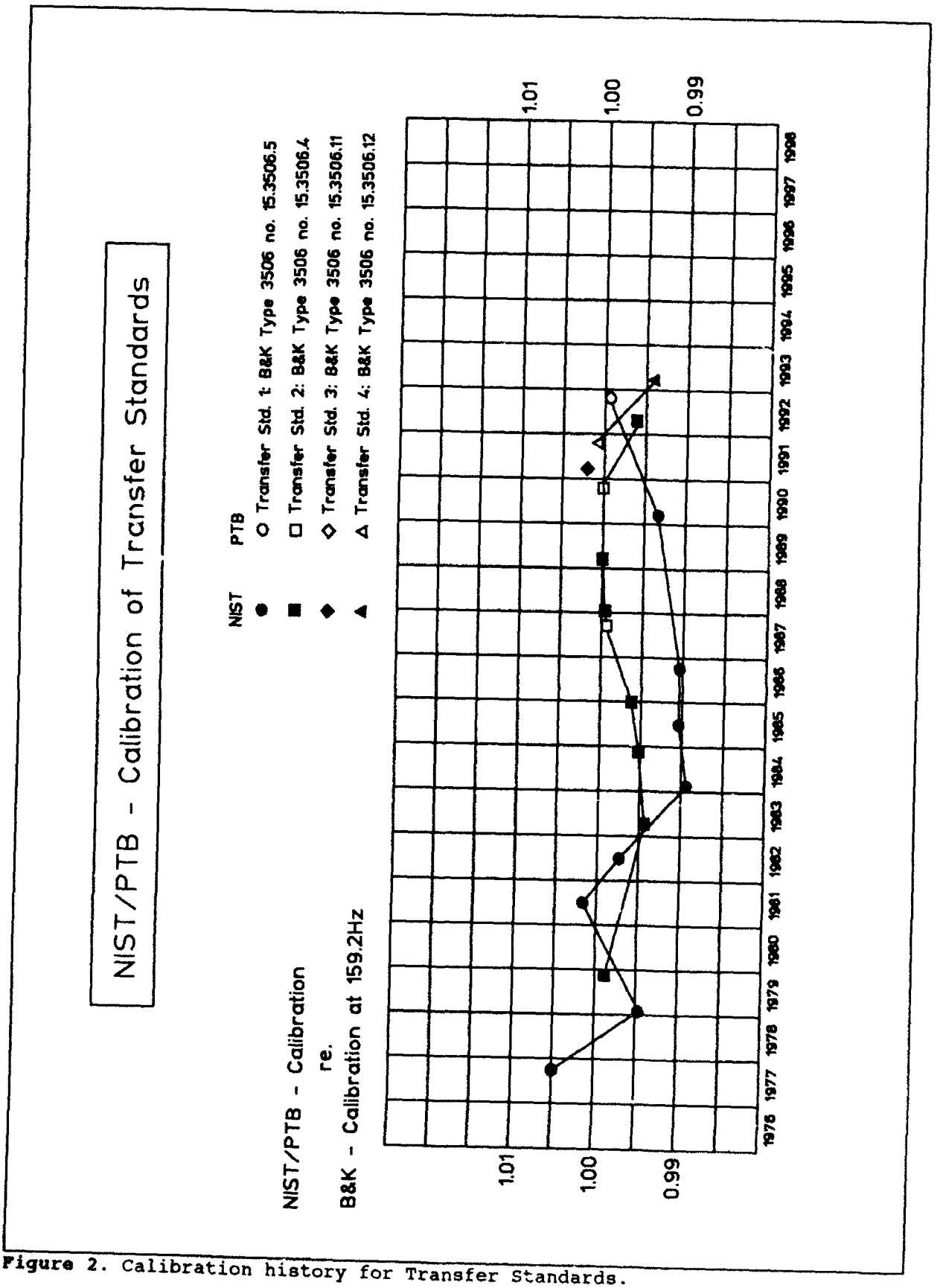

Figure 2. Calibration history for Transfer Standards.

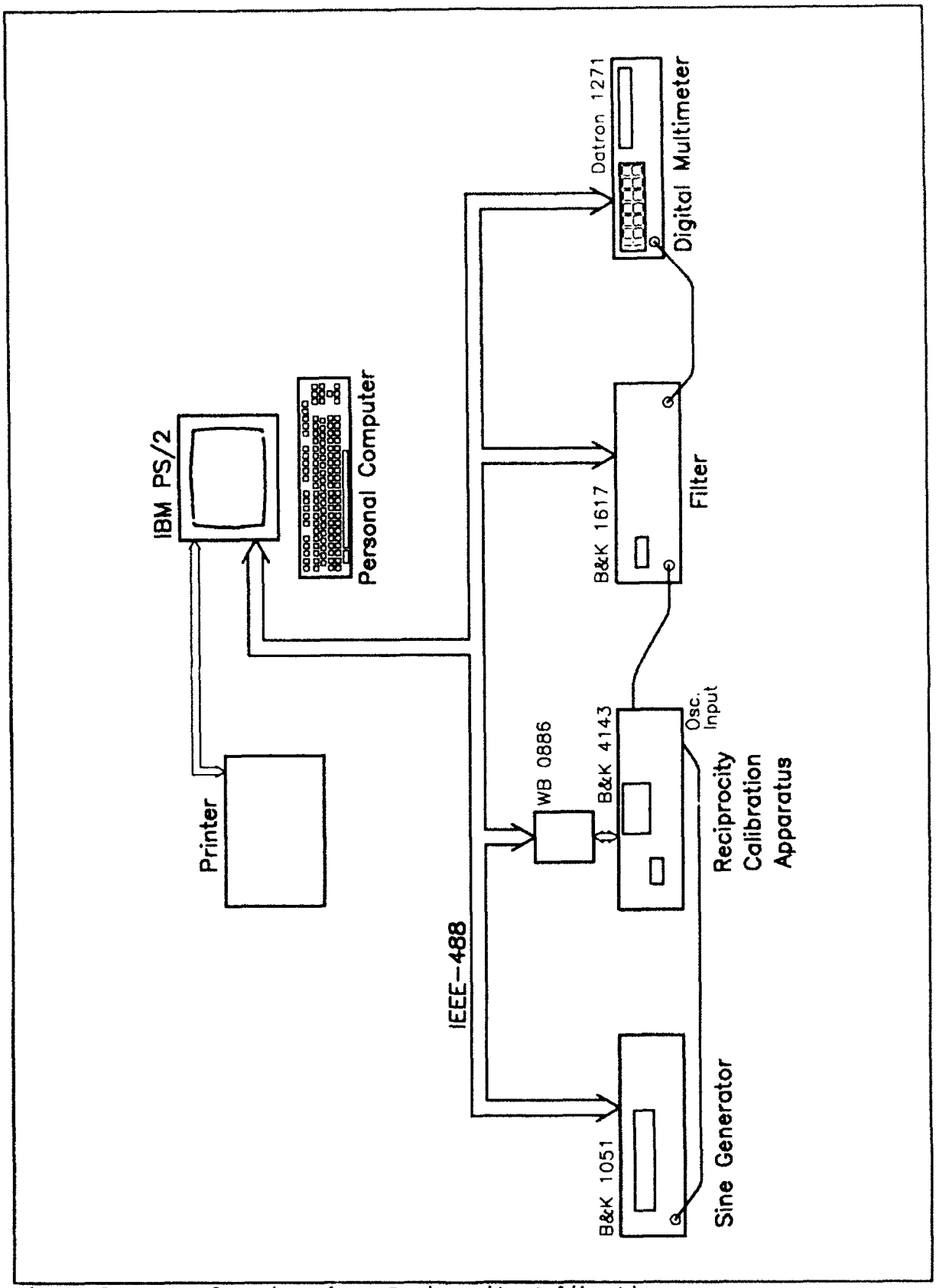

Figure 3. Setup for Microphone Reciprocity Calibration.

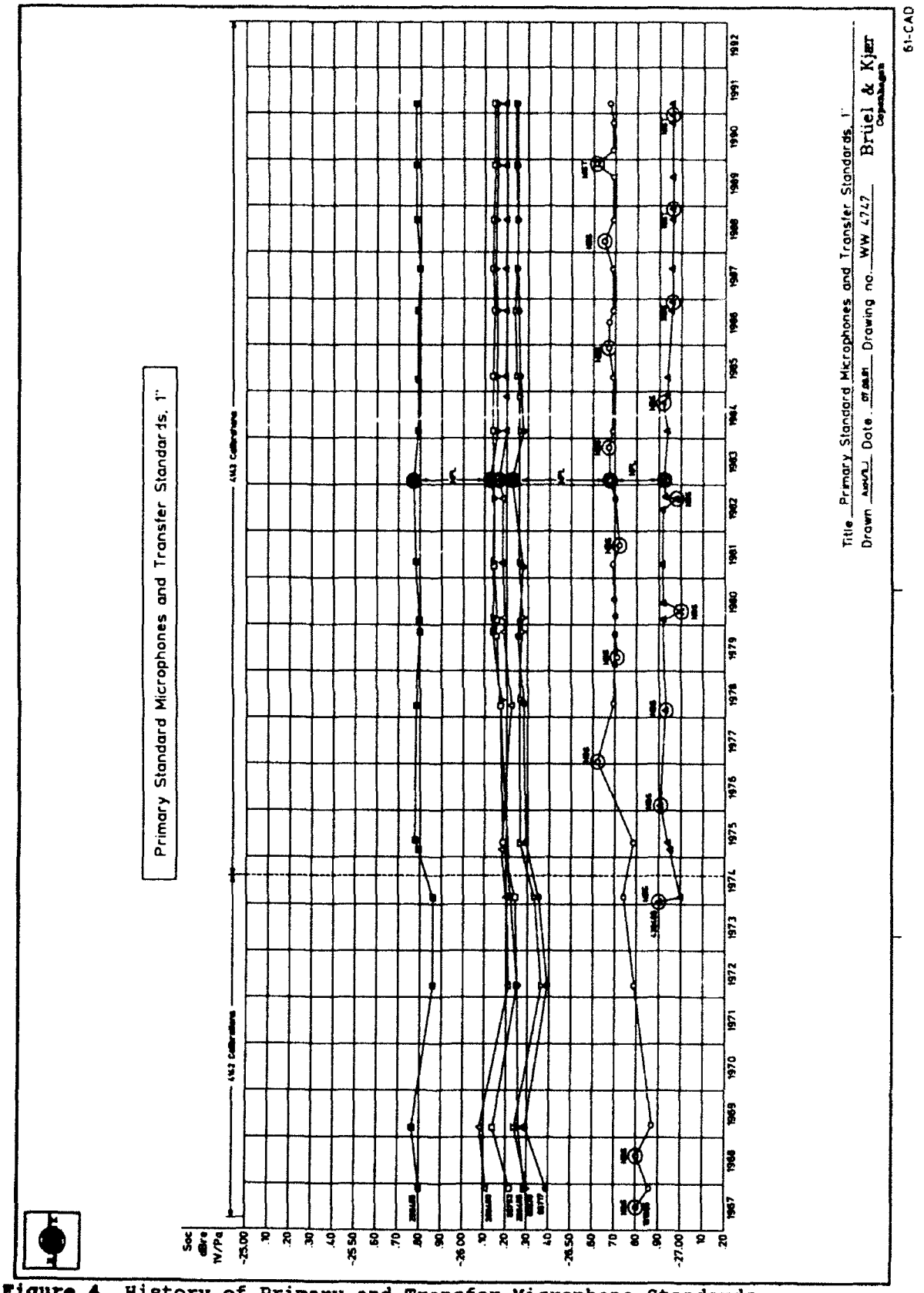

Figure 4. History of Primary and Transfer Microphone Standards.

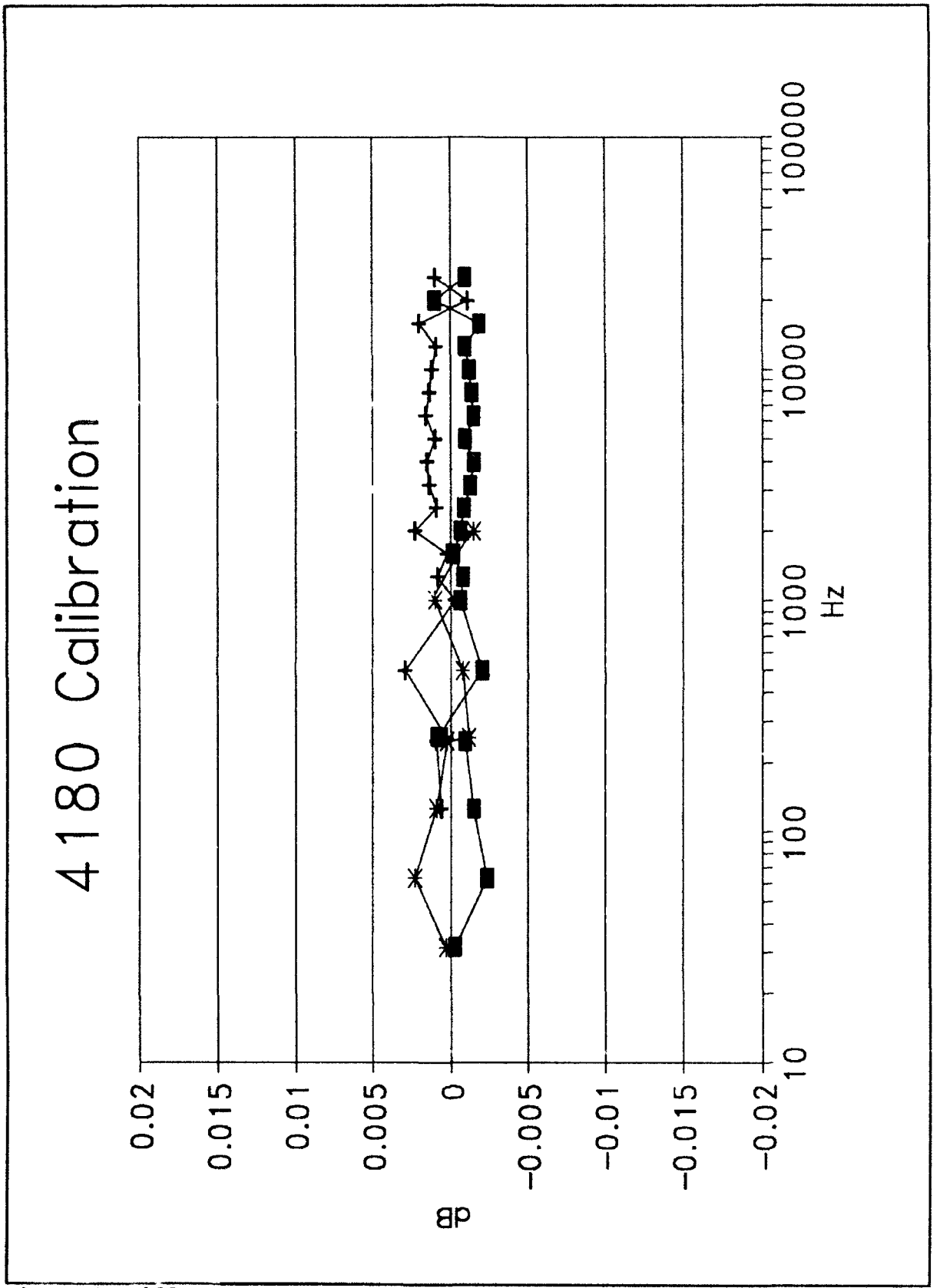

Figure 5. Differences between calibration in different couplers.